Skewed slab highway bridges

A parametric study on the design of reinforced concrete, simply supported skewed slab highway bridges

C.J.F. Hulsebosch

Witteveen + Bos

TU Delft

Cover image: northern part of the Oudenrijn highway intersection in the Netherlands.
Image obtained using Google Earth Pro [1]

Skewed slab highway bridges

A parametric study on the design of reinforced concrete, simply supported skewed slab highway bridges

by

C. J. F. (Coen) Hulsebosch

to obtain the degree of Master of Science
at the Delft University of Technology,
to be defended publicly on Tuesday May 28, 2019 at 10:30 AM.

Student number:	4177118	
Project duration:	August, 2018 – May, 2019	
Thesis committee:	Dr. ir. C. (Cor) van der Veen,	TU Delft, chairman
	Dr. ir. E. O. L. (Eva) Lantsoght,	TU Delft & Universidad San Francisco de Quito, supervisor
	Dr. ir. P. C. J. (Pierre) Hoogenboom,	TU Delft, supervisor
	Ir. P. (Pieter) Schoutens,	Witteveen+Bos, external supervisor

An electronic version of this thesis is available at http://repository.tudelft.nl/.

TU Delft

Witteveen+Bos

"Vaak moet er iets gebeuren, voordat er iets gebeurt."
Johan Cruijff

Preface

"Graduation sucks! Nobody likes it and it takes ages." This was the feeling I had towards the final chapter of obtaining my Masters degree in structural Engineering. As I got closer to the start of my graduation, I heard more and more negative stories and my enthusiasm was disappearing vastly.

Fast forward to about a year later, I am writing the last piece of my thesis. Overall, it has been quite a pleasant journey. The road towards the end was much less bumpy than expected and I can truly say that I have enjoyed most parts of the graduation process. One thing that helped me quite a lot before starting was reading the book 'Graduation - Challenge Accepted' [2], which gave me a more realistic view on the process I was about to go through.

In front of you lies the final version of my thesis, the last fulfillment in obtaining a master's degree in Structural Engineering with a specialization in Concrete Structures. The thesis contains a parametric study on the design of reinforced concrete, simply supported skewed slab highway bridges. This study was carried out under the supervision of the engineering consultancy firm Witteveen+Bos and the Delft University of Technology, both located in the Netherlands.

The idea for this thesis first started during my first weeks at Witteveen+Bos. I knew I wanted to do 'something' with parametric design and concrete, but could not formulate a much more specific topic at the start. After a lot of reading and some discussions with Pieter Schoutens, my supervisor at the company, the topic started to take shape. It was an actual proposed design of a higly skewed slab bridge in a project, which later seemed inconstructible, that fuelled the actual subject of this thesis (hence the quote by Johan Cruijff on the previous page). Not only for this start, but for his supervision throughout the entire project, I would like to thank him a lot. He has been very helpful throughout the process for me and I found that hardly any questions which I fired at him, remained unanswered.

Additionally, I want to express my gratitude towards the rest of the graduation committee. First of all, I would to thank Cor van der Veen for his feedback during our one-on-one sessions, as well as during the committee meetings. He pointed out to me that I was graduation in the specialization field of Concrete Structures, but that my thesis was still actually lacking a concrete part. Looking back, I am glad that I have added this part to my thesis. I will be one of the last graduate students under his wings, as he is retiring soon after my graduation. I wish him all the best!

Secondly, I would like to thank Pierre Hoogenboom for his contribution. Although we have only met a few times, his questions during meetings kept me sharp, especially on the topic of plates.

Next, I want to thank Eva Lantsoght, who has truly surprised me with her sharpness, extensive scientific knowledge and the speed at which she often replied me. Sometimes within a day, she went through the entire draft version of my thesis to pick out even the smallest mistakes in spelling. Looking back, I could not wished for a better 'substitute' for Dick Hordijk, who left the committee about halfway through the process. Thank you Eva!

At last, I wish to thank my parents for their support throughout my entire period of studying. Finally, I would like to give a small thanks to my roommates, who tried to motivate me by telling me how slow I was, and many thanks to all others whom I have forgotten to mention here!

Coen Hulsebosch
Rotterdam, May 2019

Abstract

In situations with spatial limitations where a bridge is desired, a skewed bridge is a solution. The bridge deck of a skewed bridge has the shape of a parallelogram, in which the angle that remains in the acute corners is defined as the skew angle. This thesis focuses on the design of reinforced concrete skewed slab highway bridges that are simply supported on discrete bearing pads. A parametric tool is created which, based on a set of values for input parameters, generates and analyzes bridge models created in a finite element method (FEM) software program. After analysis, results are summarized, which allows for a parametric study. The goal of this study is to develop knowledge for decision-making in early stages of projects.

The influence of main geometric parameters (skew angle, bridge span length, bridge road width) on the load distribution in a skewed bridge is investigated, as well as the influence of FEM mesh element size, applied plate theory, traffic load configuration and support configuration. An other important parameter, being the bridge deck height, is set to be dependent to the span length at first. Skewed slab bridges tend to span from support to support in the shortest direction. This means that loads will concentrate in the obtuse corner. Resultant quantities, mainly bending moments and shear force in the obtuse corner, are studied on their relation with the different parameters.

The obtuse corner load concentrations can require the bridge height to become larger than desired. A powerful measure is to add additional triangular sections (ATS) to the side of the bridge, which increases its width. This way, the road skew angle no longer equals the bridge skew angle. Load concentrations in the obtuse corners are reduced, which can result in a lower deck height, less reinforcement, or both. The effect of ATS addition on resultants is studied: great reduction is observed, even for relatively small ATS addition.

In order to relate the bridge deck height to bridge geometry, a reinforcement study is conducted. A procedure is described for a certain cross-section, in which the resultants are known from models generated by the parametric tool. Starting point is the longitudinal bending reinforcement based on the crack width criterion, which is usually governing in bridge design. Next, required shear reinforcement is calculated. Following, the ultimate bending moment capacity is checked, which is found to be always sufficient for crack-width-based reinforcement design. Finally, optimization (different bar diameters, add or remove a reinforcement layer, deck height reduction) is investigated and applied if possible.

Using the procedure described above, a case study is conducted. A highly skewed bridge (road skew angle of 20°) is taken. Starting with 0°, ATS is added in steps of 5°. For each geometry, a model is created with the tool after which resultants are used for the reinforcement design. For a bridge span of 13.7 m and a road width of 8.3 m, the first bridge (no ATS, skew angle of 20°) was found to lie beyond the limits of reinforced concrete. Two layers of 40 mm bars required fatigue-sensitive couplers, while detailing and proper anchorage would prove to be unconstructible. Increasing the cross-section also increased governing moments due to concrete self-weight and therefore is not an option.

Addition of a 5° ATS resulted in a 900 mm high bridge deck, which seems possible to construct. Addition of 10° resulted in a 750 mm high deck, 15° into 600 mm and further ATS addition reduced deck height even more. Although it should be noted that ATS addition increases deck surface, a significant reduction in deck height can be obtained. ATS addition is shown to be a

powerful measure. Depending on project situation, it can provide optimization and cost savings; the parametric tool is proven to be useful in investigating this.

Contents

1 | Introduction

1.1 Problem statement

In cases where a road needs to cross an obstacle below (river, other road, etc.), bridges are a solution. The simplest and most common form of a bridge is a perpendicular bridge: centre-line of the bridge with its road and the centre-line of its obstacle below cross each other at an angle of 90°. In some cases however, often due to space limitations, a perpendicular bridge is not the desired solution. In such cases, the bridge is designed to cross the underlying obstacle at an angle that is not 90°: this is called a skewed bridge. In the Netherlands, skewed bridges are becoming increasingly common at highway intersections because they are part of replacement plans for cloverleaf intersections. Such alternatives, which implement bigger radius of curvature in the horizontal alignment, allow for a smoother flow of traffic and therefore cause less congestion.

Figure 1.1: A skewed slab highway bridge in the Netherlands, where additional triangular segments were applied, from [3]

The skew angle (Dutch definition) is the angle that the center line of the bridge makes with the center line of the underlying obstacle. In other words: the skew angle is the angle that remains in the acute corners of the bridge. Bridges with a small skew (great skew angle, close to 90° crossing) are usually treated and designed as 'normal bridges', because their distribution of load is very similar to that of a rectangular (straight) bridge. However, as skew is increased (skew angle decreases), differences in force distribution compared to straight bridges are becoming increasingly significant and difficult to predict. This may lead to problems in the design of concrete slab bridges; a bridge type often applied because of its minimal system height, leading to a cost-effective design.

Higher skew (lower skew angle) can lead to high local stresses, which may require a thicker bridge slab or more reinforcement. Subsequently, fitting the reinforcement into the desired cross-section becomes problematic. To solve this, the bridge width can be increased to increase the bridge skew angle, as can be seen in Figure 1.1: an additional triangular-shaped segment (ATS) is added on both sides, which has no road on top. The bridge skew angle usually applied in such cases is 45°, which is often an aesthetic decision taken by an architect rather than being an engineering- or cost optimum. The addition of extra width also has downsides such as additional use of space and

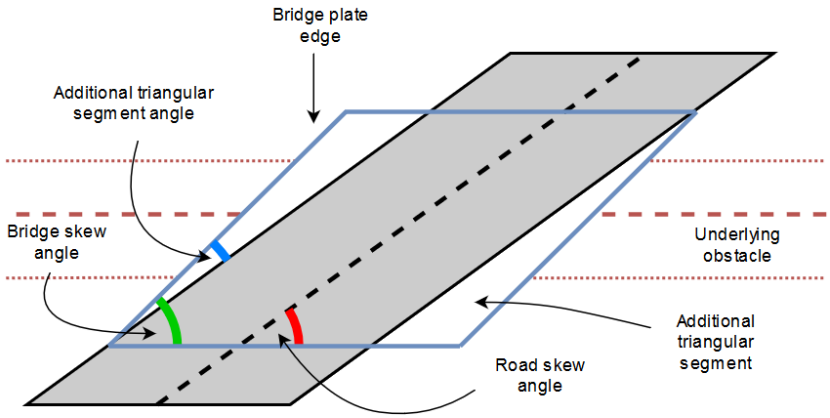

Figure 1.2: Definition of the skew angle [4]

material.

Adding ATS means that the bridge skew angle no longer equals the road skew angle. The bridge skew angle is now defined as the sum of the road skew angle α and the ATS angle β.

Decisions about bridge shapes are usually made in early stages (tender phase) of infrastructure projects. It is therefore both important and interesting to know the influence that main geometrical parameters such as the skew angle, bridge span, bridge width and bridge deck height have on skewed bridges. In this thesis, influence of such parameters is investigated. This thesis will focus on simply supported, reinforced concrete skewed slab bridges, designed for Dutch highways.

Problem statement: It is difficult to predict the consequences of decisions made in early design stages regarding simply supported, reinforced concrete skewed slab bridges.

1.2 Research objectives

The overall objective of this thesis is to gain insight into the consequences of decisions made on skewed slab bridges. This way, decisions made in early stages of an infrastructure project can be supported with a more fact-based argumentation, instead of using experience from earlier projects. Experience in itself is not a bad thing, but experience used in certain projects might be based on mistakes made earlier on, after which the 'wrongly' developed experience is used over and over again.

The first part of the objective describes gaining insight into load distribution in a simply supported reinforced concrete skewed slab bridge. This knowledge is developed by creating and utilizing a parametric bridge tool. The tool consists of a script created in the widely used Python programming language, together with a template Finite Element Model (FEM) created in SCIA Engineer version 18.1 [5]. The script allows for the parametric generation of multiple bridge geometries by combining an array of each input parameter into sets of parameters. One by one, the parameter sets are then loaded into the template FEM, after which a linear Finite Element Analysis (FEA) is executed. Results are then exported for each FEM created. Once the last analysis has finished, the script performs a generic analysis on the results and summarized them into a result sheet. The script and model will be described in the next chapter.

Results from the script/model will be used in two ways:

1. Analyze influence of the following properties (parameters) on load distribution and bridge behaviour:
    - Mesh element size and applied plate theory
    - Support configuration (vertical support stiffness of bearing pads, edge distance, centre-to-centre distance)
    - Abutment and foundation stiffness
    - Load configuration (location of the heaviest loaded lane)
    - Main geometric parameters (span length, bridge road width and bridge skew angle)
2. Obtain governing values of reinforcement design moment and vertical shear force with respect to main bridge parameters (span, width, thickness, skew angle). With the use of the parametric tool, a wide range of bridge FEMs is generated from which governing values (in terms of load quantities) can be extracted.

Next objective in the thesis is to create a 'translation' from the governing bridge loads into reinforcement layouts. Bending-reinforcement design in concrete skewed slab bridges is usually based on crack width criterion, which has proven to be governing over the ultimate bending moment. Additionally, shear reinforcement may also be a decisive criterion. A key aspect will also be looking into rejection criterion for the reinforcement: what is still physically constructible and what are the boundaries?

1.3 Research questions

Main question: What is the influence of different parameters on the load distribution in a simply supported reinforced concrete skewed slab bridge, and how can these parameters be used in the reinforcement design?

Sub-questions:

- What relations can be found between design parameters and internal load distribution?
- Which rejection criteria are key when validating a reinforcement layout?
- What is the effect of adding additional triangular segments on a skewed bridge?
- To which extent can a parametric tool be used in a preliminary design phase?

1.4 Scope

The following points describe the scope in which the research is carried out:

- Bridges investigated are highway bridges and therefore Dutch national infrastructure, managed by Rijkswaterstaat
- Bridge design should comply with the Eurocode, Dutch annexes, and Dutch guidelines for designing infrastructure (ROK)
- Bridge geometry is assumed to be a parallelogram (straight edges, opposite corners of equal angle)

- The bridges are simply supported on discrete bearing pads with a constant centre-to-centre distance
- Foundation consists of a concrete abutment beam on top of a sheet pile wall (deeply founded abutment)
- Only reinforced concrete designs are considered, prestressed concrete is not
- No earthquake, wind and impact loads are considered
- Analysis of the problem with 2.5D FEM software (no 3D elements)
- Linear analysis only, no nonlinear calculations

1.5 Thesis outline

The following steps are a rough description of the thesis outline and therefore also depict the methodology applied:

1. Literature study: investigate current state of knowledge on skewed slab bridges. Look into previous studies and their results
2. Create the parametric bridge tool (FEM-software model coupled with Python script)
3. Check and validate the model to make sure it is sufficiently accurate
4. Generate, analyze and interpret results
5. Add ATS functionality to the bridge tool
6. Conduct a reinforcement study and create sheets for quick reinforcement design
7. Perform case study on a skewed bridge with additional triangular widening segment

2 | Literature study findings

To investigate the currently available knowledge on reinforced concrete skewed slab bridges, a literature study is conducted. The full version of this literature study can be found in Appendix A. The literature study focusses on two parts that are usually present in the structural design process any reinforced concrete bridge, especially in a skewed slab bridge:

1. The effect of the bridge shape, size and loading on the force distribution in the bridge
2. 'Translation' of force distribution into required reinforcement

2.1 Part 1: Force distribution in a skewed bridge

Despite the fact that quite some literature is available on skewed bridges, not all literature is relevant. A lot of the literature focusses on skewed bridges that contain main girders. Girders strongly determine the force distribution within a bridge, since they govern the direction in which the loads are transferred. The interesting thing about skewed slab bridges is that they do not contain such girders and that their force distribution is therefore less predictable.

Key findings from the literature study are summarized below:

- Slab bridges tend to span in a direction running from support line to support line. As skew increases (skew angle becomes smaller than 90°), the difference between the skew angle and the angle of the bending moment trajectories starts to grow. [6]

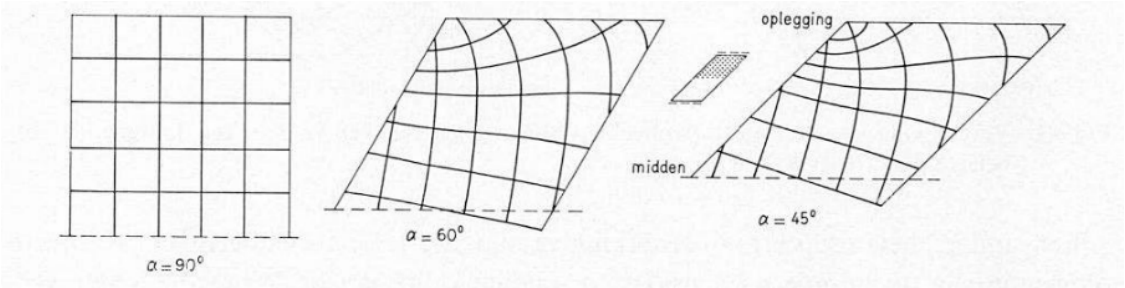

Figure 2.1: Image of trajectories for different skew angles, from [6]

- Under the conditions that the free edge and support width remain constant, and the plate is loaded by dead load only, a few conclusions are drawn. As skew increases:
  - The maximum deflection decreases
  - The maximum longitudinal bending moment decreases
  - The location of maximum longitudinal bending moment moves towards the obtuse corner (down to 0.3 l for 45°)
  - The shear forces concentrate at the obtuse corner

  - The maximum transverse moment increases

- Elastic supports allow for better distribution of support reactions. [7]
- Shear used to be of small concern in skew-slab bridges, until the collapse of a Canadian skewed slab (cantilever) bridge in 2006 happened without warning (brittle failure), raising awareness. [8]
- Shear stresses in straight slab bridges are relatively small and usually cause no problems in terms of reinforcement. However, as bridge skew increases, shear force in the obtuse corner increases dramatically.
- No study was found that applied traffic-representing Eurocode Load Model 1. A lot of studies focussed on loads from the American code AASHTO. Some of the studies only applied a constant loading.
- The last study about 'strokenverdeling' showed that application of (old) axle load-system still did not make the 'strokenverdeling' an effective method of reinforcement distribution. It recommended looking at Eurocode load models and very skewed bridges (skew angle of 30°). [9]
- Most studies cover bridges with a skew angle between $90° - 45°$. Only one study was found that investigated a bridge with a skew angle of 50°. → This thesis will cover the a range of skew angles from 90° to 30°, with a focus on $45° - 30°$.
- Skewed bridges ranging from $90° - 70°$ or even $90° - 60°$ are usually treated as straight bridges. For instance: for skew angles up to 70°, FEM and a method from AASHTO produce similar results. [10]
- According to [8], corner reaction force is not a local effect, but rather the accumulation of the vertical shear forces, that are induced by the transverse curvature.
- Several parameters can affect the amplitude of the obtuse corner forces:
  - Continuity (this thesis will treat only single-span bridges)
  - Slab geometry
  - Support configuration: continuous or discrete
  - Support stiffness
  - Cracking
  - Load configuration
- In a test with a skewed slab bridge of 40 degrees, the obtuse support was carrying about 40% of the total load. A slab strengthened at the edge (against cracks) and in the longitudinal reinforcement, showed punch-like behaviour. This research suggested doing further research into support spacing, skew and reinforcement detailing. [11]

2.2 Part 2: Determining required reinforcement

There is a lot of available literature on the automation of reinforcement calculation based on load distribution. In general, this is seen as a method of post-processing linear FEM analysis results, and NOT as a part of FEM.

Input in such methods is the stress situation, which can be obtained from the bending moments that result from FEM linear analysis. This stress situation can then be translated into reinforcement stresses. Those reinforcement stresses depend on the layout of the reinforcement, which can either be orthogonal or non-orthogonal. Non-orthogonal reinforcement layouts are shown to be highly inefficient. [12]

The reinforcement stresses at each location can be calculated into a predefined system of reinforcement (direction of the bars). A different option is to optimize the reinforcement direction, which leads to the theoretical lowest total amount of reinforcement.

However, the stress situation will depend on the location considered. This means that for every location in the plate, a different reinforcement configuration can, and probably will be found as optimal. So considering each element separately and then combining results for the entire plate, an optimal reinforcement configuration of the plate will be found which consists of a non-orthogonal layout with non-straight reinforcement bars of a non-constant diameter. This theoretical optimum is not practical at all, since it is almost impossible to construct and certainly does not lead to an economic design.

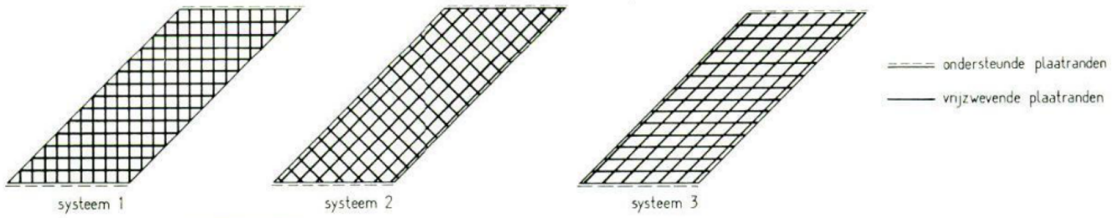

Figure 2.2: Three different reinforcement layouts, from [12]. Layout 2 will be used in this thesis

As mentioned above, a layout with straight bars is a more realistic one. The CUR reports from the 1970's [12] on skewed concrete slabs have showed that an orthogonal layout is the most optimal one, and that any deviation of this layout leads to a higher amount of reinforcement required. It should be noted though that this comment is purely theoretic. Additionally, deviations of practice from theory like cutting losses and overlap 'losses' are not considered. In some actual bridge designs, a non-orthogonal reinforcement layout may still prove to be more cost-effective in the end.

Old literature calculates only horizontal (bending reinforcement) by considering only in plane stresses, considering a disc model. Later on, plate models are considered as well, which can take into account shear stresses and calculate theoretically required reinforcement [13]. Both models are then combined into a shell model [14].

The last step of the reinforcement design step, is to go from reinforcement stresses to reinforcement surface or actual bars with diameters and centre to centre distance. In this last phase, practical considerations can also be taken into account.

However, this last step of designing an actual reinforcement layout still has not been automated in most engineering firms. In practice the structural engineer usually picks a certain reinforcement layout, and then validates this layout to see whether it meets the requirements in terms of serviceability and ultimate strength. This last step of checking is usually done with external software or through company-made calculation sheets, which are based on codes such as the Eurocode.

3 | Parametric bridge tool

3.1 Bridge tool concept

In order to study the effect of different parameters on the problem of a reinforced concrete skewed slab bridge, a parametric bridge tool is created. The Parametric bridge tool consists of two main parts: a script and a Finite Element Model (FEM) template, created with program called SCIA [5]. This chapter will focus on explaining the general outline of the tool. A brief description of the tool's properties is given, in order to make clear how it works.

Figure 3.1 shows the workflow of the tool for a single bridge model. The input parameters are defined inside the Python script, after which the script is executed. After the input is processed by the script, the parameters are transferred to the SCIA template model and the analysis is started. Once finished, SCIA will export two files: a SCIA result file, containing the model that is created and analyzed, and an excel file that contains the desired results. This is the overall workflow when analyzing a single skewed slab bridge model.

The most powerful property of the bridge tool is its ability to automatically repeat the single-bridge workflow. Instead of a single set of parameters (one value for each parameter), multiple sets of parameters can be modelled and analyzed sequentially. Finally, results from each model are extracted and gathered in a summarizing spreadsheet. This way, the tool allows for easy comparison of results from different models. A certain parameter can be varied over different models, after which the results from this variation can be investigated. Results can be force quantities or deformations and their respective maximum location.

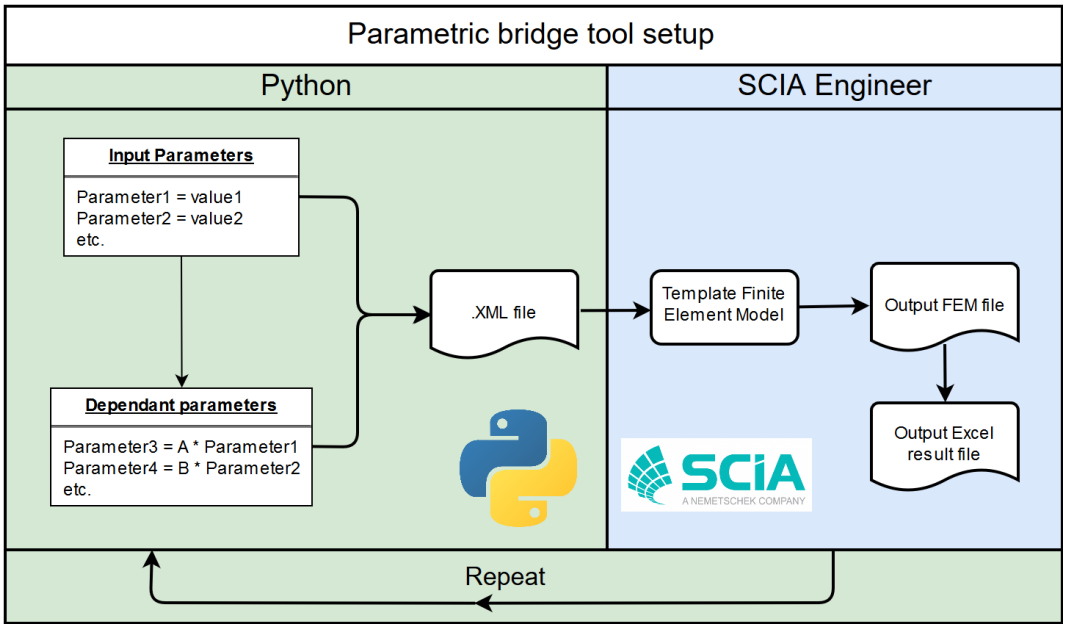

Figure 3.1: Simplified diagram of the parametric bridge tool workflow

The FEM-template is the basis for the calculation: most relations are defined within the model.

It is created in a software package called SCIA Engineer version 18.1, used by many of structural engineering firms including Witteveen+Bos. Within SCIA, it is relatively easy to set up a model, perform an analysis and obtain results. SCIA Engineer is used to perform the finite element analysis (the 'calculation') and to create result files. Additionally, SCIA offers a module which allows definition of loads, geometry and all other sorts of properties as a parameter. This means that upon creation of the model, the relations defined in the model should be known. Setting up a parametric model therefore takes more time than creation of an 'ordinary' model. However, once set up, the model (within its defined limits) is easily adjustable and changes can be applied rapidly. Therefore, if a model is to be used repeatedly due to many changes in a project or because it is reused in different projects, it will prove to be rewarding in terms of time and cost in the long run. Additionally, parametric models are great for optimization purposes.

The parametric bridge model is a tool developed in this thesis for quick determination of governing loads and deformations, given a skewed slab bridge with certain parameters. Additionally, the tool allows for generation of multiple bridge models based on an array (or multiple arrays) of values for a certain parameter (or multiple parameters), while also being able to summarize results for multiple models. This function allows for a parametric study of simply supported, reinforced concrete skewed slab bridges.

As is the case for any model, this model is a simplification of reality. A well known saying (based on a quote by George Box [15]) is:

> "All models are wrong, some models are useful"

The model has been developed with the aim of 'keeping it simple', while still being as useful (realistic) as possible: given the time frame of this graduation project and the fact that the model should still be useful (understandable and customizable) to any interested engineer (or programmer) using it hereafter. On the other hand, it should still provide a sufficiently accurate approach of 'reality' to make sure that its outcome complies with the governing codes and regulations, while assumptions and schematizations made are both plausible and re-traceable.

3.2 Script contents

The script is the backbone of the bridge tool. It is written in Python: a programming language originally conceived by a Dutchman [16] that is widely used, open-source, free of cost and considered as relatively 'easy' to read and use. Python has numerous possibilities and is considered a general purpose language. It is used for many applications: not only for scientific purpose but also for building websites (such as Google and YouTube), game development and visual effects of movies [17]. Python is great for transferring data of different formats between different software programs, which is why it is used for the bridge tool.

A small breakdown of the steps executed in the script are given below:

1. Import and activate libraries and plugins required to facilitate all functions of the script
2. Input a value or an array of values for each input parameter
3. Input the required file names and their locations
4. Creation of dependent variables (based on values of input parameters)
5. Combining the arrays of values into all possible parameter-sets
6. Sequential processing of parameter-sets through a loop:
   (a) Load a parameter-set into the SCIA template model through a .xml file
   (b) Start the linear analysis function in SCIA

(c) Export a SCIA file of the model containing the results

(d) Export a spreadsheet (Excel) file with the desired results from the model

(e) Repeat

7. Extract the results from the spreadsheet of each individual model, paste them into one summarizing spreadsheet

3.3 Template model geometry

3.3.1 Starting points

This chapter will focus on elaborating on the structure of the FEM-template. This model is based on a lot of starting points from codes and guidelines. Additionally, it contains assumptions and simplifications, which will be explained briefly here.

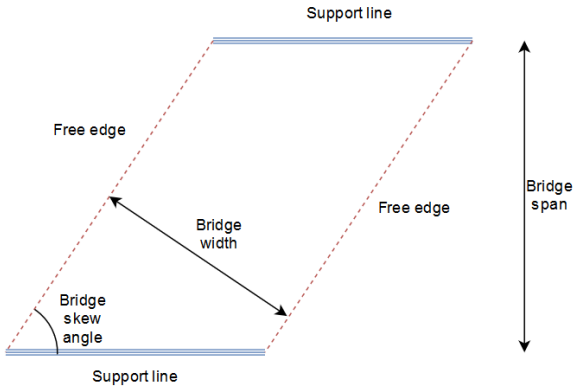

Figure 3.2: Basic definitions in a skewed bridge

The first starting point is that the amount of input parameters should be kept to a limit. To ensure this, a few simplifications are made. First of all, the bridge shape is assumed to be a parallelogram:

- All four edges of the bridge are straight lines
- The support lines of the bridge run parallel to each other
- The free edges of the bridge run parallel to each other

Main concern of the model is the influence of the bridge shape on the force distribution. The shape is mainly determined by the bridge span, the bridge width and the skew angle, as defined in Figure 3.2. A more detailed explanation of these parameters is found below.

A lot of the starting points come from one of the codes:

- Eurocodes with the national (Dutch) annex [18] [19] [20] [21] [22] [23] [24] [25] [26]
- Richtlijn Ontwerpen Kunstwerken (ROK) [27] [28] [29] (translates as Guidelines for design of infrastructural superstructures)

Eurocodes are the basis for structural design in Europe. ROK is a guideline from Rijkswaterstaat (RWS, the operating organization of the Dutch department of public works [30]), which is seen as a package of additional requirements. ROK provides requirements for designing infrastructural concrete structures for Dutch highways and bridges, which are owned, operated and maintained by RWS.

3.3.2 Geometric and parametric relations

To start with, two coordinate (axis) systems are defined, as shown in Figure 3.3.

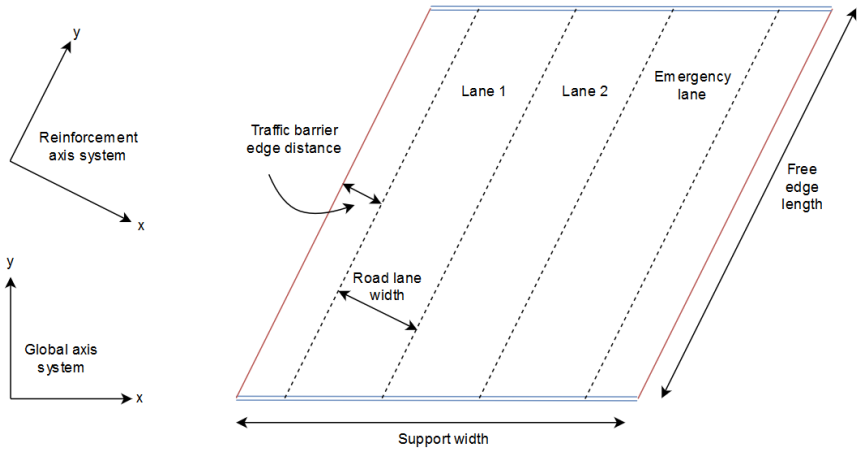

Figure 3.3: Definition of geometry parameters

The parametric bridge model allows a study on the effect of variation of important parameters. The model is defined by three types of parameters:

Constants The constants are predefined values, determined by governing codes or own decisions. Important constants are:

- Real road lane width: Standard width of a road lane in reality on a highway in the Netherlands is 3.5m (not to be mixed up with theoretical lane width).
- Traffic barrier edge distance: determines at which distance from the free edge the lanes start. This is 1.4 meters as shown in Figure 3.4
- Bearing pad size: The skewed slab bridge in this thesis is assumed to be supported by discrete bearing pads. The dimensions of the elastomeric bearing pads are chosen to be length x width x height = 400 x 300 x 80 mm. As stated before, the relative distance of the bearing pads and their edge distance will be varied.
- Thickness of the cover layer (asphalt): 140mm, according to the ROK. This layer adds to the spreading of the wheel load (see Figure 3.13), which is assumed to distribute its load under an angle of 45 degrees down till the centre of the concrete bridge ($\frac{h}{2}$). For this load distribution over deck height, 100 mm is taken into account. When calculating the load due to weight, the 140 mm is used.

Input parameters The input parameters are mostly the parameters that define the main dimensions of the bridge. By varying the input parameters, their effect on the load distribution in the bridge can be studied. The input parameters are visualized in Figure 3.2. The total required width of a road is mainly determined by the amount of lanes that it contains. For both the road on the bridge (which determines bridge width) and the underlying road (which determines the bridge span), three different configurations are chosen:

- 1 lane, no emergency lane
- 1 lane, 1 emergency lane
- 2 lanes, 1 emergency lane

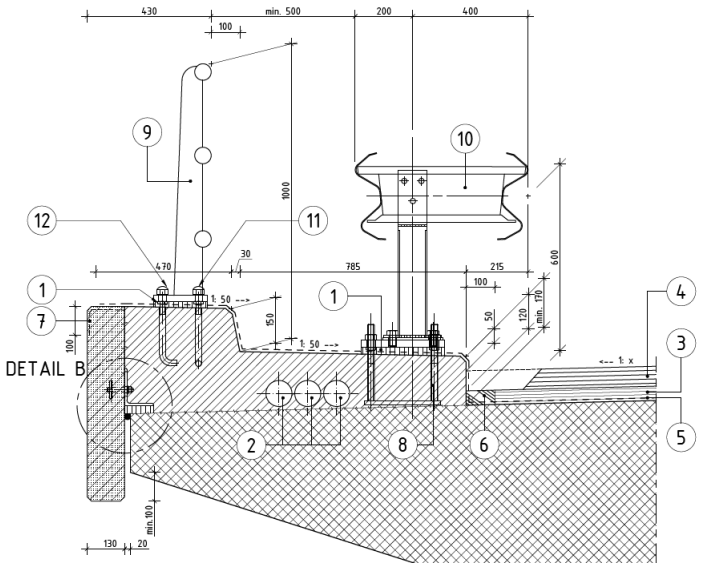

Figure 3.4: Cross-section of the edge structure from ROK annex B [29]. Edge distance is taken as distance from right side of element 10 to the edge of the bridge deck, so element 7 is not taken into account

While the standard width of a road lane (3.5 m), an emergency lane (3.7 m) and additional object distance (1.0 m) are equal for the bridge road and undergoing road, their barrier distance at the edges varies. The road on top of the bridge will have traffic barriers, which are usually placed at 1.4 m from the edge. The undergoing road, which in this case is situated between two sheet pile walls, has hardly any distance between its concrete barriers and the sheet pile walls. However, the distance between the barriers and the centre of the support line should also be taken into account, as it adds to the total span. This distance between the front of barriers and support line is assumed to be 1.0 m.

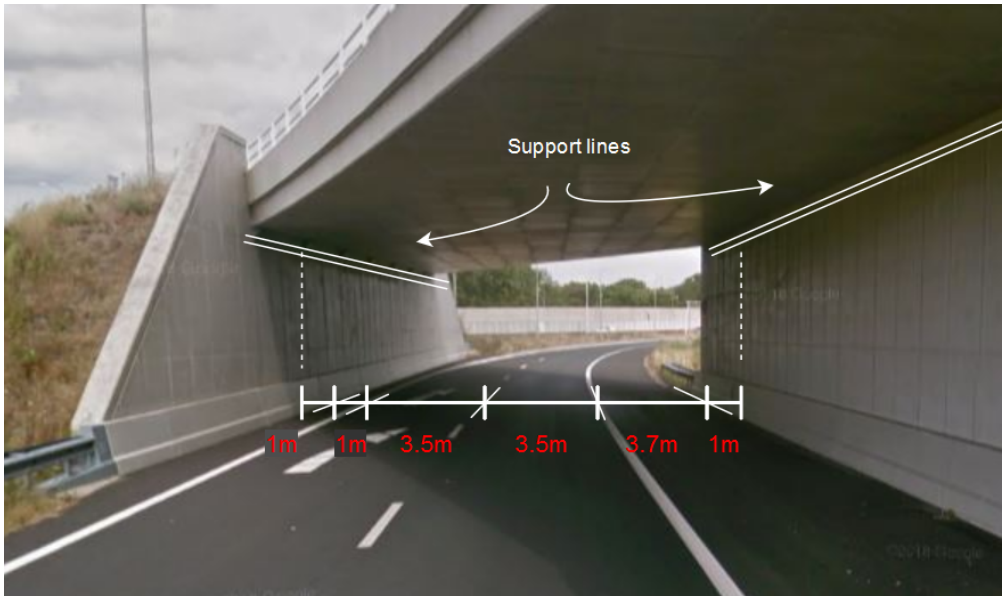

Figure 3.5: An undergoing road configuration: 2 lanes, 1 emergency lane, from [31]

- Bridge span: This is the span measured perpendicular to the support line (global y-direction). In other words, it is the required amount of space to cross the road beneath the bridge. The amount of lanes of the underlying road is governing for the Bridge span. Options are:

- 1 lane, no emergency lane: 2 * 1 + 2 * 1 + 3.5 = 7.5 m
- 1 lane, 1 emergency lane: 2 * 1 + 1 + 3.5 + 3.7 = 10.2 m
- 2 lanes, 1 emergency lane: 2 * 1 + 1 + 2 * 3.5 + 3.7 = 13.7 m

- Bridge width: This is the total width of the bridge, measured perpendicular to the free edge (in reinforcement x-direction). This width is governed by the amount of lanes that need to fit on the bridge, with dimensions similar to the Bridge span:
  - 1 lane, no emergency lane: 2 * 1.4 + 2 * 1 + 3.5 = 8.3 m
  - 1 lane, 1 emergency lane: 2 * 1.4 + 1 + 3.5 + 3.7 = 11 m
  - 2 lanes, 1 emergency lane: 2 * 1.4 + 1 + 2 * 3.5 + 3.7 = 14.5 m

  A very important note is that this definition of the bridge width is different from most definitions found in literature. In this study, the road on top of the bridge is chosen to be decisive for the width of the bridge. This means that when the skew increases and the bridge width is kept constant, the support width will also increase, leading to a higher surface of the bridge:

$$\text{Support width} = \frac{\text{Bridge width}}{sin(\text{Skew angle})} \tag{3.1}$$

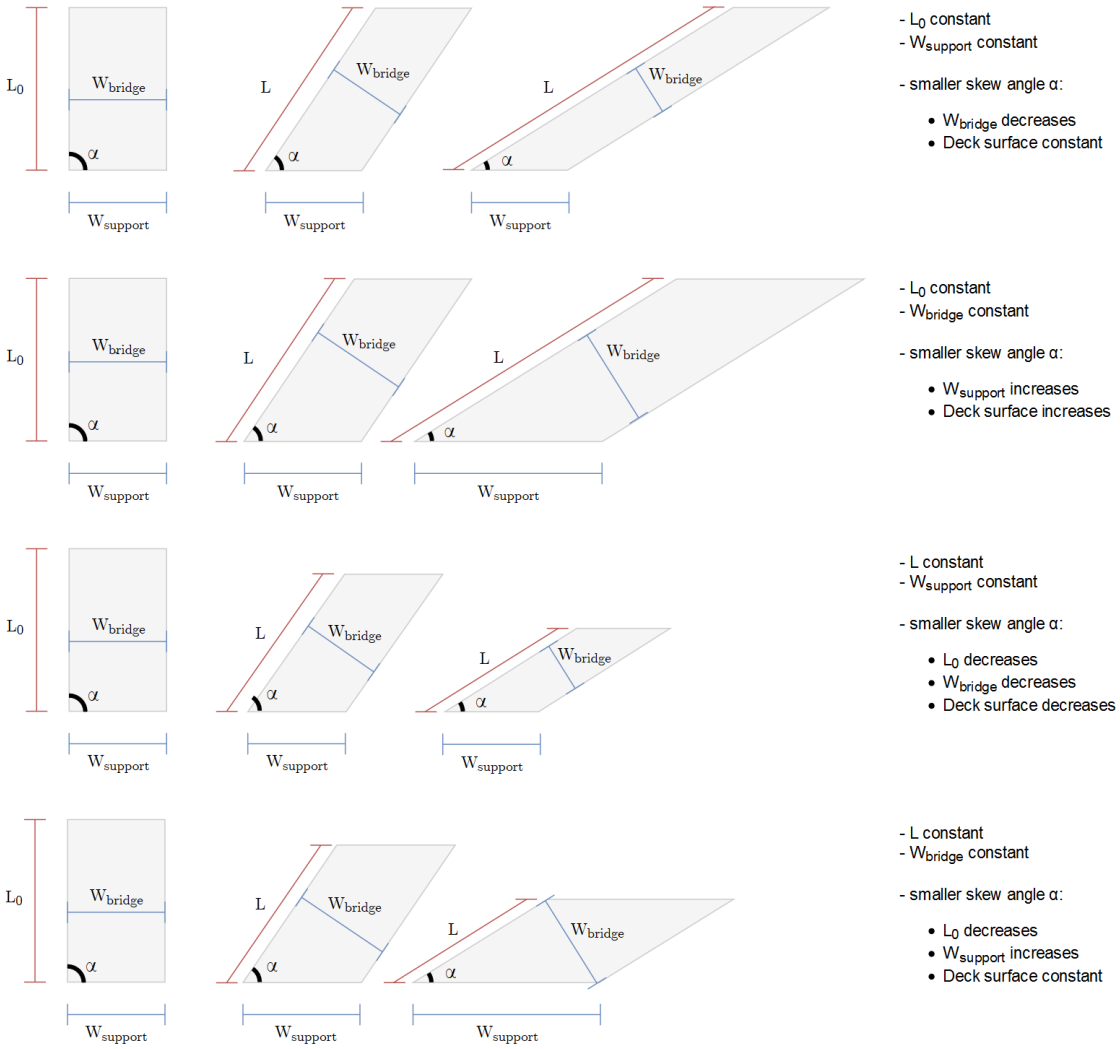

Figure 3.6: Possible geometric approaches for skewed bridges

In some literature ([6] and [32] for instance), the support width is kept constant even when skew increases. This means that for certain chosen dimensions, regardless of the skew angle, the bridge surface remains the same. This implies that with increasing skew angle, the amount of lanes that will fit on the bridge will decrease (as long as support width is kept constant).

- Skew angle: The parameter that defines the skew of the bridge. As mentioned, this thesis uses the Dutch definition: the skew angle is defined by the acute angle of the enclosed bridge shape, as shown in Figure 1.2. 90 degrees means that the bridge has a rectangular shape. Lower values for the skew angle define a more skewed bridge. The skew angles that are investigated range from 90 degrees to 30 degrees, with a focus on the range from 45 down to 30 degrees (very skewed).
- Bearing spacing: Defines the centre-to-centre distance of the bearing pads
- Bearing positioning: Defines the distance of all bearing pads to the edge of the plate (in global y-direction), and the distance of the first bearing in the obtuse corner to the plate edge (in global x-direction)

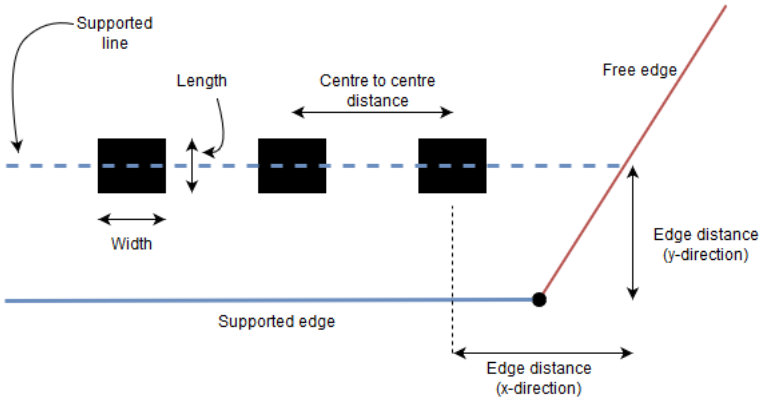

Figure 3.7: Corner definitions

Dependent parameters Dependent variables will also define the bridge model. However, they are set to be dependent on the input parameters.

- Deck height: At first, determined by dividing span length by 16, then rounding up in steps of 50. A thicker bridge has a higher internal lever arm which increases bending moment resistance of the bridge. However, it also increases the self-weight of the deck, which has significant influence on the bridge load.
- Support width: The support width is the width of the support line. This dimension directly depends on the bridge width and the skew angle as shown in equation 3.1
- Free edge length: This variable determines an important dimension of the bridge. However, it is determined by the Span length and the Skew angle:

$$\text{Free edge length} = \frac{\text{Span Length}}{sin(\text{Skew angle})} \tag{3.2}$$

- Number of supports: The amount of bearing pads depends on the width of the support line and the centre-to-centre distance of the pads, which is a predefined value.

Other code related demands:

- RWS bridges are to be treated as consequence class 3 bridges, unless specified differently in the contract.

- NEN-EN 1992-1-1 (Design of concrete structures - General rules [25]) states that when considering shear force in a horizontal element (bridge deck in this case) near a support, a reduction on the shear force can be applied. The idea behind this reduction is that (a part of) the shear force is transferred directly to the supports and thus does not require any additional shear reinforcement. It is however decided to not apply this rule.

3.4 Loads

3.4.1 Dead loads

Manual calculation of the dead loads below is done using a gravitational acceleration of $g = 10m/s^2$; this value is used only in determination of the dead loads from asphalt and the edge structure, which are added manually into the model. This value for g leads to concrete self-weight of 25 kN/m^3. SCIA itself uses 9.81 m/s^2 when calculating dead load of the deck from concrete, which leads to concrete self-weight of 24.5 kN/m^3. [1]

There are three different dead loads working on the bridge:

- Concrete dead load: determined by thickness of the bridge deck multiplied by the self-weight of concrete (Automatically added by SCIA):

$$24.5\ kN/m^3$$

- Asphalt dead load: determined by thickness of cover layer (140mm, from ROK) multiplied by the self-weight of asphalt:

$$23\ kN/m^3 * 0.14\ m = 3.22\ kN/m^2$$

- Weight of the edge structure: (see Figure 3.4)
  - Traffic barrier:

$$1\ kN/m$$

  - Handrail:

$$0.5\ kN/m$$

  - Concrete edge structure (used for anchoring the barrier and handrail):

$$0.5\ m^3/m * 25\ kN/m^3 = 12.5\ kN/m$$

  - Total, working on the free edge of the bridge:

$$14\ kN/m$$

Table 3.1: Load Model 1 loads, from [23]

Location	Tandem system *TS*	*UDL* system
	Axle loads Q_{ik} (kN)	q_{ik} (or q_{ik}) (kN/m^2)
Lane Number 1	300	9
Lane Number 2	200	2,5
Lane Number 3	100	2,5
Other lanes	0	2,5
Remaining area (q_{rk})	0	2,5

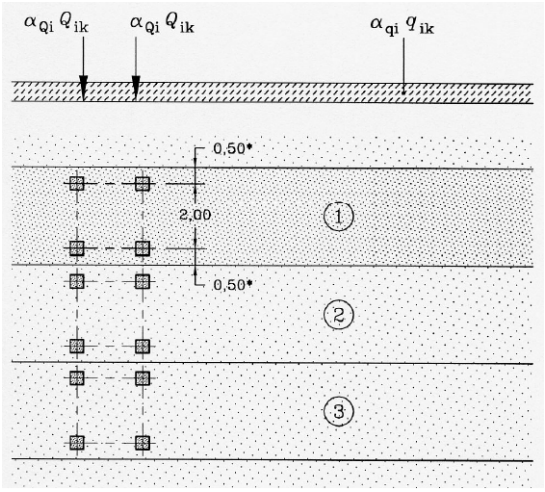

Figure 3.8: Side- and topview of Load Model 1 load configuration, from [23]. Centre-to-centre distance between wheels in lane-direction is 1.2 m

3.4.2 Live loads

Live loads on the skewed slab bridge are determined by Load Model 1 from NEN-EN 1991-2 (Traffic loads on bridges [23]). It consists of Tandem systems (TS) and uniformly distributed load (UDL) systems. An overview of the TS and UDLs, as well as their configuration is given below:

The Dutch annex states that for the heaviest loaded (cargo) lane, the correction factor should be taken as $\alpha_{q1} = 1.15$. For the other lanes, the correction factor is dependent on the total amount of theoretical lanes: $\alpha_{q2} = 1.0$ in case of 2 lanes and $\alpha_{q2..n} = 1.4$ in case 3 or more theoretical lanes are present. However, the increase in correction factor will lead to a bump in results in the transition from 2 to 3 lanes. Therefore, it is decided to keep this factor constant, regardless of the amount of theoretical lanes: $\alpha_{q2..n} = 1.0$. The configuration of the LM1 load also depends on the amount of lanes that are applied. Determination of the number of lanes and their width is found in Figure 3.2. The configuration of lanes for a certain bridge should be applied in such a way that for every verification separately, the most unfavorable situations is checked.

[1]The value of 25 kN/m^3 is actually the correct one (according to Eurocode 1 [33]), but this difference was discovered later on in the process.

Table 3.2: Distribution of road into theoretical lanes, from [23]

Carriageway width w	Number of notional lanes	Width of a notional lane w_l	Width of the remaining area
$w < 5{,}4$ m	$n_l = 1$	3 m	w - 3 m
5,4 m $\leq w < 6$ m	$n_l = 2$	$\frac{w}{2}$	0
6 m $\leq w$	$n_l = Int\left(\frac{w}{3}\right)$	3 m	$w - 3 \times n_l$
NOTE For example, for a carriageway width equal to 11m, $n_l = Int\left(\frac{w}{3}\right) = 3$, and the width of the remaining area is 11 - 3×3 = 2m.			

3.4.3 Thermal load

Thermal loads can be seen as imposed deformations. A change in temperature causes a structure to deform. As long as a structure is allowed to deform freely, imposed deformations will not lead to stresses in the structure. The thermal loading on a structure usually consists of three components:

- Constant temperature difference
- Linear temperature difference
- Non-linear temperature difference (eigentemperatures)

The NEN-EN 1991-5 (Thermal actions [21]) offers two ways to take the vertical thermal gradient on the bridge deck into account:

1. By calculating and using an equivalent linear temperature-gradient over the deck height
2. By calculating and using a non-linear temperature over the deck height

Approach 2 is probably a more accurate one. However, not all FEM-software is able to incorporate a non-linear gradient over the height of an element. The software package SCIA Engineer 18.0, used in this thesis, also has this limitation. Therefore, the non-linear temperature gradient over the deck height calculated in approach 2 is translated into a linear gradient over the height. This leads to two cases: one for cooling of the deck, and one for heating.

An imposed deformation with a linear gradient over the deck height would cause a plate element to bend. If this bending is allowed freely (without any constraints), no stresses would arise from this. However, as bending is prevented by self-weight of the bridge deck, stresses will arise. The greatest effect from this is a load due to prevented bending on the outer bearing pad(s) The linear gradient is therefore incorporated in the model. Its values depend on the total deck height, thickness of the cover layer (asphalt) and temperature conditions at location according to the national (Dutch) annex.

Example values in case the deck height is 900 mm thick: for heating of the deck during summer, the total gradient over the deck height is +8.2 degrees:

- Top of the deck: +6.0 degrees
- Bottom of the deck: -2.2 degrees

Cooling during winter time leads to a gradient of -4.1 degrees over deck height, consisting of:

- Top of the deck: -3.0 degrees
- Bottom of the deck: +1.1 degrees

3.4.4 Other loads

Normally, other loads such as wind loads and impact loading are taken into account. However, the main concern of this thesis is the plate behavior of the bridge deck. Since the impact- and wind loading hardly influence this behavior, they are not taken into account.

Additionally, the ROK describes that in cases of emergency, the heaviest LM1 tandem system could be placed on the very edge of the bridge, regardless of any barriers. However, this emergency loading is also not taken into account. The same goes for fatigue; it is not considered here.

3.5 Load combinations

Load combinations are calculated for the Serviceability Limit State (SLS), in which deformations and crack width criterion are governing, and for the Ultimate Limit State (ULS), in which the maximum bending moments and shear forces are checked with the cross-section capacity.

According to Table NB.13 - A2.4(B) from [20], the load combinations for the ULS to be considered for traffic loads on structures of consequence class 3 (all bridges that belong to national infrastructure) are:

- 6.10a - gr1a: $1.4 * G_k + (\psi_0 = 0.8) * 1.5 * Q_k$
- 6.10b - gr1a: $1.25 * G_k + 1.5 * Q_k$

According to table A2.1 in the NEN-EN 1990 (Basis of structural design [19]), thermal loads do not need to be considered in ULS checks.

The (frequent) load combinations for the SLS to be considered are:

- Traffic: $1.0 * G_k + 0.8 * Q_{traffic} + 0.3 * Q_{Thermal}$
- Temperature: $1.0 * G_k + 0.4 * Q_{traffic} + 0.8 * Q_{Thermal}$

3.6 Finite Element Template Model

This section will elaborate on the Finite Element Template Model, used for the parametric bridge tool. The model is created in a software package called SCIA Engineer 18, widely used by engineers in the industry. Within the SCIA model, all relations are defined in a parametric way. This means that if the value of a parameter is changed, all properties linked to that parameter are automatically updated to the new value. For instance, if the bridge width is increased, additional bearing pads will be added automatically; if the bridge geometry is altered, all loads will automatically be placed at the new correct position, with their correct value. Calculations for the bearing stiffness and the area over which the wheel load spreads, which can be found below, are examples. Within the template model, their properties are also linked to parameters so that they can be changed easily.

The FEM template consists of different parts, which are treated below:

3.6.1 Bridge Deck

Main part of the model is the bridge deck. The bridge deck is modelled as a 2D plate-element, of which the four corner points are defined. This 2D element can represent a 3D bridge deck by defining the thickness of the deck. The mesh size is set equal to half of the thickness, in the first case this is 450 mm. The effect of the mesh size is studied in section 4.3. The material of the deck is defined as being concrete only, so without the reinforcement. Since only linear elastic analysis is considered, stiffness of the deck is the most important parameter. The concrete class used in the model is C35/45, with an E-modulus of 34000 N/mm^2. The model is mainly used to determine governing loads and to check the deformations. Checks in SLS (crack width criterion) and ULS

(bending moment capacity, shear force capacity) will be performed later on, once the reinforcement in the cross-section is also defined.

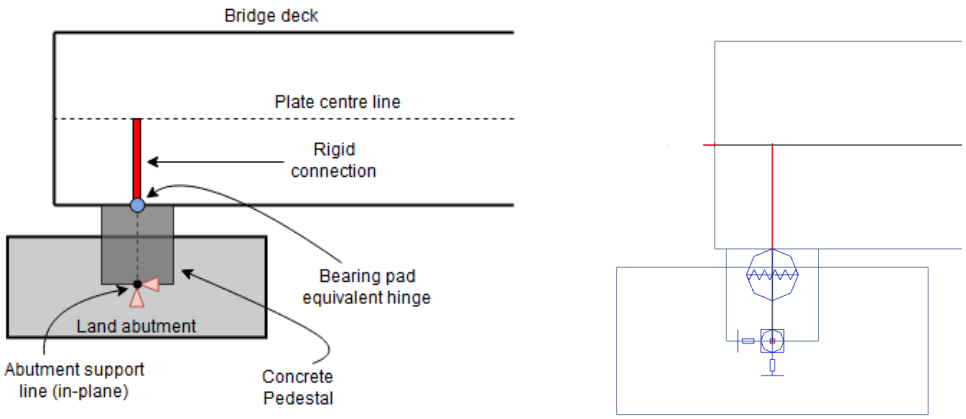

(a) Support modelling scheme

(b) Image of the support from the SCIA model

Figure 3.9: Modelling of the support structure

3.6.2 Supports and foundation

As for any boundary conditions in a structure, the supports and the foundation will influence the force distribution in the structure. The bridge deck in the model will be supported by discrete bearing pads. SCIA does not offer a direct manner to model such bearing pads. However, it does offer the option to define a hinge at the end of a 1D bar element. In this hinge, both the rotational and translational stiffness in and around all three axis can be defined. By calculating an equivalent point stiffness for the translations, the hinges will represent the bearing pads. The hinge is connected with the plate (bridge deck) by using a rigid connection. This way, the point of rotation is placed at the bottom of the plate, where the bridge deck connects with the bearing pads. The 1D bar on which the hinge is connected, represents the central axis of a concrete pedestal (voetstuk in Dutch). At the bottom of the bearing pad, the 1D element is connected to the central line of the land abutment, which is also modelled by a 1D bar element. The 1D bar representing the abutment is finally connected to an elastic line support (which represents the sheet pile wall) or a rigid line support (no deformation allowed).

Equivalent support stiffness

The value of the stiffness is determined by the dimensions and material properties of the bearing pads. The dimensions are length x width x thickness = 300 x 400 x 80 mm. The bearing pads are usually made out of combined layered elastomeric pads and steel plates. The 80 mm of thickness expresses the thickness of the elastomer only. Thickness of the steel is not taken into account in the calculation as it is about 100 times stiffer than the elastomer.

For the elastomeric material, vertical elastic property is described by a Bulk modulus of $E_b = 2000\ N/mm^2$ (according to [35] and [18]), whereas the shear modulus is taken as $G = 1.0\ N/mm^2$. The vertical equivalent stiffness will represent the vertical compressive stiffness of the bearing pad, which is the most stiff direction. The horizontal equivalent stiffness represents the shear stiffness of the bearing pad in horizontal direction. Calculation of the vertical compressive (global z-direction) stiffness:

$$k_z = \frac{A * E_b}{t} = \frac{300 * 400 * 2000}{80} = 3 * 10^6\ N/mm = 3000\ MN/m \tag{3.3}$$

Calculation of the horizontal shear stiffness (global x- and y-direction):

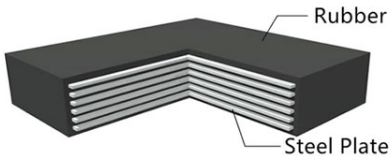

Figure 3.10: Laminated steel elastomeric bearing pad, from [34]

$$k_x = k_y = \frac{A * G}{t} = \frac{300 * 400 * 1}{80} = 1500\ N/mm = 1.5\ MN/m \tag{3.4}$$

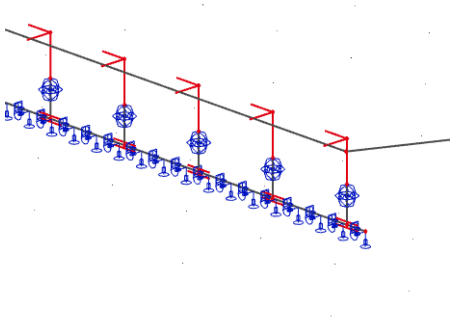

Figure 3.11: The support line showing 5 modelled bearing pads

Land abutment properties

The land abutment is a concrete beam on which the bearing pads rest. Its function is to spread the loads from the bearing pads towards the foundation. The land abutment itself is usually founded on concrete or steel foundation piles (shallow founded abutment) or on a steel sheet pile wall (deeply founded abutment). As mentioned in the scope, the land abutment in the model is assumed to be a deeply founded abutment on a sheet pile wall.

In the model, the support will be modelled as a line support. The support stiffness of this line support is set to be equivalent to that of a sheet pile wall, which in the Netherlands is usually taken around 100 MN/m.

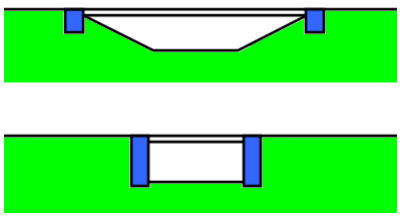

Figure 3.12: shallow founded abutment (top) and deeply founded abutment (bottom), from [36]

It now becomes clear that the vertical stiffness of the bearing pads is much higher than the foundation stiffness of the abutment beam. This foundation stiffness should therefore not be neglected when the aim of the model is to approach reality. However, if only the influence of the bearing pad

configuration (edge distance and centre-to-centre distance) is to be studied, the foundation stiffness can be set infinitely high.

As mentioned earlier, the abutment beam itself is modelled as a 1D beam with a certain cross-section. This cross-section can either be a realistic representation of a concrete bar which can deform due to bending and shear (for a more realistic spreading of bearing loads to foundation), or a rigid bar that can only be displaced as a whole.

Load input

In the NEN-EN 1991-2:2003 (Traffic loads on bridges [23]), it is stated that when performing local checks, the concentrated wheel loads should be spread horizontally up to the vertical centre line of the concrete. The wheel surface area of LM1 on surface level is assumed to be 0.4 x 0.4 meters. Spreading towards the centre line of the deck is assumed under a 1 to 1 angle (45 degrees with horizontal). Although thickness of the cover layer is usually at least 140 mm, only 100 mm is taken into account when calculating the load surface. In case the deck height is 0.9 m, the load surface at centre line becomes:

$$\begin{aligned} \text{Load surface} &= \left(\text{wheel length } ① + 2 * \text{toplayer height } ② + 2 * \frac{\text{deck height } ③}{2}\right)^2 \\ &= \left(0.4 + 2 * 0.1 + 2 * \frac{0.9}{2}\right)^2 = 1.5^2 = 2.25\ m^2 \end{aligned} \tag{3.5}$$

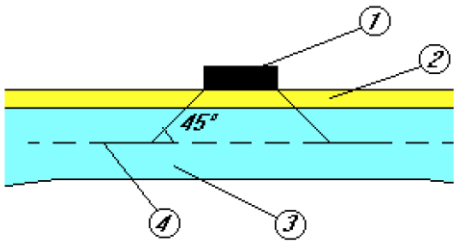

Key
1 Wheel contact pressure
2 Pavement
3 Concrete slab
4 Middle surface of concrete slab

Figure 3.13: Distribution of concentrated load over height of concrete slab, from [23]

Once the load surface is known, the load value of the tandem systems can be determined (assuming that deck height is still 0.9 m):

$$\begin{aligned} TS1 &= \frac{300 * 0.5}{2.25} = 66.67\ kN/m^2 \\ TS2 &= \frac{200 * 0.5}{2.25} = 44.44\ kN/m^2 \\ TS3 &= \frac{100 * 0.5}{2.25} = 22.22\ kN/m^2 \end{aligned} \tag{3.6}$$

The tandem systems and uniformly distributed loads from LM1 are placed on theoretical lanes. The amount of theoretical lanes and their width depends on the width of the total driveway, as mentioned before. Configuration of the TS and UDLs should be chosen in such a way that the

most unfavorable situation is checked. For most geometric bridge situations, this is usually done by placing lane 1 (with highest loads) near the edge, and the less loaded lanes away from the edge (edge-orientated configuration). For each lane active in the model, the respective tandem systems is placed over the bridge span with an increment of $\frac{1}{10}$ of the lane, so that 10 different load positions for the TS are tested. An alternative is to aim for placing the heaviest lanes in the centre of the bridge (centre-orientated configuration). This alternative is also tested (section 4.6) to see if for any geometry, this configuration leads to higher loads.

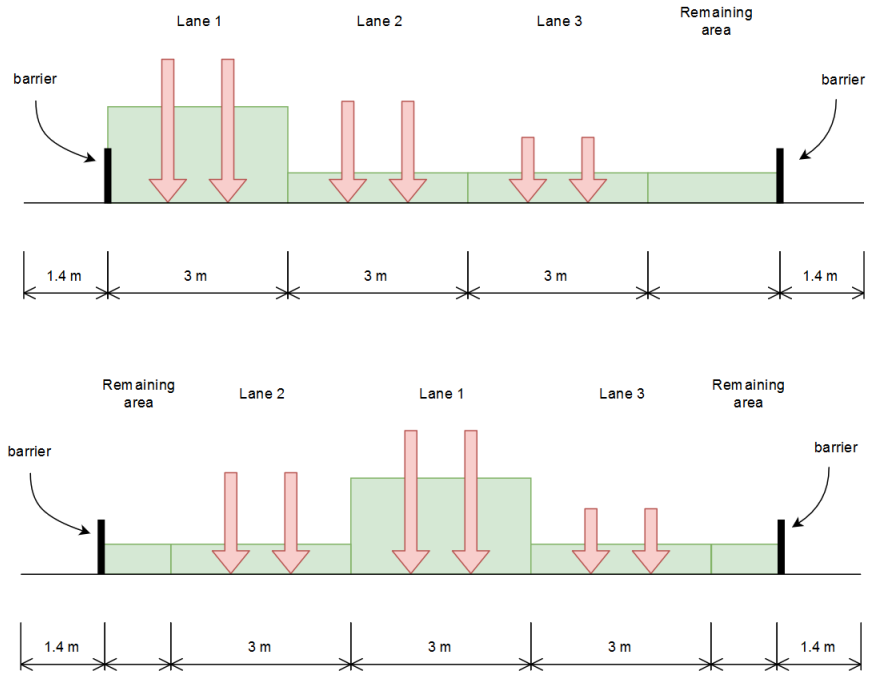

Figure 3.14: Two different load configurations: the edge-orientated (top) and centre-orientated (bottom) configuration

Load combinations

The load combinations, as stated in section 3.5 are entered into the FEM model. The software automatically generates combinations of the most governing loads. This means that for each theoretical lane, although the wheel loads are placed at 10 different locations on the lane, only the most governing one is used in the load combinations.

3.7 Model validation

Before using the model, it will be validated to make sure that it produces sufficiently accurate results which are acceptable and close to expected values or values found in literature.

3.7.1 CUR validation by support stiffness

In the CUR report 58 [7], the effect of the bearing stiffness is investigated. Results from the model and the CUR report are compared to see if they show sufficient resemblance. Investigation is done for a plate of $\alpha = 45°$ with an aspect ratio of $b : l = 1$ (see Figure 3.15), which is equivalent to $W : L = 1$, because:

$$b = \frac{W}{\sin\alpha} \; ; \; l = \frac{L}{\sin\alpha} \tag{3.7}$$

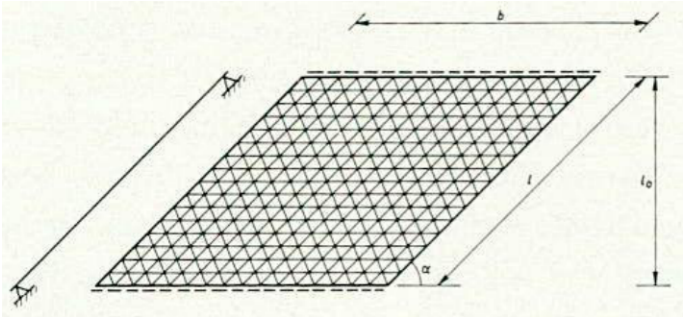

Figure 3.15: Skewed slab geometry as defined in CUR report 58 [7]

First, the total support reaction over one support line is defined as the dead load q working on half the plate:

$$R = \frac{1}{2}qbl \tag{3.8}$$

Plate stiffness K is defined as $Eh^3/12$, under the assumption that Poisson's ratio is zero. Next, the deflection w is expressed in terms of R and K:

$$w = \frac{5}{192}\frac{Rl^3}{Kb} \tag{3.9}$$

The relation between the support reaction R and the mid-span plate deflection w is shown to be of the order of Ebh^3/l^3. Finally, the total support stiffness (over one support line) C_v is defined as the load required to compress all supports (in one support line) over a unit length, and a factor f is introduced for the relation between plate stiffness K and C_v:

$$f = \frac{1}{C_v}\frac{Ebh^3}{l^3} \Rightarrow C_v = \frac{1}{f}\frac{Ebh^3}{l^3} \tag{3.10}$$

This relation means that $f = 0$ represents a rigid support ($C_v = \infty$), whereas higher values represent more elastic supports. The report mentions that $f = 0.02$ is a realistic value for uncracked reinforced plates, which are relatively stiff and the supports therefore relatively elastic. Individual support stiffness $C_{v,i}$ is calculated by dividing C_v by the amounts of supports, which is denoted as $n + 1$ (b/n defines the bearing centre-to-centre distance).

The CUR report shows normalized support reaction distributions for different values of f and different values of n. In Figure 3.16, the CUR results for $f = 0.02$ and $n = 8$ are compared with results from the model. In the model, the abutment beam and foundation are set as rigid, in order to only investigate support influence. The CUR did not give exact values for the normalized support reactions, so values have been estimated based on a figure provided. Additionally, the height of the plate element (in relation to plate dimensions b and l) are not provided in the CUR report, so they have been estimated. It can be seen that results from the model show great resemblance with the CUR results.

Next, a comparison is made for rigid supports ($f = 0$), where results from the CUR report are compared with model results. Figure 3.17 shows comparison of those results. The model with the first estimate of the plate height (same height used as above for $f = 0.02$) already seemed reasonably accurate, except for the first two supports. In the CUR report, the first support shows a very high peak, whereas the second support reaction is negative thus indicating tension. As a second guess, the plate height was decreased in order to obtain this negative value. In the figure, it can be seen that the grey columns (second guess) already approach the orange columns (CUR values) much better than the blue columns (first estimate).

Apart from the relation between the plate height its dimensions b and l, which is not defined in the report, the results from the model in terms of support reaction distribution have shown to be

reasonably accurate. It is therefore concluded that the way the supports are modeled as shown in Figure 3.9 is correct.

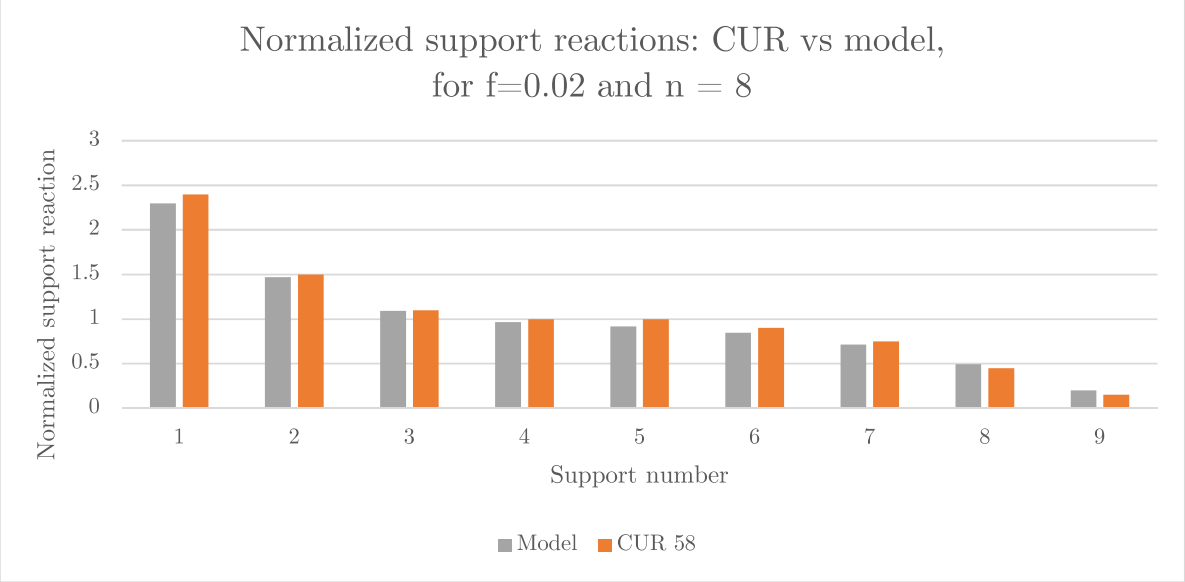

Figure 3.16: Comparison of support reaction distribution between results obtained through the parametric tool and the CUR 58 report ([7])

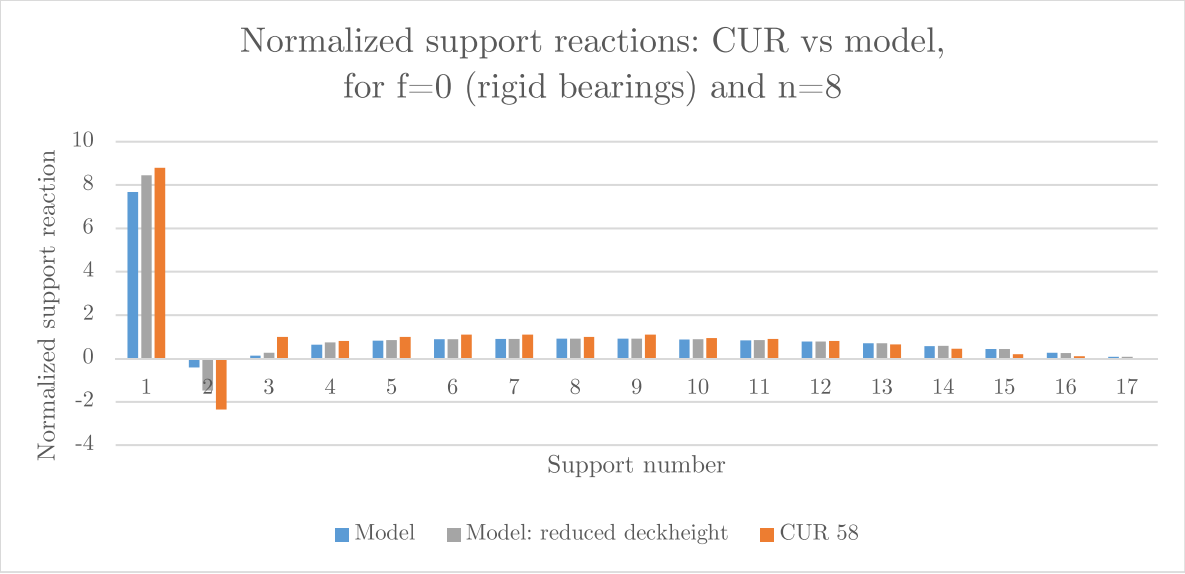

Figure 3.17: Comparison of support reaction distribution, for rigid supports, between results obtained through the parametric tool and the CUR 58 report ([7])

3.7.2 Average support deflection due to self-weight

For validation, the vertical displacement of the bridge deck at the supports is checked. As a rule of thumb, this displacement should not be larger than 1 mm. A bridge with the following properties is checked:

- Skew angle = 90° (rectangular bridge)
- Span length = 13.7 m ⇒ Total bridge length = 14.2 m (due to bearing edge distance of $2 * 0.25\ m$)
- Bridge width = 14.5 m
- Deck height = 0.9 m
- Concrete self-weight = 24.5 $kN/m^3 = 24.5 \times 10^3\ N/m^3$
- Bearing ctc-distance = 1 m ⇒ Number of supports = 15 (on each support line)
- Bearing vertical stiffness = $3 \times 10^9\ N/m$
- Foundation stiffness set as rigid

With this information, the average vertical deflection (displacement of bearing pad at bottom minus displacement at top) of the supports can be calculated:

$$\text{Average deflection} = \frac{\text{Length} * \text{Width} * \text{Height} * \text{Concrete Weight}}{2 * \text{Number of supports} * \text{Vertical support stiffness}} \tag{3.11}$$

$$\Delta u_{z,DL,avg} = \frac{14.2 * 14.5 * 0.9 * 24.5 \times 10^3}{2 * 15 * 3 \times 10^9} = 5.05 \times 10^{-5}\ m = 0.0505\ mm$$

The calculated value for the average vertical deflection of the supports is well below the rule-of-thumb maximum of 1 mm. In reality, the centre-to-center distance will be increased (less supports are required) which also means that the average deflection will increase. Nonetheless, the deflection will remain well below the 1 mm.

Next, the bridge as described above is created with the bridge model tool, in order to check if the vertical deflections found in the model are in agreement with the calculated values. The first value found for the average deflection from the model is 0.1 mm, which is about twice as much as expected. However, it seems that this is the result of rounding, since the displacements are given in millimeters with only one decimal. In order to obtain a more detailed result (and to allow for more even deflection of bearings), stiffness of the bearing pads is divided by 1000, and the linear analysis is run again. The average value found now for the deflection is 50.5 mm. Dividing this value by 1000 (correcting for the adjusted stiffness) gives 0.0505 mm, which is almost exactly the same as the calculated value (very small difference). It can therefore be concluded that the supports in the model behave as expected and that deflection of the supports under dead loads is well within the rule of thumb limit.

3.7.3 Longitudinal bending moment hand calculation

As a last validation, comparison is made between calculated and model values for the longitudinal bending moment m_y. This moment is calculated for concrete self-weight of the deck only (without load factors), and for both ULS load combinations as defined in section 3.5. The following bridge is used for validation:

- Skew angle = 90° (rectangular bridge)
- Span length = 13.7 m
- Bridge width = $3 + 2 * 1.4 = 5.8$ m (1 lane + edge distance)
- Deck height = 0.9 m
- Concrete self-weight = 24.5 kN/m^3

The bending moment at mid-span due to self-weight of the concrete deck can now be calculated by simplifying the deck as a beam on two hinged supports:

$$M_{y,concrete} = \frac{1}{8}ql^2 = \frac{1}{8} * (0.9 * 5.8 * 24.5) * 13.7^2 = 3003.5\ kNm$$
$$\Rightarrow m_{y,concrete} = \frac{3003.5}{5.8} = 517.8\ kNm/m \tag{3.12}$$

Next, in a similar way, the two ULS moments are calculated for combination 6.10a and 6.10b. Following loads (characteristic values, see section 3.4) are used:

$$\text{Total dead load: } Q_{DL} = 0.9 * 5.8 * 24.5 + 3 * 3.22 = 165.7\ kN/m^1$$
$$\text{Traffic UDL: } Q_{UDL} = 3 * 10.35 = 31.1\ kN/m^1 \tag{3.13}$$
$$\text{Traffic TS: } F_{TS} = 2 * 150 = 300\ kN$$

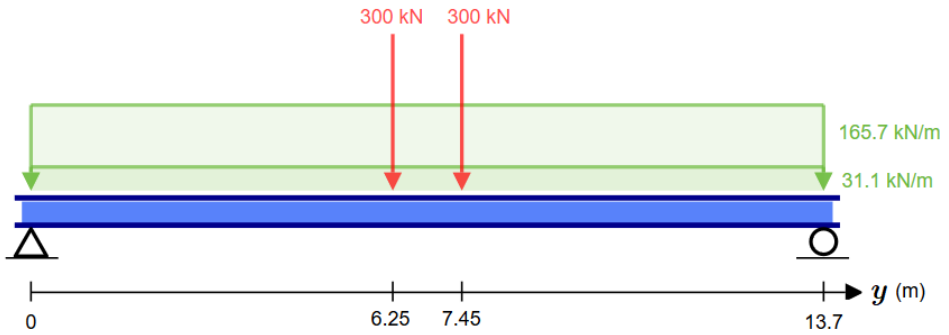

Figure 3.18: Simplified beam model used for bending moment calculation, created with [37]

The point loads F_{TS} are placed at a distance of 6.25 and 7.45 m from the origin, as shown in Figure 3.18. The following formulas are used for calculating the bending moment from combinations 6.10a and 6.10b:

$$m_{y,6.10a} = \left[\frac{1}{8} * (1.4 * Q_{DL} + 1.2 * Q_{UDL}) * L^2 + (1.2 * F_{TS}) * 6.25\right] * \frac{1}{5.8} = 1514.1\ kNm/m$$

$$m_{y,6.10b} = \left[\frac{1}{8} * (1.25 * Q_{DL} + 1.5 * Q_{UDL}) * L^2 + (1.5 * F_{TS}) * 6.25\right] * \frac{1}{5.8} = 1557.6\ kNm/m \tag{3.14}$$

Finally, results obtained with the model are compared with results from this calculation in Figure 3.3. It can be seen that differences between model and calculation for the ULS combinations are a bit bigger than difference for the bending moment of the concrete weight only. Nonetheless, differences are well within a 2% range, proving that the model produces satisfactory results. Small differences found for the ULS combinations might be caused by the fact that in the hand calculation, the tandem system is placed at exactly mid-span (both point loads at 0.6 m from centre), while in the model the governing location for the tandem system in this case is either $0.45l$ or $0.55l$. Nonetheless, results from the model and calculated results show great resemblance, once again indicating that the model works as intended.

Table 3.3: Comparison of different results, obtained through calculation and with the model

	Calculated [kNm/m]	**Model result** [kNm/m]	**Difference** [%]
$m_{concrete}$	517.8	516.6	0.24
$m_{6.10a}$	1477.3	1481.3	-0.27
$m_{6.10b}$	1511.4	1490.0	1.44

4 | Model Results

4.1 Introduction

In this chapter, the results from the parameter study will be shown and briefly discussed. The influence of the following properties and parameters of skewed slab bridged generated by the model, and the results produced are studied:

1. Mesh element size: When using the Finite Element Method, there is always a trade-off between between a smaller element size (usually more accurate) and calculation time. The effect of the mesh element size, especially near the free edge will be investigated. The relation between the mesh element size and the applied plate theory is also subject to modelling.
2. Bearing configuration: (see Figure 3.7 for definitions):
   - Edge distance in span direction
   - Edge distance of first bearing to obtuse corner
   - Centre-to-centre (ctc) distance of bearing pads
   - Support stiffness of bearing pads
3. Abutment- and foundation stiffness:
   - Vertical stiffness of sheet pile wall
   - Bending stiffness of the land abutment beam
4. Load configuration: two different lane configurations will be tested (see Figure 3.14):
   - Heaviest lanes closest to the edge
   - Heaviest lanes in the centre
5. Main geometry parameters:
   - Span Length (global y-direction)
   - Bridge Road Width (reinforcement x-direction)
   - Skew Angle

4.2 Result processing

4.2.1 Coordinate system definition

For determination of the result quantities, the direction of the reinforcement has to be chosen. In CUR report 54 [12], proof is given that laying reinforcement in a perpendicular layout (so 90° between the two directions) leads to a theoretical smaller amount of required reinforcement. In reality, the most applied layout for skewed bridges is the one where reinforcement bars are placed parallel and perpendicular to the free edge of the deck, which is a perpendicular layout. This layout is therefore taken as starting point to be able to compare the results from different models.

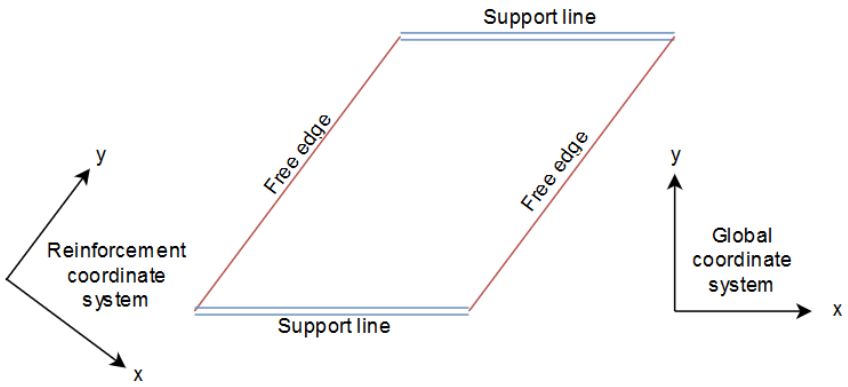

Figure 4.1: Definition of the global- and reinforcement coordinate system

- Global coordinate system: x-axis parallel to the support line, y-axis in span direction
- Reinforcement coordinate system: x-axis perpendicular to the free edge, y-axis parallel to the free edge. This orientation of this system (with respect to the global coordinate system) is dependent on the skew angle.

The most important results from the parameter study to be investigated:

- Support reaction distribution: the distribution of support reactions over the support line, where special attention is paid to the first support in the obtuse corner
- $q_{max\text{-}b}$: Maximum vertical shear force (averaged over certain width) in the obtuse corner. From hereon on, denoted as **'the shear force'.**
- m_{yD+}: Maximum longitudinal hogging moment (tension at the top of the plate), near the obtuse corner. From hereon, denoted as **the longitudinal hogging moment.**
- m_{yD-}: Maximum longitudinal sagging moment (tension at the bottom of the plate), somewhere near half-span (depending on skew). From hereon, denoted as **the longitudinal sagging moment.**
- m_{xD-}: Maximum transverse sagging moment (tension at the bottom of the plate), again somewhere near half-span (depending on skew). From hereon, denoted as **the transverse sagging moment.**

4.2.2 Positive definitions

In SCIA, the vertical z-direction upwards is set as positive. This means that quantities with a plus (+) are in the positive direction or at a positive surface (the top of the bridge deck), whereas quantities with a minus (−) are in the negative direction or at a negative surface (bottom of the bridge deck).

Shear force

In SCIA, the vertical shear force is calculated as two vertical components, acting along a plane in the x-direction (v_x) and a component along a plane in the y-direction (v_y). In order to obtain the vectoral maximized vertical shear force in a location, the modulus of both components is calculated:

$$v_{\bar{x}} = q_{max\text{-}b} = \sqrt{v_x^2 + v_y^2} \tag{4.1}$$

This maximum shear force as calculated now works on a plane $\bar{x}$, that is rotated from the normal x-plane with an angle β:

$$\beta = \frac{v_y}{q_{max\text{-}b}} \tag{4.2}$$

Rotation of the y-plane leads to a plane denoted as $\bar{y}$, with a shear force $v_{\bar{y}}$ that is zero.

Reinforcement design moment

The notation used here (and in SCIA) contains a horizontal and vertical direction component. For instance: m_{yD-} is the reinforcement design moment in the y direction, where the minus (-) sign means that the bottom reinforcement is described, hence the sagging moment.

The reinforcement design moment is a combination of (a) normal bending component(s) and a torsional bending component. This combination is based on a method first proposed by Wood and Armer [38], where angle α between two reinforcement direction is 90° since an orthogonal layout will be used. Expressions can be found in Table 4.1.

Table 4.1: Definition of design moments, from [39]

m_{xD+}	m_{yD+}
(1) $-m_x + \lvert m_{xy}\rvert$ if $m_x \leq m_y$ and $m_y \leq \lvert m_{xy}\rvert$	(1) $-m_y + \lvert m_{xy}\rvert$ if $m_x \leq m_y$ and $m_y \leq \lvert m_{xy}\rvert$
(2) $-m_x + \lvert m_{xy}\rvert$ if $m_x > m_y$ and $m_x \leq \lvert m_{xy}\rvert$	(2) $-m_y + \lvert m_{xy}\rvert$ if $m_x > m_y$ and $m_x \leq \lvert m_{xy}\rvert$
(3) $-m_x + \frac{{m_{xy}}^2}{\lvert m_y\rvert}$ if $m_x \leq m_y$ and $m_y > \lvert m_{xy}\rvert$	(3) 0 if $m_x \leq m_y$ and $m_y > \lvert m_{xy}\rvert$
(4) 0 if $m_x > m_y$ and $m_x > \lvert m_{xy}\rvert$	(4) $-m_y + \frac{{m_{xy}}^2}{\lvert m_x\rvert}$ if $m_x > m_y$ and $m_x > \lvert m_{xy}\rvert$
m_{xD-}	m_{yD-}
(1) $m_x + \lvert m_{xy}\rvert$ if $m_x \leq m_y$ and $m_x \geq -\lvert m_{xy}\rvert$	(1) $m_y + \lvert m_{xy}\rvert$ if $m_x \leq m_y$ and $m_y \geq -\lvert m_{xy}\rvert$
(2) $m_x + \lvert m_{xy}\rvert$ if $m_x > m_y$ and $m_y \geq -\lvert m_{xy}\rvert$	(2) $m_y + \lvert m_{xy}\rvert$ if $m_x > m_y$ and $m_y \geq -\lvert m_{xy}\rvert$
(3) 0 if $m_x \leq m_y$ and $m_x < -\lvert m_{xy}\rvert$	(3) $m_y + \frac{{m_{xy}}^2}{\lvert m_x\rvert}$ if $m_x \leq m_y$ and $m_x < -\lvert m_{xy}\rvert$
(4) $m_x + \frac{{m_{xy}}^2}{\lvert m_y\rvert}$ if $m_x > m_y$ and $m_y < -\lvert m_{xy}\rvert$	(4) 0 if $m_x > m_y$ and $m_y < -\lvert m_{xy}\rvert$

Anytime a bending moment is considered from hereon, it refers to a reinforcement design moment.

4.2.3 Obtuse corner section

The FEM software package used (SCIA) offers the possibility to make sections in a 2D-member. The section is a straight line that can be drawn on a 2D member, which will be the bridge deck represented by a plate element in this case. The section will then represent a cross-section at its location. Once a section has been made, results over this section can easily be displayed. Additionally, SCIA offers an option to average a result quantity over the section. This option will be used to obtain several averaged values.

When using FEM-software to analyze the load distribution within a structure, sections are a powerful tool. Localized effects such as singularities can produce results in a model that do not reflect reality properly. If used properly, sections can therefore be a powerful tool. They have the ability to average peak values, in order to give more realistic results. Using the averaging over a section also suggests a redistribution of a quantity over the sections length. The length of the section is therefore of influence on the obtained results.

In the case of skewed slab bridges, stress- and load concentrations have been observed near the obtuse corner and along the free edge [8]. An appropriate section length should therefore be chosen to obtain resultants over an assumed distribution length. In research conducted at Delft University of Technology [40], concrete slabs were subjected to a point load close to a support line. The reaction force profile was then measured along the width of the slab and compared with results

from a finite element model. The research concluded that peak shear stress found in a finite element model can be distributed over a width of $4 * d$, where d is the effective depth of the longitudinal reinforcement.

In the case of skewed slab bridges, peak shear force will be found along the edge. This means that distribution of this peak shear force can only happen in one direction: inwards (perpendicular to the free edge). For this reason, redistribution over a length of $2 * d$ is assumed. This is also the x-direction in the reinforcement coordinate system and therefore also the direction in which the transverse reinforcement will be placed.

Figure 4.2 shows the obtuse corner for a skewed slab bridge. The diagonal edge is the free edge, the horizontal edge is the support line. It can be seen that there is a shear force peak in the 4 elements that surround the obtuse corner support. This peak will be present almost regardless of the size of these elements. It is therefore decided to apply a mesh refinement around this first support. This way, the elements around the support will be rather small, so that the first section can be made relatively close to this obtuse corner support. If elements and thus the peak were larger, the section would also have to be placed at a bigger distance from the support. Further elaboration on the selected mesh element size is done in Section 4.3.

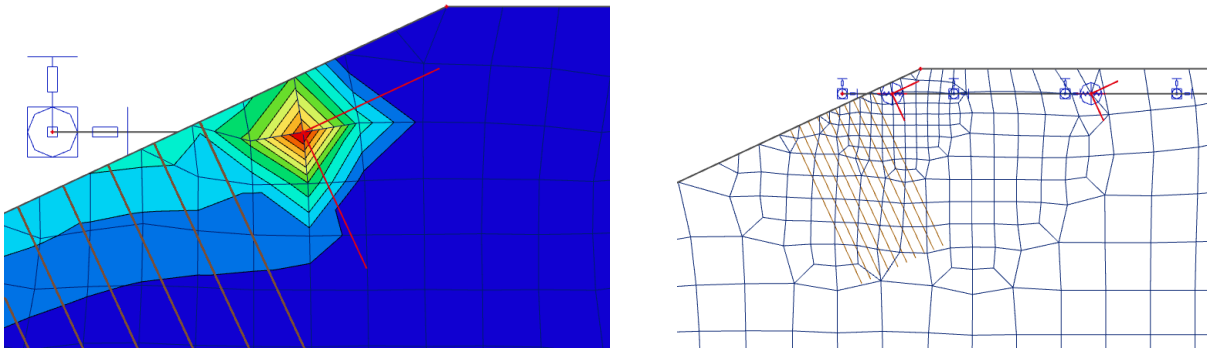

(a) Shear stress around the obtuse corner support, where a peak is visible in the 4 elements around the support

(b) Mesh refinement applied around the obtuse support

Figure 4.2: The obtuse corner in the model: sections are shown as brown lines, supports are at the intersection of two red lines, and a mesh refinement is applied around the obtuse corner support. Notice that there is at least one mesh element between the obtuse corner support and the first section

4.2.4 Deck height and result display

At first, the deck height H is set to be dependent on the (perpendicular) span length L through a ratio of $L/H = 16/1$. This ratio was found in a rather skew bridge design for the Dutch infrastructure project Blankenburgverbinding. Applying this relation means that the deck height is not dependent on the skew angle. This decision is made because the relation between skew angle and deck height is unknown. However, in reality, the skew angle will determine the skew span (length of the free edge), a parameter that will have a significant influence on the required deck height. As stated, the deck height depends on the span length. It is therefore important to notice that results from different span lengths should be compared with caution. From hereon, graphs where different span lengths are displayed will be given different colours, while graphs that are better comparable are given the same colour but with a brightness gradient.

In the following sections, most displayed results will come from Ultimate Limit State (ULS) combinations (see Section 3.5), unless specified otherwise.

A last remark on the result display is the effect of the skew angle. For most graphs (unless

specified otherwise), the span length and the bridge road width (perpendicular road width) are kept constant. The support width however is dependent on the skew angle. Since the total surface of the bridge deck is the product of the span length L and the perpendicular bridge road width W, the bridge surface will vary for different skew angles. A higher skew angle means a smaller bridge and thus a lower total bridge deck surface. This relation should be kept in mind when viewing the results below.

4.3 Mesh element size

4.3.1 Introduction

The size of the elements in the mesh should be chosen with knowledge of the consequence. Generally speaking, the decision for the mesh size is based on the trade-off that exists between model accuracy and calculation time. A very coarse mesh means that a relatively small amount of elements is required in order to model a certain structure. Running the finite element analysis (FEA) will therefore require a relatively small amount of time, meaning that results can be obtained rather quickly. However, in many situations, a coarse mesh model is insufficiently able to describe the 'true behavior' of the structure. Results obtained from the model will thus show great differences with reality.

On the other hand, a model with a very fine mesh will contain a relatively high amount of elements. In general, such a model is able to represent the behavior of the structure with more accuracy. The trade-off is a longer calculation time. For the finite element models generated by the parametric tool, a mesh size of 0.1 m was found to be the smallest measure that still produced a workable model, and will therefore be used as the minimum. Smaller meshes not only lead to longer calculation times, but especially caused very long loading time when generating results, often crashing the software. As with any model, results from a finite element model should be treated with caution. There are many cases where a finer mesh can lead to a big error if proper interpretation is lacked.

4.3.2 Plate theories: Kirchhoff vs Mindlin

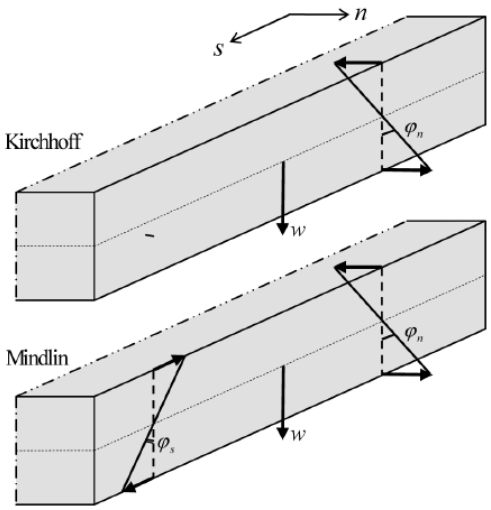

Figure 4.3: Boundary conditions for both plate theories, from [41]

The skewed slab in the finite element model is represented by plate elements. Most FEM software packages offer two alternative theories for plate bending that can be used in the analysis: Mindlin and Kirchhoff [41]. Although their names are subject of debate, their differences are more distinct.

The Kirchhoff theory does not take into account deformations due to shear forces, and is therefore regarded as thin plate theory. Consider a plate edge defined in Figure 4.3. At the free edge of a plate, Kirchhoff can only describe two degrees of freedom, being the vertical displacement w of the plate and the rotation φ_n normal to the edge. The rotation in the plane of the edge is assumed to be fully dependent on the deflection through the relation $\varphi_s = \frac{\partial w}{\partial s}$ (similar to Euler-Bernoulli beam theory). It follows that at the edge, two loads can be applied: vertical load f and moment t_n in the direction of φ_n. While the moment t_n is equal to m_{nn}, the vertical load is described as $f = v_n + \frac{\partial m_{sn}}{\partial s}$. These relations show that if no edge moment is present ($t_n = 0$), the related quantity $m_{nn} = 0$ as well. On the other hand, if vertical edge load is zero, internal quantities v_n and m_{sn} are usually not equal to zero. This means that at a plate edge which is unloaded, a twisting moment and a concentrated shear force will be present. This concentrated shear force, which is often denoted as V_s, is only present in the Kirchhoff theory. When using Kirchhoff theory in FEM software however, the concentrated shear force is not taken into account. Hence, no vertical equilibrium is found using this theory.

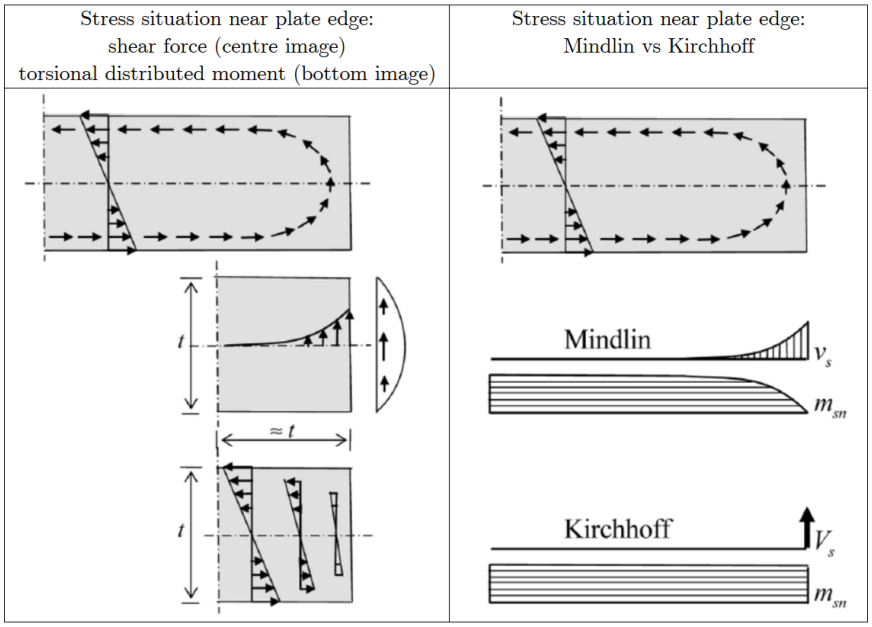

Figure 4.4: Difference in stress state at plate edge between Mindlin and Kirchhoff, from [41]

The theory of Mindlin is set as default in most FEM software. This theory, which is seen as thick plate theory, does incorporate shear deformations by decoupling the vertical deflection w and the rotation φ_s. The cross-section is now no longer assumed to be perpendicular to the (vertical) centre-line of the plate, similar to Timoshenko beam theory. This means that at a plate edge, there are now three independent degrees of freedom (see Figure 4.3): vertical deflection w, rotation φ_s parallel to plate edge and rotation φ_n normal to the plate edge. These three degrees of freedom all have their own related edge load, which are in term equal to internal quantities: vertically distributed force f related to w is equal to internal shear force v_s, distributed torque t_s related to φ_s is equal to internal torsional distributed moment m_{ns} and distributed torque t_n related to φ_n is equal to internal bending moment m_{nn}.

As opposed to the Kirchhoff theory, which shows a concentrated edge shear force V_s, the Mindlin theory is able to compute a distributed shear force v_s over an edge length that is about equal to plate thickness t. This difference is illustrated in Figure 4.4. It shows the flow of shear stress due to a torsional moment applied in a section which is normal to the free edge. For the greater part of the cross-section, excluding the edge zones, it can be observed that the torsional moment caused a linear distribution of the shear stress over the height of the plate, where a zero value is found at $\frac{h}{2}$ (centre-line). Following theory of elasticity, the shear stress in the cross-section has to 'run

around', which happens in the edge zone over a width of about t. Describing the stress state in the edge part, we can see that its direction changes and becomes vertical. Over this edge zone, the vertical component increases non-linearly (almost parabolic), while the horizontal component decreases (also non-linearly). The vertical component is maximum at the very edge, while the horizontal component has become zero here. Integration of the horizontal shear components leads to the torsional moment m_{sn}, whereas integration of the vertical component gives the vertical shear force v_s.

Summarizing and looking at Figure 4.4 again, we see that Mindlin is able to handle the flow of shear stress around the cross-section, while Kirchhoff cannot. Kirchhoff fails to handle the boundary condition $m_{ns} = 0$ and instead keeps it constant, even at the edge zone. The theory determines an integral of the local vertical stress components and creates a concentrated shear force V_s at the very edge. However, as mentioned before, most FEM software does not take this concentrated shear force into account. Considering this, it seems logical that most FEM software prefers Mindlin and sets it as its default plate theory method. However, it should be noted that most FEM software can only calculate the torsional moment m_{sn} in an element in a linear way. This means that, if one wants to describe and display this torsional moment accurately, approximately five elements are required over the edge zone of width t. When less elements are present in the edge zone, the software will not be able to properly display the flow of internal stress in the edge zone.

Some experts [42] still suggest using Kirchhoff theory and adding the concentrated vertical shear force at the edge manually. This way, a rather coarse mesh can be applied, and the user is 'forced' to consciously look and handle the problem. For straightforward problems such as rectangular plates, this might be an option. However, it will prove to be rather labor-intensive for less straightforward problems. Especially in the case of a plate that has no rectangular shape: skewed slabs for instance.

4.3.3 Effect of mesh element size

With this in mind, the question remains with which purpose the model is created. As stated above, an accurate display of the edge situation with Mindlin requires a fine mesh near the edge. This either means that the overall mesh of the model needs refinement, or that (if possible) a mesh refinement should be applied near the edge zone. However, if the goal of the model is mainly to obtain values of the shear force and torsional moment at the edge for reinforcement design, the values will be averaged over a certain width. In this thesis, peak values of the shear stress at the edge can be distributed over a distance of $2 * d$. It is therefore investigated if the mesh element size still influences the averaged shear stress peak.

In order to show the effect of a smaller mesh size, the mesh size is varied. A bridge with the following properties is chosen to display the differences:

- Span length = 13.7 m
- Bridge width = 8.3 m
- Skew Angle = 30°
- Deck height = 0.9 m

The effective depth d is assumed to be 0.85 m. In the obtuse corner near the first support, a section with a length of $2 * d = 1.7\,m$ perpendicular to the free edge is made to investigate the flow of shear force near the edge. This means that the edge zone over which the applied Mindlin theory causes a different stress state is about half the size of the section's length.

Results with Mindlin

Figure 4.5 shows the maximum vertical shear force over the sections for different mesh element sizes, ranging from a size equal to deck height h (0.9 m) to approximately $\frac{1}{8}h$ (0.1 m). As stated before,

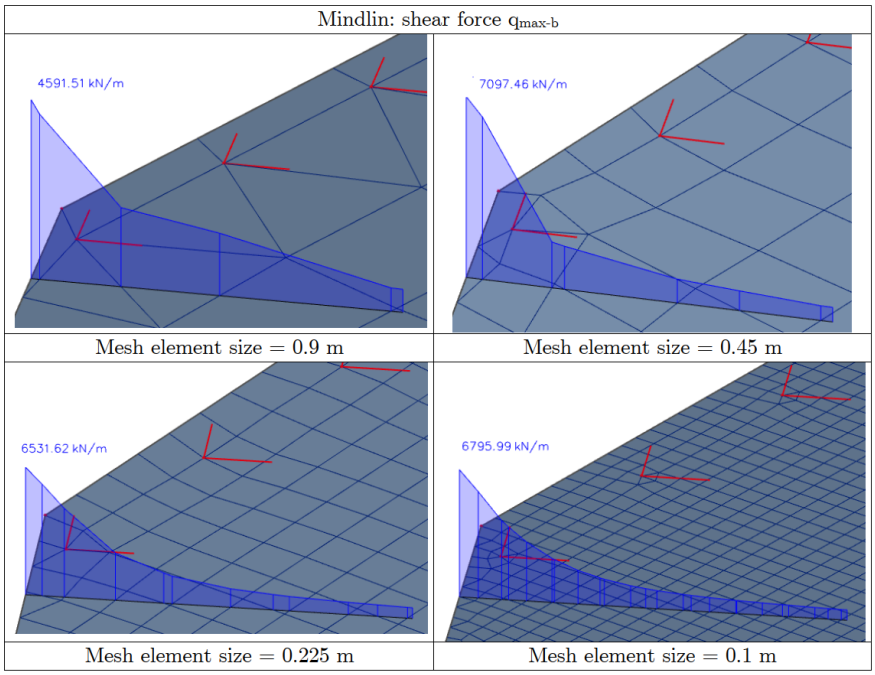

Figure 4.5: Shear force in the obtuse corner for different mesh element sizes

a large number of elements are required for an accurate representation of vertical shear force at the edge zone. This is clearly visible in the figure: the smaller the elements, the more the shear force over the section resembles the (almost parabolic) Mindlin distribution as shown in Figure 4.4. The smaller meshes also show that the right half of the shear force over the section is constant. Because the section is almost twice as wide $(2 * d)$ as the edge zone $(h \approx d)$, the right part lies outside of this edge zone and should be about constant.

Averaged values for the shear force and twisting moment over the section found using Mindlin are given in Table 4.2. Differences between the shear force values obtained for different mesh sizes are relatively small, in the order of 5%. Additionally, if one is to assume that a smaller mesh leads to a more accurate result, then the image that belongs to mesh size $0.9m$ deviates from this assumption (because it seems more accurate than 0.45 and 0.225 values). A mesh even smaller than $0.1m$ (undesired) supports this assumption as it leads to a value below the $1765kN/m$. It could be that small local effects such as element shape and size cause the average value belonging to a mesh size of 0.9 m cause some 'accidental' accuracy.

Similar to the maximum shear force, the twisting moment m_{xy} is also displayed for different mesh sizes in Figure 4.6. The same bridge configuration, section length and mesh variation are applied. Once again, it is clear that for a smaller mesh, the shape of the plot over the section starts to resemble the shape for m_{sn} in Figure 4.4, where only about the left half of the section resembles the edge zone. The right side of the section plot should be about constant because it lies outside the edge zone.

Table 4.2 shows the average twisting moment m_{xy} over the sections for the different mesh sizes. The values in this table seem to make more sense, since they converge towards a certain limit value. Differences between the values are again in the order of 5%.

Results with Kirchhoff

In the same way described above using Mindlin, the effect of applying Kirchhoff is now investigated. Figure 4.7 shows the shear force and twisting moment over the section in the obtuse corner, using Kirchhoff with a fine mesh of 0.01 m. As opposed to Mindlin, the plot for the twisting moment m_{xy} now does not approach zero towards the plate edge, but rather shows a linear distribution. This

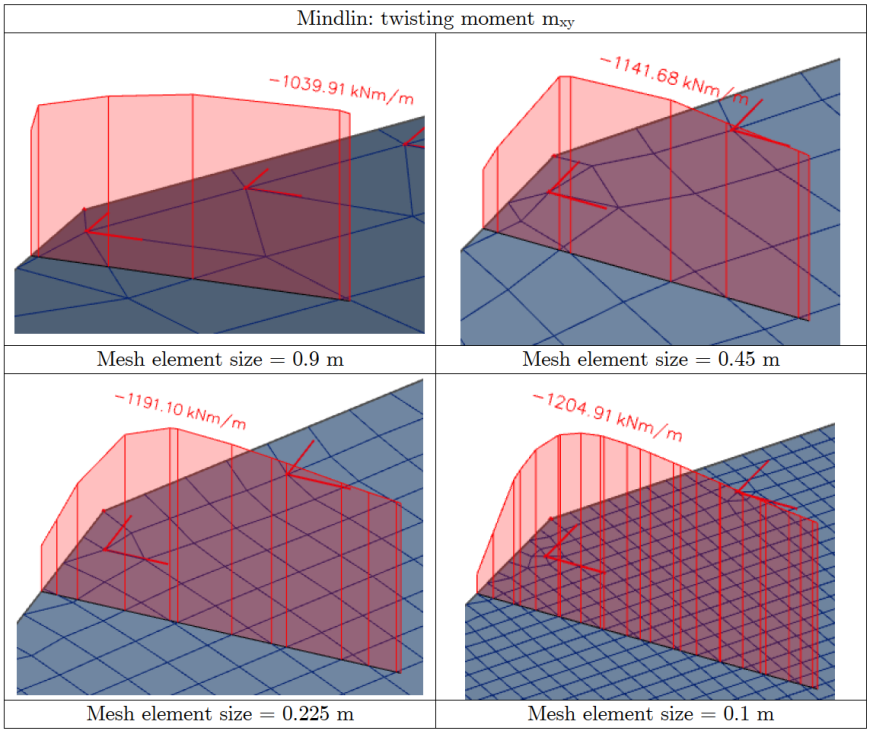

Figure 4.6: Distributed torsional moment in the obtuse corner for different mesh element sizes

Table 4.2: Sectional averaged values for the maximized shear force ($q_{max\text{-}b}$) and twisting moment (m_{xy}) obtained through using the Mindlin and Kirchhoff plate theories for different mesh element sizes

	Mindlin		**Kirchhoff**	
Mesh element size [m]	$q_{max\text{-}b}$ [kN/m]	m_{xy} [kNm/m]	$q_{max\text{-}b}$ [kN/m]	m_{xy} [kNm/m]
0.9	1797	-976	989	-1020
0.45	1851	-1021	1229	-1091
0.225	1803	-1036	1066	-1101
0.1	1765	-1042	1056	-1099

difference can also be seen looking at the sectional average values in Table 4.2 for m_{xy}: the values are slightly higher for Kirchhoff than for Mindlin.

Looking at the shear force distribution in the Kirchhoff plot in Figure 4.7, a difference with Mindlin (4.5) can be observed. Where Mindlin is able to describe the almost parabolic distribution in the edge zone, Kirchhoff is unable to resemble it. The shear force increases near the edge, but does not come close to the distribution found with Mindlin.

Conclusion

Summarizing, comparison of values obtained using Mindlin shows that values for twisting moment m_{xy} are a bit smaller than Kirchhoff because distribution does not tend to zero at the edge. Moreover, it can be seen that the values for vertical shear force $q_{max\text{-}b}$ obtained through Kirchhoff theory are a lot lower than the ones obtained through Mindlin. This difference, explained in 4.3.2, shows why in practice, Mindlin is often the preferred method. From a scientific point of view, application of Kirchhoff and manual processing of shear forces might be the preferred option. However, in reality, applying Mindlin in FEM-software and using sections to obtain averaged values for further

design of structures provides a faster and more practical method. Because this thesis will handle lots of models, Mindlin will be used. A mesh element size of 0.45 m is found to be sufficiently accurate, while producing models that are acceptable in terms of file size and therefore can be handled by the software without getting slow. For this reason, mesh element size of 0.45 m is applied in the models.

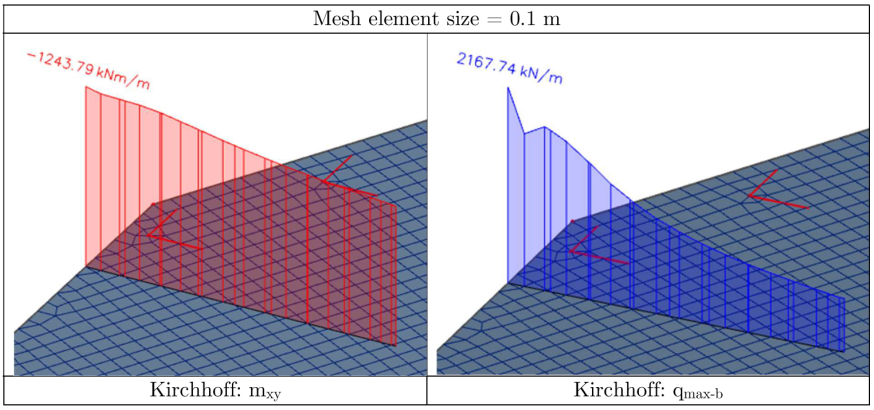

Figure 4.7: Twisting moment m_{xy} and shear force $q_{max\text{-}b}$ display for a fine mesh element size obtained applying Kirchhoff plate-theory

It should be noted that mesh size is not changed for different deck heights (plate thicknesses). The chosen 0.45 m is still smaller than the smallest assumed deck height, and should therefore be sufficiently accurate.

4.4 Bearing Configuration

Three main parameters are considered in the bearing configuration: distance of the first bearing to the plate edge in longitudinal and transverse direction, the centre-to-centre (ctc) spacing of the bearings and finally the global vertical support stiffness. Definition of those parameters can be found in Figure 3.7, where the span direction is denoted as y and the transverse direction with x. These parameters are varied to study their influence on the stress distribution in the plate, as well to check the distribution of the support reactions. For this study, the same bridge is used as in the mesh element size study:

- Span length = 13.7 m
- Bridge width = 8.3 m
- Skew Angle = 30°
- Deck height = 0.9 m

Bridge bearings provide a connection between the superstructure (bridge deck) and the substructure (abutment beam). In the case of assumed simple (hinged) supports, the bearings transfer vertical loads to the substructure while they should not prevent rotation. Moreover, the bearing pads should also prevent any significant displacement in the horizontal plane: the bridge should not be able to 'walk away'. To ensure this, the Eurocode for bearings [18] specifies that a minimum contact pressure of 3 N/mm^2 should be present at the surface between the support and the deck, under permanent loading only. This means that the assumed bearing pads of 300 x 400 mm will require a minimum of 360 kN under permanent load. This criterion is not considered in this thesis.

4.4.1 Bearing edge distances

As a first parameter, edge distance in span direction is varied slightly. This edge distance should be kept to a minimum, because it will create a cantilevering part. Any rotations due to vertical deflection over the span of the bridge, will cause the cantilevering part to move upwards. This results in height differences over the connection / expansion joint which lead to bridge deck degradation and are unpleasant or even dangerous for the traffic. Moreover, an increase of this edge length in span direction will increase total weight of the bridge because its geometry in the span direction is governed by the span length: the distance between the centre of the support lines. However, this additional weight is relatively small and will not significantly impact the bearing structure. This edge distance should therefore be seen as a measure to influence load distribution in the obtuse corner and support reactions.

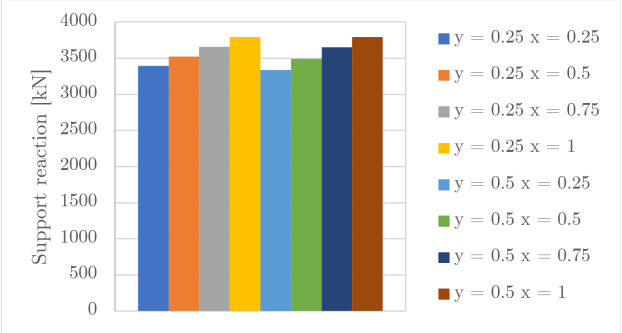

Figure 4.8: Obtuse corner support reaction for different bearing edge distances

Support reactions

First, influence of bearing configuration on the support reactions is checked. Figure 4.8 shows the distribution of the support reactions for different edge distances. Support 1 is the first support in the obtuse corner. Edge distance in span direction (y) is varied between 0.25 and 0.5 m, while edge distance of first support in transverse direction (x) is checked for values of 0.25, 0.5, 0.75 and 1.0 m. Centre to centre (ctc) distance of the bearing pads is set to 1.0 m. The figure shows that a variation of the y-distance has little effect and does not lead to significant changes of the support reactions. However, variation of edge distance in the x-direction leads to increase of the first support reaction. This makes sense because as the first support in the obtuse corner moves away from the plate edge (in transverse direction), it takes up a bigger portion of accumulated shear forces from the obtuse corner. It should be noted that a higher reaction force from support 1 also leads to a more punching shear-like behavior of the bridge deck itself, which is undesired.

Obtuse corner shear force

Next, influence of the edge distances on the shear force in the obtuse corner is investigated. This shear force is once again judged by the average value over a section with a length of $2 * d$ running in perpendicular direction from the free plate edge. The left part of Figure 4.9 shows the value of the shear force for different bearing configurations. The x-axis represents the distance of the first support to the free edge, while the averaged sectional shear force is plotted on the y-axis. The different lines show this relation for different ctc distances and different distances to the support edge in y-direction. The graph shows that for similar configurations, an increase in y-edge distance from 0.25 to 0.5 m leads to a decrease of the obtuse corner shear force. The right part of Figure 4.9 shows a graph similar to the left part, but now the variations in values for different x-edge distances have been left out by displaying the average. As the left part already suggested, the average values for equal y-distance show little difference: the three lines for $y = 0.25$ as well as the three lines for

$y = 0.5$ m can hardly be distinguished. It is however very clear that there is a difference between the lines for $y = 0.25$ and $y = 0.5$ m, which is about 16%. For the included bearing configurations, an increase in y-edge distance from 0.25 m to 0.5 m leads to a significant increase in obtuse corner shear force.

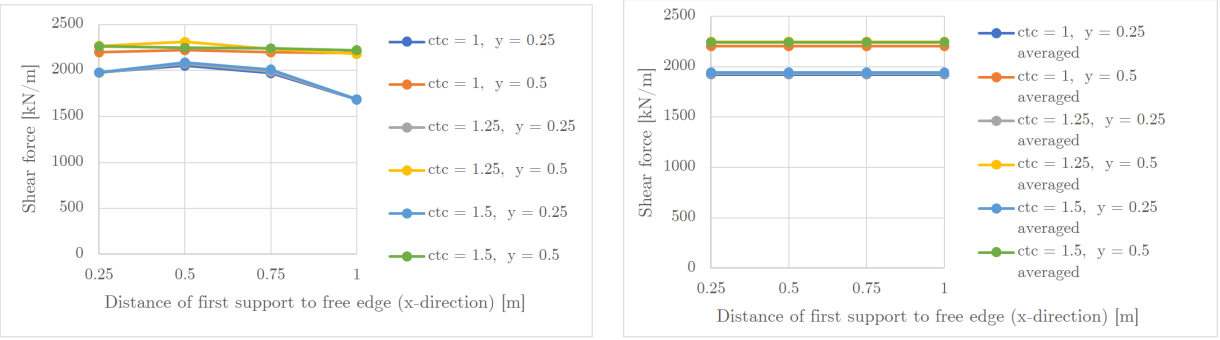

(a) Shear force for different x- and y-directions and centre-to-centre distances

(b) Similar to left graph, but values averaged for different x-distances

Figure 4.9: Bearing configuration versus the averaged sectional shear force in the obtuse corner

Longitudinal sagging moment

Finally, the effect of the bearing configuration on the bending moment in the plate is checked. This is done for the longitudinal sagging moment m_{yD-}, which describes the total bending moment quantity (consisting of bending and twisting moment component, see section 4.2.2) in the main reinforcement direction (which is parallel to the free edge) that needs to be taken up by tensile reinforcement at the bottom of the plate. Figure 4.10 shows this longitudinal sagging moment for different bearing configurations. The horizontal axis depicts the x-edge distance, wheres the different coloured lines display different y-edge- and ctc-distances. Left part of the figure shows the reinforcement moment from zero to maximum value, where the right graph shows a zoomed version of the left graph. The left graph shows that the influence of the bearing configuration on the longitudinal sagging moment is relatively small. However, as visible in the right graph, a clear linear trend is visible: increasing the x-edge distance of the first bearing from 0.25 m to 1.0 m, the sagging moment increases by about 3%.

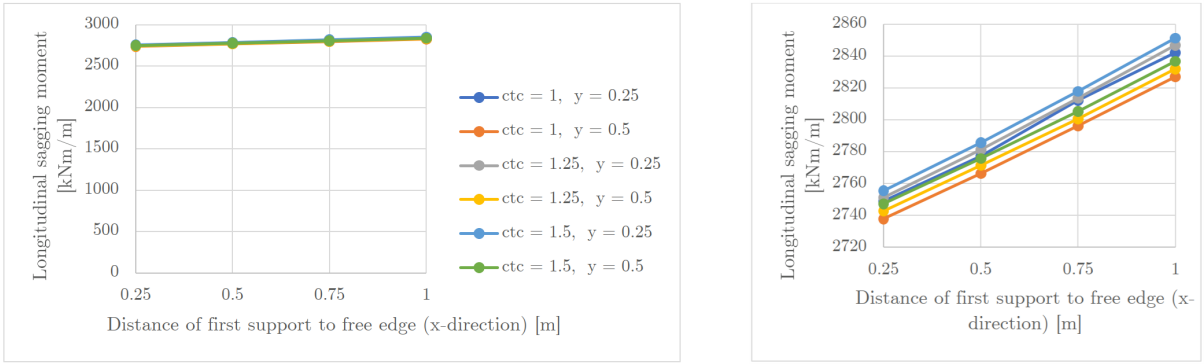

(a) Maximum longitudinal sagging moment for different bearing configurations

(b) Zoomed in representation of the left graph

Figure 4.10: The maximum longitudinal sagging moment m_{yD-} plotted versus the bearing edge distance in global x-direction. Line colors depict different edge distances in y-direction and bearing centre-to-centre distance

4.4.2 Bearing centre to centre distance

An increase in the centre-to-centre (ctc) distance of the bearing pads assures that a smaller number of bearing pads is required to support the total structure. Although this might lead to a cost saving, it also means that the load per bearing pad increases, which can lead to a punching shear-like failure mechanism of the bridge deck. However, in order to prevent displacement of the bridge deck in its horizontal plane, certain minimum contact pressure due to dead load only has to be assured between the bearing pad and the bridge deck. If this requirement leads to concentrated support reactions that are considered too high, the size of the bearing pads can be decreased, together with increasing the number of bearings. This way, the minimum contact pressure is still reached, while creating a better distribution of reaction forces along the support line.

Support reactions

First of all, the ctc-distance is varied for different edge-distance configurations and the changes in support reactions are studied. Figure 4.11 shows that variation of the ctc-distance from 1 to 2 m has the same effect for different edge-distances. Doubling the ctc-distance means that the amount of supports is halved and the average support reaction therefore doubles. However, looking at the Figure 4.11, we see that the first support reaction only increases by about 12% when ctc-distance is doubled from 1 to 2 m. This can be explained by the fact that the first support already takes up a disproportionately large share of the load. After all, a significant portion of the first support reaction comes from an accumulation of shear forces along the free edge towards the obtuse corner. Therefore, the first support reaction should be expected to double upon doubling the ctc-distance.

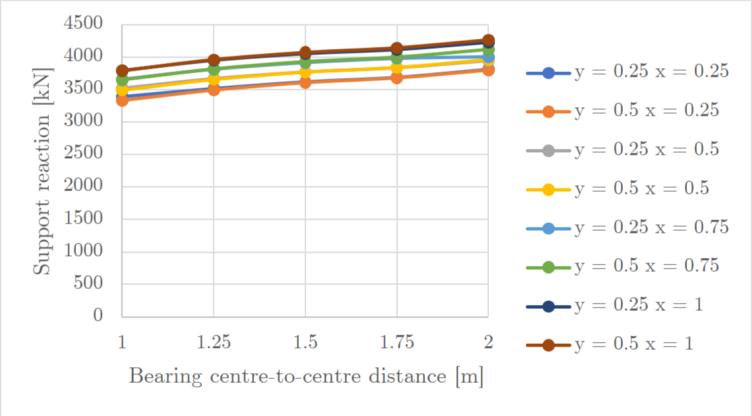

Figure 4.11: Obtuse corner support reaction versus the bearing centre-to-centre distance, for different global x- and y-direction edge distances

Obtuse corner shear force

Secondly, the effect of the ctc-distance on the obtuse corner shear force ($q_{max\text{-}b}$) and longitudinal sagging moment (m_{yD-}) is checked. Figure 4.12 shows both quantities plotted on the vertical axis, whereas the horizontal axes show the bearing ctc-distance. The left graph clearly shows a horizontal line, indicating that no significant changes in the longitudinal sagging moment take place as a result of the variation. This is hardly surprising, because this moment is mainly a function of the bridge geometry, which is not changed. Similarly, the right graph also shows nearly horizontal lines although it must be said that there is a very slight increase of obtuse corner shear force when increasing the bearing ctc-distance.

As stated before, an obtuse corner support reaction that is too high can lead to unwanted effects. A measure that is sometimes applied is adding an additional bearing pad between support 1 and 2, let us name this support 1.5. Figure 4.13 shows two plots of the distribution of support reactions

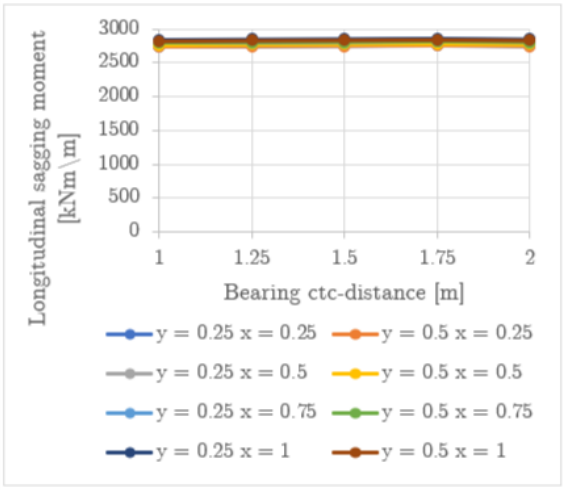

(a) Longitudinal sagging moment versus bearing ctc-distance: hardly any influence

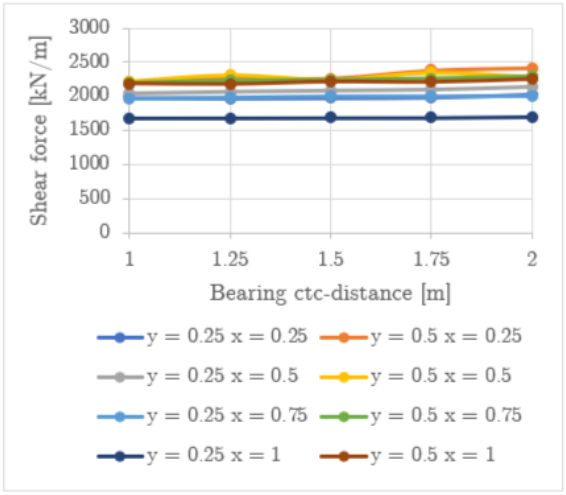

(b) Obtuse corner shear force versus bearing ctc-distance: little influence

Figure 4.12: Variation of the bearing ctc-distance shows little influence on the longitudinal sagging moment and the obtuse corner shear force

for different ctc-distances, where the top graph has an equal distribution of bearing pads, whereas the bottom graph has the aforementioned support 1.5 added. A first look at the graphs shows that both shapes are rather similar: overall support distribution over the support line has not changed in behavior. The value of the first support in the obtuse corner of the graph with support 1.5 is on average about 14% lower compared to the graph without the support 1.5. This shows that adding the support 1.5 is an effective way of reducing support reaction 1.

Like Figure 4.11 already showed, doubling the ctc-distance from 1 to 2 m, does not lead to doubling of the first support reaction. Figure 4.13 shows that an increase of about 100% or more does take place for other supports. The lighter-coloured lines, which depict a higher ctc-distance, show higher support reactions compared to more dark-coloured lines. Some locations show a more than doubled support reaction, others show less relative difference.

Longitudinal hogging moment

The last quantity to be checked is m_{yD+}, the hogging moment in free-edge direction. The bottom of Figure 4.14 shows a plot of this moment in which the concentration around the first obtuse support becomes very clear. Figure 4.14 also shows both components of the bending moment m_x and m_y, as well as the twisting moment m_{xy} for the global- as well as the reinforcement coordinate system (see 4.2.1).

Negative values for m_x, m_y and m_{yD+} indicate tension at the top of the bridge deck (therefore requiring reinforcement). Generally speaking, top reinforcement is only required at a clamped or continuous support, and not around a simple support. However, the plots indicate tension at the top of the bridge deck. The biggest bending moment (peak value of -1919 kNm/m) is found in the top left plot, which shows m_x in the global coordinate system (GCS): a direction parallel to the support line. The bending moment m_y in the reinforcement coordinate system (peak value of -1846 kNm/m) approaches the aforementioned peak of m_x in the GCS. Maximum value of this negative moment is found when the reinforcement axis system is rotated a little more, somewhere between 0° and 30°. This indicates that the plate is sort of clamped around the first obtuse support: due to the load that is 'hanging' on this obtuse support due to high skew (30° in this case) of the bridge, the deck to the left of the obtuse support wants to move upwards since the stiff deck tends to remain straight. However, this upward bending is prevented by the load resting on the supports

next to the obtuse support. These loads on both sides, countered by the obtuse support, generate the negative bending moment which leads to tension in an area above the obtuse support. In other words: due to high skew, a sort of continuous plate exists which mainly rests on the obtuse corner support. Loads on both sides cause the negative moment, which causes tension at the top and therefore requires reinforcement at an area around the obtuse support. The influence of the main geometry parameters on this positive bending moment is investigated later on in section 4.7.

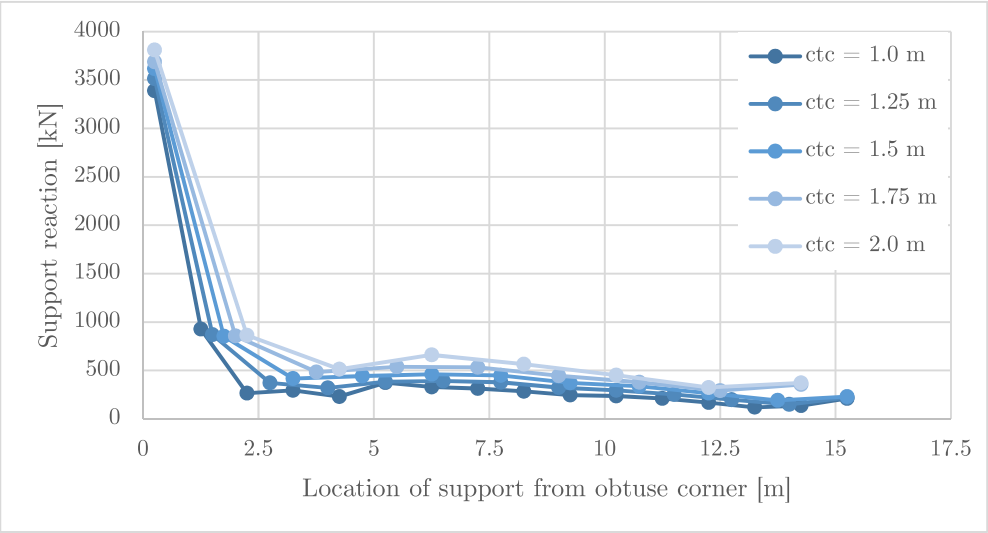

(a) Distribution of support reactions for equal ctc-distances

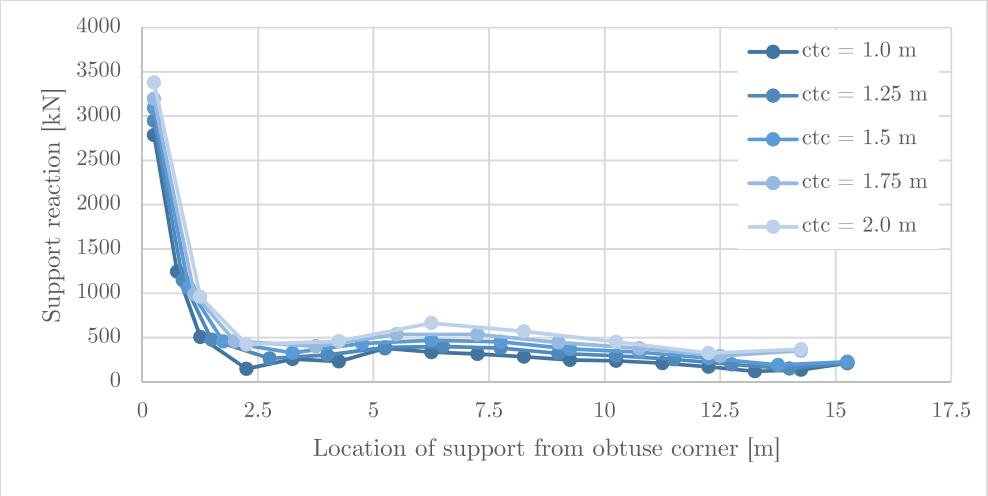

(b) Distribution of support reactions in case an extra bearing pad is added between support 1 and 2

Figure 4.13: Distribution of the support reactions for different bearing centre-to-centre distances

Checking of the relation between the bearing configuration and the longitudinal hogging moment in the obtuse corner is done by once again averaging the moment value over a certain length. The length of this section, perpendicular to direction of the reinforcement, is taken as $2 * d$, which is once again 1700 mm as described in 4.4. Figure 4.15 shows the averaged sectional longitudinal hogging moment for different bearing configurations: the x-axis shows three different ctc-distances, whereas the line colours represent two different edge-distances. The graph shows that neither the edge distance nor the centre-to-centre distance has any significant effect on the longitudinal hogging moment. Figure 4.16 shows that the peak value for the hogging moment is a rather local effect,

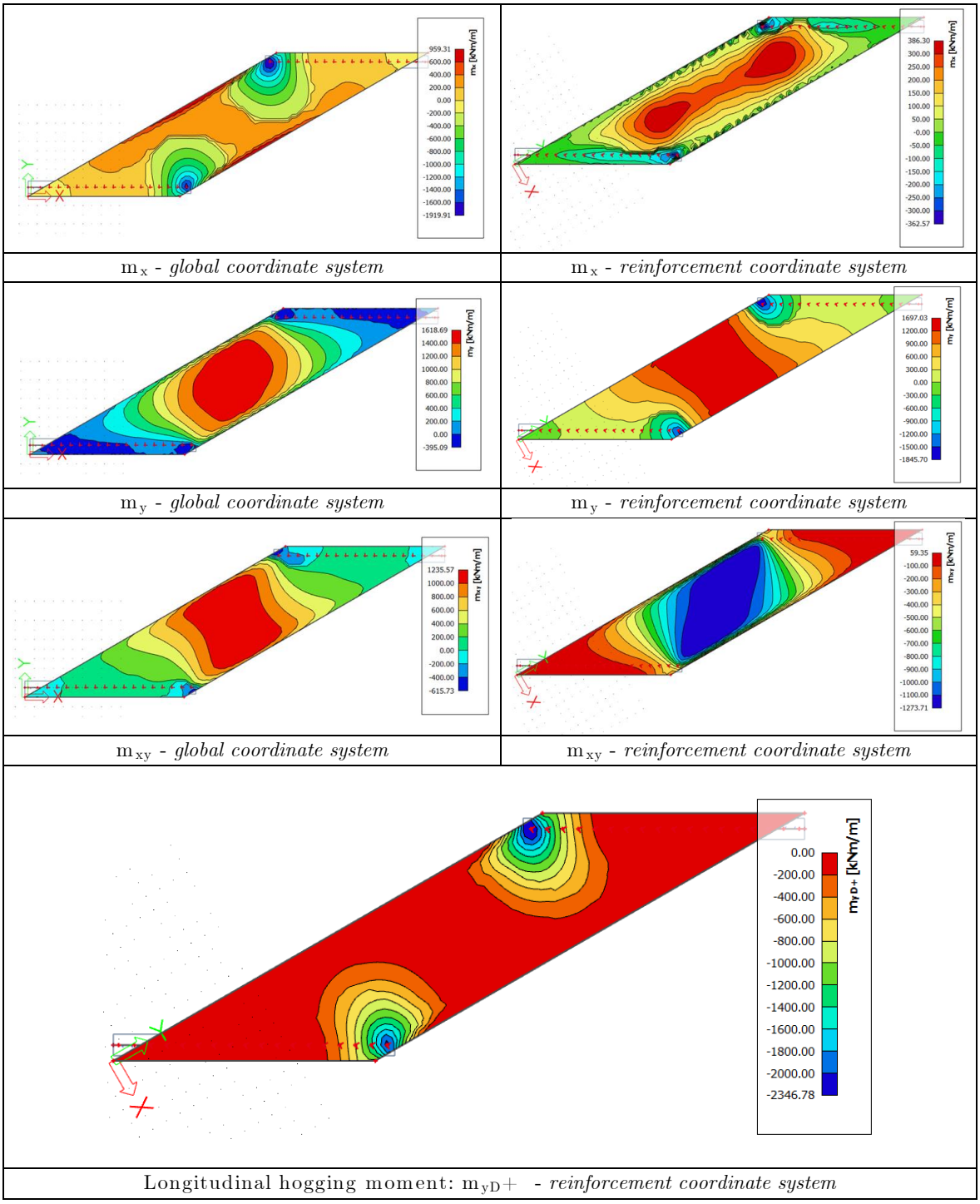

m_x - *global coordinate system*

m_x - *reinforcement coordinate system*

m_y - *global coordinate system*

m_y - *reinforcement coordinate system*

m_{xy} - *global coordinate system*

m_{xy} - *reinforcement coordinate system*

Longitudinal hogging moment: m_{yD+} - *reinforcement coordinate system*

Figure 4.14: Plots of the longitudinal hogging moment m_{yD+} and bending and twisting moment quantities in two different axis systems

concentrated around the obtuse support. It can be seen that the length of the sections are rather large compared to the peak area. This probably explains why Figure 4.15 shows little deviance: differences in the longitudinal hogging moment between different bearing configurations are reduced by averaging over a relatively large area. Moreover, it is probable that this hogging moment is far more dependent on the global geometry of the plate rather than relatively small local differences in bearing configuration.

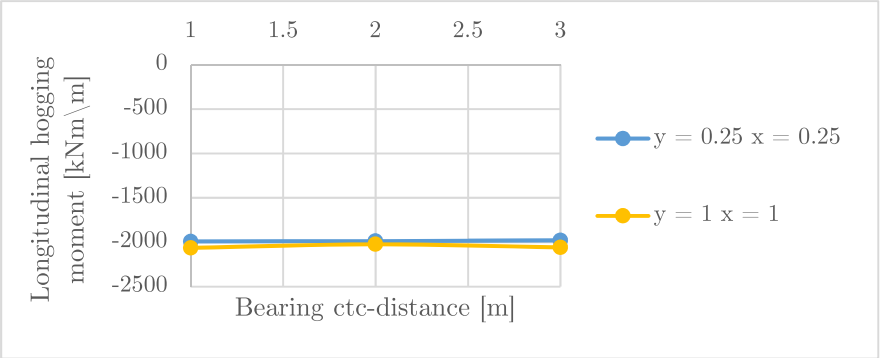

Figure 4.15: The longitudinal hogging moment m_{yD+} for different bearing configurations

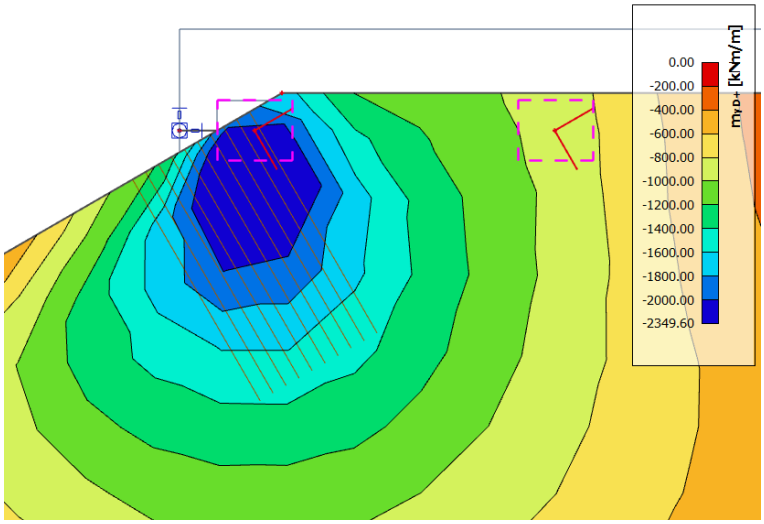

Figure 4.16: Longitudinal hogging moment at the obtuse corner. Note the section length versus the peak value area

4.4.3 Bearing support stiffness

Support reaction distribution

The effect of changing the bearing pad stiffness was investigated in CUR report 58 [7], which showed that more elastic pads lead to better redistribution. The same conclusion can be drawn looking at Figure 4.17: a lower support stiffness leads to a more even distribution. The peak value of the first support drops significantly as the support stiffness is lowered, while second and third support reaction increase a bit. For rigid supports, a small negative value at third support can be observed, which indicates tension. The damping effect of the more elastic supports seems to have most of its effect on the first six supports. Starting from support 7, hardly any difference can be observed.

Other result quantities

The result quantities that are mostly related to the obtuse corner support reaction are the corner shear force and the longitudinal hogging moment. Since it was shown that reduction of the support stiffness leads to a lower obtuse corner support reaction, lowering the bearing stiffness also leads to a decrease of the obtuse corner shear force and the longitudinal hogging moment. After all, more elastic bearings are shown to lead to better redistribution, which means that there is less concentration of forces at the corner.

The better load distribution that follows from reducing support stiffness, also means that the

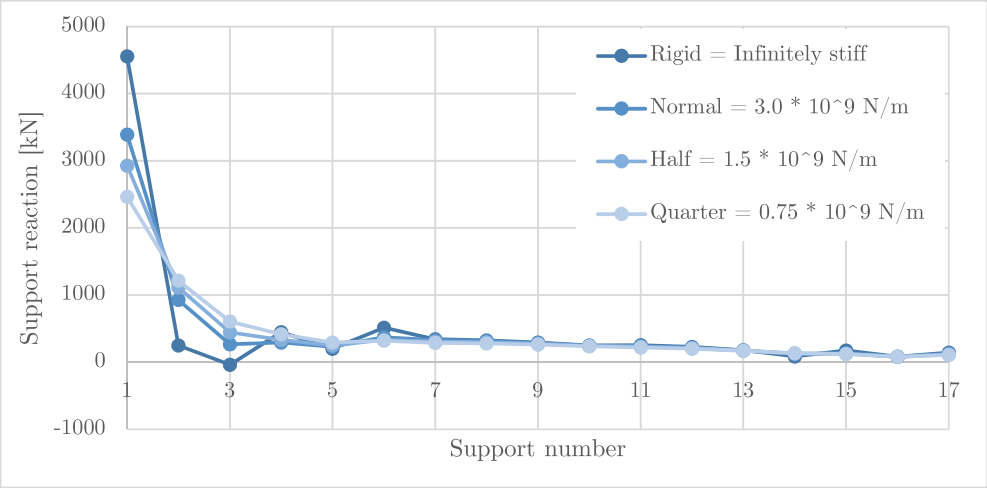

Figure 4.17: Distribution of support reactions for different bearing stiffness, with a centre-to-centre distance of 1 m

longitudinal sagging moment slightly increases; as less load is concentrated along the free edge, more load is transferred through the location where the maximum sagging moment is found. Reversibly, the transverse moment decreases as the support stiffness is decreased.

4.5 Abutment and foundation stiffness

Next, the influence of both the abutment and foundation stiffness on stress distribution within a skewed slab bridge as well as the distribution of the support reactions is investigated. A skewed slab bridge with the same geometry as used in the previous chapters (see 4.4) is again used for this investigation, with a bearing ctc-distance of $1m$ and x- and y-edge distances of $0.25m$. In total, four different bridge models are compared, as shown in Table 4.3, where both foundation and abutment beam (bending) stiffness are taken as normal (modelled realistic) and rigid. A plot of the support reaction distribution is given in Figure 4.18. These results, as can be seen in the graph, have proven that the support reactions for model 2, 3 and 4 (as defined in Table 4.3) are almost exactly the same. This means that a rigid abutment beam has the same effect on the support reaction distribution as a rigid foundation. Application of both a rigid foundation and a rigid abutment beam leads to the same results. This makes sense since the abutment beam is resting directly on top of the foundation. If one of both (or both) are set to be rigid, there is no deformation capacity that can cause any redistribution between supports. Therefore, model 2, 3 and 4 lead to the same support distribution.

Looking at the differences between model 1 and model 2,3 and 4, we see that rigid abutment configuration leads to a slight increase of support reaction 1 and 2. The greatest difference is in support reaction 3 (+27%) and support reaction 4 (-32.6%). Overall, applying rigid abutment configuration leads to a less favorable support distribution, because more load is taken by the first two obtuse supports.

Table 4.3: Configuration of different models used

Model number	**1**	**2**	**3**	**4**
Foundation stiffness	normal	rigid	normal	rigid
Abutment beam	normal	normal	rigid	rigid

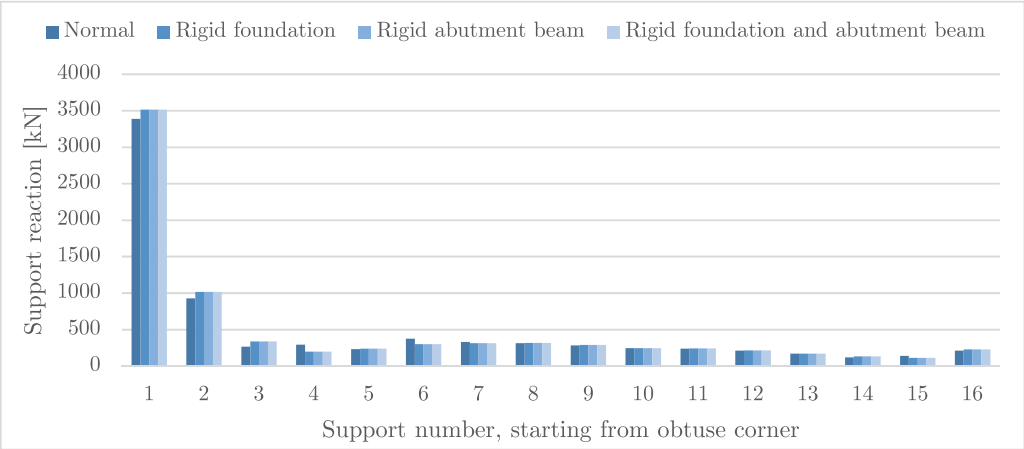

Figure 4.18: Support reactions resulting from different abutment and foundation stiffness

4.6 Load configuration

In this section, resulting force distribution from the two different load configurations as shown in 4.19 are compared: an edge-orientated configuration (heaviest lanes at edge) and a centre-orientated configuration. The comparison shows that the load configuration that aims to place the heaviest load at the edge of the bridge mostly leads to the highest results in terms of:

- Longitudinal sagging moment
- Longitudinal obtuse corner hogging moment
- Obtuse corner shear force
- Obtuse corner support reaction

For some of the above quantities, the centre-oriented configuration does lead to a slightly higher result. However, this differences observed always remain within 1%.

Only for the transverse sagging moment, the centre-orientated configuration leads to significantly higher results, of which 13% was the highest observed difference. In CUR report 58 [7], it was already shown that the highest secondary principal moment m_2, which is closely related to m_{xD-}, is obtained by placing a point-load in the centre of the plate. The higher values that are obtained through the centre-oriented configuration confirm this finding.

There are two ways of handling the higher values obtained through the centre-oriented layout:

- Determine and apply a correction factor on the transverse sagging moment m_{xD-} to compensate the difference in results found between edge-oriented and centre-oriented layout. This way, for a certain geometry, only the edge-oriented layout needs to be modelled
- Model both layouts for each bridge configuration considered, and take the highest transverse sagging moment resulting from both layouts

The latter is chosen as preferred method.

4.7 Main geometry parameters

In this section, influence of following the main geometry parameters (as defined in 3.3) on the bridge behavior is investigated:

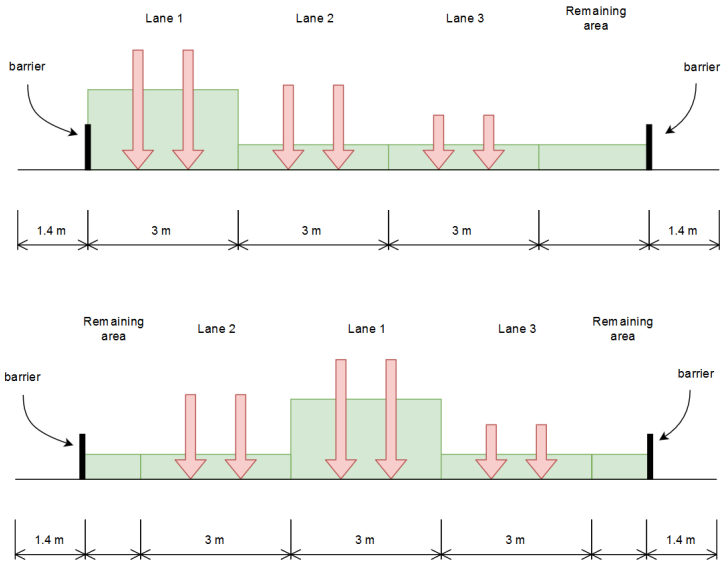

Figure 4.19: Two different load configurations: the edge-orientated (top) and centre-orientated (bottom) configuration

- Skew angle α
- Span length L
- Bridge width W

It is important to mention that the parameter bridge width is defined as the width of the bridge deck measured in perpendicular direction from the free edge, because this width is in order to accommodate the lanes of the crossing road. This means that for a certain span length and bridge width, a lower skew angle leads to a wider bridge deck and thus a higher bridge deck surface area:

$$A_{total} = W_{support} * L = \frac{W}{\sin \alpha} * L \tag{4.3}$$

4.7.1 Skew angle

Obtuse corner support

First of all, influence of the skew angle on the support reactions is investigated. Figure 4.20 shows the first obtuse support reaction plotted against the skew angle, for different bridge aspect ratios ($W : L$). For all aspect ratios, the graph shows rather big amplification factors. Those amplification factors, which show the magnitude by which the obtuse support reaction is multiplied when going from a straight crossing bridge ($\alpha = 90°$) to a highly skewed bridge ($\alpha = 30°$), range from 5.6 to 6.2. These factors show just how great the load concentration effect can get in a skewed slab bridge. An increase of great magnitude has been found before in [8], although continuous supports were applied and stiffness of those supports was not mentioned. Similarly, the CUR report 58 [7] found rather high magnifications as well, but now for discrete supports. It also showed that reduction of stiffness of the bearing pads leads to increased distribution of reaction forces. Additionally, [32] also finds great increase in obtuse corner support reaction for dead load as well as two live load cases that represent heavy trucks. It must be said that in literature cited above, upon increasing skew (thus decreasing skew angle), the free edge is kept at a constant length, rather than aiming for a constant bridge span as applied in this thesis. This means that upon increasing skew, the actual bridge span is reduced. Consequently, magnification factors found in this thesis cannot be compared one on one with such values from literature.

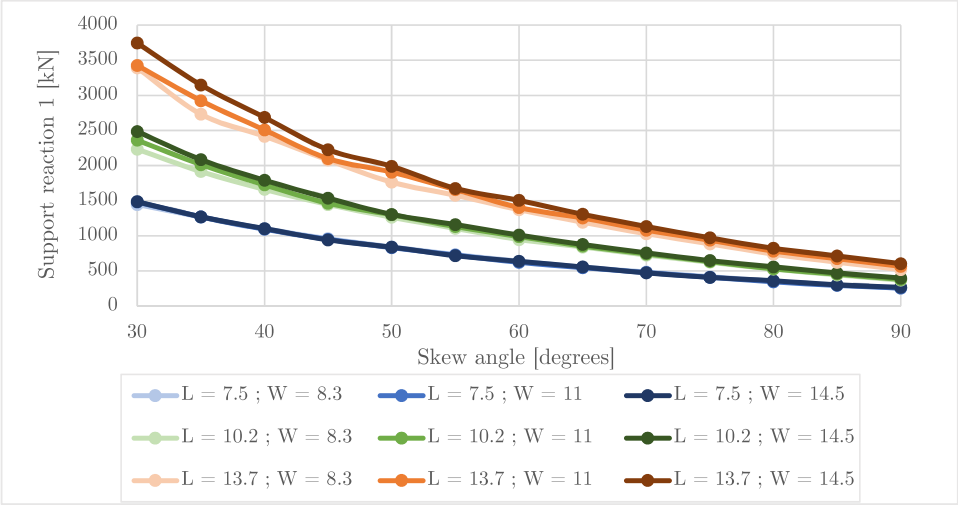

Figure 4.20: Support reaction in the obtuse corner vs the skew angle for different bridge geometries

Looking at the plots of bridges with the same span length, differences between those bridges can be spotted. The three plots that belong to the smallest span ($L = 7.5\ m$) can hardly be separated from each other: their obtuse support reactions are very similar. These three bridges have an aspect ratio ($W : L$) ranging from 1.11 to 1.93 (higher is relatively wider). The second set of plots, which belongs to the three bridges with a span of $L = 10.2\ m$, show more distinctive lines. It can be seen that the bridges with a higher aspect ratio (ranging from 0.81 to 1.42) have a slightly higher obtuse support reaction. This does however not mean that the amplification factor also increases for relatively wider bridge. The aforementioned difference between bridges with the same span length is best visible for the set of three with the longest span ($L = 13.7\ m$, aspect ratios from 0.61 to 1.06). Once again, the bridge with the highest aspect ratio leads to the biggest obtuse support reaction.

It is important to emphasize that in the above, no relation has been found between the bridge aspect ratio and the amplification factor. Only a small relation between the aspect ratio and the absolute obtuse support reaction is found, whereas the amplification factor describes the relative magnitude of this obtuse corner support reaction.

Support reaction distribution

For the overall distribution of support reactions for different skew angles, two figures are presented. The first one, Figure 4.21 shows the support distribution for a bridge with dimensions $L = 7.5\ m$; $W = 8.3\ m$, where a lighter-coloured line represents a less skewed bridge. As shown before, a highly skewed bridge gives a very uneven support reaction distribution, with the obvious peak at the obtuse corner support (number 1). As the bridge skew decreases, the support distribution plot lines become more horizontal, indicating a more even distribution of support reactions.

A perpendicular bridge ($\alpha = 90°$) with (continuous) line supports and only uniformly distributed loads over the entire bridge deck would lead to straight horizontal plot line for support load distribution. However, looking at the light-coloured line that belongs to the 90° bridge, it can be seen that there are still differences between support reactions and that distribution is not equal. This is caused mainly due to the the bridge model being loaded non-uniformly. For this model, two theoretical lanes loaded by different tandem systems and distributed loads are present. The lanes start at 1.4 m from the edge of the bridge, which can be seen as an explanation why support 3, 4 and 5 are loaded heaviest for this configuration. Figure 4.21 shows an increased last support reaction (the most right dot for each line), with a value that can be more than two times as high as the second-last support. This increased support reaction is mainly caused by the temperature load.

Figure 4.22 shows a graph with distribution support for a bridge of similar span, but now of a

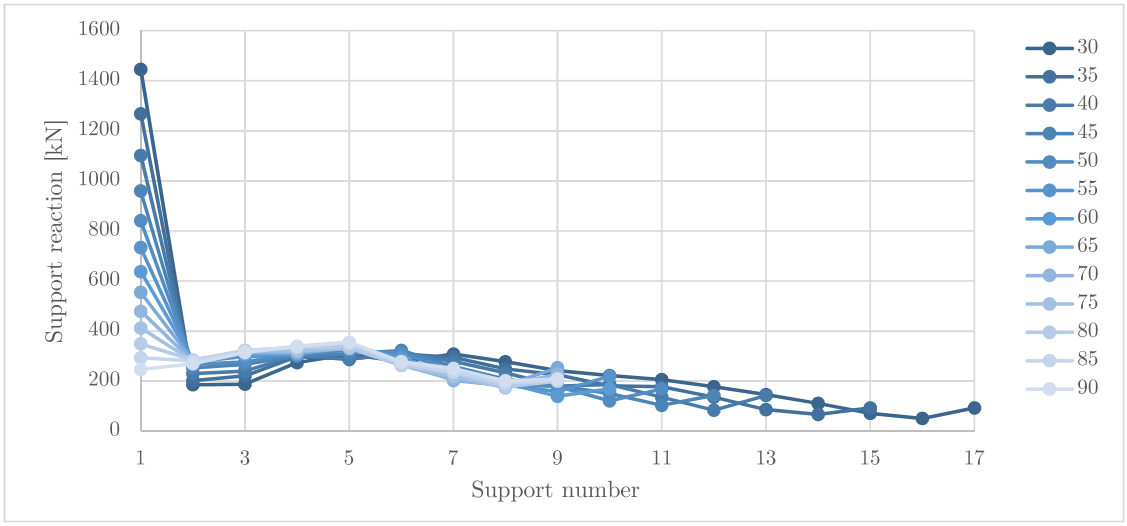

Figure 4.21: Distribution of support reactions for different skew angles. Bridge geometry: $L = 7.5\ m$; $W = 8.3\ m$

different width: $L = 7.5\ m$; $W = 14.5\ m$. It can be seen that this graph has great resemblance with Figure 4.21: the distributions and their support reaction values are much alike. This shows that the effect of the skew angle on the support distribution is not really dependant on the width of the bridge. In other words: the bridge width has very little influence on the support distribution. Once again, the increase in the last (acute corner) support reaction is present.

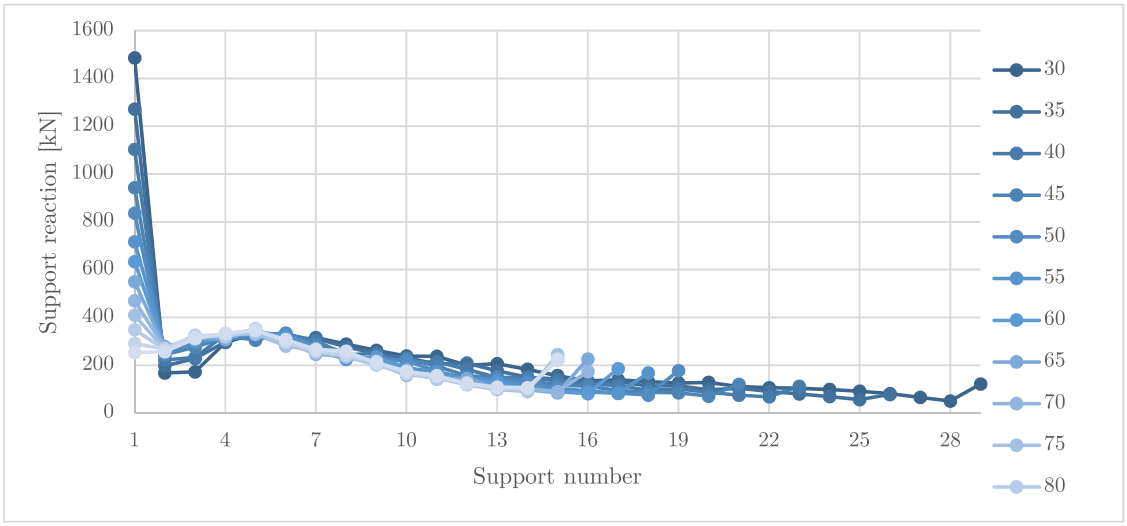

Figure 4.22: Distribution of support reactions for different skew angles. Bridge geometry: $L = 7.5\ m$; $W = 14.5\ m$

Shear force in the obtuse corner

For investigation of the effect of the skew angle on the obtuse corner shear force $q_{max\text{-}b}$, the shear force is once again averaged over a section with a length of $2 * d$, where d is the effective depth, depending on the thickness of the slab. Figure 4.23 shows a graph in which the shear force is plotted against the skew angle, for the 9 different bridge aspect ratios. The graph shows that the plots for bridges with the same span length follow roughly the same curve, where local deviations from that curve seem rather random. Overall, the graph looks less smooth than graphs produced

for other quantities. This is probably due to a local effect that differs per skew angle, since most plots seem to follow a similar deviation pattern. It might be that the sectional averaged shear force is more sensitive to local deviations in mesh element shape and size and therefore has greater deviation. Alternatively, the deviations could be a result from the incremental placement of the tandem systems, which are moved over the theoretic lanes in increments of $\frac{1}{10}$, resulting in different governing positions for different skew angles.

Looking at the difference between the shear force for perpendicular bridges (90°) and the very skewed bridges (30°), a magnification factor of over 4 can be found. This means that the averaged obtuse corner shear force can become more than 4 times as high as the bridge skew is increased down to (30°). As mentioned before, increasing skew in this thesis leads to an increase of the free edge length as opposed to most literature. The paper by Theoret [8] states that the vertical shear forces due to transverse curvature accumulate along the free edge. A longer skew span (longer free edge) will therefore surely boost this magnification of the shear force.

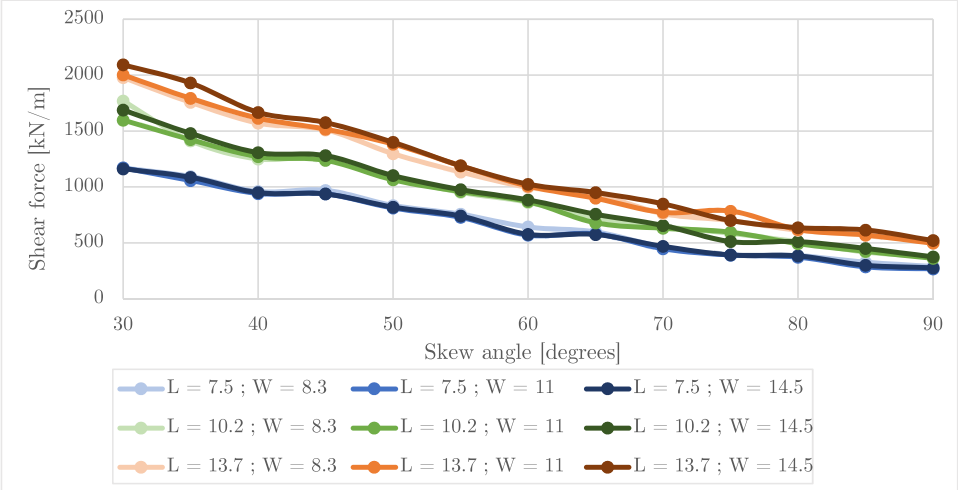

Figure 4.23: Obtuse corner shear force versus skew angle for different bridge aspect ratios

Longitudinal hogging moment in the obtuse corner

The positive longitudinal sagging moment m_{yD+} is, similar to the vertical shear force, highly dependant on the skew angle. Firstly, high skew makes the obtuse support reaction a sort of intermediate support, which causes the moment. Secondly, longitudinal reinforcement lies somewhat in the direction of the support line for highly skewed bridges, which is indicated by m_x in the global coordinate system in Figure 4.14 . As skew decreases, longitudinal reinforcement descends from this global m_x direction. Dependence on the skew angle is therefore twofold. Figure 4.24 shows this high dependence: as skew angle goes up to 90°, the positive bending reinforcement moment m_{yD+} diminishes and approaches zero. Only the twisting moment component remains, which is relatively small in those cases. Nonetheless, for high skew, the corner top moment should not be ignored since it leads to rather high moments.

Magnitude and location of maximum longitudinal sagging moment

Figure 4.25 shows the relation between the maximum longitudinal sagging moment versus the skew angle. The graph shows that this moment increases for a lower skew angle. This makes sense, since the skew span (free edge length) increases as skew increases. The average magnification factor for this moment between 90° and 30° is 1.45.

The location of the maximum moment described above, is plotted against the skew angle in Figure 4.26. It can be seen that the individual plots are rather bumpy. Most lines, and therefore the average, do not end at 0.5 L(halfway of the span) as expected for 90 degrees, but at 0.44 L.

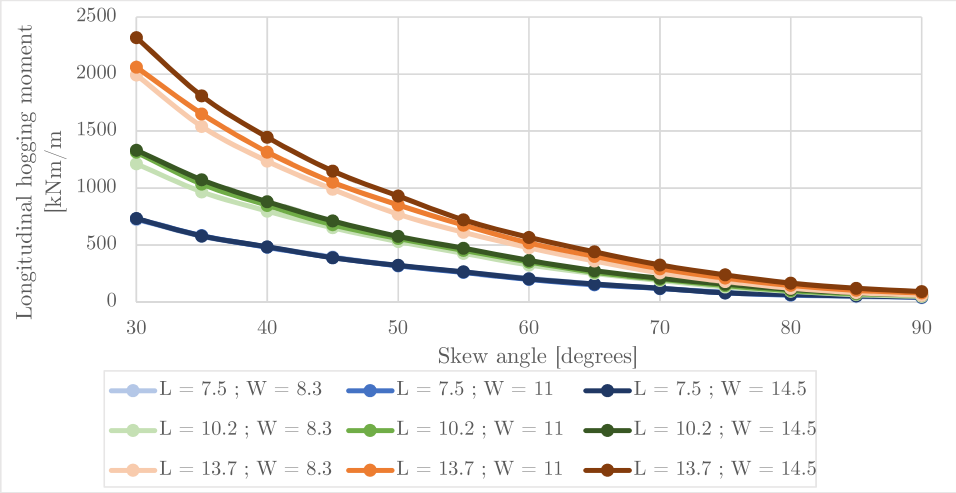

Figure 4.24: The obtuse corner longitudinal hogging moment versus the skew angle

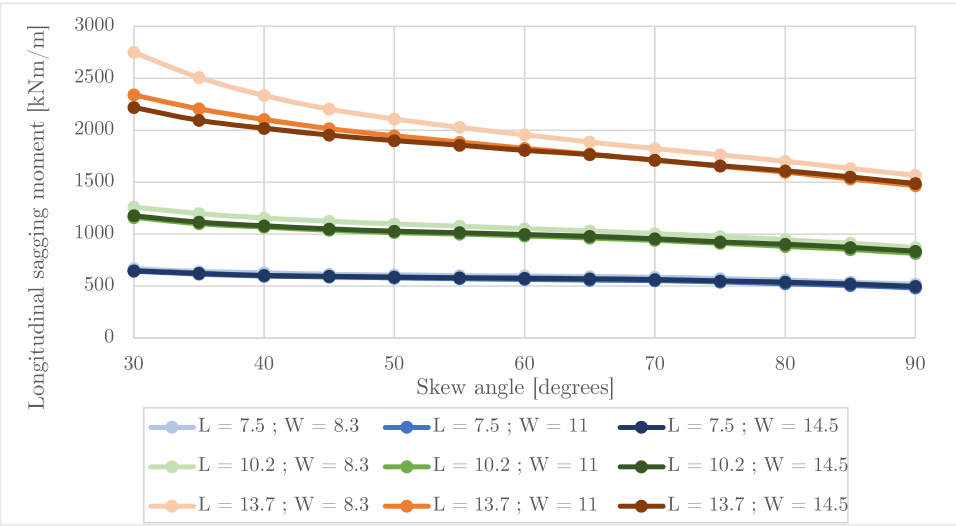

Figure 4.25: Longitudinal sagging moment versus skew angle, for different bridge aspect ratios

This result seems a bit weird, but can be explained by the fact that the tandem systems are moved over the bridge with an increment of $L * \frac{1}{10}$, where they are placed at 0.45 L and 0.55 L. This might also explain why the plot is less smooth: maximum locations found jump from one location to another. Additionally, because the wheel loads are spread out over a rather big area as explained in 3.6.2, the maximum moment will also be spread out over a larger area, making it less relevant to search for the exact location of the maximum. It is therefore more interesting to look at the overall trend.

Another reason for the bumpy graph is that for the longitudinal sagging moment m_{yD-}, the maximum is calculated at the corner of the elements, in order to obtain the coordinates related to the maximum in SCIA. The 'jumps' in the graph are therefore more or less equal to element size. Additionally, 'jumps' in the graphs become smaller for bridges with a larger span, because the element size relative to the bridge span becomes smaller (element size remains 0.45 m, while bridge span increases). This could be due to the fact that the maximum moment is rather spread out due to wheel load, so the exact location might not be so accurate.

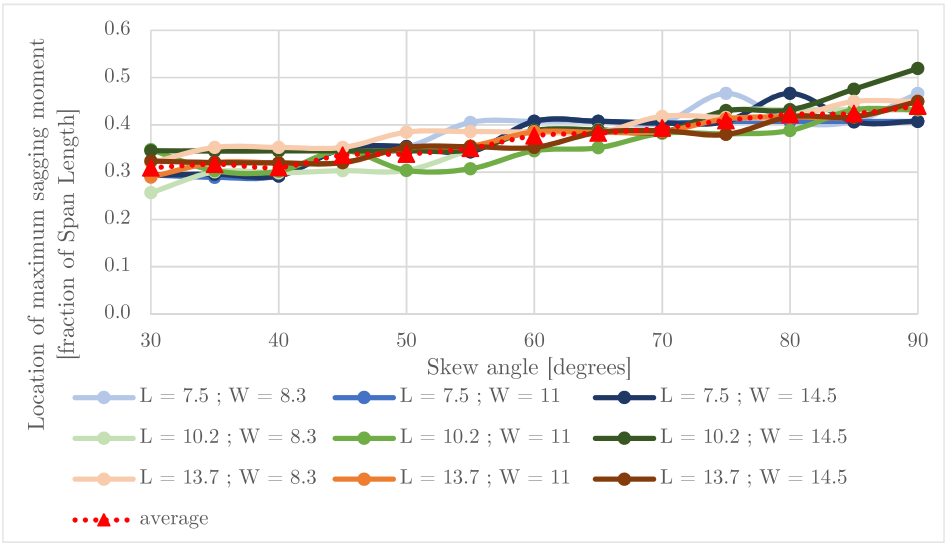

Figure 4.26: Location of the maximum longitudinal sagging moment from the obtuse corner vs the skew angle for different bridge aspect ratios

Direction of main principal bending moment

The main principal moment m_1 is a pure bending moment in a certain direction that does not have to (and mostly will not) coincide with the reinforcement axis system (parallel and perpendicular to the free edge). The direction of this principal moment often follows the trajectories for bending in the longitudinal direction.

CUR report 53 [6] contains a graph (shown in Figure 4.27) that shows the relation between skew angle and principal moment direction. In the bridge related to this graph, free edge length and support width are kept constant and only dead load is applied. The image shows that as skew increases, the plates tend to span in a direction parallel to the free edge, but with a certain lag (or 'sense of dislike' as mentioned in [6]).

A similar graph is produced using results produced with the parametric tool. Figure 4.28 shows the result. The blue line, which represents an averaged value of the principal moment m_1 for different aspect ratio, very much resembles the upper dashed line in Figure 4.27.

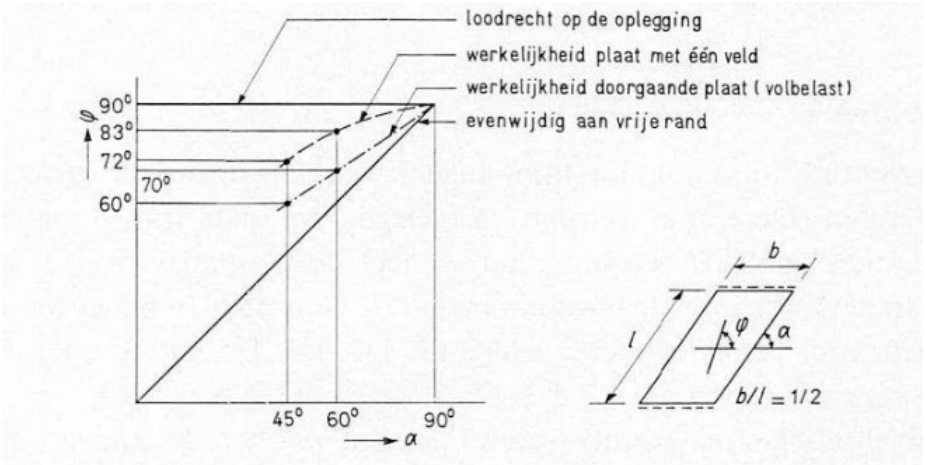

Figure 4.27: Image of the direction of trajectories φ versus the skew angle α, from [6]. The upper dashed line indicates a simply supported bridge

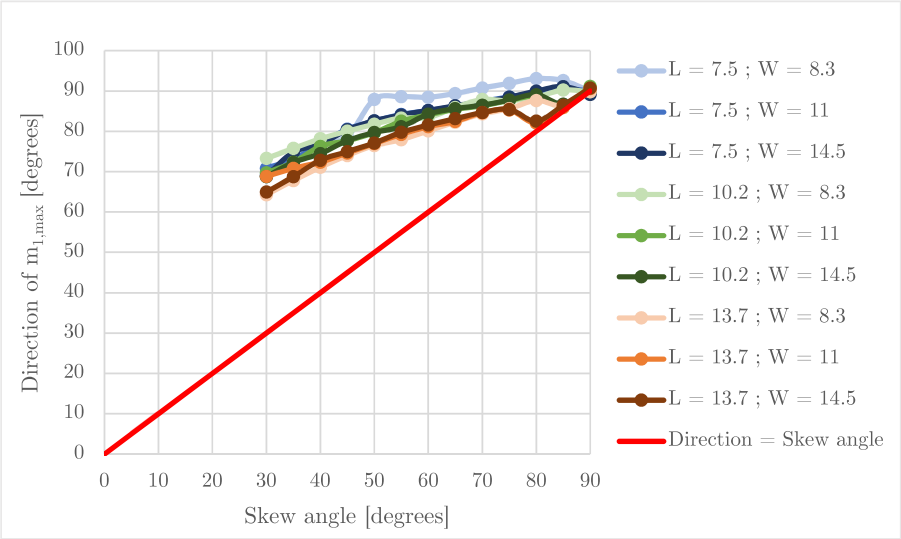

Figure 4.28: Direction of the main principal moment versus the skew angle. This image very much resembles Figure 4.27

Maximum transverse sagging moment

The transverse reinforcement direction lies perpendicular to the free edges. Figure 4.29 shows that the sagging moment in this transverse direction can reach a significant value. The graph shows a high influence of the skew angle, with magnification factors ranging from 3.43 up to 7.68. The transverse moment magnification also seems to be slightly dependent on the aspect ratio of the bridge, where a more slender bridge has a lower magnification factor. In other words, in a wider bridge the transverse sagging moment as result of higher skew will be relatively higher compared to more narrow bridges.

It should be noted that for each data point in Figure 4.29, the maximum value resulting from the edge-orientated and centre-orientated load configuration is taken. Section 4.6 showed that the centre-oriented configuration can be governing for the transverse sagging moment.

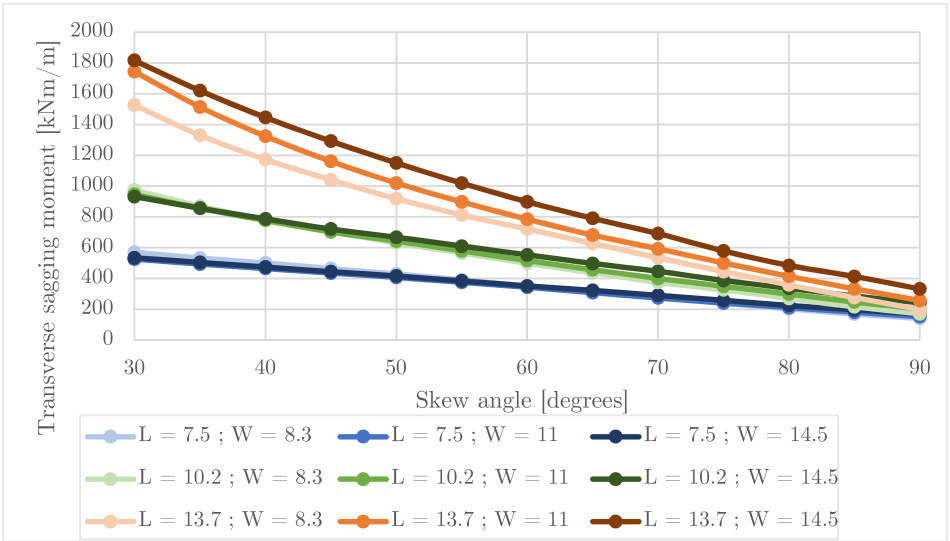

Figure 4.29: Maximum transverse sagging moment vs the skew angle, for different bridge aspect ratios

4.7.2 Span length and bridge width

Longitudinal sagging moment

In a straight beam or a perpendicular plate the relation between the span length and the bending moment is of quadratic order. A relation of the same order can be observed in Figure 4.30, where the longitudinal sagging moment is plotted versus three different bridge spans. The left graph belongs to the smallest bridge configurations (bridge width $W = 8.3\ m$), whereas the right graph shows plots for the widest bridges (bridge width $W = 14.5\ m$) analyzed. Although per bridge configuration only three different spans are calculated ($7.5\ m$, $10.2\ m$ and $13.7\ m$), quadratic relation between this span length and the longitudinal moment seems evident.

Going from narrow to wide bridges, a drop in longitudinal moment can be observed in Figure 4.31. The graphs show the longitudinal moment, now plotted for different bridge widths. The most narrow bridges are found at the left data-points of the right graph ($W = 8.3\ m$, $L = 13.7\ m$), while the widest bridges are found at the right data-points of the left graph ($W = 14.5\ m$, $L = 7.5\ m$). The decrease in longitudinal moment is the strongest for the narrow bridges, while for the wider bridges the effect seems to be absent.

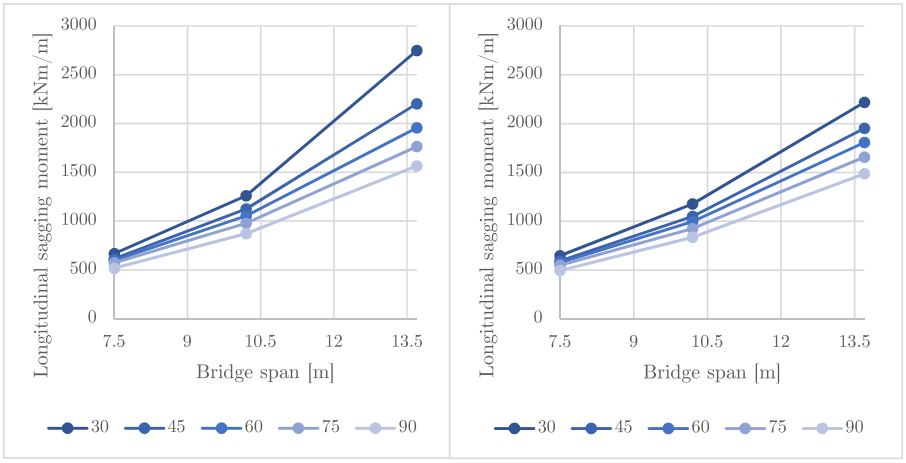

Figure 4.30: The longitudinal sagging moment m_{yD-} plotted against the bridge span length for different bridge widths (left and right graph) and different skew angles (line brightness)

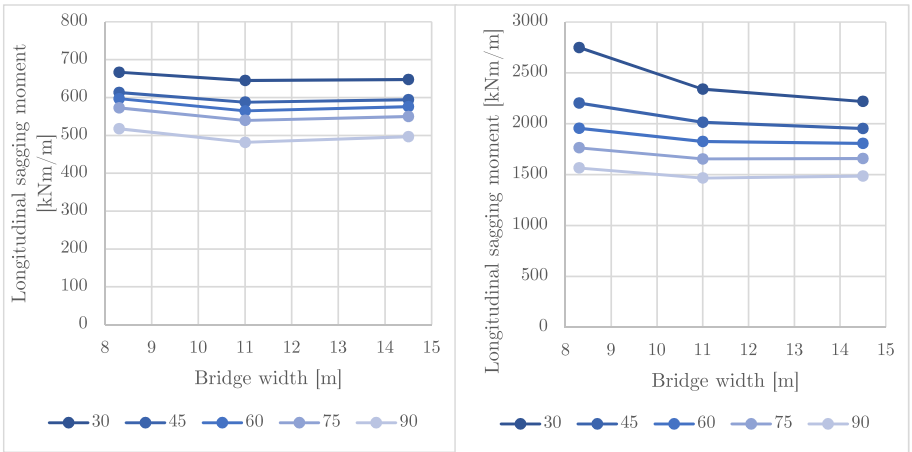

Figure 4.31: The longitudinal sagging moment m_{yD-} plotted against the bridge width for different span lengths (left and right graph) and different skew angles (line brightness)

Transverse sagging moment

Similar to the longitudinal moment, the transverse sagging moment is now plotted against the bridge span and the bridge width for different skew angles. Figure 4.32 shows that a greater span leads to a higher transverse moment. The left graph, which represents 8.3 m-wide bridges, shows a relation between the bridge span and the transverse sagging moment that appears to be linear. However, looking at the right graph which represents 14.5 m-wide bridges, a higher increase can be observed. Apparently, a wider bridge could lead to a higher increase of the transverse moment due to span increase.

This relation is investigated with the use of Figure 4.33. It shows plots of the transverse moment versus the bridge width, for two span lengths and different skew angles. In the right graph, a slight increase can be observed in the transverse moment as the bridge width is increased. This result can be linked to the right graph seen in Figure 4.31: as the bridge width is increased, the longitudinal moment decreases while transverse moment increases. However, this effect only seems present when a narrow bridge is widened to an aspect ratio of about 1 ($W \approx L$). This is confirmed by looking at the left part of Figure 4.33, which represents bridges with an aspect ratio of 1 and wider. An increase seems to be present only for the 90° bridge, whereas the more skewed bridges (30° and 45°) show a slight decrease in transverse moment as bridge width is increased. This behavior is difficult to explain.

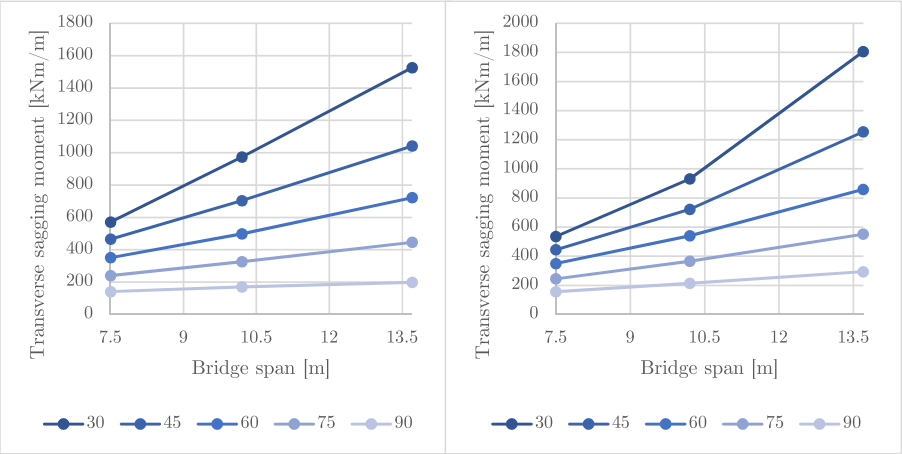

Figure 4.32: The transverse sagging moment m_{xD-} plotted against the bridge width for different span lengths (left and right graph) and different skew angles (line brightness)

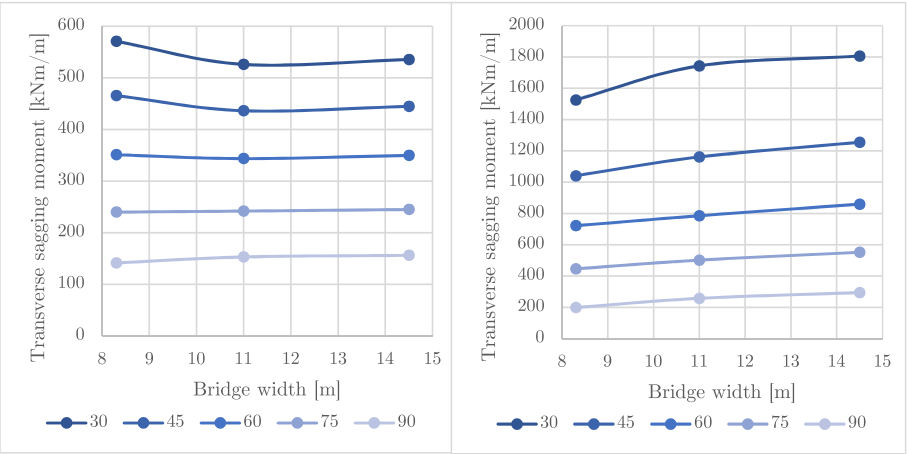

Figure 4.33: The transverse sagging moment m_{xD-} plotted against the bridge width for different span lengths (left and right graph) and different skew angles (line brightness)

Obtuse corner shear force

The obtuse corner shear force shows a clear increase as the bridge span is increased: Figure 4.34 depicts this. Both the left and the right graph show that when the bridges become wider, the (span-dependent) increase becomes smaller but is still evident.

Looking at the relation between the shear force and the bridge width, Figure 4.35 makes quite clear that there is none. Apart from some small deviations, shear force seems to remain constant as the bridge width is increased.

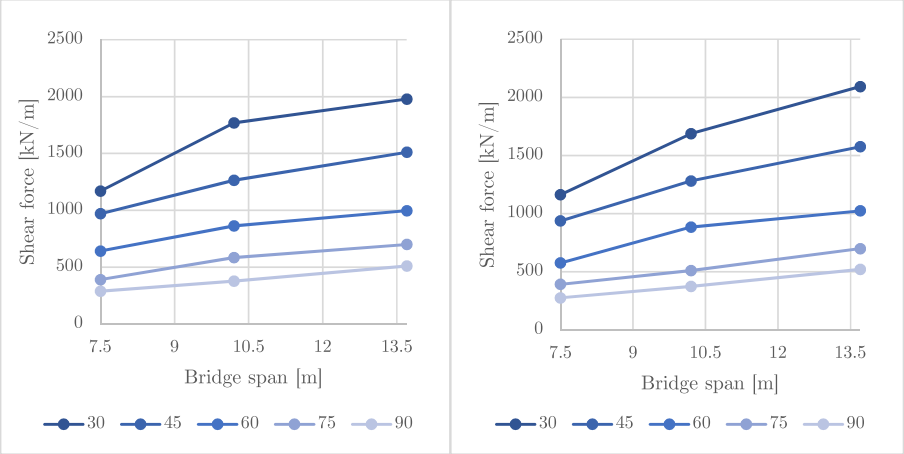

Figure 4.34: Shear force versus bridge span, for different skew angles and two different bridge widths

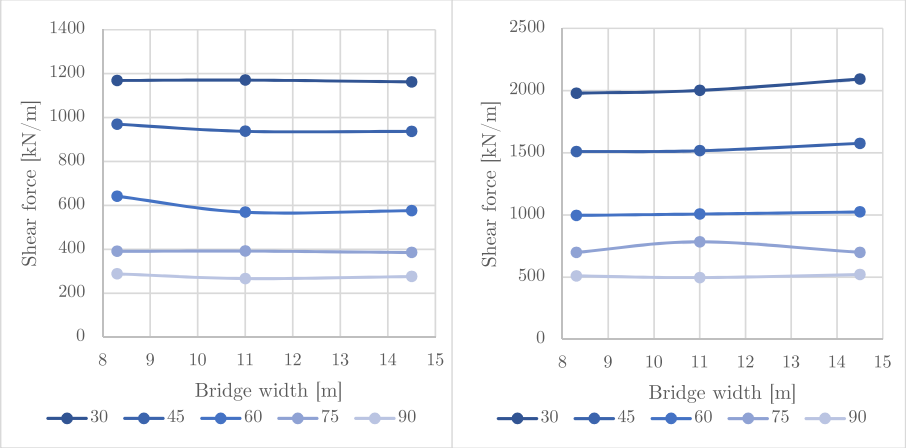

Figure 4.35: shear force versus bridge width, for different skew angles and two different span lengths

Obtuse corner longitudinal hogging moment

It was observed before that the longitudinal top moment in the obtuse corner is very much dependent on the skew angle. It is therefore most interesting to look at the lines that depict the skewed bridges in Figure 4.36: they show a mostly linear relation between this top corner moment and the bridge span. Apparently, a longer span causes a greater part to 'hang' on the first support, causing the top moment to increase.

Looking at Figure 4.37, the top moment seems to be rather independent of the bridge width. Only the larger bridges seem to show a slight increase as a result of a higher bridge width.

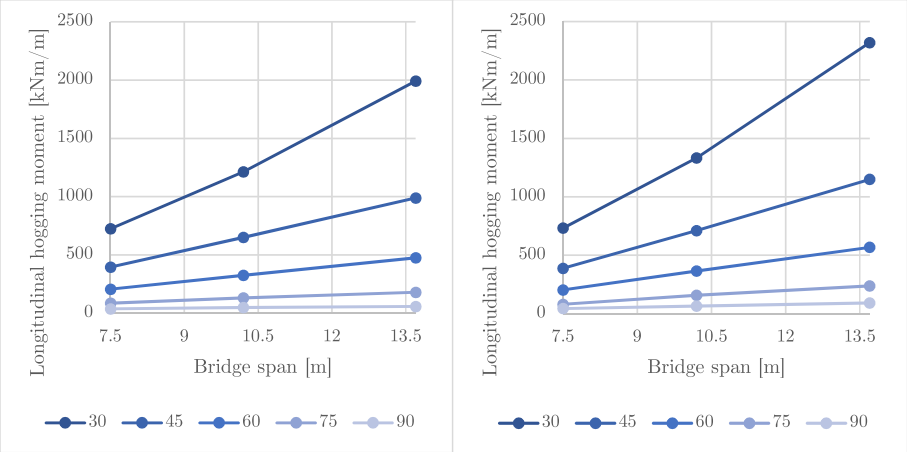

Figure 4.36: Longitudinal hogging moment versus bridge span, for different skew angles and two different bridge widths

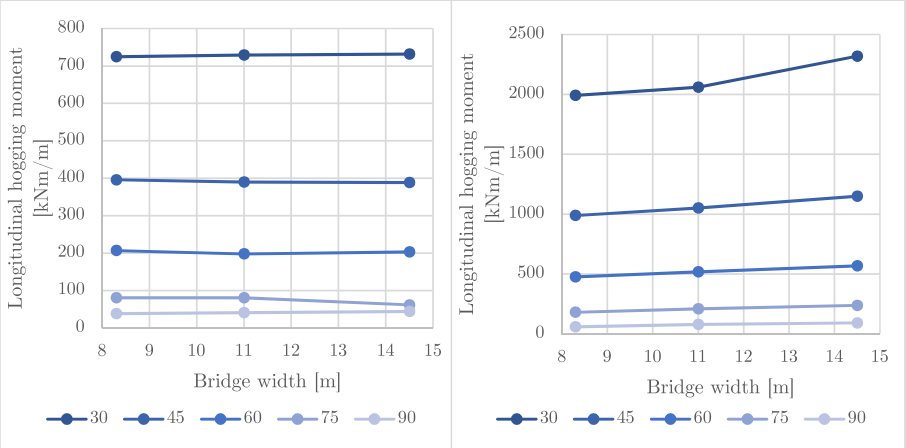

Figure 4.37: Longitudinal hogging moment versus bridge width, for different skew angles and two different span lengths

5 | Study of additional triangular segments (ATS)

In this chapter, the effect of adding an additional triangular segment (ATS) is investigated. First, the required changes in the model and its geometry are elaborated. Next, a small case study is conducted, where one bridge configuration is chosen. Addition of ATS on this bridge is investigated in terms of the result quantities.

5.1 Model adjustments

In a skewed bridge without ATS, the (initial) support width is determined by bridge width, which is based on the amount of driving lanes that need to fit on the bridge. With the addition of ATS, the new total support width is determined by the initial support width and the additional width. Figure 5.1 shows definitions for a skewed bridge with ATS added.

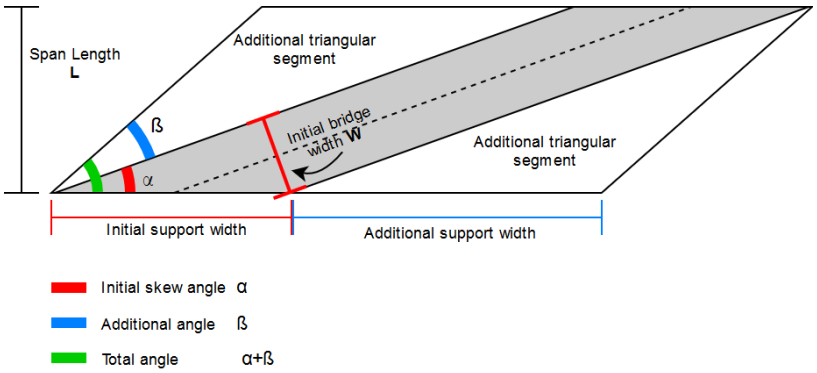

Figure 5.1: Geometric definitions for a bridge with additional triangular segments

The new total support width is calculated using the following formula:

$$\text{Total support width} = \frac{\mathrm{W}}{\sin\alpha} + \frac{L}{\tan\alpha} - \frac{L}{\tan(\alpha+\beta)} \tag{5.1}$$

The loads on the bridge model as defined in section 3.4 have to be altered slightly to fit the new bridge model with the ATS. In the first model, the edge of the bridge was loaded by traffic barriers, handrails and a concrete edge structure by means of a line load on the edge, with a total of 14 kN/m. In the new model with the ATS, this edge load is split in two parts:

- Bridge edge load: handrails and most of the concrete edge structure
  $\frac{3}{4} * 14 = 10.5\ kN/m$
- Road edge load: traffic barrier and a part of the concrete edge structure to support it
  $\frac{1}{4} * 14 = 3.5\ kN/m$

Figure 5.2 shows a bridge model with ATS applied, where the dead loads as explained above are displayed, as well as the asphalt load on the road.

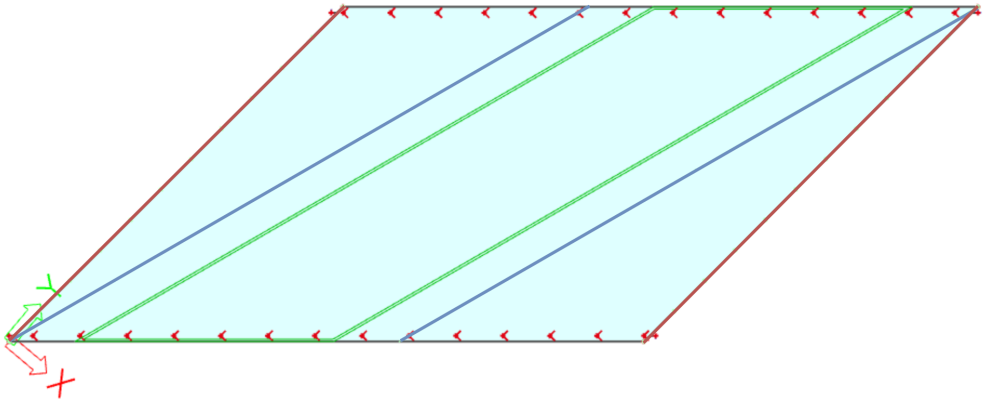

Figure 5.2: Dead loads displayed on an ATS model: red indicates the free edge line load, blue indicates the road edge line load, green indicates the road with the surface load from the asphalt

5.2 ATS model validation

Before using adjusted model with the ATS included, it needs to be validated. A skewed bridge with the following geometry is taken:

- Span length $L = 13.7\ m$
- Road width $W = 8.3\ m$
- Angle of road crossing $\alpha = 30°$
- ATS angle $\beta = 15°$
- $\rightarrow$ Total bridge skew angle $\alpha + \beta = 45°$

Previous validation of loads on the model were done by comparing model results in terms of bending moment with results from hand calculation. However, due to the more skew geometry now, hand calculation of bending moment will be inaccurate and therefore much less suitable for a validation.

SCIA offers a function that can calculate and display the resultant of all support reactions. This resultant support reaction is equal to the total vertical load chosen in the resultant calculation. For validation, two calculations are made:

- Resultant support reaction due to (concrete) self-weight only
- Resultant support reaction due to ULS combination 6.10a (as shown in 3.5)

The validation shows that the resultant support reaction from the model is exactly equal to the calculated resultant reaction, both for the self-weight only and the ULS combination. A detailed calculation can be found in Appendix C.

5.3 ATS model results

In this section, results from the ATS model are shown. Main focus is once again on the following resultant quantities:

- Obtuse corner shear force: sectional average over $2d$
- Longitudinal sagging moment
- Transverse sagging moment
- Longitudinal hogging moment in obtuse corner
- Obtuse corner support reaction

Results will be displayed for a bridge with of the following geometry:

- Span Length $L = 13.7\ m$
- Total Road width (barrier - barrier) $W = 8.3\ m$
- Deck height $= 0.9\ m$
- Road skew angle $\alpha = 20° - 60°$
- ATS angle β varied so that $\alpha + \beta = 20° - 60°$
- Bearing centre-to-centre distance of $2\ m$

5.3.1 Bridge deck surface

Before displaying the resulting differences in resultant quantities from adding ATS, the effect on the overall geometry is elaborated. Figure 5.3 shows a plot of the bridge deck magnification for bridges with a different road skew angle. For every line, the left data-point indicates the bridge geometry without addition of ATS. For each data-point to the right from thereon, an ATS of 2.5 is added.

Purpose of the graph is to show that even addition of an ATS of only $\beta = 2.5°$ can mean an increase in support width, and therefore an increase in bridge deck surface, of about 20%. As will be shown next, addition of ATS might prove to be an effective measure in reducing governing resultant quantities, which might make it possible to reduce thickness of the deck and save material. Nonetheless, as Figure 5.3 shows, the significant increase in bridge deck surface and therefore the (potential) increase in material use should not be forgotten.

5.3.2 Obtuse corner shear force

Figure 5.4 shows a plot of the bridge angle versus the obtuse corner shear force $q_{max,b}$. The line colour indicates the road skew angle, whereas the horizontal axis depicts the total bridge angle. In other words: for every line, the leftmost data-point has no ATS, and the more right data-points per line represent configurations with a greater ATS.

It can be seen that for the bridges with a high road skew angle, adding ATS can be very beneficial in terms of reducing the shear stress in the obtuse corner. Looking at the curve that belongs to $\alpha = 20°$ for instance, the difference between $\beta = 0°$ and $\beta = 2.5°$ results into lowering the obtuse corner shear stress from roughly 3150 kN/m down to 2500 kN/m; a reduction of about 20%.

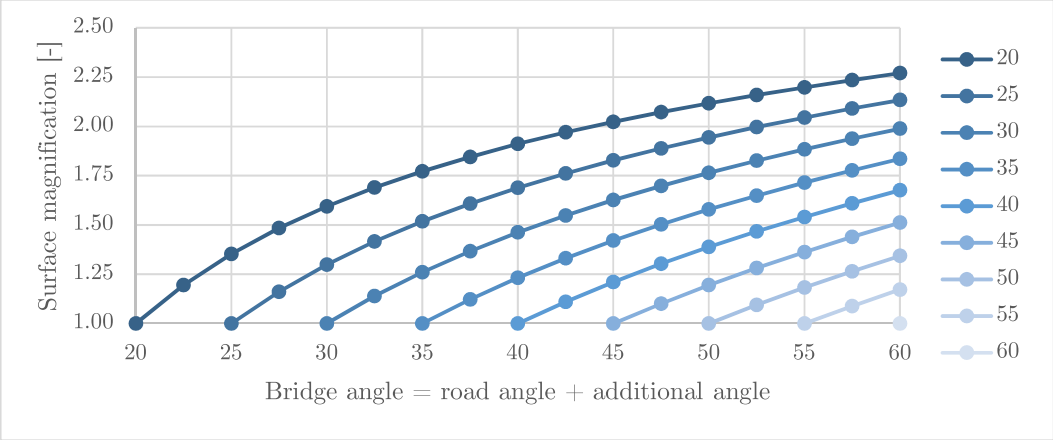

Figure 5.3: Magnification of the brdige deck surface plotted versus the bridge skew angle, for different road skew angles

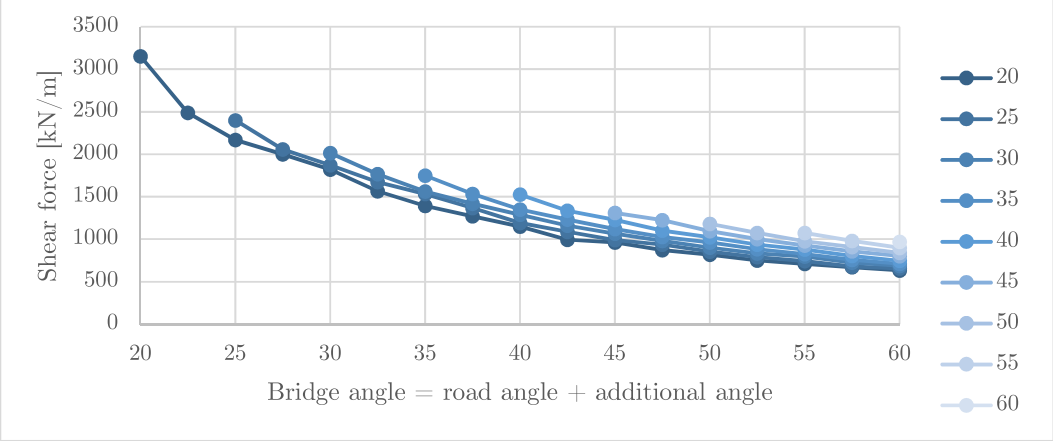

Figure 5.4: Obtuse corner shear force versus the Bridge skew angle, for different road skew angles

5.3.3 Longitudinal sagging moment

The longitudinal sagging moment is plotted against the total bridge angle for different road angles in Figure 5.5. Looking at the difference between the first and second data-point of each curve, the difference in terms of longitudinal sagging moment is quite remarkable. Similar to shear force, addition of only a small ATS of $\beta = 2.5°$ can make a great difference in moment reduction. For the 20° curve, addition of a $\beta = 2.5°$ ATS causes a drop in sagging moment from 3700 $kNm/$ to 2500 kNm/m; a reduction of 32%. This reduction that occurs between first and second data-point becomes smaller for smaller road angles α, but reduction is still quite significant.

The governing longitudinal sagging moment occurs near the free edge, and is caused mainly by the self-weight of the concrete and the live loads on the lane near the edge. Adding the ATS increases the distance between the bridge edge and the road, which ensures that governing traffic loads are placed further away from the free edge. Additionally, the ATS decreases bridge skew angle, and therefore reduces the length of the free edge. This length, often named the free-span, is therefore effectively reduced by addition of ATS. As the graph has shown, adding ATS is a highly effective measure for reduction of the longitudinal sagging moment.

5.3.4 Transverse sagging moment

This one is a bit more difficult to explain. Bridge becomes wider, so one might expect an increase in transverse moment. As can be seen in the graph, this is not the case.

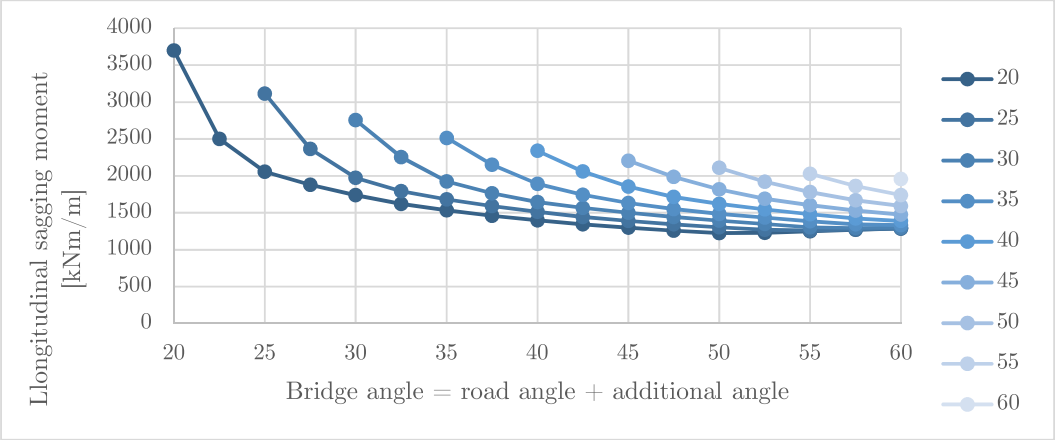

Figure 5.5: Longitudinal sagging moment versus the Bridge skew angle, for different road skew angles

The transverse direction is perpendicular to the free edge. For highly skewed bridges, this direction is rather close to the straight span direction (perpendicular to the support line). Since ATS addition means that this transverse direction diverts from straight span direction, it makes sense that the transverse sagging moment is also reduced. It could be said that this reduction is therefore more a result of a rotation of the axis system rather than resulting from the actual addition of bridge deck surface.

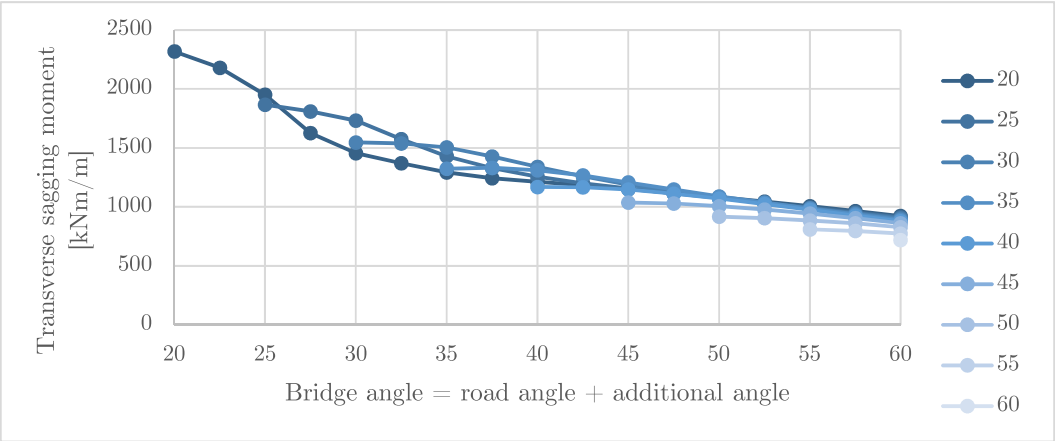

Figure 5.6: Transverse sagging moment versus the Bridge skew angle, for different road skew angles

5.3.5 Longitudinal hogging moment

Similar to before, this effect is strongly dependant on bridge skew angle. Therefore a high decrease at low skew angles can be observed, which shows that for this moment, ATS addition is a highly effective measure for reduction.

5.3.6 Obtuse corner support reaction

This graph is rather similar to the one for shear force. There is a high decrease at first, since high concentration of shear forces is present in the obtuse corner.

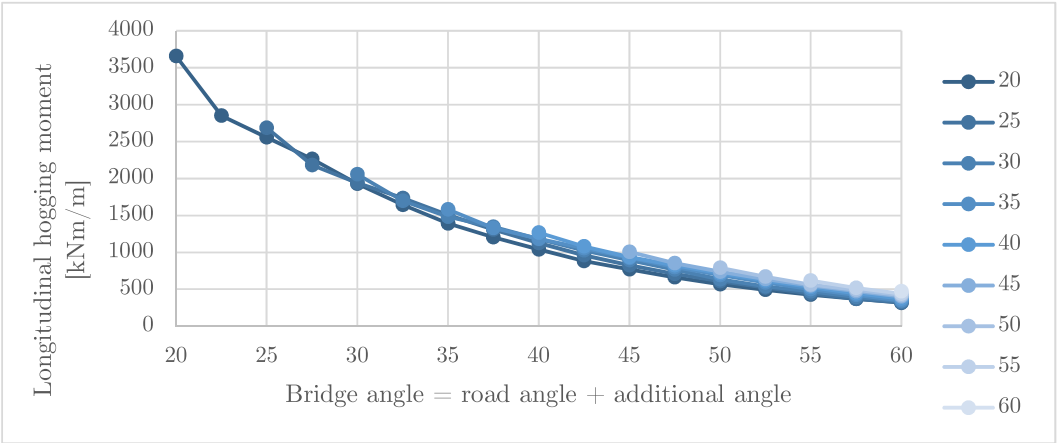

Figure 5.7: The obtuse corner longitudinal hogging moment versus the Bridge skew angle, for different road skew angles

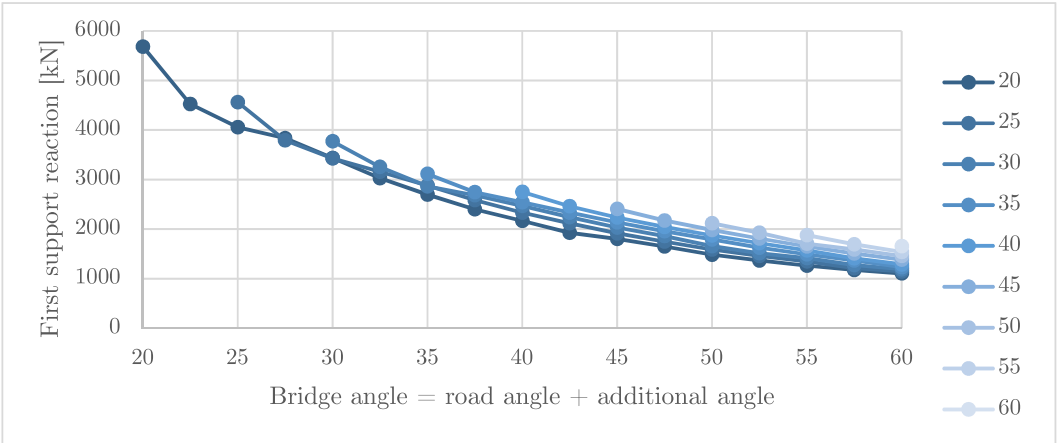

Figure 5.8: The obtuse corner support reaction versus the Bridge skew angle, for different road skew angles

5.4 Results for different bridge aspect ratio

As equation 5.1 showed, the total support width under addition of ATS is dependent on both the Span length L and the Total road width W. This dependence could cause differences in results for different bridge aspect ratios. Therefore, an aspect ratio different from the above, is also investigated on its result concerning ATS addition. The Total road width W is increased to from 8.3 to 14.5 m, result graphs are presented in Appendix D.

Overall, results between the two different bridges are small. The graphs are of similar shape, indicating similar behavior. The most significant differences are summarized below. For the wider bridge:

- surface magnification factors are significantly lower. D.1 shows magnification due to greatest ATS addition does not reach a value above 1.75, while 5.3 showed a magnification of over 2.25.
- the decrease in longitudinal sagging moment resulting from ATS addition is smaller (less steep curve in Figure D.3): maximum reduction found is 54% versus 67% for the more narrow bridge from Figure 5.5.
- addition of ATS is more effective for reduction of the transverse sagging moment

6 | Reinforcement capacity study

In this chapter, resulting force quantities from the model are assumed to be known. Next step in preliminary bridge design is the reinforcement calculation. This calculation consists of a few steps:

1. The bridge deck is divided into a number of zones. For each zone, separate reinforcement layout will be determined, based on governing moments and vertical shear force
2. Starting point in terms of resultants is the bending moment in the Serviceability Limit State (SLS). In most infrastructure, the crack width criterion based on this moment is governing in terms of the flexural bending reinforcement. For each zone, the flexural bending reinforcement is determined.
3. With the flexural reinforcement now known, shear reinforcement can be determined. Depending on the assumed angle for the shear diagonal, which determines the equilibrium in the truss-model, extra tensile capacity may be required in the flexural reinforcement.
4. For each zone, the Ultimate Limit State (ULS) bending capacity, based on the flexural reinforcement calculated earlier, is determined. If capacity is insufficient, a layout is chosen which satisfies both the SLS and ULS requirements.

As stated before, it is desired to 'translate' resultants from the model into a reinforcement layout with sufficient capacity to withstand those resultants. However, the Eurocode is mainly a guide for validation of a cross-section. This means that a cross-section and its related geometrical and material properties need to be chosen first, together with a reinforcement layout. The Eurocode then provides guidance in validating whether this chosen configuration provides the required capacity.

It is however desired to have a somewhat opposite workflow: force resultants from the model that lead to a reinforcement layout, instead of a reinforcement layout that leads to a certain capacity. This could be achieved by creating an automated, repetitive validation process. An array of values would be inserted for each parameter of the validation process, after which results from validation are saved in a table or database. Such a database allows for the selection of a reinforcement layout based on governing model results, which is the desired workflow.

However, since creating such a database takes too much time, it was decided not to proceed with this step. To speed up the process of validation, validation-sheets are created: the different Eurocode validations (SLS moment crack width check, ULS moment capacity check, ULS shear force check) are interpreted and translated stepwise into a spreadsheet for each validation. These spreadsheets are still very helpful and will be used in the case study of Chapter 7.

6.1 Flexural reinforcement determination based on crack width criterion

The method used for determination of the flexural reinforcement based on the crack width criterion, is described by R. Braam in [43], and is mainly based on the Eurocode 2 [25]. Calculation of the crack width is done by assuming an effective tensile area around the flexural reinforcement. Since

results from the model in terms of principal stress show only compression (except for some very local effects), pure bending is considered in the determination of the flexural reinforcement (conservative approach).

Eurocode 2 describes calculation of the upper limit for the crack width w_k by multiplying the distance between the cracks $s_{r,max}$ with the difference in average strain between the steel and the concrete $(\epsilon_{sm} - \epsilon_{cm})$. This method should be seen as a validation that checks whether a cross section with a certain reinforcement layout has an upper limit crack width that is below the maximum allowable width, which is based on durability criterion from Eurocode 2 (Concrete structures) [25].

However, as Braam shows, it is also possible (with some assumptions) to determine the required amount of steel A_s that is required to keep the crack width below a certain limit. To do this, the SLS bending moment should be known, and a diameter for the flexural reinforcement should be chosen. After reinforcement is determined, the crack width is calculated with the method from the Eurocode 2, and it should be checked whether this calculated value is below the desired limit.

Further elaboration on the reinforcement determination based on crack width can be found in Appendix E.

6.2 Shear reinforcement calculation

Once the longitudinal reinforcement based on the SLS crack width criterion is chosen, the shear reinforcement calculation can be performed. The most important parameters for this calculation are:

- shear reinforcement layout:
  - shear reinforcement bar diameter ϕ_{shear}
  - amount of vertical bars in cross-section per meter width n_{bars} (1 stirrup = 2 bars)
  - in plane centre-to-centre distance of shear bars s
- assumed angle of compressive diagonals for equilibrium in truss-model θ

Once again, these parameters will be varied and the shear capacity resulting from them will be output in a result table. A short overview of the shear capacity calculation is given below, a more detailed one can be found in Appendix F:

1. Capacity of only the concrete cross-section is determined
2. With the assumed angle θ, an equilibrium in the truss-model is created. This truss-model has two failure mechanisms with a related capacity:
   - the concrete compressive diagonals fail under compression: $V_{Rd,c,max}$
   - the vertical shear reinforcement capacity is reached (vertical bars start yielding): $V_{Rd,s}$
3. final cross-section capacity V_{Rd} is the lowest value of $V_{Rd,c,max}$ and $V_{Rd,s}$ (first failure mechanism to occur)

6.3 Reinforcement detailing

An important aspect of reinforcement design is the detailing. Proper detailing makes sure that the calculated cross-section capacity can actually be reached without unexpected failure. Consequently, rules on detailing result in limitations for certain reinforcement types. This section will treat some of those rules and show the limitations imposed. Guidelines for detailing rules are given in Eurocode 2 (Design of concrete structures [25]).

6.3.1 Centre-to-centre distance of bars

Centre-to-centre distance should be large enough to ensure that both pouring and compacting can be done properly. According to Eurocode 2, the minimum distance between two reinforcement bars is the largest value of:

- the bar diameter ϕ
- the largest aggregate size (usually 32 or 16 mm) + 5 mm
- 20 mm

For larger bar diameters, the first criterion becomes governing. Looking at longitudinal reinforcement, bars also need a certain overlap length to ensure transition of forces between bars. Overlapping bars are usually placed in the same (horizontal) layer as the longitudinal bars. This means that the distance between two longitudinal bars needs to be increased by 1 times the diameter. The distance between two separate bars then becomes $2 * \phi_l$. Subsequently, the minimum centre-to-centre distance becomes $3 * \phi_l$. If this limitation of $3 * \phi_l$ becomes problematic, an alternative for overlapping bars can be chosen such as bar couplers, to make sure that the ctc-limit stays at $2 * \phi_l$. A bar coupler can couple two bars together with a screwed connection, see Figure 6.1. An alternative is to weld bars together, although this is considered a labor-intensive and therefore expensive option. For further calculations, the minimum centre-to-centre distance is assumed to be at $2 * \phi_l$.

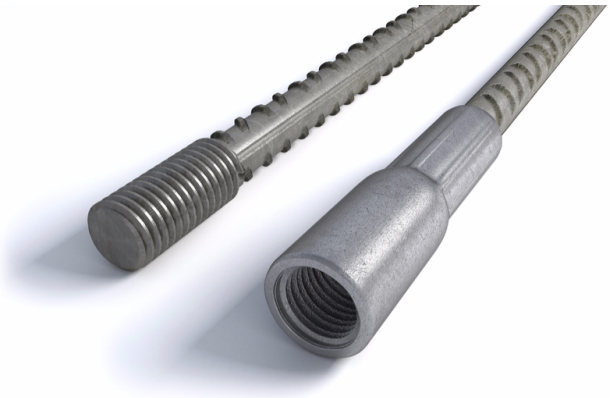

Figure 6.1: Example image of a reinforcement bar coupler, from [44]

In a situation where a very high amount of longitudinal reinforcement is required, it could be that the required bars do not fit into one layer of reinforcement. It can then be decided that reinforcement is placed in two horizontal layers. If so, the bars in the two layers need to be placed above each other to allow the concrete to be cast in between the bars, as well as leaving space for a compacter. For the vertical space between bars, the same rules apply as between horizontal bars. A minimum centre-to-centre spacing of $2 * \phi_l$ is again assumed from now on, based on application of couplers.

Placing reinforcement in a second (inner) layer is however less effective than reinforcement in one layer. The internal lever arm of the inner layer becomes smaller.

6.3.2 Shear reinforcement

Shear reinforcement usually consists of stirrups, which are placed around longitudinal reinforcement. If stirrups prove to be problematic, there are alternatives available on the market, although they will not be considered here.

At the edge of a plate, hairpins should be placed to prevent the edge of the slab from breaking off due to shear stresses.

6.3.3 Reinforcement anchorage

Reinforcement should always be anchored properly to ensure proper transition of stresses between reinforcement and another reinforcement bar or the concrete. Although proper anchorage is a very important detail in design and execution of reinforced concrete, no special attention is payed to anchorage here.

7 | Case study

In this case study, results from the ATS model and the reinforcement capacity study are combined. A bridge with the following properties (similar to the bridge in Chapter 5) is studied:

- Span Length $L = 13.7\ m$ (perpendicular distance of support line to support line)
- Total Road width (barrier - barrier) $W = 8.3\ m$
- Road skew angle $\alpha = 20°$
- ATS angle β varied so that $\alpha + \beta = 20° - 45°$
- Bearing centre-to-centre distance of $2\ m$

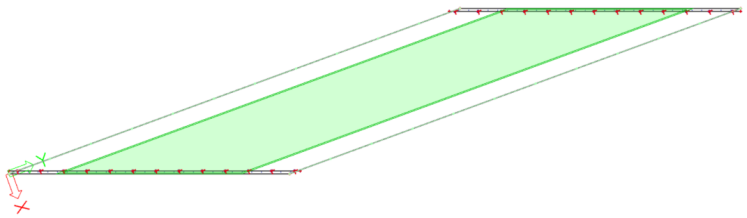

(a) $\alpha + \beta = 20° + 0°$

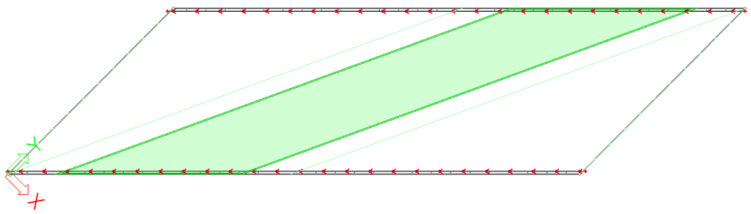

(b) $\alpha + \beta = 20° + 25°$

Figure 7.1: The minimum and maximum bridge size in the considered range of ATS extension

For a bridge with the requirements as specified above, configurations with different ATS additions are investigated. The range of this investigation runs from $\alpha + \beta = 20° + 0° = 20°$ to $\alpha + \beta = 20° + 25° = 45°$. Addition of ATS is done in steps of $\beta = 5°$. For each configuration, the required deck height is determined based on a reinforcement capacity study. For this determination, the following assumptions are made:

- Longitudinal reinforcement per direction is placed in one or two vertical layers
- Coupling of reinforcement: no lap splice applied at first, so minimum ctc-distance is $2 * \phi_l$
- Construction class S5
- Concrete cover of 50 mm on the shear reinforcement
- Transverse reinforcement layout is not governing for cross-section height and therefore not taken into account at first

7.1 Bridge height and reinforcement determination procedure

Determination of the required bridge deck height and reinforcement is done in a certain procedure. This procedure roughly contains the following steps:

1. Model the configuration with the ATS model tool, where the deck height is based on an estimation
2. Summarize the resultant quantities from both SLS and ULS and select the governing SLS moment: either the sagging field moment m_{yD-} or hogging corner moment m_{yD+}
3. Estimate the required longitudinal reinforcement amount $A_{s,l,req}$ (see Appendix E) for certain assumed longitudinal and shear reinforcement bar diameter, and calculate the centre-to-centre distance for a 1-layer and 2-layer configuration
4. Validate the estimated longitudinal reinforcement layout, in terms of crack width, using the Eurocode 2 method. If crack width is too high, increase the reinforcement amount and re-validate. Repeat this until the crack width is limited at the desired criterion ($w_k = 0.2\,mm$). Additionally, check if the centre-to-centre distance is not smaller than $2\phi_l$. If validation is successful, the longitudinal layout is temporarily accepted
5. If not done already, repeat the above procedure for the longitudinal hogging moment m_{yD+}
6. Choose a shear reinforcement layout (bar spacing), based on the bar diameter assumed earlier. If the resulting capacity is sufficient, this shear reinforcement layout is temporarily accepted
7. Validate the reinforcement layout in terms of the ULS bending moment. This validation should be done for the location with the highest ULS moment (same location as max SLS moment).
8. Review the different reinforcement layouts and look for optimization:
   - Reduce the deck height
   - Reduce the diameter of the shear reinforcement
   - Reduce the diameter of the longitudinal reinforcement
   - Switch between 1 or 2 longitudinal reinforcement layers

7.2 Example 1 - ATS angle = 0 degrees

For the first configuration, a bridge with a skew of $\alpha + \beta = 20° + 0°$, the aforementioned procedure is followed, and determination of the reinforcement layout will be shown as an example. For the cross-sections, a meter of width is considered. Therefore, all resultant quantities are also defined in result per meter width.

Step 1: Modelling the desired configuration

This step is straight forward: enter the desired geometry in the parametric tool, and let it generate the bridge and its configuration. Starting point is a bridge with a deck height of 0.9 m.

Step 2: Summarizing the result quantities

The governing result quantities are presented below:

It can be seen that the governing SLS moment is the longitudinal sagging moment: $m_{yD-,sls} = 2600\,kNm/m$.

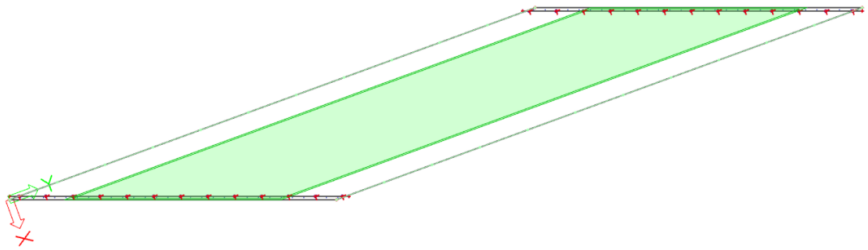

Figure 7.2: Geometry of the bridge without ATS

Table 7.1: Results for $\alpha + \beta = 20° + 0°$

Rounded resultant quantities	**SLS**	**ULS**
Obtuse corner shear force [kN/m]	2200	3150
Longitudinal sagging moment [kNm/m]	2600	3700
Obtuse corner longitudinal hogging moment [kNm/m]	2550	3650

Step 3 and 4: Estimate reinforcement, validate crack width

Using the method described in Appendix E, the required amount of reinforcement is estimated. First, bar diameters are estimated: for the longitudinal reinforcement $\phi_l = 40\ mm$ is chosen, whereas for the shear reinforcement $\phi_{shear} = 25\ mm$ is picked. Estimated amount of reinforcement for 1 layers is 22085 mm^2. This results in a centre-to-centre distance of 57 mm, which is much smaller than the minimum of $2 * \phi_l = 80\ mm$. Therefore, for this cross-section, a longitudinal reinforcement configuration in 1 layer is rejected.

Estimated amount of reinforcement for 2 layers is 24761 mm^2/m. Calculation of the crack width for this reinforcement amount gives $w_k = 0.23\ mm$, which is too high. Therefore, the amount of reinforcement is increased and crack width is calculated again. This is repeated until the desired crack width is not exceeded: this is the case for $A_s = 28200\ mm^2/m$, which leads to a centre-to-centre distance (assumed equal for both layers) of 89 mm, which is above the minimum of 80 mm. Additionally, this leads to a reinforcement ratio of $\rho_l = 3.69\%$, whereas the maximum according to Eurocode 2 is at 4%. Therefore, this longitudinal reinforcement layout is temporarily accepted.

Step 5: Determine longitudinal reinforcement layout for the hogging moment

The obtuse corner longitudinal hogging moment value $m_{yD+,sls} = 2550\ kNm/m$ lies very close to the longitudinal sagging moment. Following step 4, the required reinforcement amount becomes $A_s = 27700\ mm^2/m$. This leads to 2 layers of $\phi_l = 40\ mm$, $ctc_l = 91\ mm$

Step 6: Determine a shear reinforcement layout for the obtuse corner

In step 3 a diameter $\phi_{shear} = 25\ mm$ was chosen for the shear reinforcement. The governing shear force in ULS is 3150 kN/m. Using the shear reinforcement capacity calculation from the Eurocode as explained in Appendix F, a configuration can be chosen. For a configuration with $s = 5$ vertical bars per meter width of cross-section, an in-plane centre-to-centre distance of $ctc_l = 200\,mm$ and an assumed angle $\theta = 35°$ for the concrete compressive diagonal in the truss-model, the cross-section ULS shear capacity becomes $V_{Rd} = V_{Rd,s} = 3467\ kN/m$. It should be noted that this already is quite a lot of shear reinforcement. As stated, failure of the shear reinforcement is governing in the assumed truss-model for this configuration.

The assumed truss-model also induces an additional tensile load, which has to be taken up by the tensile reinforcement. This tensile load depends on the governing shear force. In this case, value for this additional tensile load is $\Delta F_{td} = 2249\ kN$.

Under the centre-to-centre distance (89 mm) calculated for the longitudinal reinforcement ($\phi_l = 40\,mm$), it was found that fitting stirrups in between the longitudinal bars becomes problematic. Inner radius of a bent stirrup of $\phi_{shear} = 25\ mm$ is $2.5 * 25 = 62.5\,mm$. Consequently, the outer diameter becomes $3.5 * 25 = 87.5\,mm$, which is the distance at least required from the centre of a longitudinal bar, so that at least $87.5 - 40/2 = 67.5\,mm$ is required in between bars. This space is simply not present, which means that this shear reinforcement layout is already not constructible. An option is to later reduce shear bar diameter and re-determine and validate a shear reinforcement layout.

Step 7: Validation of ULS moment capacity

Last step is checking the ULS moment capacity for the governing cross-section. The governing ULS moment is once again the sagging moment, with a value of $m_{yD-,uls} = 3700\ kNm/m$. A reinforcement amount of 28200 mm^2 leads to a ULS moment capacity of the cross-section of $M_{Rd} = 5100\ kNm/m$; the unity check becomes 0.73. This ULS overcapacity proves that the SLS crack width criterion is indeed governing for the longitudinal bending reinforcement.

Additionally, the capacity in the obtuse corner needs to be checked. Here, the ULS moment is slightly lower than the longitudinal sagging moment. However, from equilibrium assumed in the truss-model used for the shear capacity calculation, a tensile load ΔF_{td} was found. It should also be checked whether this tensile load can be taken by the reinforcement. The unity check for this location becomes:

$$UC = \text{Max}\left[\frac{m_{yD+,uls}}{M_{Rd}}\,;\,\frac{\Delta F_{td} * z}{M_{Rd}}\right] = \text{Max}\left[\frac{3650}{5100}\,;\,\frac{2249 * 0.561}{5100}\right] = 0.72 \tag{7.1}$$

It can be seen that the assumed equilibrium for the shear force does not impose a governing tensile load in the longitudinal reinforcement when compared with the governing bending moment.

Step 8: Reflection and possible optimization

According to the steps which are elaborated on above, this example bridge seems to fall within the theoretical limits of reinforced concrete capacity. However, it was already shown that shear reinforcement cannot be placed in between the longitudinal reinforcement, when using stirrups. Although there are alternatives for shear reinforcement, such options are not desired here.

The assumption that ULS crack width criterion is governing for the longitudinal reinforcement, is proven to be valid for this configuration: reinforcement determined from the SLS bending moment (unity check = 1.0) leads to a unity check for the ULS bending moment of 0.72. However, some remarks need to be made on the reinforcement layouts chosen.

First of all, centre-to-centre distances of non-round numbers such as 89 mm are not practical at all. A contractor will prefer bar distances rounded by 10 or even 25 mm which are less prone to errors.

Secondly, a centre-to-centre distance for $\phi_l = 40\,mm$ of about 90 mm will in practice prove to be very difficult to construct. Pouring the concrete in between the bars might prove to be difficult. A solution to this can be to pick a smaller size for the greatest aggregates. Standard size is 32 mm, but smaller sizes such as 16 or even 8 mm are also available. In between bars, there should also be enough space for a needle vibrator to enter, which is required for compacting the concrete.

The minimum spacing between bars is based on the assumption (made in Chapter 6) that reinforcement couplers are used. This way, no overlap bars are required, which significantly reduces the centre-to-centre distance of bars from $3\phi_l$ to $2\phi_l$. This decision was made to discover the limits of theoretical cross-section capacity. However, application of couplers has two disadvantages. The first one is the cost: application of couplers is usually more expensive than the application of lap splices. However, in this case, if application of couplers lead to a more slender cross-section, extra costs due to couplers can be compensated by savings in material use. The second disadvantage is

the sensitivity of couplers to fatigue damage. Couplers transfer the load between reinforcement bars through screw thread. Within screw thread, stress concentrations will develop. Highway bridges are subject to cyclic loading, since an order of 2 million heavy vehicles can pass a bridge each year. With a design lifetime of 100 years, this could mean up to 200 million cycles of a bridge in its lifetime. The combination of this many load cycles and the stress concentrations make the screw thread very prone to fatigue failure, which can mean brittle fracture of the connection between two reinforcement bars.

In addition to detailing problems, the longitudinal reinforcement layout is shown to lead to a reinforcement ratio of $\rho_l = 3.69\%$. A general rule of thumb for plates is that the maximum (desired) reinforcement ratio lies somewhere around 2%. This limit is heavily exceeded.

The Eurocode 2 [25] provides additional rules for bar diameters that are greater than a certain size that is considered 'large'. The Dutch annex on Eurocode 2 [26] defines a bar diameter of 32 mm to be large. The additional rules then apply to bar diameters greater than 32 mm: the $\phi_l = 40$ mm that is used above should therefore at least comply with some of the most important of those rules:

- Crack width may be controlled using surface reinforcement: applying bars with a small diameter outside of the stirrups

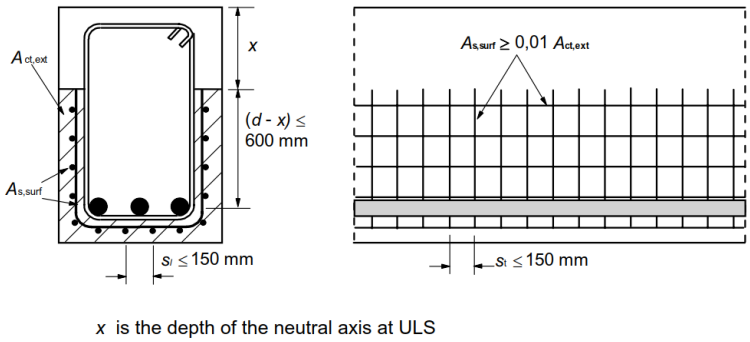

Figure 7.3: An example of surface reinforcement, from [25]

- All the longitudinal bars need proper anchorage, either from mechanical anchorage or by enclosing them with a stirrup

- Generally speaking, for any cross section smaller than 1.0 m (which applies to most bridge configurations in this thesis), no overlap is allowed. An exception can be made if tension in the bars does not exceed 80% of the ultimate strength. This may well be the case for structures in which longitudinal reinforcement is governed by SLS crack width criterion, rather than ultimate strength limitations

- In areas of anchorage where there is no compression present, transverse reinforcement should be added to the stirrup anchorage mentioned before

Considering all of the remarks above, it could be concluded that practically speaking, a bridge configuration of $\alpha + \beta = 20° + 0°$ is not constructible using reinforced concrete.

Additionally, it should be noted that increasing the cross-section height is not really an option. Although this might look like a favorable measure in terms of crack width control and increasing cross-section capacity, it also leads to significantly higher values for the moments and shear force. Increasing cross-section height to 1.5 m for instance, leads to a governing SLS moment of 4100 kNm/m. For the crack width control, with 2 layers of $\phi_l = 40$, this cross-section requires 23850 mm^2/m, which means $ctc_l = 105$ mm for both layers. It can be seen that an increase from $h = 900$ to $h = 1500\,mm$ does not lead to a great reduction in required reinforcement. On the contrary, the

amount of concrete increases by more than 50%, which is a significant increase in cost. Moreover, a thicker deck will also require a stronger foundation, more formwork and requires more soil for a higher abutment.

All in all, this configuration does not lead to a practical and economical design when reinforced concrete is chosen. It should not be forgotten that although the perpendicular span is 13.7 m, the actual skew span (length of the free edge) is $L/sin(\alpha) = 40\,m$. An option is to apply prestressed concrete, which however lies outside the scope of this thesis. The other alternative, adding an additional triangular segment (ATS), is investigated next.

7.3 Example 2 - ATS angle = 5 degrees

In the next example, an ATS of 5° is added. For this new geometry, the reinforcement design procedure is followed again. Figure 5.5 already showed that the addition of an ATS of $\beta = 5°$ leads to a significant reduction of the longitudinal sagging moment, in the order of 40%. Although this figure showed bending moments in ULS, similar reduction can be expected for the SLS moment.

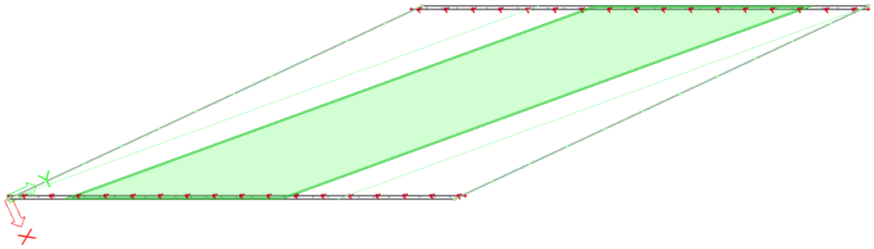

Figure 7.4: Geometry of the bridge with ATS of 5°

Step 1 and 2: Modelling the desired configuration, summarizing the result quantities

Top view of this configuration can be seen in Figure 7.4. Results are summarized in Table 7.2.

Table 7.2: Results for $\alpha + \beta = 20° + 5°$

Rounded resultant quantities	SLS	ULS
Obtuse corner shear force [kN/m]	1550	2200
Longitudinal sagging moment [kNm/m]	1500	2050
Obtuse corner longitudinal hogging moment [kNm/m]	1800	2550

Step 3 and 4: Estimate longitudinal reinforcement, validate crack width

Table 7.2 shows that the obtuse corner longitudinal hogging moment is now governing: $m_{yD+,sls} = 1800\,kN/m$. Assuming a shear reinforcement bar diameter of $\phi_{shear} = 16\,mm$, reinforcement is first determined for 1 layer of $\phi_l = 40\,mm$. This configuration requires $A_s = 15750\,mm^2/m$, which corresponds with $ctc_l = 80\,mm$. As said before, this is already at the very theoretical limit of constructability, and therefore rather undesired. Therefore, a configuration with 2 layers of bars is investigated.

2 layers of $\phi_l = 40\,mm$ requires $A_S = 17650\,mm^2/m$, which means $ctc_l = 142\,mm$. This already seems like a reasonable layout. However, since using $\phi_l = 40\,mm$ leads to additional requirements, it might be desired to use a smaller diameter: $\phi_l = 32\,mm$. This diameter, again applied in two layers, requires $A_s = 16450mm^2/m$, which leads to $ctc_l = 98\,mm$. This centre-to-centre distance is well above the set minimum of $2 * \phi_l$ based on the use of couplers. Additionally, it also lies above

the limit of $3 * \phi_l$, which means that lap splices can be applied as well (see Figure 7.5). This layout is temporarily accepted.

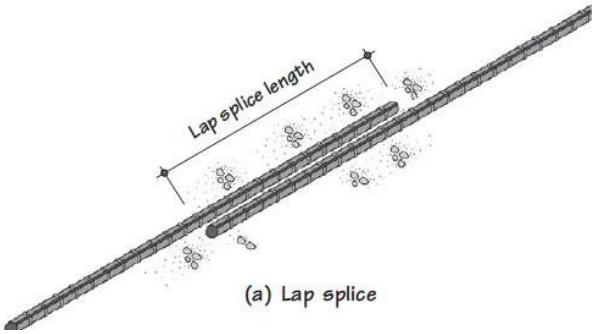

Figure 7.5: Connection of reinforcement bars through lap splice, from [45]

Step 5: Determine longitudinal reinforcement layout for the sagging moment

The SLS longitudinal sagging moment has a value of $m_{yD-,sls} = 1500\,kN/m$. Applying bars with a diameter of 32 mm in two layers (and again assuming shear bar diameter of 16 mm), the required amount of reinforcement becomes $A_s = 13700\,mm^2/m$, which results in $ctc_l = 117\,mm$ for both layers. This also seems acceptable.

Step 6: Determine a shear reinforcement layout for the obtuse corner

Governing shear force found in the obtuse corner has a value of 2200 kN/m. The assumed diameter of the shear reinforcement is $\phi_{shear} = 16\ mm$. Applying 4 bars per meter width, with an in plane centre to centre distance of $ctc_{shear} = 225\ mm$ and assuming an angle θ of 25°, a capacity of $V_{Rd} = V_{Rd,s} = 2406\ kN$ is reached. This still is quite a lot of shear reinforcement, but does offer sufficient capacity. This shear configuration for now is temporarily accepted.

Step 7: Validation of ULS moment capacity

Governing ULS moment is the obtuse corner longitudinal hogging moment, with a value of 2550 kNm/m. With the reinforcement configuration based on the SLS crack width criterion, a total capacity of $M_{Rd} = 4500\ kNm/m$ can be reached. Besides the prevailing moment, the tensile load that rises from the assumed truss-model from the shear capacity calculation also needs to be checked:

$$UC = \text{Max}\left[\frac{m_{yD+,uls}}{M_{Rd}}\,;\,\frac{\Delta F_{td} * z}{M_{Rd}}\right] = \text{Max}\left[\frac{2250}{4500}\,;\,\frac{2359 * 0.627}{4500}\right] = 0.50 \tag{7.2}$$

With a unity check of 0.50, a clear overcapacity is present. This once again shows that for the longitudinal bending reinforcement, the SLS situation is governing.

Step 8: Reflection and possible optimization

It can be seen that with the addition of an ATS of 5°, the reduction in resultants also leads to a quite significant reduction in required reinforcement. Longitudinal bar diameter applied is reduced from 40 down to 32 mm (compared with the 0° example), while centre-to-centre distance is increased to above $3\phi_l$. Resulting reinforcement ratio is $\rho_l = 2.09\%$, which is close to the rule of thumb-percentage of 2%.

The resulting shear reinforcement layout seems reasonable, although still quite a lot of shear reinforcement is required. Reduction of bar diameter does not make sense as it would require even

more shear reinforcement, which is more labor-intensive. It can therefore be concluded that unless a smaller shear bar diameter is really desired (longitudinal reinforcement becomes more effective), an optimization need not be done.

A more interesting optimization is the reduction of the deck height. This leads to significant savings in required amount of concrete. However, a reduction in deck height also results in a reduction in capacity: a reduction in internal lever arm means a lower bending moment resistance and greater crack width. Reduction of deck height is therefore only possible if either the governing moment also drops in value, or if the current configuration uses small bars (not the case here) or rather big centre-to-centre distances (also not the case here).

Figure 7.6 shows a graph in which both the longitudinal sagging (blue line) and the longitudinal obtuse corner hogging moment (orange line) are plotted for the SLS. Geometry of the bridge is the same as the one used in the case study here. The road skew angle is kept constant at $\alpha = 20°$, and the graph shows the total angle $\alpha + \beta$. It can be seen that between a total angle of 20° and 35°, the longitudinal hogging moment is the governing one. With this observation in mind, Figure 7.7 should be inspected. It shows the relation between deck height and both SLS bending moments, for a bridge of $\alpha + \beta = 20° + 5°$. The most important observation is that upon decreasing the deck height the sagging moment decreases, while the hogging moment increases.

Summarizing, both graphs together show that when the hogging moment is governing over the sagging moment, reduction of the deck height is not an effective measure of optimization in terms of moment reduction. This means that unless the current configuration contains room for improvement (bigger bar diameter, smaller ctc distance), decreasing the deck height need not be considered. As Figure 7.6 shows, this conclusion is valid for bridges in this case study with an ATS smaller than $\beta = 15°$ (35° total).

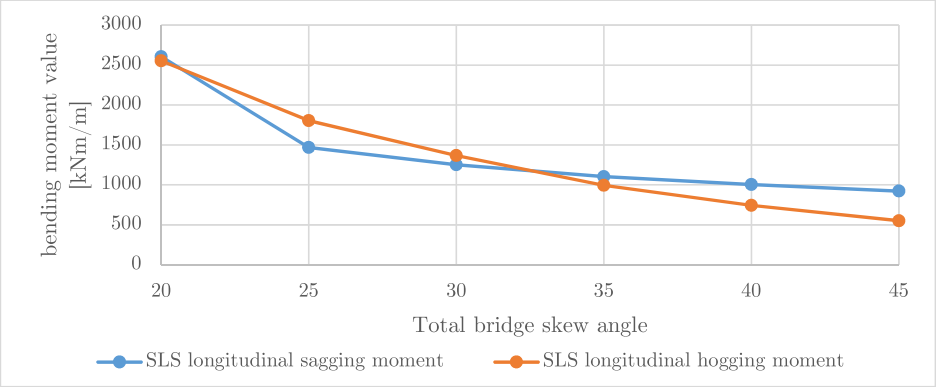

Figure 7.6: SLS bending moments for $\alpha = 20°$ and different ATS angles β, for $h = 900\ mm$

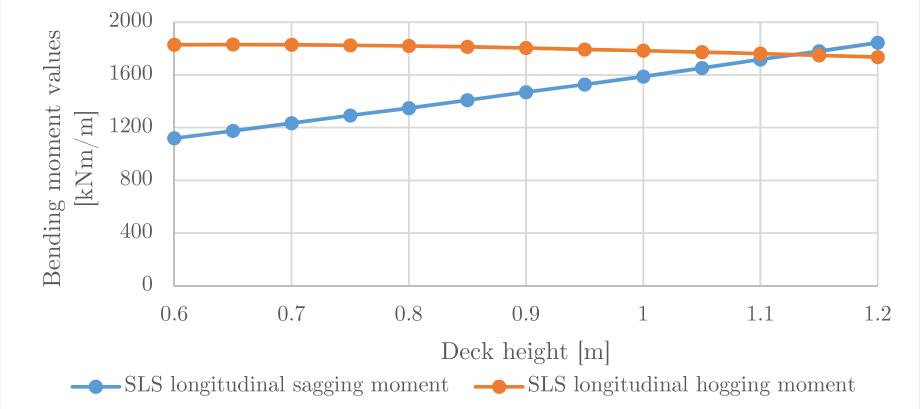

Figure 7.7: SLS bending moments versus the deck height, for $\alpha + \beta = 20° + 5°$

In step 3, the longitudinal reinforcement layout based on the SLS hogging moment was $\phi_l = 32\ mm$ and $ctc_l = 98\ mm$. Since reducing the cross-section height would not reduce the governing SLS moment, a greater bar diameter or smaller centre-to-centre distance (or both) would have to be chosen. As stated in example 1, both are not really desirable. It is therefore chosen to accept the longitudinal reinforcement layout.

The shear reinforcement was shown to be reasonable, and a reduction of bar diameter is not desirable.

All in all it can be concluded that under the assumptions made, this configuration seems constructible. A centre-to-centre distance of 98 mm, apart from being a theoretical value, is however still quite tight. If this proves to be the main issue of this configuration however, it should not be seen an unsolvable one.

Looking at the resulting span to height ratio, two boundary values can be identified:

- Straight span / height ratio $= \dfrac{13.7}{0.9} = 15.22$
- Skew span / height ratio $= \dfrac{13.7/\sin 25°}{0.9} = 36.02$

The straight span / height ratio, on which the initial deck height of the parametric tool is based, is rather low, as has been concluded before. On the other hand, the skew span / height ratio at a value of 36.02 is rather high. With Figure 4.28 in mind, it is known that the direction in which the plate tends to span lies somewhere between the two boundaries of 90° (straight span direction) and 25° (skew span direction). It can therefore be stated that there is also a fictional span/height ratio, that lies somewhere between the two boundaries found above.

7.4 Result overview

For the next examples, which are created by adding ATS in steps of 5°, the steps followed for the reinforcement determination are no longer fully elaborated on. Their results can be found below

7.4.1 Example 3: $\beta = 10°$

- Final deck height: 750 mm
- Governing longitudinal reinforcement layout: $\phi_l = 32\ mm$ - $ctc_l = 105\ mm$ - 2 layers - $\rho_l = 2.04\%$
- Shear reinforcement layout: $\phi_{shear} = 12\ mm$ - 6 bars per meter width, ctc in-plane of 175 mm, $\theta = 25°$
- shear UC $= \frac{2000}{2122} = 0.94$
- ULS moment UC $= \frac{1950}{3250} = 0.60$

In this geometry, the longitudinal hogging moment has again dropped significantly (down to 1400 kNm/m). A reduction in deck height from 900 to 750 mm could therefore be realized, while maintaining a realistic longitudinal reinforcement layout.

7.4.2 Example 4: $\beta = 15°$

- Final deck height: 600 mm
- Governing longitudinal reinforcement layout: $\phi_l = 32\ mm$ - $ctc_l = 110\ mm$ - 2 layers - $\rho_l = 2.43\%$

- Shear reinforcement layout: $\phi_{shear} = 12\ mm$ - 6 bars per meter width, ctc in-plane of 150 mm, $\theta = 25°$
- Shear UC = $\frac{1650}{1769} = 0.89$
- ULS bending UC = $\frac{1400}{2000} = 0.70$

Once again, the hogging moment has dropped (down to 1000 kNm/m) and a reduction of the deck height could be afforded in terms of reinforcement.

7.4.3 Example 5: $\beta = 20°$

- Final deck height: 500 mm
- Governing longitudinal reinforcement layout: $\phi_l = 32\ mm$ - $ctc_l = 114\ mm$ - 2 layers - $\rho_l = 2.83\%$
- Shear reinforcement layout: $\phi_{shear} = 12\ mm$ - 7 bars per meter width, ctc in-plane of 150 mm, $\theta = 25°$
- Shear UC = $\frac{1450}{1619} = 0.90$
- ULS bending UC = $\frac{1100}{1350} = 0.82$

In this configuration, the hogging and sagging longitudinal moments are about equal in value. Deck height is reduced down to 500 mm.

7.4.4 Example 6: $\beta = 25°$

- Final deck height: 450 mm
- Governing longitudinal reinforcement layout: $\phi_l = 32\ mm$ - $ctc_l = 101\ mm$ - 1 layer - $\rho_l = 1.78\%$
- Shear reinforcement layout: $\phi_{shear} = 12\ mm$ - 6 bars per meter width, ctc in-plane of 175 mm, $\theta = 25°$
- Shear UC = $\frac{1150}{1250} = 0.92$
- ULS bending UC = $\frac{800}{1100} = 0.74$

In this example, the sagging moment has become governing. A slight reduction in deck height is obtained. Additionally, longitudinal reinforcement can now be placed in one instead of two, which results in a significant reduction of reinforcement (reduced to 1.78%).

7.5 Transverse reinforcement

At the beginning of this case study, the assumption was made that the transverse reinforcement layout is not governing for the cross-section height of the skewed slab bridges considered. In theory, this assumption will hold because for no configuration throughout the entire study, the transverse sagging moment was found to be the governing bending moment. However, it should be noted that for most bridges, transverse sagging moment cannot be called insignificant. In normal concrete slabs, rule of thumb is to apply about 20% of the longitudinal reinforcement amount as transverse reinforcement. For skewed slab bridges, such an amount would be highly insufficient.

The transverse reinforcement is placed in the same direction as the stirrups (shear reinforcement). If forms of reinforcement are to be put in the same zone, detailing issues may occur. Putting

both reinforcement in the same layer might therefore not be a desired option. An alternative is to place the transverse reinforcement in a layer below the longitudinal reinforcement. This would however mean that this reinforcement becomes much less effective, from which capacity problems may arise. Such capacity problems could mean that in some exceptional cases, transverse reinforcement (in combination with the shear reinforcement) is so problematic that it becomes governing for the cross-section height. As stated, transverse reinforcement requires further research.

7.6 Getting rid of shear reinforcement

A rather common rule is that concrete slabs in general do not require shear reinforcements. Skewed slab bridges are an exception to this rule. However, it would be interesting to know for which bridge configurations shear reinforcement would no longer be required. The bridge configurations considered in this case study however all seemed to require shear reinforcement. It could well be that under the assumption of distribution of shear force perpendicular to the free edge over a length of $4 * d$, a configuration (certain ATS angle) can be found for which shear reinforcement is no longer required. This is an interesting topic for future research.

7.7 Conclusion

It can be seen that reinforcement determination is not quite a linear process. It contains quite some iteration steps and decisions based on experience and insights. Automating such a process, which was intended at first, should still be possible, but since every decision then needs to be made by a computer, decision criteria should first be understood and made visible by the engineer.

ATS addition is shown to be an effective measure in achieving a reduction in cross-section height. Under the assumptions made, a configuration of $\alpha + \beta = 20^\circ + 5^\circ$ seems constructible. However, a more detailed study should be conducted to conclude whether such a configuration is actually physically constructible. Additionally, greater ATS addition is shown to potentially facilitate a significant decrease in cross-section height. It can therefore be said that this is most definitely an interesting option that should be considered in the design of any skewed slab bridge.

8 | Conclusion, Discussion and Recommendations

8.1 Conclusions

The conclusions are divided into two subsections: technical conclusions and process-related conclusions. The technical conclusions elaborate on the results found with the model and elsewhere and are targeted towards the problem of a reinforced concrete simply supported skewed slab bridge. The process-related conclusions are directed towards the findings and observations gathered in the process of creating a parametric model and the way results were handled.

8.1.1 Technical conclusions

Main question: What is the influence of different parameters on the load distribution in a simply supported reinforced concrete skewed slab bridge, and how can these parameters be used in the reinforcement design?

In order to be able to answer this rather broad main question, four sub-questions have been posed. They are answered briefly below:

What relations can be found between design parameters and internal load distribution?

- The first parameter to be checked was the mesh element size in combination with the chosen plate theory. Investigation showed that a smaller mesh element size produced a representation of shear force and twisting moment in the edge zone that corresponded with the applied plate theory more accurately. Additionally, it was found that the application of Mindlin plate-theory in the finite element model produced more realistic results, especially in terms of the shear force. It was therefore decided to apply the Mindlin theory.
- Since the shear force in the edge-zone is assumed to distribute over a width of $2 * d$ (d being the effective height of longitudinal reinforcement in the cross-section), sections are applied within the models. Within these sections, the shear force (and later on also the longitudinal hogging moment) are averaged over the section to obtain resultant quantities, to be used for reinforcement design. Because of this averaging, an accurate representation of shear force distribution in the edge zone becomes less useful. After a verification, it is concluded that application of a mesh element size of 0.45 m, equal to $h/2$, provides sufficiently accurate results.
- The bearing configuration contains a couple of parameters, which can be altered to change the distribution of support reactions. An increased x-distance of first support to the free edge

leads to increased first support reaction, because the first support takes more load and an even bigger portion of the edge zone. Therefore x-distance should be kept small; there is no reason to increase it.

- An increased y-distance of the supports to the supported edge gives increased shear force. Therefore, the y-distance should be kept to a minimum that is required for bearing placement and reinforcement detailing (anchorage).

- The bearing centre-to-centre distance influences average load per bearing. This distance should be altered to make sure that the minimum load per bearing is reached to prevent horizontal movement. However, distance between supports should not become too great, because this will promote punching shear-like behavior.

- The bearing support stiffness is an important parameter. Both literature and results from the model clearly show that more elastic supports lead to a more equal support reaction distribution.

- The abutment and foundation stiffness can influence the support reaction distribution. Once one of both is set as infinitely stiff, stiffness of the other is of very little influence because they are directly connected to each other. Similar to bearing stiffness, an increased foundation stiffness leads to a more uneven support reaction distribution.

- For most result quantities, an edge-oriented load configuration leads to the highest values. Only exception is the transverse sagging moment, which is often higher for the centre-oriented load configuration.

- Under the conditions of a constant span length, deck height and bridge road width, an increase in skew (decrease in skew angle) leads to a significant increase in load concentration in the obtuse corner. This results in a higher first support reaction (in absolute and relative sense), a higher obtuse corner shear force and a higher longitudinal hogging moment.

- Increase of skew also causes an increase of the longitudinal sagging moment, although the increase is less strong than for most corner effects. This increase is mainly caused by an increase of the free edge length, also called the skew span. Skewed bridges tend to span in a direction that lies somewhere between the free edge direction and the straight span direction (perpendicular to support line). Additionally, as skew increases the location of the maximum longitudinal sagging moment shifts from $0.5L$ for $90°$ towards about $0.3L$ from the obtuse corner for $30°$.

- The transverse sagging moment also shows to be greatly influenced by the skew angle.

- The two other major geometrical parameters are the span length L and the bridge road width W. The span length has great influence on results, and while in most projects this parameter cannot be changed for the better (width of the underlying object is predetermined), its influence is still investigated. All dead loads and uniformly distributed traffic loads increase linearly with an increased span length, but the tandem systems do not change in magnitude. The relation between the span length and the longitudinal sagging moment is expected and shown to be almost quadratic. Both the obtuse corner shear force and the longitudinal hogging moment show somewhat linear increase upon increasing the span length, the same goes for the transverse sagging moment.

- The bridge road width W, which is determined by the amount of lanes that need to fit on the bridge, shows to have hardly any influence on the following resultants: shear force, longitudinal sagging moment, longitudinal hogging moment and transverse sagging moment.

Which rejection criteria are key when designing and validating a reinforcement layout?

- In determination of the longitudinal reinforcement layout, the crack width based on the SLS moment is shown the be governing over the ULS moment.

- When designing and validating a reinforcement layout, longitudinal reinforcement centre-to-centre distance is very important. This distance should not be too small in order to allow concrete to be cast in between the bars, as well as leaving space for a compacter needle. This centre-to-centre distance appeared to be limiting in the design of the case study bridges. Bars of a large diameter ($\phi_l = 40\ mm$) were avoided because they have additional requirements. Coupling of bars through lap splices is the preferred method from an economic point of view, although it requires a greater centre-to-centre distance. Alternatives are mechanical screwed couplers (more fatigue sensitive) or welding bars together (highly labor intensive).

- In skewed slab bridges, the amount of reinforcement required is rather high. This could induce brittle fracture: failure of the structure without warning (yielding of reinforcement). However, since longitudinal bending reinforcement is governed by SLS crack-width criterion, the ULS bending capacity in which this brittle fracture may occur will not be reached. In the case studies, the highest unity check for ULS bending found was at 0.82 and was therefore considered safe.

What is the effect of adding additional triangular segments on a skew bridge?

- One of the few 'tools' a structural engineer has in designing a skewed slab bridge is the addition of additional triangular segments (ATS): adding an extra piece of bridge, that does not directly carry a road on top. A direct effect of ATS addition is that the bridge deck surface is increased. The aim of ATS addition is the reduction of governing resultants, which can lead to a saving in the amount of reinforcement required, a reduction of the deck height or both.

  This reduction in governing results is shown to be very significant: obtuse corner shear force (and first support reaction), longitudinal sagging moment and longitudinal hogging moment can be reduced dramatically, even when adding an ATS of just 2.5°. The lower the initial road skew angle (higher skew), the more effective the addition of ATS is.

- In order to further investigate the effects of ATS addition, and to relate it to possible reduction in cross section height and/or required reinforcement, a case study is conducted. A highly skewed bridge with an initial road skew angle of $\alpha = 20°$ is taken as starting point, after which addition of ATS in steps of $\beta = 5°$ is investigated. For each geometry, resultants are obtained through the parametric tool, after which reinforcement layouts are determined and validated.

  It appears that the highly skewed bridge of $\alpha + \beta = 20° + 0°$ is not really constructible. The governing criterion was the SLS crack width, which required too much reinforcement, even when applying 2 layers of $\phi_l = 40\ mm$ bars. After addition of an ATS of $\beta = 5°$, a reasonable reinforcement layout was found for a deck height of 900 mm. For $\beta = 10°$, deck height could be reduced to 750 mm. Further addition of ATS lead to greater reductions in deck height.

- It was found that for the highly skewed bridges, the obtuse corner hogging moment was governing. For those bridges, reducing deck height did not lead to reduction of this hogging moment. Under the assumption of distribution of shear force over a width of $2 * d$, shear force reinforcement was never found governing for the required deck height.

To which extent can a parametric tool be used in a preliminary design phase?

- In early design stages, the parametric skewed slab bridge tool developed can be very useful for investigating different geometrical designs. Given certain spatial limits, different bridge designs can quickly be generated and the results summarized. Even in the case of applying prestressed concrete, the tool can provide insights in load distribution, although it will be less accurate.

- Once a more detailed design is required, the bridge tool will become less relevant. Since it contains quite some simplifications in terms of geometry and loading, differences in obtained resultants will probably become too great once design needs to go into detail. The developed tool should therefore be seen as helpful when quickly investigating different variants; it is not created with the intention to design a complete skewed slab bridge from a to z.

8.1.2 Process-related conclusions

Parametric modelling

Creating a parametric tool (script and model) required a quite high investment in terms of time (thus money in most cases), which was present for this master thesis. In engineering companies, work is often very project-oriented. On each project, profit needs to be made. Small projects will therefore probably never offer direct possibilities in which profit in terms of time savings (thus money) can be made by creating a parametric model, this might be different for big projects. However, for recurring problems, creating a parametric model can be very rewarding, and the option of doing so is definitely worth investigating.

Before creating a parametric model, two things are very important. First one is clarity about the relation between all parameters. In other words; what should the model look like, and which parametric relations are going to be incorporated? Secondly, any limitations imposed by software or calculation methods should be investigated and known upfront. A parametric model that still requires some steps to be done by hand, will quickly prove to be time consuming. Parametric modelling should therefore be seen as an all or nothing-situation: almost completely parametric is not parametric.

Reinforcement automation

At the start of the reinforcement capacity study, it was intended to automate the reinforcement determination. However, throughout the process, it appeared to be too difficult. Reinforcement design and validation is not a linear process. It requires insight into all aspects involved, and contains iterative improvement steps. If one is to fully automate the reinforcement design process, a full insight into this process is required. Additionally, all preferences and experience-based choices made by structural engineers should be captured and programmed. This will prove to be quite a difficult thing to do.

8.2 Discussion

The parametric bridge model tool in this thesis is created completely by the author. It does therefore not contain any assumptions or irregularities generated by other persons. The only uncertainties can be caused in the process of using the finite element method program SCIA Engineer. The models created with SCIA have been validated to make sure they behave as expected. If applicable, results obtained through the parametric tool have been compared with results from the literature, which mostly showed great resemblance.

Nonetheless, the process of parametric modelling and automatic result collection means that not every model is checked after it is created. It is therefore still possible that some results obtained

are not as valid as expected. Especially the automatic generation of sections in the obtuse corner might be sensitive to certain errors. Most results generated were however part of a series of results. This means that any deviations in model results due to localized errors are picked out easily, as they stand out from the results from other models (assuming that those are correct). Additionally, quite some automatically generated models were still opened and checked by hand, during which little mistakes were found. This makes the chance of models with errors that remain unnoticed rather small.

Conducting a parametric study often involved changing one parameter, while keeping all others at a certain constant value. In the beginning of the study, picking those constant values proved to be rather difficult in some cases. After all, the influence of each parameter was not known at that time. This resulted in quite some trial and error at the start and lead to a lot of data to be discarded due to later discovered errors.

Despite the simplifications (perpendicular bridge, reinforced concrete only) and decisions made in terms of parameters (3 bridge road widths, 3 span lengths), insightful results have been generated. The decision to base a bridge geometry on the amount of lanes below and on the bridge for instance, meant that upon increasing skew, the total bridge deck surface also increased. This decision causes some results to be more difficult to interpret. From a design point of view however, it is a logical choice. The selected span to height ratio for the parametric study appeared to be very much on the conservative side. In other words: rather thick bridges have been generated, in which the effect of self-weight might have pushed effects caused by the traffic loads away a bit. Additionally, the factor $\alpha_{q2..n}$ for uniformly distributed traffic load was set to 1.0 while it should be 1.4 if more than 2 theoretical lanes are present. This decision (to prevent a 'bump' in result between 2-lane and 3-lane bridges) also slightly reduces the effect of the uniformly distributed traffic loads.

The bridge deck is modelled with a stiffness equal to the secant modulus E_{cm} of concrete that belongs to the chosen concrete class (C35/45). However, normal engineering practice when modelling a reinforced concrete structure is to set the stiffness equal to $E/3$ as a representation for cracked reinforced concrete. This lower stiffness allows for better redistribution of peak stresses, which is favorable. On the other hand, deflections found will be higher, although they have not been considered in this thesis. Quick investigation shows that the lower E-modulus can lead to reduction of shear force and longitudinal hogging moment of around 10 to 15% (more statically indeterminate behavior around this obtuse corner support). Reduction in longitudinal sagging moment is rather small, in the order of 1 to 2%.

The case study conducted in this thesis is done using quite a lot of simplifications and assumptions. In could be said that this case study is a rather 'coarse' study. A lot of rules from codes, details and effects have been left out intentionally or have remained unnoticed. Aim of this case study was not to produce bridges ready for design. The study was rather aimed to investigate the limits of applying reinforcement in skewed slab bridges, in combination with the application of additional triangular segments. In the study, deck heights were determined after conducting a simple reinforcement capacity study and some simple optimization steps (cross section reduction, switching between 1 and 2 layers of reinforcement, changing bar diameters). The reinforcement required for the transverse sagging moment was assumed not to be governing for the cross-section height. Additionally, concrete cover was assumed to be only 50 mm, whereas 65 mm is not uncommon in infrastructure design. This smaller assumed cover is a rather favorable one. However, as stated before, concrete stiffness (E-modulus) used in the model is of an unfavorable value. Nonetheless, the cross-section heights obtained in the case study are probably a bit slender. In other words, the bridges investigated might require a greater cross-section height in reality.

8.3 Recommendations

8.3.1 Practical recommendations

- First step in designing longitudinal reinforcement should be to determine the required reinforcement to limit the crack width resulting from the SLS bending moment.
- If reduction of deck height is desired and the space for additional support width is available, additional triangular segments should be applied. This is shown to be a very effective measure in reducing the governing loads and therefore facilitating reduction of the cross-section height.
- Centre-oriented traffic load configuration can lead to governing transverse sagging moment, and should therefore always be taken into account when possible.
- Placement of reinforcement in two layers is a great way of obtaining additional bending moment capacity. In the aim of designing a slender slab bridge, this should almost always be applied, or at least considered.
- Alternatives to lap splices allow a reduction of longitudinal reinforcement centre-to-centre distance from 3ϕ down to 2ϕ and therefore have the potential to unlock a great amount of additional capacity. However, they also induce new problems in terms of detailing and concrete compacting.
- The proper factor for uniformly distributed traffic loads (according to the Eurocode) should be applied.

8.3.2 Recommendations for future work

- Besides reinforced concrete, prestressed concrete sometimes offers a solution in highly skewed concrete slab bridges (although prestressed girder bridges are more common). In this thesis, the reinforced concrete slab is assumed to be of isotropic concrete material. In the case of prestressed concrete, the bridge deck will tend to span more in the direction of the cables. It would therefore be interesting to set up a parametric tool for research of prestressed skewed slab bridges and to investigate the differences between reinforced and prestressed bridges with similar geometry.
- Integral bridges are also often applied as a solution for skewed bridge problems. They basically span in a monolithic way from abutment to abutment. Although construction of such bridges is often more expensive, they require less maintenance because no bearings or expansion joints need to be applied. A parametric study can be conducted on integral bridges, in order to explore their advantages and limitations.
- In the parametric study, a rather conservative value was chosen for a span/height ratio. This ratio related the straight span (perpendicular direction from support line to support line) to the total deck height. However, it is more realistic to incorporate the skew angle in some way into the span to height ratio. One option would be to relate the skewed span length (free edge length) to the deck height. This way, the effect of the skew angle is incorporated in the span/height ratio: higher skew leads to a longer skewed span thus requires a higher deck height. Alternatively, a fictional span length could be determined, based on the direction of the maximum main principal bending moment for instance, which could then be used to determine a (fictional) span to height ratio.
- In search of the most governing location for tandem systems, a more repetitive workflow can be used. In this thesis, the tandem systems were placed on bridge in increments of $\frac{1}{10}$ of the span length. In the second calculation of a repetitive workflow, 10 new locations could be

tried in between the 2 most governing locations found in the first calculation, in order to find a more precise value and location for the sagging moments.

- Further research could focus on determination of rules of thumb. Input would be the required width of the driveway, length of the straight span and initial road skew angle. The most important outcome would then be the thickness of the bridge deck and the angle β of the additional triangular segments to be added. In order to set up these rules of thumb, more thorough research into reinforcement design and detailing requirements and limitations is needed.

- Regarding the distribution of shear forces in the edge zone of skewed concrete slabs, test experiments should be conducted. The concrete capacity of redistribution for both slabs with and without shear reinforcement should then be investigated, as well as the influence of the skew angle on this distribution capacity.

- It has been shown that the shear forces resulting from sectional averaging over a length of $2 * d$ can be taken up by shear reinforcement, even for highly skewed bridges. Since the shear force along the edge increases towards this edge, averaging over a smaller length will lead to a higher value. It can therefore be investigated for which section length (smaller than $2 * d$), shear forces near the obtuse corner edge can still be taken up by shear reinforcement without having to increase the cross-section height for increased shear capacity. The advantage of more shear reinforcement near the edge zone is reduced (shear) crack width, which leads to improved durability.

- An other interesting topic is to investigate if under an assumed shear force distribution length of $4 * d$, an angle β for the ATS addition could be found for which shear reinforcement is no longer necessary.

Bibliography

[1] *Google Earth Pro*. URL: https://www.google.com/earth/versions/#earth-pro.

[2] Alexander de Haan and Elianne de Regt. *Graduation - Challenge Accepted*. 2014, p. 188. ISBN: 9789462364868.

[3] *A9 - Google Maps*. URL: https://goo.gl/maps/P7Ban1C31EP2.

[4] *Draw.io | Most unreferenced images have been created with this online tool*. URL: https://www.draw.io/.

[5] *Structural Analysis and Design Software - SCIA Engineer*. URL: https://www.scia.net/en/software/scia-engineer.

[6] Johan Blaauwendraad. *Rapport 53 - Scheve platen: gelijkmatig verdeelde belasting*. Tech. rep. CUR, IBBC-TNO, 1972. URL: http://www.sbrcurnet.nl/producten/kennisarchief/scheve-platen-gelijkmatig-verdeelde-belasting.

[7] J. Blaauwendraad and Th. Monnier. *Rapport 58 - Scheve platen: puntlasten, temperatuur, dwars contractie coëfficiënt, verende ondersteuningen*. Tech. rep. CUR, IBBC-TNO, 1973. URL: http://www.sbrcurnet.nl/producten/kennisarchief/scheve-platen-puntlasten-temperatuur-dwarscontractiecoefficient-verende-ondersteuningen.

[8] Patrick Théoret, Bruno Massicotte, and David Conciatori. "Analysis and Design of Straight and Skewed Slab Bridges". In: *Journal of Bridge Engineering* 17.2 (2012), pp. 289–301. ISSN: 1084-0702. DOI: 10.1061/(ASCE)BE.1943-5592.0000249. URL: http://ascelibrary.org/doi/10.1061/%28ASCE%29BE.1943-5592.0000249.

[9] H. W. M. van der Ham. *Strokenverdeling voor het wapenen van scheve plaatveldviaducten*. 2004.

[10] C Menassa et al. "Influence of skew angle on reinforced concrete slab bridges". In: *Journal of Bridge Engineering* 12.2 (2007), pp. 205–214. ISSN: 1084-0702. DOI: 10.1061/(ASCE)1084-0702(2007)12:2(205). URL: http://www.scopus.com/inward/record.url?eid=2-s2.0-33847148425&partnerID=40&md5=e4d3a551bab56c1245d4d552812dff13.

[11] Denby Grey Morrison and Gustav R. Weich. "Free-Edge and Obtuse-Corner Shear in R/C Skew Bridge Decks". In: *ACI Structural Journal* 84.1 (1987), pp. 3–9. ISSN: 08893241.

[12] Th. Monnier. *Rapport 54 - Wapenen van platen*. Tech. rep. CUR, IBBC-TNO, 1972, p. 62. URL: http://www.sbrcurnet.nl/producten/kennisarchief/wapenen-van-platen.

[13] C.R. Braam and F.G. de Haas. "Wapenen op basis van belastingen in- en/of uit-het-vlak". In: 12 (1993), pp. 54–59.

[14] René Braam and Johan Blaauwendraad. "Van spanning naar wapening". In: *Cement* (2014), pp. 28–31.

[15] George E. P. Box. "Science and Statistics". In: *Journal of the American Statistical Association* 71.356 (1976), pp. 791–799. URL: http://ir.obihiro.ac.jp/dspace/handle/10322/3933.

[16] Bill Venners. *The Making of Python*. 2003. URL: https://www.artima.com/intv/pythonP.html.

[17] Prof. Dr Ir. Jacco Hoekstra. "Goodbye Matlab! Hello Python!" In: *Leonardo Times* (2012), pp. 24–25. URL: https://repository.tudelft.nl/islandora/object/uuid%3A677d695b-2030-4032-b0be-93c2a93fd858.

[18] Normcommissie 353 068 "Opleggingen". *NEN-EN 1337-3: Structural bearings - Part 3: Elastomeric bearings*. 2005.

[19] Normcommissie 351 001 "Technische Grondslagen voor Bouwconstructies". *NEN-EN 1990: Eurocode: Basis of structural design*. 2013.

[20] Normcommissie 351 001 "Technische Grondslagen voor Bouwconstructies". *National Annex to NEN-EN 1990: Eurocode: Basis of structural design*. 2017.

[21] Normcommissie 351 001 "Technische Grondslagen voor Bouwconstructies". *NEN-EN 1991-1-5: Eurocode 1: Actions on structures - Part 1-5: General actions - Thermal actions*. 2011.

[22] Normcommissie 351 001 "Technische Grondslagen voor Bouwconstructies". "National Annex to NEN-EN 1991-1-5: Eurocode 1: Actions on structures - Part 1-5: General actions - Thermal actions". In: december (2011).

[23] Normcommissie 351 001 "Technische Grondslagen voor Bouwconstructies". *NEN-EN 1991-2: Eurocode 1: Actions on structures - Part 2: Traffic loads on bridges*. 2015.

[24] Normcommissie 351 001 "Technische Grondslagen voor Bouwconstructies". *National Annex to NEN-EN 1991-2: Eurocode 1: Actions on structures - Part 2: Traffic loads on bridges*. 2016.

[25] Normcommissie 351 001 "Technische Grondslagen voor Bouwconstructies". *NEN-EN 1992-1-1: Eurocode 2: Design of concrete structures – Part 1-1: General rules and rules for buildings*. 2011.

[26] Normcommissie 351 001 "Technische Grondslagen voor Bouwconstructies". *National Annex to NEN-EN 1992-1-1 Eurocode 2: Design of concrete structures - Part 1-1: General rules and rules for buildings*. 2014.

[27] Rijkswaterstaat. *Richtlijnen Ontwerp Kunstwerken 1.4*. 2017. URL: http://publicaties.minienm.nl/download-bijlage/97120/rtd1001-rok1-4-april2017.pdf.

[28] Rijkswaterstaat. *Richtlijnen Ontwerp Kunstwerken 1.4 - Bijlagendocument deel A*. 2017. URL: http://publicaties.minienm.nl/download-bijlage/97121/rtd1001-rok1-4-bijlagea-april2017.pdf.

[29] Rijkswaterstaat. *Richtlijnen Ontwerp Kunstwerken 1.4 - Bijlagendocument deel B*. 2017. URL: http://publicaties.minienm.nl/download-bijlage/97122/rtd1001-rok1-4-bijlageb-april2017.pdf.

[30] *Rijkswaterstaat | Onze organisatie*. URL: https://www.rijkswaterstaat.nl/over-ons/onze-organisatie.

[31] *Knooppunt Kethelplein - Google Maps*. URL: https://goo.gl/maps/EcJ2cWuyDACcqQdX8.

[32] B. V. Sindhu et al. "Effect of Skew Angle on Static Behaviour of Reinforced Concrete Slab Bridge Decks". In: *International Journal of Research in Engineering and Technology* (2013), pp. 50–58.

[33] Normcommissie 351 001 "Technische Grondslagen voor Bouwconstructies". *NEN-EN 1991-1-1: Eurocode 1: General actions - Densities, self-weight, imposed loads for buildings*. 2012.

[34] *Elastomeric Bearing with Steel Plate Reinforced*. URL: http://www.bridgebearing.org/bridgebearing/laminated-elastomeric-bearing-pad.html.

[35] S. Pinarbasi and U. Akyuz. "Investigation of Compressive Stiffness of Elastomeric Bearings". In: *6th International Congress on Advances in Civil Engineering* October (2004), pp. 6–8.

[36] *BrugLandhoofd.png*. URL: https://upload.wikimedia.org/wikipedia/commons/9/9a/BrugLandhoofd.png.

[37] *Free Beam Calculator | Used to create beam image | SkyCiv*. URL: https://skyciv.com/free-beam-calculator/.

[38] R.H. Wood. "The Reinforcement of Slabs in Accordance with a Pre-Determined Field of Moments". In: *Concrete* 2.2 (1968), pp. 69–76.

[39] *SCIA Engineer Help - Calculated results for 2D members*. URL: https://help.scia.net/17.0/en/index.htm#rb/results/calculated_results_for_2d_members.htm%3FTocPath%3DResults%7CResults%2520on%2520slabs%7C_____1.

[40] Eva O.L. Lantsoght, Ane de Boer, and Cor van der Veen. "Distribution of peak shear stress in finite element models of reinforced concrete slabs". In: *Engineering Structures* 148 (2017), pp. 571–583. ISSN: 18737323. DOI: 10.1016/j.engstruct.2017.07.005. URL: http://dx.doi.org/10.1016/j.engstruct.2017.07.005.

[41] J. Blaauwendraad. *Plates and FEM - Surprises and Pitfalls*. Vol. 171. Springer, 2010. ISBN: 978-90-481-3595-0. DOI: 10.1007/978-90-481-3596-7. URL: http://link.springer.com/10.1007/978-90-481-3596-7.

[42] J. Blaauwendraad. "Platen en programma's". In: *Cement* (2010), pp. 80–85. URL: https://www.cementonline.nl/artikel/platen-en-programmas.

[43] C.R. Braam. "Scheurwijdte". In: *Cement* 2 (2010), pp. 93–97. URL: https://www.cementonline.nl/artikel/scheurwijdte.

[44] *Euro Accessories Ltd - Reinforcement Couplers*. URL: http://www.euroacc.co.uk/products/reinforcement-couplers/.

[45] Tayyaba Sarwar. *Lap splice - Pinterest page*. URL: https://nl.pinterest.com/pin/482729653782198663/?lp=true.

[46] RJ COPE. "Flexural Shear Failure of Reinforced Concrete Slab Bridges." In: *Proceedings of the Institution of Civil Engineers* 79.3 (1985), pp. 559–583. ISSN: 1753-7789. DOI: 10.1680/iicep.1985.838. URL: http://www.icevirtuallibrary.com/doi/10.1680/iicep.1985.838.

[47] R.M. van Vulpen. *Strokenverdeling voor het wapenen van scheve plaatveldviaducten*. 2002.

[48] Marcel 't Hart. "Uitgangspunten QS Platen 2012 (PRB) - Scheefheidsfactoren 2012". 2013.

[49] C. J.A. Ter Berg et al. "Expert judgement based maintenance decision support method for structures with a long service-life". In: *Structure and Infrastructure Engineering* (2019), pp. 1–12. ISSN: 17448980. DOI: 10.1080/15732479.2018.1558270.

Appendices

A | Literature Review

A.1 Introduction

In order to understand the behaviour of reinforced concrete (RC), simply supported skewed slab bridges, a literature study is conducted. This study aims to get an insight into the current state of knowledge on the subject, and to provide a summarized overview of it.

The literature overview is divided into two parts, which both are fundamental in the structural design process of a RC skewed slab bridge:

- The effect of the bridge shape, size and loading on the force distribution in the bridge
- 'Translation' of force distribution into required reinforcement

A lot of the available literature does not actually focus on bridges, but on concrete plates, shells or slabs in general. This literature is still relevant because a concrete skewed slab bridge, with the right approach, can be modelled as such. As long as the boundary conditions are the same (simply supported in this case), the plate- and shell-models are able to provide valuable insights into behaviour of RC skewed slab bridges.

A.1.1 Definition of skew angle

When studying the available literature, a difference in definition of the skew angle was found. Most international literature written in English defined the skew angle as the angle of deviation from the 'standard' 90 degree crossing angle. However, from now on the Dutch definition will be used, as defined below:

The skew angle is the angle α, which is enclosed by the support line and the free edge

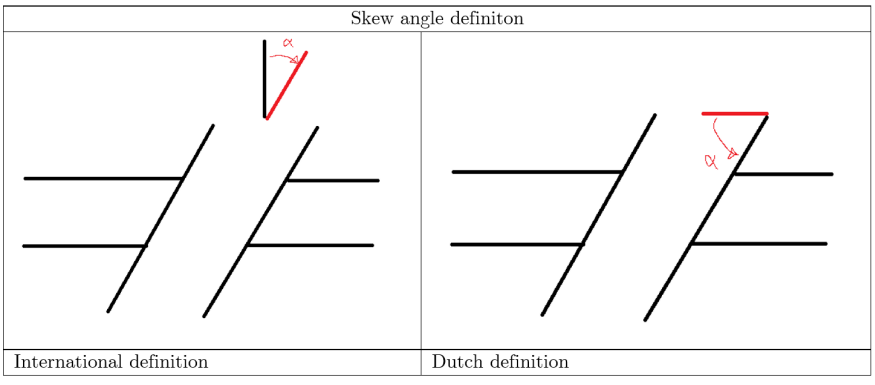

Figure A.1: Two definitions of the skew angle found in literature

This means that bridge with a higher skew is defined by a lower skew angle. Note that the international definition and the Dutch definition together make an angle of 90 degrees. As mentioned above, all skew angles found in literature are translated to the Dutch definition from now on (with the exception of some graphs and images, in which case it will be mentioned).

A.2 Part 1: Force distribution in a skew bridge

In the 1970's, a Dutch committee was doing research into the force distribution of skewed slabs (or plates). Back then, the committee already mentioned that solving a skewed plate problem with the help of a computer had become normal practice. Nonetheless, as they viewed it, extended knowledge and insights into skew problems could prove to be valuable for the design of skewed structures. This view from 50 years ago is still relevant today and partially describes the relevance of this thesis.

A.2.1 CUR Rapport 53: Scheve platen – gelijkmatig verdeelde belasting, Blaauwendraad, J. (1972) [6]

The first research of the committee into skewed plates is quite insightful, but also has its limitations. It only considers uniformly distributed loads and slabs supported by an infinitely stiff line support on two sides. Additionally, the poisons ratio used is 0.

Nonetheless, the research served as a good starting point for understanding the behaviour of skewed plates. Continuous plates are also investigated in the report, but they have been left out in this literature review as they are less relevant.

Back in the days, it was quite common to simplify a skewed slab by replacing it with an equivalent straight slab. The length of this equivalent slab was set as the length of the free edge of the skewed slab. The report mentions that this method of simplification may lead to a useful structure, but it does not give any insight into the actual behaviour of a skew plate.

Gaining insight into skewed slab behaviour is done by analyzing the force distribution in a number of representative slabs. The paper mentions two options to do so: using the yield-line theory and theory of elasticity. The first one is not really suitable, since each load case leads to a different yield pattern, which means that the principle of superposition cannot be applied. This leaves the latter option, which can make use of superposition, making it a more suitable option.

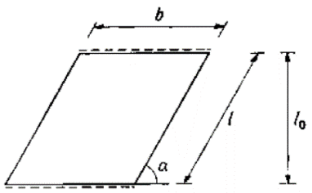

Figure A.2: Definitions of the length and width as used in [6]

The report focusses on slabs with a skew angle of 45° and 60° degrees, while a slab with a skew angle of 90 degrees (straight bridge) is used for comparison. The dimensions of the bridge are expressed in terms of slenderness as b/l, where b is the width of the support line and l the length of the free edge. Three different values for the slenderness are considered:

- $b/l = \frac{1}{2}$, a slender plate
- $b/l = 1$, which is explained as a crossing of two roads of equal width (equal amount of lanes)
- $b/l = 2$, a wide plate

The plates in this report are analyzed with the finite element method (FEM), where triangular elements were used. It is mentioned that an accurate calculation of moments requires the use rather small elements.

Trajectories of the principal moments

The results show that a skew plate prefers to span in a direction perpendicular to the support line. This effect is stronger for wider plates, while smaller plates show a greater deviation from the effect.

The effect of the skew angle on the trajectories is investigated for slabs with a slenderness of $b/l = \frac{1}{2}$, and displayed in the image below. Due to symmetry, only top half of the plates (lengthwise) are displayed. It can be observed that at mid-span, trajectories in the transverse direction are almost straight. Trajectories in longitudinal directions enclose an angle ϕ with the centre line parallel to the support line. This ϕ shows the direction in which the slab tends to span.

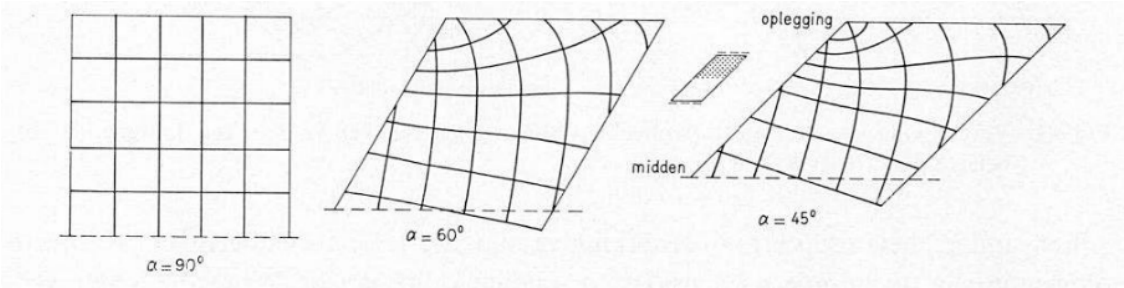

Figure A.3: Trajectories of half a bridge for different skew angles from [6]

The angle ϕ is also graphically displayed in the image below, which shows that when the angle α decreases (skew increases), the longitudinal trajectory at the centre also decreases, but at a lower rate. In the report, this is noted as the plate which, with a 'sense of dislike', starts to span in a direction parallel to the free edge.

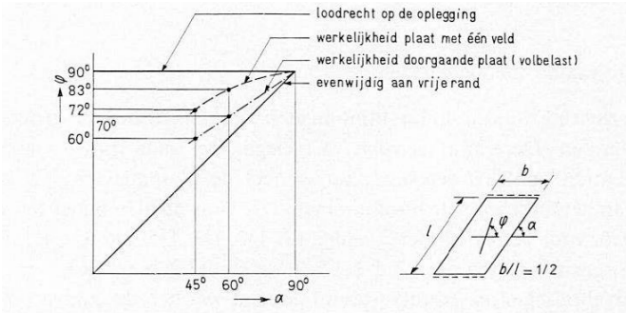

Figure A.4: Longitudinal trajectory angle φ versus the skew angle α from [6]

A last important conclusion drawn with respect to the trajectories, is that the image of trajectories near the obtuse corner should be seen as independent of (not influenced by) the slenderness ratio b/l. The report speaks of a corner solution, which is to be used as a correction on the total image of a plate (which does depend on the b/l ratio).

Magnitude of the principal moments

The biggest value of the principal moment m1 is usually found along the free edge. For a straight slab ($\alpha = 90°$) this point, at a distance c from the obtuse corner, lies halfway along this edge. As a plate becomes more skew, this point of maximum moment shifts towards the obtuse corner. The limit for distance c, for an infinitely wide slab lies at $0.35l$ for $\alpha = 60°$ and $0.30l$ for $\alpha = 45°$, where the principal moment have magnitudes of $0.130ql_0^2$ and $0.143ql_0^2$ respectively ($0.125ql_0^2$ for straight plate). Further research once again shows that for an increasing width the value of m1 approaches the value of a straight plate, which means that this part of the plate can be seen as rectangular.

Support reactions and deflections

As mentioned before, the line support considered here is assumed to incompressible. The distribution of reaction force in the line support can be described as the sum of a few reactions: a constant distributed support reaction along the entire line, a concentrated support reaction near the obtuse

corner and a concentrated moment in the obtuse corner. This moment means that in some situations, a part of the line support near the obtuse corner will have to provide a tensile support reaction.

When translating line support into support reactions in discrete supports (bearing pads), the concentrated moment in the obtuse corner should be replaced by a force couple in the first two pads of this obtuse corner. Additionally, the constant support reaction should be divided over the supports, where the load on the two outer pads should equal half the value of the inner pads. It is mentioned that creating any support configuration that leads to a concentrated moment or tension is undesirable and should be avoided.

Graphs in the report show that similar to the maximum bending moment, the point of maximum deflection at the free edge slightly shifts towards the obtuse corner as plate skew is increase (angle α is decreased). Considering the deflection in the centre line of the span (parallel to support line), the deflection is the smallest in the centre and increases towards the free edge. This effect increases with the increase of skew.

A.2.2 CUR Rapport 58: Scheve platen – puntlasten, temperatuur, dwarscontractiecoëfficiënt, verende ondersteuningen. Blaauwendraad, J. & Monnier, T. (1973) [7]

This report should be seen as an addition to the previous report A.2.1. Its goal is to provide insight into the force distribution and behaviour of skewed slabs, in terms of:

- The effect of concentrated loads
- The effect of a temperature gradient over the height of the plate
- Application of a poisons ratio of 0.2
- The influence of discrete, elastic supports

To study these effects, plates with a slenderness of $b/l = 1$ and a skew angle of $\alpha = 45°$ are considered. The report also considers continuous plates, but they are left out of this literature review.

Point loads

When increasing the span of skew plates, load systems will start to behave more like local point loads. For this reason, a few characteristic positions for point loads are chosen to investigate bending moment behaviour. The magnitude of the bending moments is expressed in Pl_0/b, where P is the point load, l_0 the span perpendicular to the support line and b the width of the support line. Over a cross-section at mid span of a skewed slab subjected to central point load P, the total bending moment equals $\frac{1}{4}Pl_0$ and the average bending moment is $\frac{1}{4}Pl_0/b$. The expression of the bending moments in Pl_0/b therefore allows for easy comparison and a dimensionless overview.

For the first comparison, three different location for the point load are compared. The location of the point load is denoted by two coordinates: (relative distance along support line, relative distance along free edge), where the origin lies in the obtuse corner. The three locations of the point load considered are: $P(\frac{1}{2}, \frac{1}{2})$, $P(\frac{1}{4}, \frac{1}{2})$ and $P(0, \frac{1}{2})$. Comparison of the bending moment trajectories that follow from the three point loads at their different locations confirm that the conclusions from the uniformly loaded skew plates from report 53 do not significantly change. The point load at the free edge $P(0, \frac{1}{2})$ leads to the biggest change in trajectories, although trajectories along the free edge still coincide with the ones from the uniformly loaded plates.

Considering elementary plate theory, changes in shape can only be caused by bending and torsional moments. Point loads lead to an infinitely large bending moment on an infinitesimal element. However, in the report, numerical approximation is applied, which makes this phenomena

impossible to occur. Practically speaking, the point load is replaced by an equivalent distributed load over a small area the size of an element. Earlier CUR reports advise taking into account a moment of $P/3$ underneath a point load, as an approximation. For the plates considered in this report with a skew angle of 45°, this equals 0.47 Pl_0/b.

When comparing the advised equivalent 0.47 Pl_0/b, the biggest moment found caused by the central point load $P(\frac{1}{2}, \frac{1}{2})$ leads to a greater principal moment, having a value of 0.55 Pl_0/b. The smallest principal moment (90° direction from principal moment) has a value of 0,37 Pl_0/b. Taking the average value of those two, a value of 0.46 Pl_0/b is found, which is really close to the equivalent value as advised in earlier reports. A bit surprised about the remarkably accurate result produced, the report concludes that dispersion of the load in the applied system of elements matches the earlier found results. It also concludes that even in the area close to the point load, the moments calculated should be considered as a reasonably accurate reflection of 'reality'.

Moving the point load towards the free edge creates a bigger different between the two principal moments. The point load $P(\frac{1}{4}, \frac{1}{2})$ leads to moments of 0.63 Pl_0/b and 0.32 Pl_0/b (average of 0.475 Pl_0/b). A point load $P(0, \frac{1}{2})$ which is applied at the very edge, gives a major principal moment of 1.36 Pl_0/b, while the minor principal moment almost equals zero. It can be observed that a point load at the edge tends to generate a major principal moment in the direction of the free edge. When moving the point load away from the free edge, the direction of the major principal moment quickly changes to span-span direction.

As mentioned before, a point load at the free edge of the skew plate generates the biggest bending moment. Putting a point load on the free edge at a quarter distance from the obtuse corner $P(0, \frac{1}{4})$ or at three quarters distance $P(0, \frac{3}{4})$ gives major main bending moments of 1.25 and 1.26 Pl_0/b. Again, comparison with values (corrected for the 45° skew) from a straight plate shows differences are very small. The report finally notes that in reality, point loads will never be on the very edge of a slab/bridge, but always a bit more inwards. Nonetheless, the magnitude of those moments found are accurate.

A point load on or near the free edge has a remarkable effect in the obtuse corner. Here, a large negative minor principal moment m_2 can be found, with maximum values of –1.0 Pl_0/b. Nothing is mentioned on the cause of this moment.

The magnitudes of the principal moments found when placing a point load along the free edge as described above, where found for a ratio of slenderness b/l of $\frac{1}{2}$. These magnitudes can also be used for wider plates ($b/l > \frac{1}{2}$), but they do not apply for plates smaller than $b/l = \frac{1}{2}$ .It can be concluded that for the plate with a skew angle of 45° investigated here, bending moments found are in agreement with the magnitudes found in a straight plate. It would be interesting to investigate whether this is still the case for an even skewer plate, when $\alpha = 30°$.

It can be concluded that a load system on a skewed slab bridge, when compared to a uniformly distributed load, does not lead to significant changes in terms of principal moments and their trajectories, only their values might change. A point load P in the centre of the skew plate will lead to moments with a magnitude of $P/3$, while a point load P on or very near the free edge will have the order of magnitude of P.

Temperature effects and Poisson's ratio

When concrete changes temperature, it wants to deform. If such deformation is restricted, stresses will appear in the concrete. It is therefor important to look at the temperature gradient in a skewed plate. A constant temperature gradient over the height of the plate, will lead to normal deformations in an unrestrained plate. A gradient that is not constant over the plate height gives rise to curvature. Where a restrained normal deformation leads to normal stresses, a restrained curvature leads to bending moments.

It is shown that when a skewed plate is subjected to a linear temperature gradient over its height, the greatest principal moment is in the direction parallel to the support line. This is explained by the fact that deformations in the direction of the supports is constrained. The minor principal

moment works in a direction that is almost perpendicular to the support line. However, its values are hardly significant besides the values along the free edge.

Effects on the support reactions can be explained as a bending moment in the obtuse corner, to be taken up by a support couple (compression in edge support, tension in the next support on the inside). Additionally, a great compressive force is to be taken in the very end of the acute corner.

Next, the report checks whether incorporation of a poisons ratio of 0.2 instead of 0 makes a significant difference. It can be concluded that this is not really the case. Longitudinal bending moments are not really influenced by the poisons ratio. It is observed that slightly bigger transverse moments are generated. However, as these transverse moments are still well below the capacity of the minimal transverse reinforcement capacity, they do not need much attention.

Elastic supports

In case a bridge would be subjected to only one, non-changing load throughout its lifetime, it would be possible to choose the support configuration (amount of pads, distance and elasticity) in such a way that the support reactions are equal to those of an infinitely stiff support. In reality however, the loads in a bridge will vary over the lifetime. In practice, skewed slab bridges are supported by bearing pads of equal elasticity at equal distance. This configuration will allow for a more favourable distribution of reaction forces compared to stiff line support (as was the case in CUR report 53).

The redistribution depends mostly on the elasticity of the pads and the distance between the pads. Influence of these parameters is investigated, once again for a plate with slenderness ratio of $b/l = 1$ and skew angle $\alpha = 45°$.

Stiffness of the supports is chosen with respect to the dimensions of the skewed slab. First of all, the total reaction force R on one side of the slab equals $\frac{1}{2}qbl$. Next, the deflection w is expressed in terms of this reaction force, which becomes:

$$w = \frac{5}{192}\frac{Rl^3}{Kb} \tag{A.1}$$

Using:

$$K = \frac{Eh^3}{12} \text{ (for } v = 0) \tag{A.2}$$

the expression for w becomes:

$$w = \frac{5}{16}\frac{Rl^3}{Ebh^3} \tag{A.3}$$

The relation between the support reaction R and the deflection at midspan w is in the order of magnitude of Ebh^3/b^3. This relation can be seen as an equivalent stiffness for the plate itself. Next, the elastic stiffness of the support Cv is defined as the total force required to compress all bearing pads in a support line, over a distance of unit length. Finally, a parameter for the relation between plate stiffness K and support stiffness Cv is defined as f:

$$C_v = \frac{1}{f}\frac{Ebh^3}{l^3} \Leftrightarrow f = \frac{1}{C_v}\frac{Ebh^3}{l^3} \tag{A.4}$$

Investigation of the support configuration is done for a few values of parameter f. For an equal plate stiffness, a smaller f leads to a greater support stiffness. Hence, if $f = 0$, the support is infinitely stiff and represents a rigid support.

The report mentions that prestressed slabs can be represented by $f = 0.002$, while reinforced plates in uncracked condition can be represented by $f = 0.02$. Finally, a value of $f = 0.2$ is mentioned to be a boundary value for slabs found in practice, and is therefore also used in the research.

Besides the different values for f, the number of support pads is varied because it was suspected that application of a small number of pads might lead to different directions for the principal

moments. The division of the support line into n equal parts, makes the distance between the blocks b/n. The number of required support pads then becomes $n+1$. For n, values of 2,4,8 and 16 are investigated. The moments calculated are expressed in ql_0^2, while the average support reaction per pad is expressed as $\frac{1}{2}qF/(n+1)$ and the deflections are denoted as ql_0^4/K.

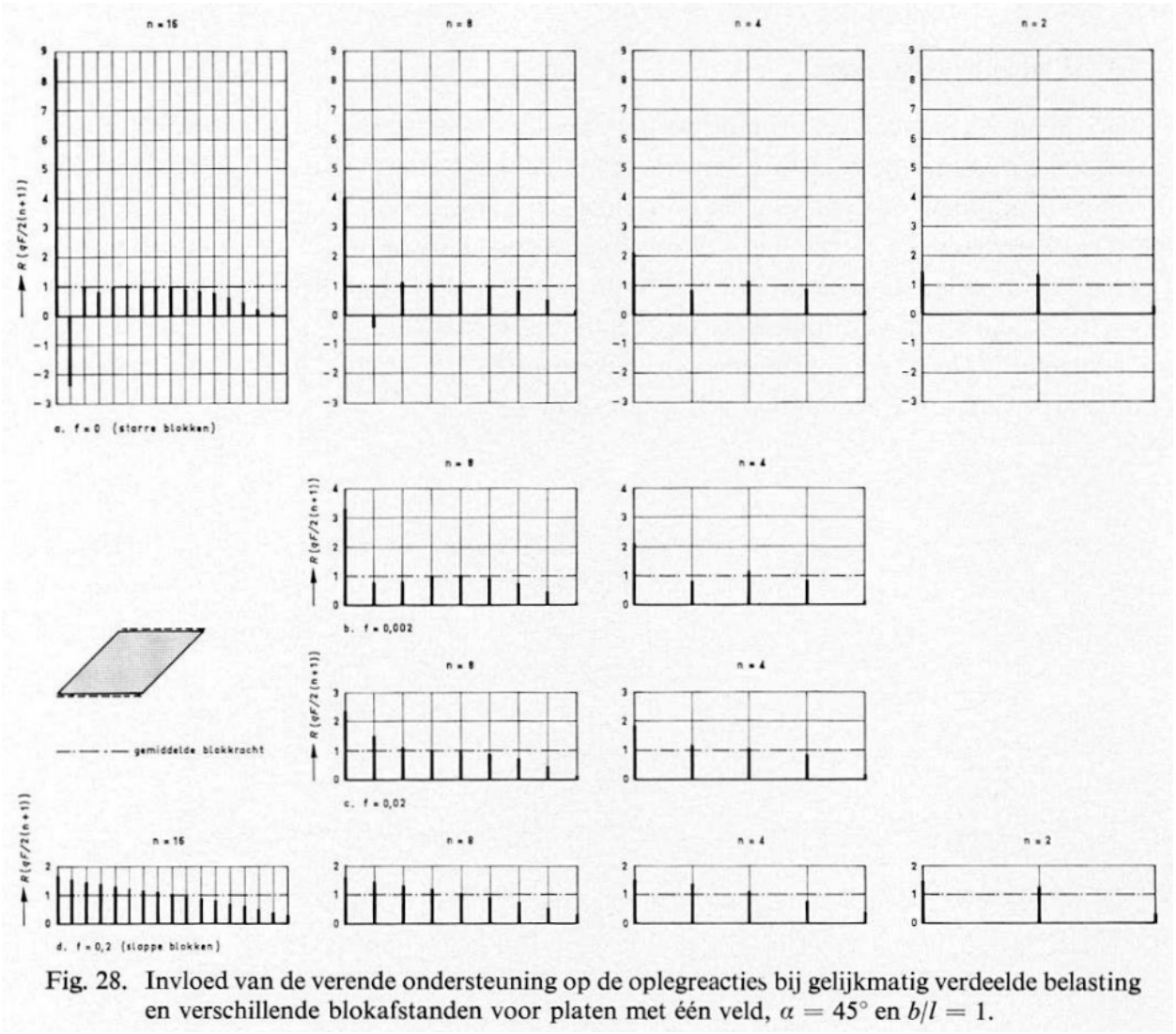

Fig. 28. Invloed van de verende ondersteuning op de oplegreacties bij gelijkmatig verdeelde belasting en verschillende blokafstanden voor platen met één veld, $\alpha = 45°$ en $b/l = 1$.

Figure A.5: Display of support reaction distribution from uniformly distributed load, for varying support stiffness (top images show rigid supports, lower more elastic) and for different number of supports (amount of lines per plot: n+1) from [7]

When considering the principal moments, it is observed that for rigid support pads, variation in the pad distance n (related to number of pads) makes no notable difference. Additionally, for a certain number n, variation of f makes a small difference. Only the minor principal moments at f = 0.2 show a noticeable difference, but not of great importance.

Looking at the individual support reactions, the number of pads does make quite a difference. For rigid supports ($f = 0$), the tensile reaction near the obtuse corner (in the 2^{nd} pad from obtuse corner) disappears when the amount of pads is reduced (present at $n = 16$ and 8, disappeared for n =4 and 2).

When looking at the support reactions, differences are big between very elastic ($f = 0.2$) and rigid supports ($f = 0$), especially for a larger amount of supports ($n = 16$ and 8). The very elastic supports clearly show a more evenly distribution of support reactions. The highest support reaction for n=16, present in the obtuse corner can be reduced to about 20% of the value for rigid supports.

For $n = 8$, this obtuse corner reaction can be reduced to about 40% of the corner value for rigid supports.

The conclusions on the support reactions for $f = 0.2$ mostly count for $f = 0.02$ (reinforced slab) as well. The reduction on the corner reaction force when going from rigid support to $f = 0.02$ is now a bit smaller: it is reduced to 60% of the rigid value. Looking at the difference between rigid supports and $f = 0.002$, the reduction has become even smaller: 80% of the original peak reaction in the obtuse corner remains.

Deflections of the slab increase with more elastic supports. Similar to support reactions, the deflections in the obtuse corner are the largest. As the supports become more elastic, the deflection pattern of the support line starts to resemble the deflection pattern in the centre of the slab.

Summarizing, it can be concluded that the influence of the bearing pad properties and their relative distance (related to number of pads) on the bending moments in a skewed slab are small. However, the support configuration does have a big influence on the support reactions. As the relative stiffness of the supports (slab stiffness divided by support stiffness) increases, a more equal distribution of reaction forces can be observed. Additionally, tensile reaction forces disappear. The obtuse corner reaction force for a reinforced slab ($f = 0.02$) can become twice as big as the average reaction force, whereas the corner reaction force in a prestressed slab ($f = 0.002$) can become three times as big as the average.

A.2.3 Flexural shear failure of reinforced concrete slab bridges, Cope, R. (1985) [46]

This paper elaborates on a research into reinforced concrete slab bridges with a skew angle, and focusses on flexural shear failure. The paper was published in 1985 in England. It states that at the time, the English codes did not give any guidance for flexural shear failure due to wheel loads. It also states a lack of guidance on punching shear perimeters for closely spaced bearings. Five one-fifth scale models of skewed slab bridges are tested, with skew angles of 60, 45 (3 slabs tested) and even 30 degrees (very skew). All slabs tested had a thickness of 100 mm, a free edge of 1880 mm and a width of 1880 mm. The tests are set up to produce shear failure.

Shear forces were not measured directly, shear cracking was detected only when it intersected slab surface. Development of visible shear cracks and the reactions were recorded, and have been reported. Other data was not reported. It is concluded that ductile behaviour after initial shear cracking can be provided by making sure that there is continuity between the top and bottom reinforcement layers. This also increases the length of the cross-section that provides shear resistance at failure.

The article concludes that a punching shear calculation is appropriate for slabs in which the obtuse corner bearings carries most of the loads. This is the case for most skew bridges, and the obtuse corner bearing carries (relatively) more load as a bridge becomes more skew. Shear behaviour found during the tests in the opposite obtuse corners of slabs were seen to produce very similar results (makes sense due to symmetry).

A.2.4 Free-edge and obtuse-corner shear in R/C skew bridge decks, Morrison, D., Weich, G. (1987) [11]

Somewhere in the US, a road-over-rail bridge was constructed. It consisted of three spans and had an angle of skew of 40 degrees. Soon after construction, inclined cracks were observed along the free edge of the longest span.

The aim of the study is to investigate cracking in the obtuse corner and along the free edge due to shear forces. The bridge type studied here is simply supported RC skew deck bridge. For investigation, two models of quarter-scale are tested in a lab, where the reinforcement ratio and the amount of stirrups was varied.

The meaning of the two test slabs is as following:

- slab 1 is supposed to represent the actual bridge
- slab 2 is an improved version of slab 1, where flexural reinforcement is added as well as stirrups to prevent the cracking at the edge. The aim of the improvements is to 'force' a punching shear-like failure in the obtuse corner.

The test slabs have a span of 6.2 m, a width of 3.4 m, and a thickness of 0.25 m. The slabs were subjected to an additional dead load, which totals three times the weight of the slab itself, to compensate for the smaller scale of the experiment slabs.

For both slabs, longitudinal bottom reinforcement is placed in the direction parallel to a line from obtuse to obtuse corner (which equals a skew angle of 70°). Transverse reinforcement is placed in a direction parallel to the support lines. Model 2 was also given additional stirrups at the free edge. An overview of the reinforcement layouts can be found below.

Horizontal reinforcement

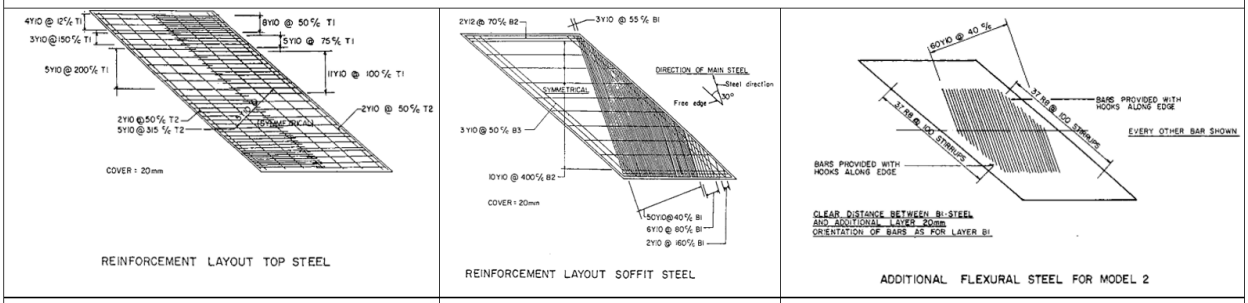

Top reinforcement in longitudinal and transverse direction	Bottom reinforcement (reinforcement only displayed on half the plate)	Model 2: additional flexural reinforcement in the bottom layer

Figure A.6: Longitudinal (horizontal) reinforcement applied in the test models of [11]

Shear reinforcement

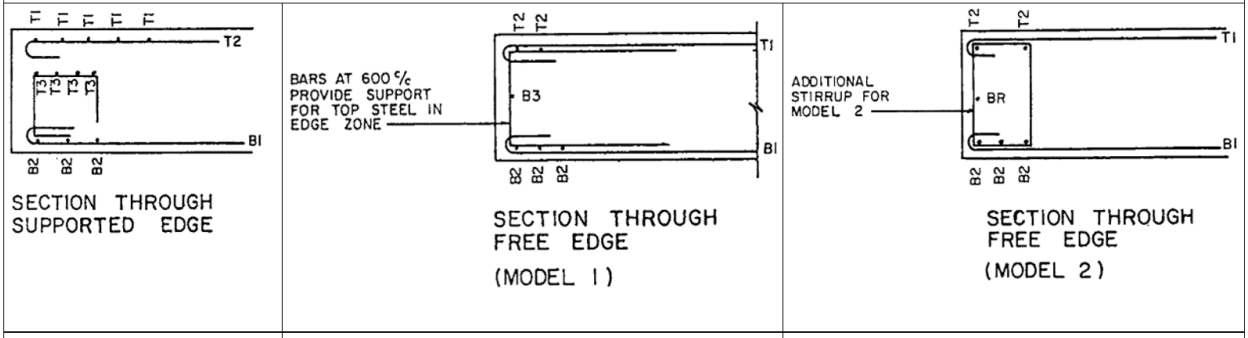

Support	Free edge of model 1	Free edge of model 2

Figure A.7: Shear reinforcement applied in the test models of [11]

The supports of the quarter-scale models were designed to have the same relative stiffness between the reactions as in the original bridge. The picture below shows the test setup. Notice that in the obtuse corner, the distance between the first three supports is larger compared to the rest. This is done to increase the effect of punching shear.

Results from the tests can be found below:

Flexural strength The flexural strength was first calculated by using measured concrete and streel strength properties. A yield line was assumed parallel to the support line. The flexural

strength of slab S1 behaved as expected and reached a load that was within 5 percent of the calculated flexural strength (based on the yield line). The flexural strength found for the improved slab S2 was 60 percent higher than for S1. However, the calculated value for S2 was 30% higher than the value reached in the test. It was concluded that S2 did not achieve a flexural failure.

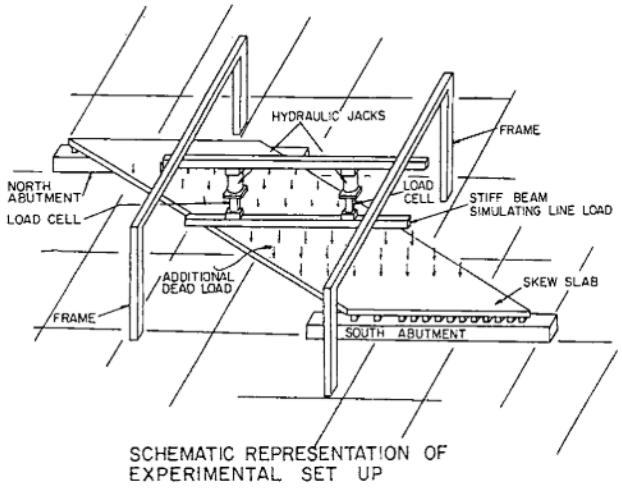

Figure A.8: A schematic overview of the experiment set up from [11]

Obtuse corner shear When the maximum load capacity was reached by the first support in the obtuse corner, the capacity of this support remained almost constant, although the crack width in the obtuse corner increased severely from 0.1 mm up to 10 mm. Increasing the load on the slab even further showed that now the second support took most of this additional load.

Calculation of an average prevailing shear stress around the obtuse support once it reached its maximum capacity were in good agreement with calculated shear stress capacity. The ratio of the maximum capacity of the obtuse support of S1 versus S2 showed relation similar to the concrete (shear) strength properties measured in those slabs.

Finally, the fraction of total load taken by the obtuse corner was measured and calculated. Calculation was done (in a different article) with elastic thin plate theory (which neglects shear deformations), where a value of approximately 40 percent was found. The experiment with slab S1 and S2 showed that for values between full dead load and strength limits, a value of 42 percent was found which corresponded with the calculated value.

Free-edge shear When analyzing the skewed slab bridges with elastic thick plate theory, high shear stress concentrations along the free edge become visible. The article mentions that it was hard to quantify those stresses in the experiment slabs. In the free edge between the obtuse corner and the loading position (halfway at span), inclined cracks where found. Those cracks started appearing at a load level just above the full dead load. The cracks increased in size as the applied load was increased, although cracks in S2 did not grow above 0.3 mm in size. Despite a smaller load applied, the cracks in S1 grew up to 3 mm. This difference was caused by stirrups with were placed in S2, but were not present in S1.

Serviceability and strength The image below shows a plot of the total load versus the mid displacement, where the circles mark different stages throughout the loading process. At a load level of 'only' 1.2 times the dead loads, cracks in slab S1 had developed to 0.3 mm, which could lead to serviceability problems. For S2, crack width at such load remained limited to 0.1 mm.

In the obtuse corner, inclined cracks started to grow quite rapidly after appearing. However, as mentioned before, Slab S1 still obtained its flexural strength limit, despite the obtuse corner cracks.

Therefore, it can be said that the obtuse corner cracks did not lead to a strength reduction.

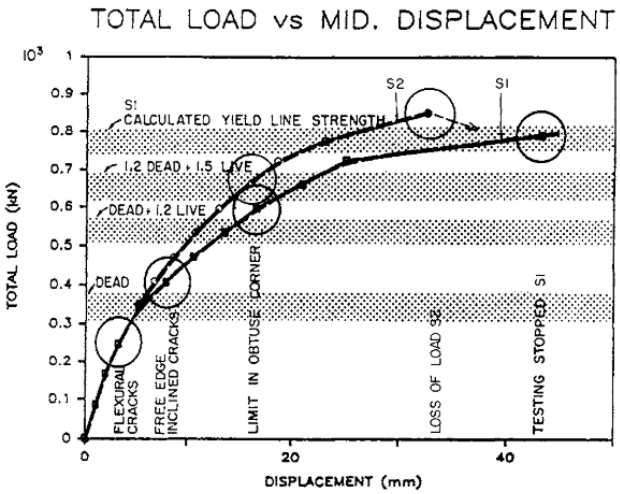

Figure A.9: A plot of the applied load versus the displacement for the two different test models from [11]

Conclusions:

The report mentions 10 conclusions, which are summarized below:

- The flexural strength, also called the yield-line limit, was hardly influenced by the inclined cracks along the free edge and the shear stresses in the obtuse corner.
- The assumption of a flexural failure under a yield-line at mid span (parallel to the supports) lead to a calculated ultimate strength of the slab that was very close to the actual capacity of slab S1
- The calculated shear stress at a distance of $d/2$ from the obtuse support (d being the effective depth) was within 30 percent of the calculated shear strength of the concrete, so not that accurate.
- The obtuse corner showed remarkable ductility, carrying up to 75% of the specimen strength, even though severe cracks were present.
- In a range from dead load up to obtuse corner limit, the obtuse corner supports carried about 40% of the load found through calculation as well as experiment.
- Linear analysis using thick plate theory, which incorporates shear deformations, showed a satisfactory accurate prediction of shear stresses along the free edge, which could be taken up by stirrups.
- The inclined cracks along the edge could be problematic in terms of serviceability (crack width), although they did not affect the strength of the skewed slab.
- The quarter-scale tests proved to be sufficiently accurate for prediction of shear related behaviour, even though aggregate size was of the scale models was the same as in the real bridge.
- A design guide with respect to shear stresses for punching shear is proposed. However, this design guide may only be valid for a similar slab as considered in the experiment. Changes in bearing configuration, as well as slab dimensions and skew probably require a different design guide.

- It is proposed to conduct further tests which investigates support spacing, skew effect and reinforcement detailing.

A.2.5 Influence of skew angle on reinforced concrete slab bridges, Mennassa et. al. (2007) [10]

As the title mentions, this paper investigates the influence of the skew angle on simply supported reinforced concrete slab bridges. It reports on a study where 96 case study bridges where subjected to finite element analysis: (4 span lengths x 4 lane configurations x 6 skew variations = 96 bridges):

- Span lengths 7.2 – 10.8 – 13.8 – 16.2 m
- Lane configurations: 1 – 2 – 3 – 4 lanes
- Skew angles: 90° – 80° – 70° – 60° – 50°

The bridges are subjected to a truck load HS-20 as defined in the AASHTO (American Association for State Highway and Transportation Officials) codes. FEM results from the truck loads are reported, and compared to two different codes:

1. AASHTO standard specifications
2. AASHTO LFRD Design specifications procedure

Comparison of the results with the codes showed that the codes overestimated the longitudinal bending moment, where the overestimation increased as skew increased (angle of skew decreased). Further elaboration on code comparison is not really relevant here. Looking at the results however is interesting.

In the parametric study, the maximum longitudinal bending moment for the skewed bridges is compared to the maximum value for a straight bridge, and expressed in a ratio of the skewed moment divided by the related straight moment M_α/M_0:

- Skew angle 90-70 degrees – ratio is almost 1
- $60 <$ skew angle < 66 – ratio goes to 0.75
- Skew angle 40 – ratio is 0.5

The ratios above show that as skew increases, the longitudinal bending moment ratio decreases. At the same time, a similar ratio for the transverse moment (TM_α/TM_0) will increase by up to 75% as skew angle drops from 90 to 40 degrees.

The ratio between the FEA maximum deflection under live-load for skewed and straight bridges decreases with skew angle decrease:

- Skew angle > 80 – ratio is one
- $40 <$ skew angle < 50 – ratio decreases to 0.6

An important recommendation given in the article is that bridges with a skew angle greater than 70 degrees, can be designed as straight (non-skewed) bridges. Once the skew angles goes below the 70 degrees, it is recommended to perform 3D finite element-analysis.

A.2.6 Analysis and design of straight and skewed slab bridges, Théoret, P., Massicotte, B., Conciatori, D. (2012) [8]

Nowadays, it is becoming increasingly easy to perform refined analysis as software becomes more easy to use and hardware capabilities have vastly increased. However, this does not necessarily mean that simpler, less refined methods for analysis become useless. Simple methods and models can still be used for verification purposes or in early design stages.

This research is aimed at determining bending moments and shear forces, which are required to conservatively design skewed concrete slab bridges using the equivalent-beam method. While the method is still used in North American bridge codes (both American and Canadian), it is not popular in the Netherlands. Therefore, conclusions from the report in terms of the equivalent-beam method are not really relevant for this literature study, but the general findings on skewed bridge behaviour are relevant.

It is mentioned that the 2006 collapse of the Concorde bridge, a deep cantilever solid slab bridge in Canada, raised attention on the shear strength of slab bridges and called for more understanding of their shear behaviour. The two graphs below show the ratio of the vertical reaction force (local divided by average reaction force) versus the transverse location. The figure requires some effort to interpret, as it contains a lot of information. Note that for the top image, symmetry does not apply.

It is known from the plate theory of Mindlin-Reissner that transverse curvature causes additional reaction forces in the corner, which can be seen below. The graphs shows normal and limit cases such as fixed rotation and a Poissons ratio of $v = 0$, as well as a varying plate thickness, 10 and 12 m wide bridges and two skew angles. Note that the skew angles mentioned in the graphs are the international notation. (translation to Dutch definition: $\theta = 0° \Rightarrow 90°$ skew angle, $\theta = 30° \Rightarrow 60°$ skew angle).

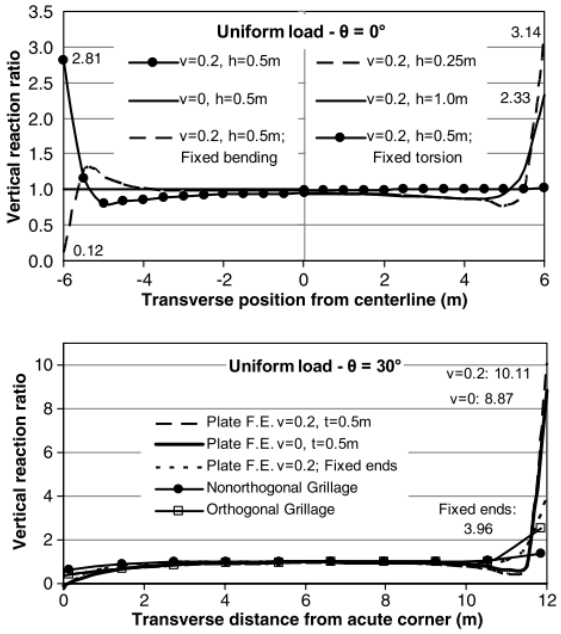

Fig. 6. Plate-element vertical reaction at support for a uniform load

Figure A.10: Vertical support reactions for various plate models and properties, from [8]

The top graph, representing a straight bridge, shows that a thinner slab gives a higher relative corner reaction. It also shows that fixed bending greatly reduces the corner reaction. Fixed torsion or Poisson's ratio of 0 account for a constant line: all supports are more or less equal.

The bottom graph, which represents a skewed bridge, once again shows that the support reaction in the obtuse corner is the highest. The support applied in the research is a continuous support, so

no discrete pads or points are used. This is done as representation for several existing structures. Although support stiffness is not mentioned in the article, a obtuse corner reaction 10 times the size of the average suggests that the supports applied are rigid.

The high support reaction magnification factor which was obtained through 2D plate FEM (10.11 in the graph), raised questions about the actual magnitude. Application of grillage models, which is considered to be more refined than equivalent-beam models, resulted in values for support reaction magnification of 2.52 (orthogonal grillage) and 1.36 (non-orthogonal grillage).

A comparative study was conducted with FEM-software ABAQUS using 8-noded elements to generate a model for a straight slab. This model (3D FEM) resulted in a stress concentration factor in the support corner of 2.6, while the model with plate elements (2D FEM) resulted in a concentration factor of 2.6 (see top graph, top left). The solid finite element analysis also showed that along the free edge, in a strip as wide as the thickness of the slab, additional vertical shear stresses are present. This is illustrated in Figure A.11. The article states that the corner reaction force should not be seen as a local effect, but as an accumulation of vertical shear forces induced by transverse curvature. In other words: shear force caused by transverse curvature 'gathers' at this strip at the free edge, and is lead to the corner support along this free edge strip. Finally, it is mentioned that the shear forces mentioned here can be relatively small for a solid slab. However, when there is severe loading present on this shear strip along the free edge, such as a sidewalk or an axle system, the shear stresses can become problematic.

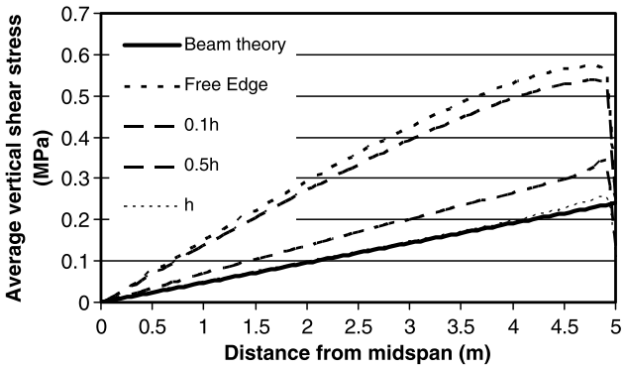

Figure A.11: Comparison of shear stresses in the edge zone of a slab, from [8]

Other tests in the research show that for as mentioned before, uniform loading on a straight slab still leads to magnification of corner reactions. However, truck loads on a straight slab hardly show any shear magnification in the corner supports. In the case of a skewed slab, it can be seen that both uniform loading as well as truck loads lead to magnification of obtuse corner support. The location of the truck load has influence on the magnification factor, which does not reach the magnitude of the uniformly loaded slab. Finally, the report draws the conclusion that when using more refined models for analysis such as the grillage method, corner reactions should be viewed separately because they cause shear stress situations that are not comparable with the rest of the slab.

It is stated that the amplitude of corner forces is influenced by many parameters, such as support stiffness, support (dis)continuity, slab dimensions, load configuration and cracking, but that further investigation of those parameters lies outside the scope of the research. However, obtained results show that two phenomenon have great impact on the corner forces: bending and its related transverse curvature, and the skew geometry.

Figure A.12 shows two graphs that illustrate influence of slab slenderness ratio B/L and skew angle (NOTE: graphs show international definition of skew angle) on the corner reaction. The corner forces (R_c) here are defined as a summation of shear forces beyond the beam-theory shear-force level at the corners. These corner forces are caused by a summation of the two phenomenon mentioned above: a bending component and a geometry component. The top graph shows that

there is a certain limit of the beam-theory shear at a vertical shear ratio of 2, which is reached at slenderness ratios B/L of 1 and higher.

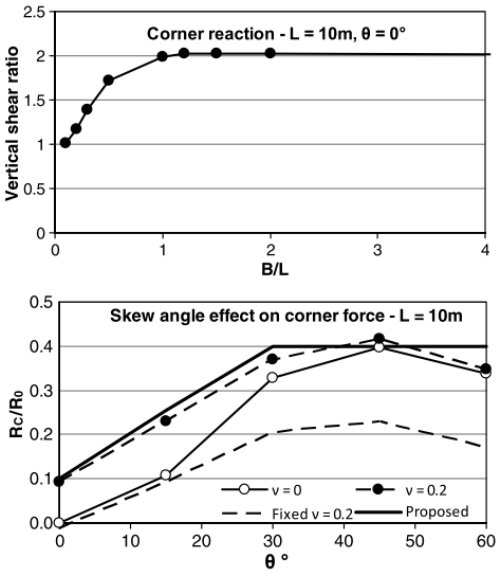

Figure A.12: Influence of slenderness and skew angle on corner reaction force, from [8]

The bottom graph shows the influence of the skew angle on the ratio R_c/R_0, where R_c stands for the corner forces as described above, and R0 is the load applied to a quarter of the slab. The line with a Poisson's of $v = 0$ represents a limit case with extensive cracking, and shows that highly skewed bridges, even without coupling of longitudinal and transverse bending, can still experience important reaction forces. Finally, it is concluded that corner forces associated with skewed geometry become important for a skew angle below 70° (Dutch definition) and that for skew angles below 60° (Dutch definition) about 40% of the dead loads are concentrated at corners.

A.2.7 Effect of skew angle on static behaviour of reinforced concrete slab bridge decks, Sindhu, B. (2013) [32]

This article describes a parametric study on 90 bridge deck models, which are subjected to uniformly distributed loads as well as Indian IRC load models. Behaviour of the bridges and their maximum in terms of longitudinal bending moment, deflection, torsional moment and support reaction are investigated. This is done for a number of different skew angles, so that the effect of the skew angle on those maximums becomes clear. For each bridge, edge beams have been added so that their effect can be checked.

The outcome of the research is similar to earlier researches. Results are summarized in a qualitative way below:

Deflection For all types of load and bridge deck aspect ratios, the maximum deflection decreases when skew increases (skew angle decreases). As skew increases and the slab span (length of the free edge) is constant, the distance from support line to support line actually decreases. Since flow of forces tends to follow the stiffest direction and span from support line to support line, rather than parallel to the free edge, it makes sense that an increase of skew decreases the maximum deflection. After all, a shorter span accounts for a stiffer structure.

A graph has been made that shows the deflection ratio D_α/D_0 as a function of the skew angle. Notice that once again the skew angle shown here is the international definition. The graph shows that the aspect ratio of the bridge deck hardly makes any difference on its deflection ratio. Results in the graph account for a bridge subjected to dead load only, where the ratio went down from 1 to

about 0.26 . The Indian load models showed a similar graph where the aspect ratio did not matter. A decline in the deflection ratio was found there as well, although it was less steep (from 1 down to 0.64). Bridges with edge beams showed smaller deformations than their twins without edge beams.

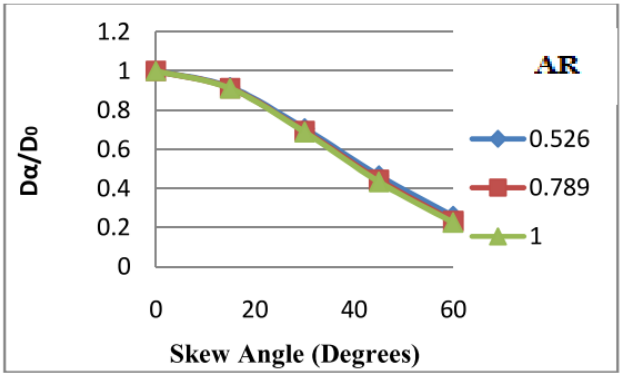

Figure A.13: The deflection ratio for different skew angles and aspect ratios, from [32]

Longitudinal bending moment Longitudinal bending moment behaviour showed to be similar to that of the deflection. As skew increases, max longitudinal bending moment decreases. Application of edge beams causes even more decrease. Once again, a normalized graph was produced, which now shows the longitudinal bending moment ratio M_α/M_0. It can be seen that this graph, as shown below, has a shape similar to that of the deflection graph. As with the deflection curve, the decrease in ratio is the greatest for the dead loads (1 to 0.33), where the decrease for Indian load models was smaller (1 to 0.74 $\sim$ 0.79) .

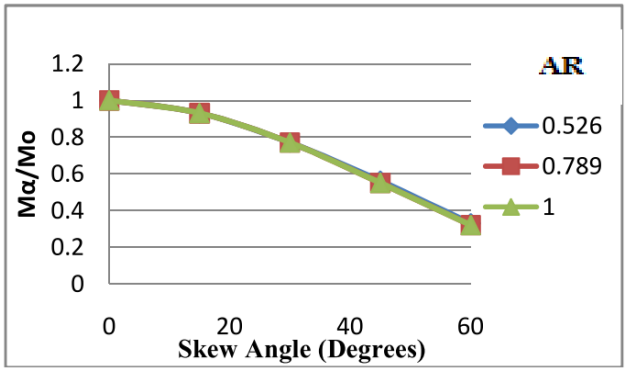

Figure A.14: The moment ratio for different skew angles and aspect ratios, from [32]

Torsional moment As opposed to deflection and the longitudinal moments, the torsional moments actually increase as the skew increases when 'starting' from a straight slab. The graph shows the torsional moment ratio TM_α/TM_0 as a function of the skew angle (international definition again). A peak is reached at around 30°, after which the torsional moment reduces. The angle at which this peak occurs, depends on the type of loading (dead load or load model) and whether or not an edge beam is present. The maximum angle at which this peak can be found is 45°.

Once again, the normalized graph shows a very similar behaviour for different aspect ratio's, although it can be seen that higher aspect ratio leads to slightly lower torsional moment ratio. The height of the peak depends on the type of loading, where for dead loads and load models similar values can be reached.

Looking at the influence of an edge beam on the torsional moment, it is observed that adding an edge beam can account for a reduction of this torsional moment of almost 50%.

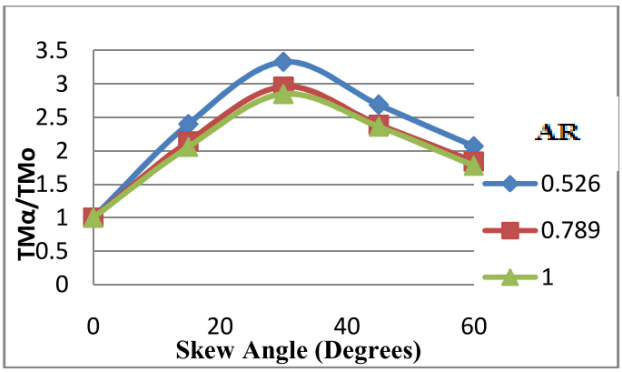

Figure A.15: The transverse moment ratio for different skew angles and aspect ratios, from [32]

Support reaction in the obtuse corner The modelled bridge slabs in this article are said to be simply supported. Although further details are not provided in the article, this probably means that the bridge supports are rigid. Because support reactions are viewed separately, it is assumed that discrete supports are used.

As the skew of a bridge increases, the relative reaction force in the obtuse corner also increases. For a skew angle of 30 degrees (Dutch definition), an 80% increase in value over the average can be found. Looking at the normalized support reaction S_α/S_0 for the obtuse corner reaction, values as high as 10 can be found for certain load models. It once again becomes clear that an increase of skew leads to concentrated support reactions in the obtuse corner.

A.3 Part 2: Calculating required reinforcement

Quite some literature is available on automated reinforcement design. Most methods and algorithms provided in such literature lead to a reinforcement design that is economic and effective in theory. However, such a design will often prove to be very unpractical in the execution phase, making it an inefficient and uneconomic design after all. This gap between theory and practice is something that engineers have been trying to overcome. There are plenty of software packages available in which reinforcement design is automated. However, to this day, such software still has not proved to be satisfactory in their output design. One of the reasons for this is that most codes only provide methods to validate designs. As the article Aanzet tot consistent wapenen van schijven, platen en schalen, Blaauwendraad, J. & Lourenço, P. (1995) puts it: "Sadly enough the most important characteristic of all validation techniques is that they do not indicate what we should do, but only what we shouldn't do." Nonetheless, the methods of reinforcement design in literature provide useful insights into different reinforcement layout designs for RC skewed slab bridges. Therefore it is still worthwhile to look into the available literature.

A.3.1 CUR Rapport 54: Wapenen van platen, Monnier, T. (1972) [12]

Most standard concrete elements (beams, columns, one-way spanning floors) have a clear direction of span. Such a direction usually governs the direction in which reinforcement is designed. However, for instance the case of plates supported on all sides or skewed bridges, reinforcement needs to be designed in a direction that does not coincide with the direction of the bending moments. This report focusses on such cases.

The report states that previous literature contains different theories on calculating reinforcement quantities for cases where trajectories and reinforcement direction do not coincide. A clearly preferred method is hard to indicate at first. However, comparative studies show that (almost) all of those theories lead to very similar results. This makes sense considering that most of them are based on the same assumptions and aim for equilibrium of forces.

The theories lead to certain forces in the direction of the reinforcement, that will provide equilibrium with the moments present due to loading. Force distribution (moments) is calculated under the assumption of theory of elasticity. This focus on equilibrium of forces means that deformation-related cracking and redistribution of forces are left unattended.

In the method of reinforcement calculation described below, the reinforcement layout is taken as a starting point. This means that the direction of the bars in both longitudinal and transverse direction are known and can be seen as input. Given a problem with a known force distribution, the total required amount of reinforcement for a certain layout can then be determined. In theory and for a certain situation, the layout that leads to the smallest amount of reinforcement is the most favourable one.

For the case of a skewed slab bridge, there are three possible reinforcement layouts that should be considered. The three layouts can be found below:

1. Parallel and perpendicular to supported edge (orthogonal)
2. Parallel and perpendicular to the free edge (orthogonal)
3. Parallel to support edge and parallel to free edge (nonorthogonal)

Calculation of required reinforcement

This part will focus on calculation of required reinforcement amounts. Calculation is based on a few assumptions:

- All tensile forces are taken by the reinforcement steel

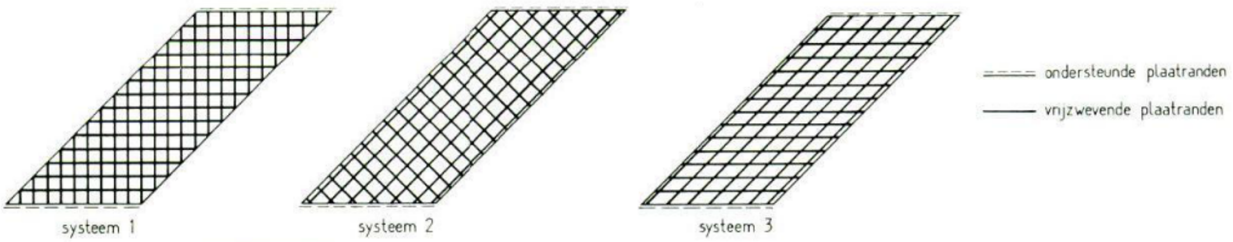

Figure A.16: Three different possible reinforcement layouts in a skewed slab, from [12]

- The reinforcement steel takes no shear force
- The reinforcement steel does not deviate from its original direction
- The concrete only takes up compressive forces
- Equilibrium of forces is considered, deformations are not

The last assumption needs a little more explanation. Reinforcement calculation for a certain layout and problem also requires the distribution of forces (moments) to be known. In this distribution of forces, deformation can (should) be taken into account, because the problem is viewed on a global scale. Calculation of reinforcement however primarily happens on an element scale. It is on this element scale that the assumption is made that deformations do not influence force distribution. In other words, the force distribution does not change when, due to cracking of the concrete, the reinforcement steel takes over the forces in the concrete.

The equilibrium of forces can be worked out in many different ways. Usually, the tensile zone of the plate is considered and the problem is treated using a disc model at first. In this disc, forces are converted into stresses. This consideration of stresses can also be used for the entire plate, because moments and stresses are related through the section modulus.

From the assumptions follows that a reinforced plate problem can be solved by taking the flat stress state considered in the disc model. The flat stress state in the tensile zone is decomposed into three line stress states, where tensile line stresses are to be taken up by the reinforcement and the eventual compressive line stress is taken up by the concrete. Direction of the tensile line stresses are determined by the direction of the reinforcement; the direction of the concrete compressive line stress remains free.

It is mentioned that compressive stresses in the tensile zone should be viewed as a fictive resultant from a complex stress sate, that rises from the fixation of the reinforcement. The method described above will never be able to reflect the true stress states in a reinforced concrete slab problem. It should be seen as a tool that produces a reasonable and reliable calculation of reinforcement, given an elastic distribution of moments.

Determination of the required reinforcement under the assumptions as described above, can be done in multiple ways. The report describes three ways:

1. Analytic decomposition of the flat state stress
2. Method of compression diagonal
3. Yield-line theory

All three methods lead to the same results. A practical way of applying the relevant formulas will be given now.

Practical way of working out the reinforcement

As mentioned above, calculation of reinforcement can be done by considering a disc model and the stresses working on it. Alternatively, a plate model can be used with the according moments. This second model is preferred and will used in the calculation of the reinforcement.

Case 1: both moments have the same sign convention (both positive or both negative)

Below, the formulas for calculating the reinforcement moments m1 and m2 are given. In this first case, both bending moments must have the same sign convention. The sign for the bending moments should be chosen so that the reinforcement considered is in tension.

$$m_1 = \frac{1}{\sin\varphi^2}\left[m_I \sin^2(\delta+\varphi) + m_{II}\cos^2(\delta+\varphi) \pm \frac{1}{k}\left|m_I \sin\delta \sin(\delta+\varphi) + m_{II}\cos\delta\cos(\delta+\varphi)\right|\right] \tag{A.5}$$

$$m_2 = \frac{1}{\sin^2\varphi}\left[m_I \sin^2\delta + m_{II}\cos^2\delta \pm k\left|m_I \sin\delta \sin(\delta+\varphi) + m_{II}\cos\delta\cos(\delta+\varphi)\right|\right] \tag{A.6}$$

$$k = \frac{\sin\beta}{\sin(\varphi-\beta)} \tag{A.7}$$

The definition of the angles δ and φ is illustrated below. φ is defined as the angle between the compression diagonal and moment direction 1: m_1. Similar,φ is the angle between the compression diagonal and moment direction 2: m_2.

The parameter k is a ratio of the angles between the reinforcement directions that are divided by the compression diagonal. The report shows that in most cases the lowest amount of reinforcement is achieved when the compression diagonal lies on the bisection of the reinforcement directions. This leads to $k = 1$.

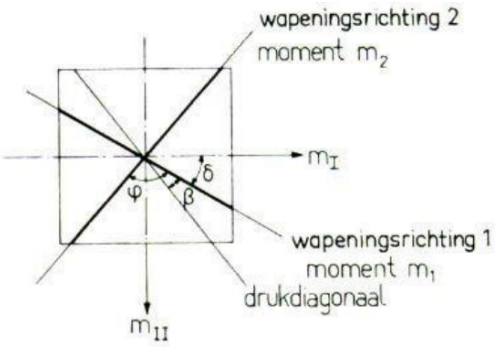

Figure A.17: Definitions of relative reinforcement directions and related angles, from [12]

The expressions m_1 and m_2 as stated above are expressed as a function of the relative angles of the reinforcement and the compression diagonal. An alternative way is to express them as a function of the occurring bending and torsional moments:

Bottom reinforcement:

$$m_1 = \left[m_\xi + \frac{1}{k} |m_{\xi\eta}| \right] \frac{1}{\sin \varphi}$$
$$m_2 = \left[m_\eta + k |m_{\xi\eta}| \right] \frac{1}{\sin \varphi} \tag{A.8}$$

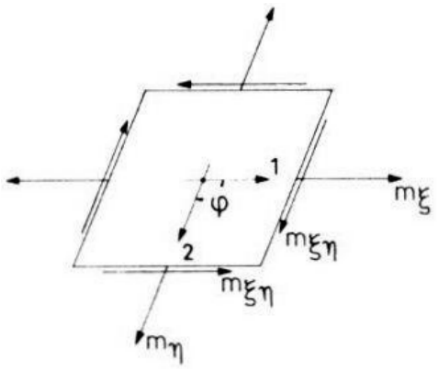

Figure A.18: Definitions of stress-directions, from [12]

Top reinforcement:

$$m_1 = \left[m_\xi - \frac{1}{k} |m_{\xi\eta}| \right] \frac{1}{\sin \varphi}$$
$$m_2 = \left[m_\eta - k |m_{\xi\eta}| \right] \frac{1}{\sin \varphi} \tag{A.9}$$

The formulas provided above can be simplified under the assumption of $k = 1$ and a value of $\varphi = 90°$. This leads to :

Bottom reinforcement:

$$m_1 = m_x + |m_{xy}|$$
$$m_2 = m_y + |m_{xy}| \tag{A.10}$$

Top reinforcement:

$$m_1 = m_x - |m_{xy}|$$
$$m_2 = m_y - |m_{xy}| \tag{A.11}$$

Case 2: the moments have a different sign (one is positive, one is negative)

Use of the formulas above may lead to reinforcement moments that cause compression in the reinforcement instead of tension. In such case, the reinforcement moment should be set to 0. Such case can lead to a new value for k that is not equal to 1, which leads to a smaller amount of reinforcement:

$$m_2 = \left[m_\eta - k \left| m_{\xi\eta} \right| \right] \frac{1}{\sin \varphi} \tag{A.12}$$

From this, it follows that:

$$k = \left| \frac{m_\eta}{m_{\xi\eta}} \right| \tag{A.13}$$

The formula for m_1 now becomes:

$$m_1 = \left[m_\xi - \frac{1}{k} \left| m_{\xi\eta} \right| \right] \frac{1}{\sin \varphi} = \left[m_\xi - \frac{m_{\xi\eta}^2}{m_\eta} \right] \frac{1}{\sin \varphi} \tag{A.14}$$

The formula for m_1 above might lead to a value that is greater than 0. Such a moment with a positive value means that only tension in the bottom is present, and that with respect to the bending moments, the top reinforcement can be left out entirely (since m_2=0 was assumed as well). As opposed to theory, practice usually still calls for reinforcement to prevent cracking. It is mentioned that the required reinforcement moments can easily be calculated with the help of a computer. In practice, the governing moments are calculated for different load combinations. Current software is usually able to show a bending moment envelope, which combines the values from different load combinations and shows the maximum for each location. This way, the reinforcement can be designed to resist the maximum moment at each location. The use of such moment envelopes, or maximum plots for other stresses or deformations, should be done with caution as such plots often do not provide sufficient insight into behaviour of a structure. The book Plates and FEM - Surprises and Pitfalls, Blaauwendraad J. (2010) mentions the following:

Blameworthy use of envelopes of load cases

A really blameworthy practice is to consider an envelope of load cases and combination results, rather than judging the result of each load case and combination individually. In that way the structural engineer cannot pick up how the structure behaves, and will have no idea about actual safety levels. Apart of this, the approach is not economic. Structural engineers should investigate results of load cases and combinations individually, at least for the most important ones.

Figure A.19: Small note on the use of envelopes of load cases, from [41]

The last step in the reinforcement design process, is converting the reinforcement moments into a practical reinforcement design. A helpful tool in this step can be creating a plot for each reinforcement layer (top and bottom) and direction (longitudinal and transverse). Such plots can easily be generated by a computer nowadays.

Under the assumption that the reinforcement moments do not influence each other, the reinforcement moments can be translated into a practical configurations (bar diameter and centre to centre distance) by considering each reinforcement layer and direction to be present in a beam of unit width. This is done using the formula below:

$$A_1/a_1 = \frac{m_1}{f_{yd} z_1} \tag{A.15}$$

Where A_1 stands for the cross-section of a reinforcement bar $[mm^2]$, a1 stands for the centre to centre distance of the bars $[mm]$, m_1 stands for the reinforcement moment $[Nmm/mm]$, f_{yd} is the yield strength of the reinforcement steel and z_1 represents the inner lever arm of the corresponding bar to the compressive zone $[mm]$.

Following this procedure, failure of the plate in this case is started by yielding of the reinforcement steel. To ensure a ductile way of failure, the amount of reinforcement applied needs to be above the minimum (to prevent brittle fracture) and below the maximum (to prevent compressive zone failure) amount of reinforcement.

In case the maximum reinforcement ratio is exceeded somewhere, a different value for k can be adopted to correct the problem without having to alter the plate. Say that the reinforcement moment for bottom reinforcement leads to a reinforcement ratio that is above the maximum. The formula used for such reinforcement is:

$$m_1 = \left[m_\xi + \frac{1}{k} \left| m_{\xi\eta} \right| \right] \frac{1}{\sin \varphi} \tag{A.16}$$

The maximum allowable reinforcement in the bottom is called $m_{1,max}$. It follows then that k is determined by:

$$k = \frac{\left| m_{\xi\eta} \right|}{m_{1,max} \sin(\varphi) - m_\xi} \tag{A.17}$$

This means that for the bottom, the reinforcement in the other direction is determined by:

$$m_2 = \left[m_\eta + \frac{m_{\xi\eta}^2}{m_{1,max} \sin(\varphi)} \right] \frac{1}{\sin \varphi} \tag{A.18}$$

Next, it should be checked whether the resulting reinforcement is below the maximum ratio. If so, then the value for k has been adopted successfully. If not, different measures need to be taken where increasing the thickness of the plate is the most straightforward measure. For a reinforcement configuration where φ is not equal to 90° (nonorthogonal layout), it is possible that the reinforcement layout combined with the principal moments result in reinforcement moments that are smaller than the greatest principal moment. In such a case, thickness of the plate is limited by the maximum reinforcement ratio that takes up the biggest principal moment with reinforcement in the direction of that principal moment. In all other cases, the greatest reinforcement moment can be used for determining the plate thickness and the maximum reinforcement ratio.

To demonstrate the efficiency of the three most used reinforcement layouts, the research has calculated the total amount of reinforcement required when using those layouts. A graphical depiction is shown below. The plates in the image have been subjected to a uniform load only. The amount of reinforcement is determined by taking the reinforcement moments for each location. It therefore uses an assumption that the reinforcement can be altered to match those reinforcement moments. In other words: a purely theoretic amount of reinforcement is calculated based on the reinforcement layout. In practice, reinforcement nets would be applied, meaning that in most locations, more reinforcement is applied than necessary. This method of reinforcement calculation should therefore not be seen or used to make a realistic and practical design. It does however give a decent indication on where bending moment reinforcement is required. Additionally, it allows for comparison of different reinforcement configurations.

The following can be concluded when observing the image:

- Looking at the total amount of reinforcement required (part c of the image), it becomes clear that layout 3 requires far more reinforcement than the other two layouts. This goes for plate slenderness ratio b/l of 0.25 and up. Below such ratio, the plate starts to behave more like a beam, and the difference between layout 2 and 3 becomes small.

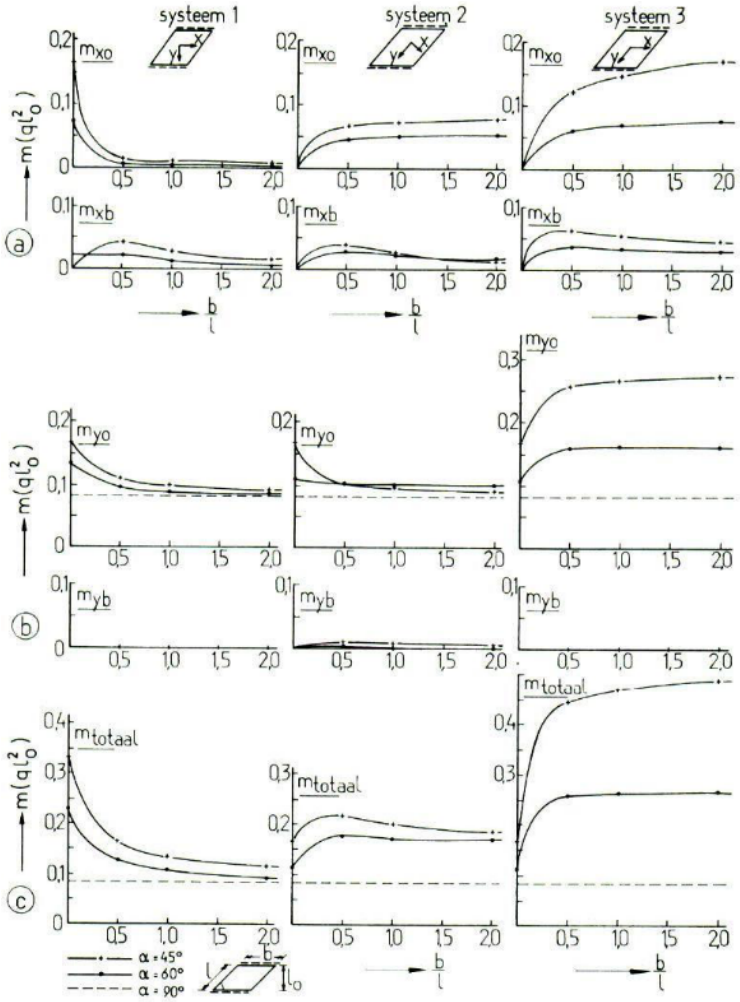

Figure A.20: Comparison of different reinforcement layouts for different skew angles and bridge aspect ratios, from [12]. o = bottom reinforcement, b = top reinforcement

- For system 1, it can be seen that for an increasing ratio of b/l, the amounts of required reinforcement start to approach the (dashed) line of the straight slab. In CUR report 54, it was mentioned that wider slabs start tend to span from support line to support line, which kind of resembles a straight plate. The amount of longitudinal bottom reinforcement becomes similar to that of a straight slab, while the other reinforcement amounts, required for the edge 'disturbance' become relatively less important and start to approach 0.
- When comparing the orthogonal layouts 1 and 2, it can be seen that from $b/l > 0.5$, layout 2 needs about 50% more reinforcement than layout 1. This is mainly due to transverse bottom reinforcement, which needs to be present over almost the entire plate in layout 2, while layout 1 only requires transverse reinforcement along the free edge.
- Layout 1 shows a reduction of bottom longitudinal reinforcement amount as the skew decreases (skew angle increases). Layout 2 shows similar behaviour only for small values of b/l, which means that the plate behaves more or less like a beam.
- As b/l increases, layout 2 and 3 require a lot more reinforcement than layout 1. As mentioned before, the plates starts to span from support line to support line. Hence, layout 1 is much more efficient in such case as the reinforcement follows this direction of span.

The figure has shown that a nonorthogonal reinforcement layout leads to inefficient design and requires much more reinforcement. Additionally, orthogonal reinforcement tends to perform better

in terms of cracking when a slab is subjected to special loads for which the slab initially was not designed. In case of nonorthogonal layout, the smallest angle made by the two reinforcement directions contains a relative small amount of effective reinforcement. It is in a direction between this angle that severe cracks may occur in cases of special loads.

A.3.2 Wapenen op basis van belastingen in- en/of uit-het-vlak, Braam, C. & de Haas, F. (1993) [13]

The CUR-report 54, which is summarized above, focussed on determining reinforcement for bending. Loads on the plate where translated into moments, which could be taken up by reinforcement moments. Loads out of plane however, were not considered (neglected).

This article proposes a method of calculating reinforcement in case loads from both a disc-model (in-plane) and a plate-model (out-of-plane) are present: a combined model of the two is called a shell-model. Reinforcement for a shell model does not only consist of flexural reinforcement (in-plane direction), but also of shear reinforcement (perpendicular to the plane).

Bending moments

The article builds up the calculation method step wise. First, the disc-model is considered, where only in-plane membrane stresses are present. Next, the plate-model is considered, which takes into account bending and torsional moments and shear forces. The shear forces in this model are considered separately from the moments, and will be treated later on. When adding the disc-model and plate-model together, a shell-model is created. Without consideration of shear forces, the shell model looks at forces in a cross section (x and y), in which a normal force and a moment are present. These forces need to make equilibrium with their reinforcement counterparts. The formulas used here look rather similar to those in CUR-report 54, although membrane stresses are now also included:

For a cross section in the x-plane:

$$n^*_{xx} = n_{xx} + |n_{yx}| m^*_{xx} = m_{xx} \pm m_{xy} \tag{A.19}$$

And a cross-section in the y-plane:

$$n^*_{xx} = n_{xx} + |n_{yx}| \tag{A.20}$$

Shear force

The shear force capacity of a certain reinforced shell-model can be divided into two parts: the shear force capacity of the concrete itself and the shear force capacity of the shear reinforcement. Shear force in the concrete itself is mainly transferred by the concrete compression zone. This capacity is influenced by normal forces working on the concrete: a compressive force increases the shear capacity of this zone while a tensile force reduces it. Considering a plate, two shear forces are present: q_x and q_y, working along the respective planes. The maximum shear force can be found with the formula: $q_{\overline{x}} = \sqrt{q_x^2 + q_y^2}$ This shear force no longer works on the x-plane, but on a plane of which the normal $\overline{x}$ is rotated from the normal x. This angle of rotation is denoted by α. Where rotation of the x-plane leads to a plane on which the maximum shear force is working, rotation of y to $\overline{y}$ leads to $q_{\overline{y}}$, which is equal to zero. The angle α of rotation can be determined by:

$$\sin\alpha = \frac{q_y}{\sqrt{q_x^2 + q_y^2}} \tag{A.21}$$

This shear force was calculated for a plate-model. Since plate models do not consider in-plane forces, this shear force will not be influenced by such force. However, since we want to

work towards a solution in a shell-model, influence of normal forces needs to be considered. The easiest way to do this is by considering x and y-directions independently. This way, a sort of beam mechanism is assumed. The required amount of shear reinforcement in this x-beam is now determined by subtracting the contribution of n_{xx}, on the compressive zone in this fictive beam, from q_x. Calculation is similar in y-direction, but now n_{yy} and q_y should be considered. Finally, the amounts for x and y-direction should be summed to obtain the total amount of required shear reinforcement for a location.

The article mentions two objections to this method of shear consideration:

- In-plane shear stress, denoted by $n_{xy} = n_{yx}$, are not taken into account. Since they do influence the concrete compressive zone, the considered capacity of this zone might be incorrect
- Two shear forces are considered separately, without giving attention to the maximum shear force that arises from them.

The first point can be solved by considering the principal stresses and then calculating $q_{\overline{x}}$ and $q_{\overline{y}}$. The second point can be dealt with by calculating the maximum vertical shear force, and then calculating the accompanying values of $n_{\overline{xx}}$ and $n_{\overline{yy}}$. Next, a method of calculations is proposed that considers all possible directions, by calculating shear reinforcement for angles α between 0° and 90°. α is once again defined as the angle between the original x-axis and the new $\overline{x}$-axis. For this new axis-system, the following formulas can be used:

$$\begin{aligned} \sigma_{\overline{xx}} &= \sigma_{xx}\cos^2\alpha + \sigma_{yy}\sin^2\alpha + 2\sigma_{xy}\sin\alpha\cos\alpha \\ \sigma_{\overline{yy}} &= \sigma_{xx}\sin^2\alpha + \sigma_{yy}\cos^2\alpha - 2\sigma_{xy}\sin\alpha\cos\alpha \\ q_{\overline{x}} &= q_x\cos\alpha + q_y\sin\alpha \\ q_{\overline{y}} &= -q_x\sin\alpha + q_y\cos\alpha \end{aligned} \tag{A.22}$$

In the next step, the reinforcement can be calculated. The required amount of reinforcement in the $\overline{x}$-direction can now be found by considering shear force $q_{\overline{x}}$ and taking into account $n_{\overline{xx}}$ when considering the concrete compressive zone. The y-direction requires similar approach, using $q_{\overline{y}}$ and $n_{\overline{yy}}$. Once again, the total required amount of shear reinforcement is obtained by summing up the individual amounts of the two directions. This method might show a complication when calculating the influence of the concrete compressive zone. The old Dutch code considered in the article gives an expression for calculating the share of this compressive zone, denoted by τ_1. One of the things it takes into account is the reinforcement percentage. However, the directions of the flexural reinforcement x and y do not coincide with the newly used directions $\overline{x}$ and $\overline{y}$. The reinforcement percentage can be converted into the new axis system, although this makes the formula from the code less valid. It is therefore advised to take the most conservative value for τ_1. For calculation of the contribution of the concrete compressive zone, an internal lever arm is usually taken as $d = 0.9 * h$. It should be noted that the methods described above only look at the problems on a failure level. Serviceability is not considered in these formulas.

A.3.3 Strokenverdeling voor het wapenen van scheve plaatveldviaducten, Van Vulpen, R. (2002) [47]

This thesis looks at the influence of skew on the bending moment distribution in a concrete slab bridge. Shear forces are not considered in this thesis. It also investigates a way of simplifying the design process of the reinforcement by dividing the bridge in strips.

This division into strips comes from the NEN 6720 (old Dutch code), and is done with the aim of reducing the total amount of reinforcement by applying a more efficient distribution of reinforcement (compared to a uniform reinforcement design over the entire bridge). If a strip is subjected to higher bending moments, more reinforcement is applied here. This way, reinforcement is placed in the strips where it is required the most. Finally, an automatic process of determining reinforcement is considered making use of iterations.

Four different cases are considered in terms of skew: 90° (rectangular bridge), 75°, 60° and 45°. For the calculation, DIANA (FEM software) is used, where a load is applied that consist of the dead load and a uniform live load.

Division of strips is done in three parts: two strips at the edges, each of a quarter of the width ($l/4$), and a middle strip half as wide as the slab ($l/2$). This is also done for reinforcement in the other direction (so $b/4$ at both edges, $b/2$ in the middle).

For each strip, the reinforcement moments are determined by taking the average bending moment in the strip. Using NEN-6720, the reinforcement is dimensioned to this average moment. After that, a nonlinear calculation is done to validate whether the design failure factor is reached. Finally, a comparison is done between reinforcement designed with the strip method, and reinforcement which is uniform over the entire plate.

The non-linear calculation showed that determination of reinforcement using the average moments leads to the expected failure factor. Difference in reinforcement between the strips is small.

For this reason, division into strips gives no significant improvement up to a skew angle of 60°. The thesis also adds that the reinforcement difference between strips could lead to error during the execution phase (I personally do not consider this to be likely). At a higher skew (acute angle of 45 degrees in this case), division into strips does lead to a significantly better division of reinforcement.

Determination of reinforcement in this thesis is done by hand, by following the Dutch code NEN 6720. Finally, it is investigated if this process could be automated. For this, a method by P.B. Lourenco is considered, which is based on CEB-FIP Model code 90. The amounts of reinforcement found using this method are in agreement with the amounts found earlier on (methods described above). Additionally, this method can also incorporate membrane forces, making it an interesting tool for reinforcement design.

Early on in the thesis, the decision is made to leave out the case of nonorthogonal reinforcement, as it is considered inefficient, leading to higher amounts of reinforcement. In Bijlage 2 (appendix of the respective thesis [47]), additional comments are made on nonorthogonal reinforcement layouts. A graph is presented (see Figure A.21), in which both magnification factors for σ_{xy} and σ_{yy} are plotted against the reinforcement angle β. As this angle goes down from 90°, the magnification factors soon start to rise significantly, indicating that more reinforcement is required.

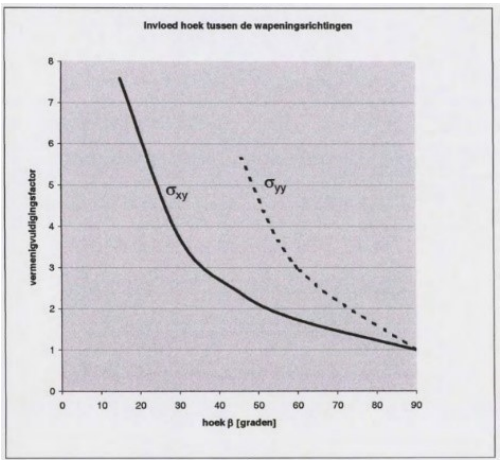

Figure A.21: Magnification factors of σ_{xy} and σ_{yy} versus relative reinforcement angle β, from [47]

In a follow up study, influence of a load model on the viaduct and the above mentioned membrane

forces can be looked at. For this thesis, the assumption is made that local loads will hardly effect the global bending moment distribution, and hence has hardly any effect on the required amount of reinforcement.

A.3.4 Strokenverdeling voor het wapenen van scheve plaatveldviaducten, Van der Ham, H.(2004) [9]

This research can be seen as sort of a follow up of the 'first part' by R. van Vulpen. It considers the same subject and has the exact same name, but focusses on different aspects. The new aspect considered in this research is the effect of axle load-systems. It once again looks at division of the bridge in different strips, in order to obtain a more effective reinforcement layout (compared to uniform reinforcement over entire bridge) for cost savings.

As was done in the previous thesis, four models are set up with an angle of skew of 90° (rectangular bridge), 75°, 60° and 45°. The skewed plate bridges considered in this thesis are subjected to a constant load and an axle load-system. The research is conducted with a numerical analysis using the FEM package DIANA.

First, the bending moments are determined. From this, reinforcement with the strip-method is determined. This method resulted in a higher amount of reinforcement, compared to the 'conventional' method which takes the average bending moment over the entire plate cross-section.

The (higher) reinforcement layout which resulted from the strip-method is then checked using a non-linear calculation, in which the load is increased step-wise until the structure fails. It appears that this layout leads to a higher failure factor (= lower Unity Check). This makes sense as more reinforcement is applied.

To determine the real effect of the strip-method, the amount of reinforcement is optimized. By use of iterations, the reinforcement amount is reduced to match the amount from the 'conventional' method (uniform reinforcement over entire bridge). This way, both layouts can be compared more realistically because the amounts are the same but the layout is different. From this comparison, it followed that the layout obtained with the strip-method has an equal factor of failure compared to the 'conventional' layout.

Next, both layouts are compared in terms of crack formation. It is concluded that in the strip-method layout, the maximum crack-strain is reduced, leading to smaller cracks. This applies for all angles of skew. However, when looking at crack-strain over the entire cross-section, there is hardly any difference.

From the results as described above, it can be concluded that the reinforcement layout obtained using the strip-method (and then reduced to match the reinforcement amount currently used), does not lead to any significant benefits. Finally, recommendations for future research are given:

- Check the influence of the new European codes (= Eurocode load models)
- Check highly skewed bridges with a 30° skew angle.

A.3.5 Van spanning naar wapening, Braam R. & Blaauwendraad J. (2014) [14]

This is a more recent article on the 'translation' of FEM-obtained force distribution into required reinforcement amounts. The approach used here is quite similar to the one used in Wapenen op basis van belastingen in- en/of uit-het-vlak, Blaauwendraad J., Lourenço P. (1993). A disc element and a plate element are considered separately at first, and then combined into a shell element. This shell element is also included in an annex of Eurocode 2 as a 3-layer sandwich model.

Disc model

This model once again only considers in-plane stress. The reinforcement in this model is assumed to be orthogonal and to coincide with the x- and y-axis. The stresses working on the disc are n_{xx}, n_{yy}, $n_{xy} = n_{yx}$ and are assumed to be known results from a FEM calculation. The FEM stresses on the disc-model are taken up by three line-stresses: n_c, n_{sx} and n_{sy}. The first one is assumed to be positive when compressive, the latter two are assumed to be positive when tensile. Direction of the compressive diagonals is the same as the direction of the related compressive stress, and there is no shear-stress present between those diagonals. The angle between the diagonals and the y-axis is denoted as φ.

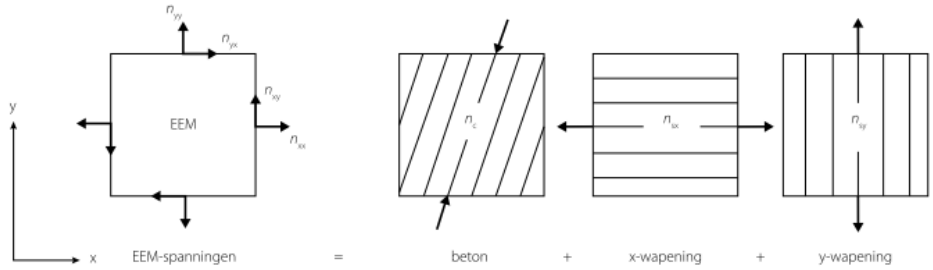

Figure A.22: Stress components in the disc-model, from [14]

Two questions concerning this approach are:

- How much reinforcement is required?
- Is it possible to optimize (reduce) this amount of reinforcement?

Considering the disc element, three equations can be derived:

$$\begin{aligned} n_{xx} &= n_{sx} - n_c \sin^2 \varphi \\ n_{yy} &= n_{sy} - n_c \cos^2 \varphi \\ n_{xy} &= n_c \sin \varphi \cos \varphi \end{aligned} \tag{A.23}$$

Next, the equations are rewritten in terms of the unknowns:

$$\begin{aligned} n_{sx} &= n_{xx} + n_{xy} \tan \varphi \\ n_{sy} &= n_{yy} + n_{xy} \cot \varphi \\ n_c &= \frac{n_{xy}}{\sin \varphi \cos \varphi} \end{aligned} \tag{A.24}$$

The total required amount of reinforcement in this disc model is $n_{s,total} = n_{sx} + n_{sy}$. Now, similar to the earlier paper, a term k is introduced (although the expression is slightly different): $k = \tan\varphi$. The total required amount of reinforcement can now be written as:

$$n_{sx} + n_{sy} = n_{xx} + n_{yy} + n_{xy}(k + k^{-1}) \tag{A.25}$$

As can be seen in Figure A.23, the term $(k + k^{-1})$ shows a minimum for $k = 1$, which leads to $\varphi = 45°$. Using this k-factor, the expressions look familiar again:

$$\begin{aligned} n_{sx} &= n_{xx} + |n_{xy}| \\ n_{sy} &= n_{yy} + |n_{xy}| \end{aligned} \tag{A.26}$$

Force in the concrete compressive diagonal:

$$n_c = 2n_{xy} \tag{A.27}$$

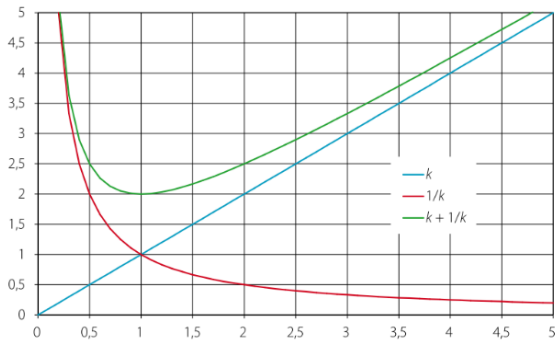

Figure A.23: A graph showing the minimum at $k = 1$, from [14]

Until now, it was assumed that reinforcement is required in both directions. In other words, both terms n_{sx} and n_{sy} are assumed to be positive. This is however not always the case. A negative value for one of these terms (or both) means that no reinforcement is required for this direction (under the assumption that the compressive forces can be taken up by the concrete). If one of these terms is negative, k needs to be re-evaluated. Say that a certain stress situations leads to a negative value for n_{sx}, then k is found by setting $n_{sx} = 0$. The same goes for a negative stress in y-direction and n_{sy}.

In total there are 4 cases that can be separated. They depend on two things: reinforcement required in x-direction (yes or no) and reinforcement required in the y-direction (yes or no). Transition between this requirement of reinforcement happens in the situations $n_{xx}/|n_{xy} = -1$ and $n_{yy}/|n_{xy} = -1$.

Figure A.24 that there is also a situation in which no reinforcement is required at all. The transition curve that encloses this situation is described by $n_{xx}n_{yy}/(n_{xy})^2 = 1$.

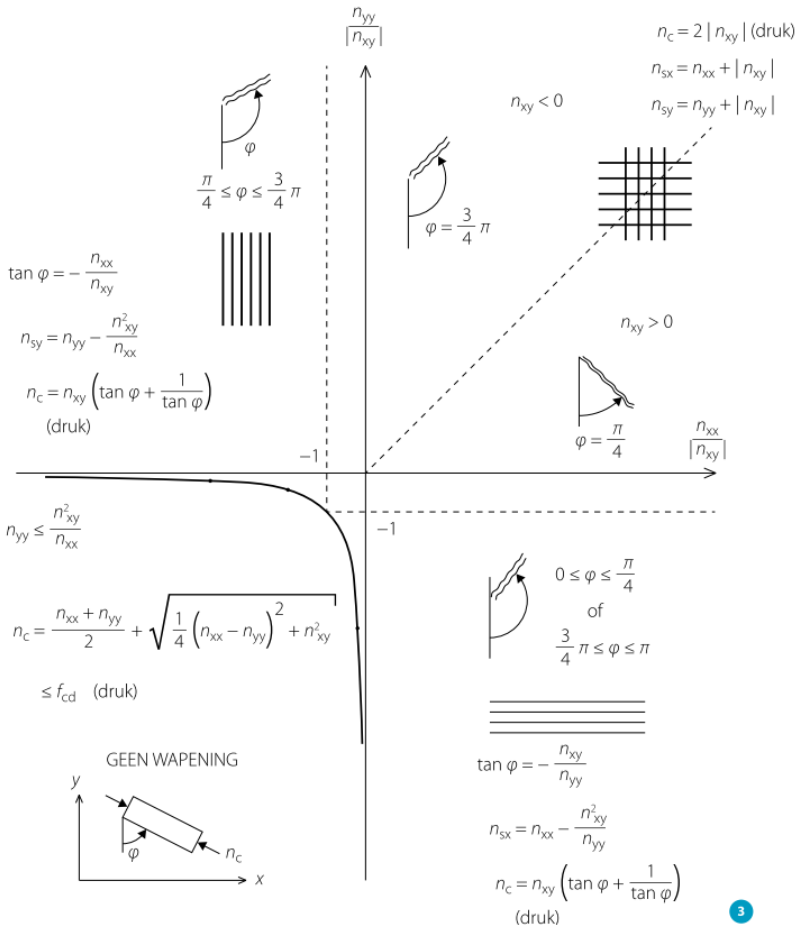

Figure A.24: 4 different quadrants for the disc model, from [14]

Plate model

A plate model deals with out-of-plane forces: bending moments, torsional moments and shear force. To determine the required reinforcement to counter those forces, the plate model is divided into three layers: a sandwich model. The outer layers are considered to be only loaded in-plane: by replacing the moments with a force-couple, this is realized. Next, the outer layers can be treated in the same way as the disc models because they are once again loaded in-plane only.

The inner layer, also called the core, deals with the vertical shear force. The output from FEM calculations usually consists of two components (shear forces): v_x working along the x-plane and v_y working along the y-plane. Similar to earlier methods, calculation of shear reinforcement is done by taking into account the maximum shear force: $v_0 = \sqrt{v_x^2 + v_y^2}$. This maximum shear force works along a vertical plane that makes an angle φ_0 with the x-axis. The angle can be determined using $\tan \varphi_0 = v_y / v_x$. The maximum shear force 'activates' compressive diagonals in this core, which make an angle θ with the horizontal plane. According to the Eurocode, this angle lies between 21.6° and 45°.

When checking the shear force capacity, the amount of reinforcement in x- and y-direction are important. Their contribution in the direction of the maximum shear force v_0 needs to be calculated to incorporate them: $\rho_l = \rho_x \cos^2 \varphi_0 + \rho_y \sin^2 \varphi_0$. Next, the shear force capacity of the concrete (without shear reinforcement) needs to be calculated. If the capacity is sufficient, no shear reinforcement is required.

In case of insufficient shear capacity of the concrete itself, shear reinforcement is required. In this case, a truss-model will also create additional normal forces, which need to be added to the outer two layers. Alternatively, the additional reinforcement tensile force that is required can be calculated.

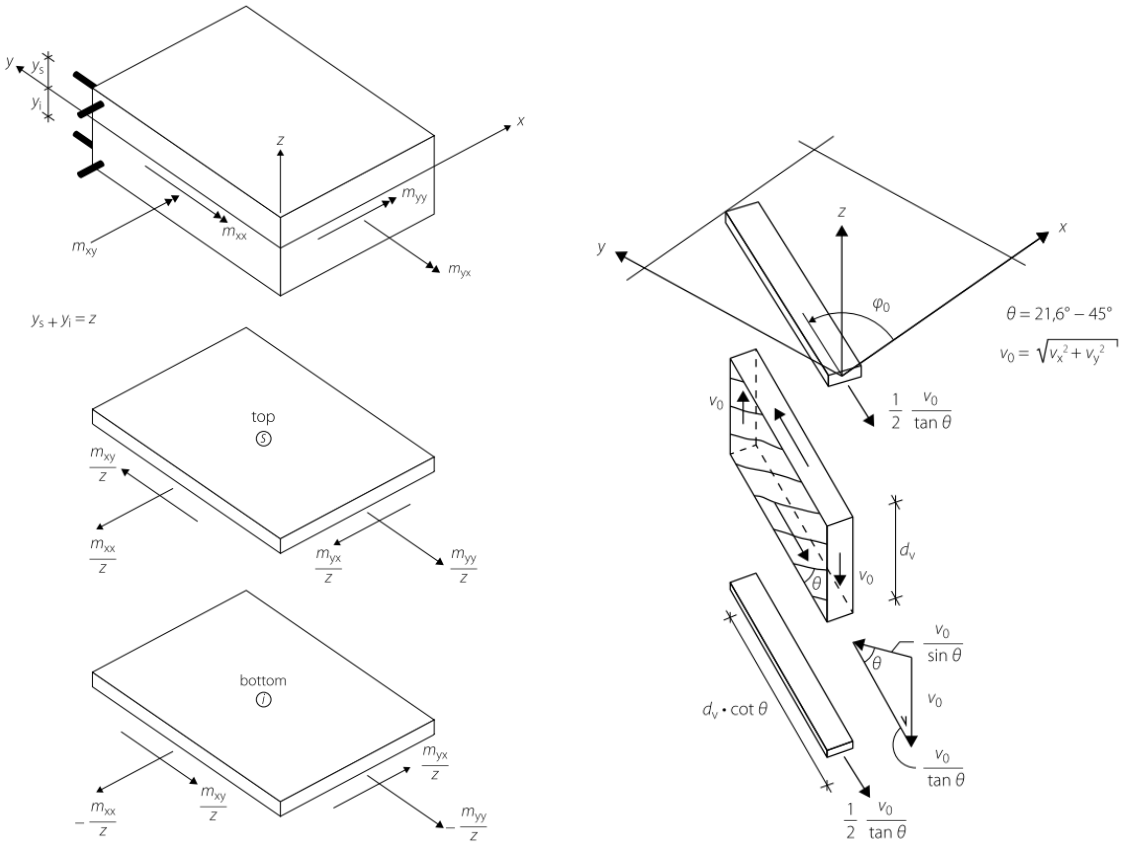

(a) The sandwich model, consisting of two discs **(b)** The truss model that takes up the shear forces

Figure A.25: Sandwich and shear-truss model, from [14]

Shell model

The shell model combined the plate- and disc model, and is quite like the plate model. The two outer layers of the sandwich model (in the shell model now) now also take up the in-plane normal and shear forces, which are divided among those outer layers. This division is done proportionally to the eccentricity of the outer layers with respect to the central axis, where the difference between x- and y-layers is usually neglected. The figure below shows all forces and moments working on the outer layers of the shell model. The factor γ determines the portion of the forces and moments taken by the top layer, while the complementary factor $\gamma - 1$ accounts for the bottom layer. Application of those factors accounts for a significant simplification of terms.

The three layer sandwich model from Eurocode 2 as treated here is useful in cases of moderate amounts of reinforcement and non-dominate torsion, which are quite common. The model is of course still a theoretical simplification, and does for instance not account for minimum reinforcement. It mainly considers elastic load resistance with concrete and reinforcement, but does not look at serviceability. In practice, cracking of concrete can account for significant redistribution of forces.

This consideration on element scale can provide useful insight, but it will not lead to a practical reinforcement design. Since the stress situation will depend on the location considered, every location in the plate will lead to a different reinforcement configuration found as optimal. So considering each element separately and then combining results for the entire plate, an optimal reinforcement configuration of the plate will be found which consists of a nonorthogonal layout with non-straight reinforcement bars of an inconsistent diameter. This theoretical optimum is of course not practical at all, since it is almost impossible to construct. The model also ignores other practicalities like required anchorage and overlap length and cutting losses.

All in all, the shell-sandwich model from the Eurocode may prove to be a useful tool for checking required amounts of reinforcement. It is however not at all a tool for making complete and sufficient reinforcement designs that satisfies serviceability limit state nor ultimate limit state.

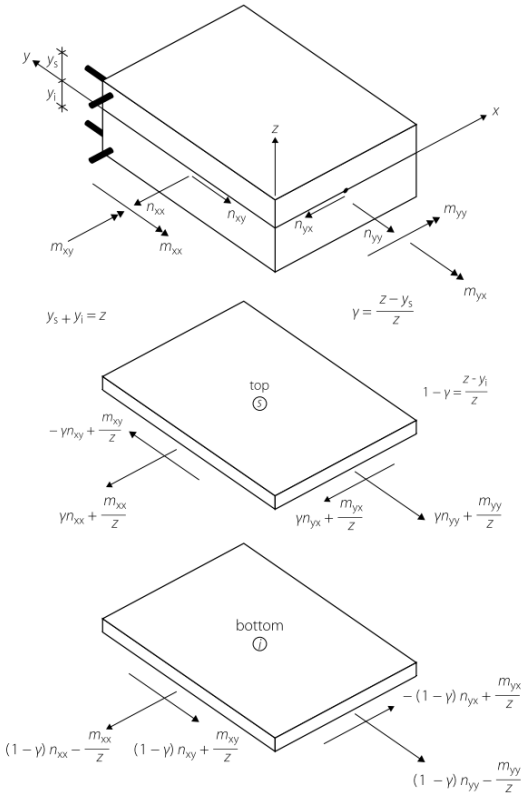

Figure A.26: The shell model

B | Magnification factors from Rijkswaterstaat

B.1 Introduction

A lot of the existing highway infrastructure in the Netherlands was built during the 1960's and 1970's. This infrastructure consists of a lot of concrete bridges, which were designed for a lifetime of 50 years. This means that in the current, the lifetime of such bridges is about to expire or has already expired.

However, design lifetime is a theoretical thing; in reality, the bridges will not collapse at their 50^{th} anniversary. Most of the concrete bridges are still sufficiently able to fulfill their requirements. To ensure this, the concrete bridges are checked on their structural integrity. This is done in steps (assessment levels), where a quick scan is usually the first step and the most conservative and coarse approach. If a bridge does not pass the quick scan, more thorough research is required, which is more detailed and less conservative. This follow up research can consist of linear finite element analysis, non-linear finite element analysis, (scale) lab tests and even proof loading of the actual structure.

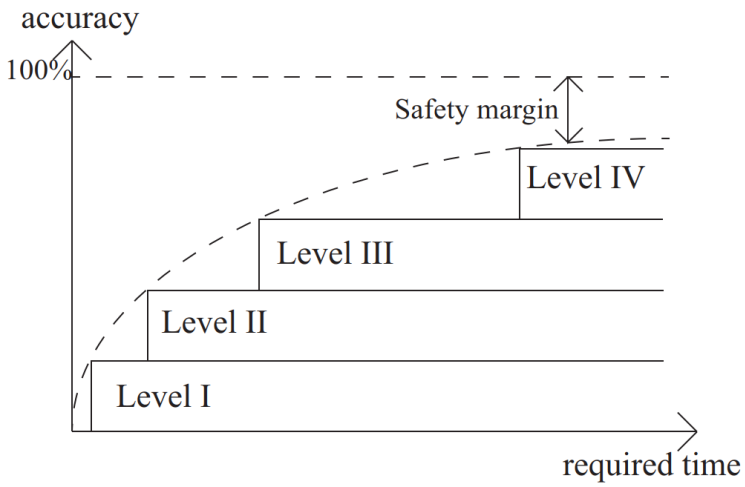

Figure B.1: Visualization of the assessment levels for existing bridges, from [40]

Rijkswaterstaat (RWS), which is the operating organization of the Dutch Ministry of Infrastructure [30], has conducted a small parametric study [48] on skewed slab bridges in order to obtain magnification factors (scheefheidsfactoren in Dutch) for the averaged sectional shear force in and near the obtuse corner. Those magnification factors are to be used in quick scans, which are based on rectangular (non-skewed) slab bridges. Magnification factors can then account for the effects caused by skew, allowing for quick analysis of skewed slab bridges, which is the purpose of the quick scans.

B.2 Model choices and geometry

In the study reported in the document, the following parameters are varied:

- Skew angle: 90° to 45°, in steps of 9°
- Free edge distance of the section (for shear force): 3 options
- Span length: 3 configurations (most occurring in practice)

The width of the bridge, defined as the perpendicular distance between the two free edges, is kept constant. The thickness of the slabs is set to be depending on the span.

Geometry of the model was chosen based on the most common bridges in practice, where a database of over 2000 spans from 281 reinforced slab bridges was used. Since about 70% of the bridges from the database consist of 3 or 4 spans with a constant slab height, it was decided to model a bridge with 4 spans, where the middle 2 spans are larger than the 2 end spans. Above the supports, a support bar is modelled, which has a width of 800 mm and a height of 1.5 $*$ the slab height. The supports are modelled as a line support, with a vertical support stiffness of 1000 $kN/mm/m$ (based on pile foundation).

In most old bridges, the free edge of the bridge was strengthened and reinforced with stirrups over a certain width. Therefore, cracking and failure of the concrete deck mostly occurs just next to the strengthened edge. As stated above, three different edge distances will be checked: 1.4, 0.95 and 0.5 m.

Table B.1: Geometry of the bridges used in the RWS document

Configuration	**Main span** [m]	**End span** [m]	**Slab height** [mm]	**Effective height** [mm]
1	19.00	14.25	900	860
2	13.50	10.00	600	560
3	8.20	6.00	400	360

The model from the RWS document was created in a 3D FEM program called DIANA, where 8 noded shell elements (CQ40S, Mindlin) were used. Near the obtuse corner where the shear force is investigated, a mesh refinement was applied: a mesh of 10 x 10 cm^2 ($\sim \frac{1}{5}h$) was created there.

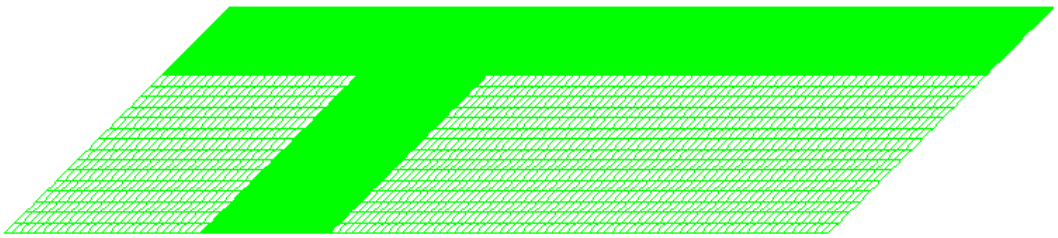

Figure B.2: Image from part of the RWS model, showing the stiffened edge (horizontal solid green) and a part of the support beam (diagonal solid green)

The bridge decks are modelled with orthotropic properties: stiffness in direction of the lanes (x-direction) is taken as the E-modulus of uncracked concrete, while for transverse and vertical stiffness a reduced modulus (40 %) is taken:

- $E_x = 30000\ MPa$
- $E_y = E_z = 12000\ MPa$

- $G_{xy} = G_{yz} = G_{xz} = 6000\ MPa$

The support beams are modelled as being isotropic.

B.3 Loads

Although the model from the document contains various loads (self-weight, dead-load, edge-load, uniformly distributed traffic loads and traffic tandem systems), only self-weight will be considered here. Results from self-weight allow for easy comparison between results from the RWS model and the model created for this thesis.

B.4 Result approach

For determination of the shear force, a section is created in the obtuse corner over a distance of 4*d, where d is the effective height of the bridge deck (taken as deck height - 40 mm), as determined in [40]. In lane direction, the section is placed at 0.5 $*h$ from the support line, as indicated by the blue line in Figure B.3. As stated before, in transverse direction the section is placed at a varying edge distance: 1.4, 0.95 and 0.5 m are taken. This edge distance represents the strengthened (vertical stirrup reinforcement) edge zone, which is much less prone to cracking. The section zone represents the location where cracking and eventual failure is expected to happen first.

Within this section, shear force is averaged. This vertical shear force is determined using a formula similar to the one used in 4.2.2:

$$V_{max} = \sqrt{V_{xz}^2 + V_{yz}^2} \tag{B.1}$$

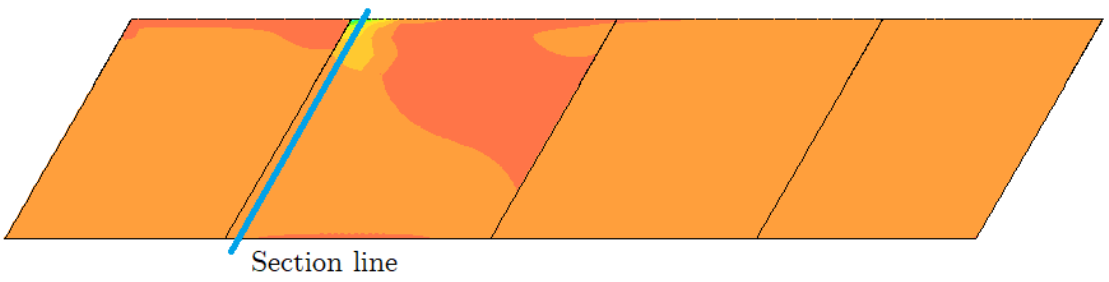

Figure B.3: Display of shear force contour plot on the 4-span bridge, where the possible location of the section indicated by the blue line

Finally, the shear force for the different parameters is checked, after which the shear magnification factors are calculated. The magnification factor for a certain skew angle α is defined as:

$$\text{Shear magnification factor} = \frac{\text{Sectional shear force for } \alpha}{\text{Sectional shear force for } 90^\circ} \tag{B.2}$$

Results from the RWS document are displayed in Figure B.2. It can be seen that magnification factors found are rather low. Moreover, geometry 1 shows a relatively lower magnification factor for the section closer to the free edge. Since shear force is concentrated along this free edge, magnification is expected to be higher in areas closer to the free edge. This result therefore contradicts with the expected.

Next, the parametric bridge tool from this thesis is configured to resemble the RWS model as much as possible. A bridge with a span length of 13.5 m, a total bridge width of 13.6 m and a deck height of 600 mm is created, in accordance to Geometry 2 (see Table B.1). Resulting shear force

Table B.2: Obtuse corner shear force magnification factors from the RWS document [48], resulting from dead load for the different configurations

3.3 Eigen gewicht – scheefheidsfactoren

Geometrie 1	Randafstand		
Hoek (graden)	1.4m	0.95m	0.5m
90	1.00	1.00	1.00
81	1.04	1.05	1.04
72	1.07	1.08	1.07
63	1.08	1.08	1.08
54	1.08	1.08	1.08
45	1.11	1.06	1.06

Geometrie 2	Randafstand		
Hoek (graden)	1.4m	0.95m	0.5m
90	1.00	1.00	1.00
81	1.04	1.05	1.04
72	1.07	1.08	1.08
63	1.10	1.10	1.10
54	1.11	1.11	1.11
45	1.11	1.12	1.11

Geometrie 3	Randafstand		
Hoek (graden)	1.4m	0.95m	0.5m
90	1.00	1.00	1.00
81	1.04	1.04	1.03
72	1.08	1.07	1.06
63	1.10	1.09	1.10
54	1.11	1.10	1.11
45	1.08	1.10	1.11

Table B.3: Magnification factors obtained from model results generated with the parametric tool, best compared with Geometry 2 from table B.2

section edge distance [m]	**1.40**	**0.95**	**0.50**
shear force magnification factor: 90°	1.00	1.00	1.00
shear force magnification factor: 45°	1.42	1.43	1.65

from dead load only is calculated in sections with a length of $4*d = 2240\ mm$, at the three different distances from the free edge. Results obtained from the tool are displayed in Table B.3 below.

It can be seen that magnification factors obtained are much higher than the ones from the RWS report (Table B.2). This shows that both models used are not so suitable for comparison. Some differences (parametric tool model versus RWS model) are:

- use of 2D elements versus 3D elements
- isotropic versus orthotropic deck material properties
- single-span versus multi-span
- discrete support versus semi-continuous support (support beam with discrete supports)
- homogeneous edge zone versus stiffened edge zone

All in all, these differences between the two models proved to be difficult for comparison. This

underlines the importance of properties other than the geometry of a model on the outcome it can produce.

C | ATS model validation

Validation of the model with the additional triangular segment (ATS) function added, is done for a bridge with the following geometrical properties:

- Span length $L = 13.7\ m$
- Road width $W = 8.3\ m \rightarrow$ 2 theoretical 2.75 m-wide lanes (driveway = 5.5 m wide)
- Angle of road crossing $\alpha = 30°$
- ATS angle $\beta = 15°$
- $\rightarrow$ Total bridge skew angle $\alpha + \beta = 45°$

For validation, SCIA can calculate the resultant of support reactions for certain load settings (load case, load combination or result class). This function is used to calculate the resultant support reaction for the following two load settings:

1. Resultant support reaction due to (concrete) self-weight only
2. Resultant support reaction due to ULS combination 6.10a (as shown in section 3.5):

$$\text{6.10a - gr1a: } 1.4 * G_k + (\psi_0 = 0.8) * 1.5 * Q_k$$

For the two load settings above, a hand calculation is made as well. This way, resultants from the model can be compared with the hand calculation for validation.

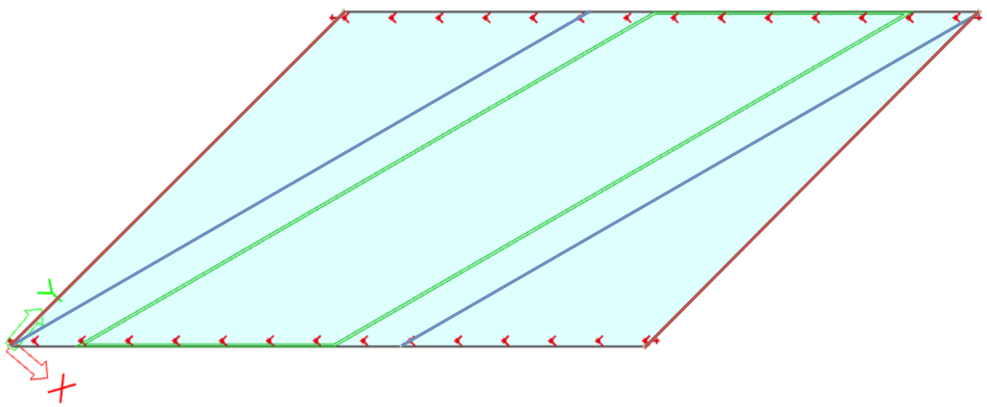

Figure C.1: Geometry of the model for validation. Different dead loads are highlighted with colours: red indicates the free edge line load, blue indicates the road edge line load, green indicates the road with the surface load from the asphalt

C.1 Hand calculation 1: concrete self-weight resultant

For the first hand calculation, the resultant from the concrete self-weight is calculated. This resultant is equal to the total load of the concrete elements on the supports:

- Bridge deck
- Abutment beam (2 x)
- Concrete pedestals (2 x 14 in this case)

C.1.1 Bridge deck

The total width of the bridge deck is calculated using the following formula:

$$\text{Total support width} = \frac{\text{W}}{\sin\alpha} + \frac{L}{\tan\alpha} - \frac{L}{\tan(\alpha+\beta)} \tag{C.1}$$

The total length in the direction perpendicular to the support lines is calculated with:

$$\text{Total length} = \text{Span length} + 2 * \text{Edge distance in y-direction} \tag{C.2}$$

The total load from the concrete bridge deck becomes:

$$\begin{gathered} G_{k,c,deck} = \text{Total length} * \text{Total support width} * \text{Deck height} * \text{Concrete self-weight} \\ G_{k,c,deck} = 14.2\,m * 27\,m * 0.9\,m * 24.5\,kN/m^3 = 8461.1\,kN \end{gathered} \tag{C.3}$$

C.1.2 Abutment beam

There are two abutment beams in the model: one for each support line. Total weight of the beam is determined by the cross-section of the beam ($0.64\ m$ by $1.35\ m$) and its length ($27.5\ m$)

$$G_{k,c,abut} = 2 * 27.5\,m * (0.64\,m * 1.35\,m) * 24.5\,kN/m^3 = 1165.2\,kN \tag{C.4}$$

C.1.3 Concrete pedestals

Each bearing pad is supported by a concrete pedestal. The pedestals have a height of $0.4\ m$ and a cross-section of $0.4\,m$ by $0.5\,m$. Each support line has 14 supports in this geometry and therefore also 14 pedestals. Total load due to the pedestals:

$$G_{k,c,ped} = 2 * 14 * 0.4\,m * (0.4\,m * 0.5\,m) * 24.5\,kN/m^3 = 54.9\,kN \tag{C.5}$$

C.1.4 Total load due to concrete self-weight

Now that the contribution of all components is calculated, they can be summed up:

$$\begin{gathered} G_{k,c,total} = G_{k,c,deck} + G_{k,c,abut} + G_{k,c,ped} \\ G_{k,c,total} = 8461.1 + 1165.2 + 54.9 = 9681.2\,kN \end{gathered} \tag{C.6}$$

C.2 Hand calculation 2: ULS combination 6.10a

The resultant support reaction now consists of the following dead loads and live loads, which can be seen in Figure C.1:

- Dead loads:
  - Concrete self-weight as calculated above: $9681.2\,kN$
  - Self-weight from the asphalt (surface load)
  - Road edge-load (line load)
  - Bridge edge-load (line load)
- Live loads:
  - Uniformly distributed loads from theoretical lane 1 and 2
  - Tandem systems on theoretical lane 1 and 2

C.2.1 Self-weight from asphalt

The driveway with asphalt has a total width of 5.5 m. The total surface of the driveway can be calculated by multiplying the total length of the bridge (in global y-direction) with the width of the driveway in support direction (global x-direction). The surface load from the asphalt is 3.22 kN/m^2 (see section 3.4).

$$\text{Asphalt load} = \text{Total length} * \frac{\text{Driveway width}}{\sin\alpha} * \text{ Asphalt weight}$$
$$\text{Asphalt load} = 14.2\,m * \frac{5.5\,m}{\sin 30^\circ} * 3.22\,kN/m^2 = 503.0\,kN \tag{C.7}$$

C.2.2 Road edge load

The road edge load works on the edge of the road, which is on both sides of the driveway (at a distance of 1.4 m from driveway edge). Edge line load is 3.5 kN/m. The total road edge load then becomes:

$$\text{Total road edge load} = 2 * \frac{\text{Total span}}{\sin\alpha} * \text{Road edge load}$$
$$\text{Total road edge load} = 2 * \frac{14.2\,m}{\sin 30^\circ} * 3.5\,kN/m = 198.8\,kN \tag{C.8}$$

C.2.3 Bridge edge load

The free edge of the bridge is loaded with a line load of 10.5 kN/m. The total bridge edge load then becomes:

$$\text{Total bridge edge load} = 2 * \frac{\text{Total span}}{\sin(\alpha+\beta)} * \text{Bridge edge load}$$
$$\text{Total bridge edge load} = 2 * \frac{14.2\,m}{\sin 45^\circ} * 10.5\,kN/m = 421.7\,kN \tag{C.9}$$

C.2.4 Total dead loads

Total sum of all dead loads, including the self-weight of the concrete elements:

$$\begin{aligned} G_{k,total} &= G_{k,c,total} + G_{k,asphalt} + G_{k,road\,edge} + G_{k,bridge\,edge} \\ G_{k,total} &= 9681.2 + 503.0 + 198.8 + 421.7 = 10804.7\,kN \end{aligned} \tag{C.10}$$

C.2.5 Traffic loads

The driveway on the validation bridge consists of two 2.75 m-wide lanes. The total surface of those lanes is calculated first by multiplying the lane length in global y-direction (Total length = 14.2 m) by the width of the lanes in global x-direction. Finally, the total loads from the UDLs of Eurocode Load Model 1 are calculated:

$$\begin{aligned} \text{Total area per theoretical lane} &= \text{Total length} * \frac{\text{lane width}}{\sin\alpha} \\ \text{Total area per theoretical lane} &= 14.2\,m * \frac{2.5\,m}{\sin 30^\circ} = 78.1\,m^2 \\ Q_{k,UDL,1} &= 78.1\,m^2 * 10.35\,kN/m^2 = 808.3\,kN \\ Q_{k,UDL,2} &= 78.1\,m^2 * 3.5\,kN/m^2 = 273.4\,kN \end{aligned} \tag{C.11}$$

Characteristic values of the Tandem Systems on theoretical lane 1 and 2 are 600 kN and 400 kN respectively. Since the total live load is equal to the total load from traffic, the total (characteristic) live load becomes:

$$\begin{aligned} Q_{k,total} &= Q_{k,UDL,1} + Q_{k,UDL,2} + Q_{k,TS,1} + Q_{k,TS,2} \\ Q_{k,total} &= 808.3 + 273.4 + 600 + 400 = 2081.7\,kN \end{aligned} \tag{C.12}$$

C.2.6 Total load from ULS combination 6.10a

With the total dead load and live load now known, the total ULS combination load can be calculated, which should equal the total resultant from support reactions for that ULS combination:

$$\begin{aligned} \text{Total vertical load from ULS combination 6.10a} &= 1.4 * G_{k,total} + 1.25 * Q_{k,total} \\ &= 1.4 * 10804.7\,kN + 1.25 * 2081.7\,kN = 17728.7\,kN \end{aligned} \tag{C.13}$$

C.3 Comparison of hand calculations with model results

In table C.1, results from hand-calculation and the model are compared. It can be seen that the calculated values and values from the model show exact agreement, and that difference thus is 0%. It can therefore be concluded that the ATS model creates a bridge with geometry and loads as expected.

Table C.1: Comparison of total vertical resultant from hand-calculation versus model results

	Hand calculation [kN]	**Model result [kN]**	**Difference**
Concrete self-weight resultant	9681.2	9681.2	0.0 %
ULS combination 6.10a resultant	17728.7	17728.7	0.0 %

D | Additional ATS results

Below, results of ATS addition to a bridge with the following configuration are shown:

- Span Length $L = 13.7\ m$
- Total Road width (barrier - barrier) $W = 14.5\ m$
- Deck height $= 0.9\ m$
- Road skew angle $\alpha = 20° - 60°$
- ATS angle β varied so that $\alpha + \beta = 20° - 60°$
- Bearing centre-to-centre distance of $2\ m$

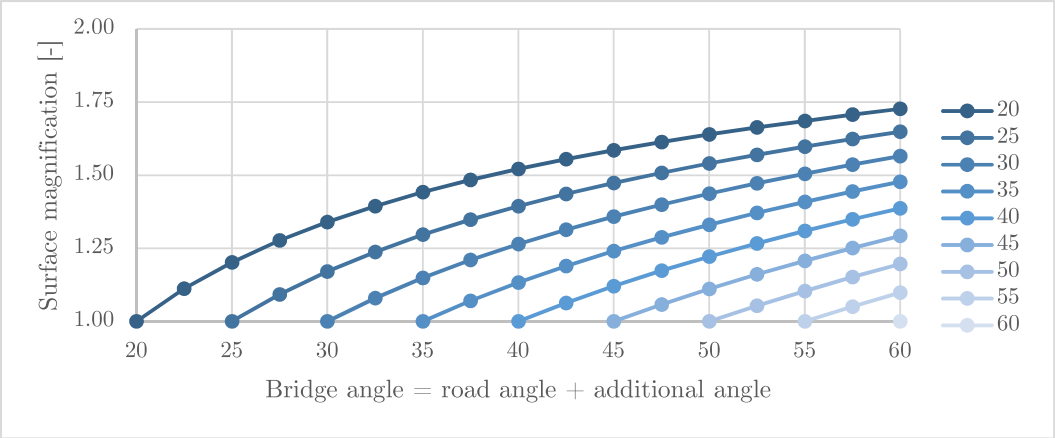

Figure D.1: Bridge deck surface magnification versus the total bridge skew angle, for different road skew angles

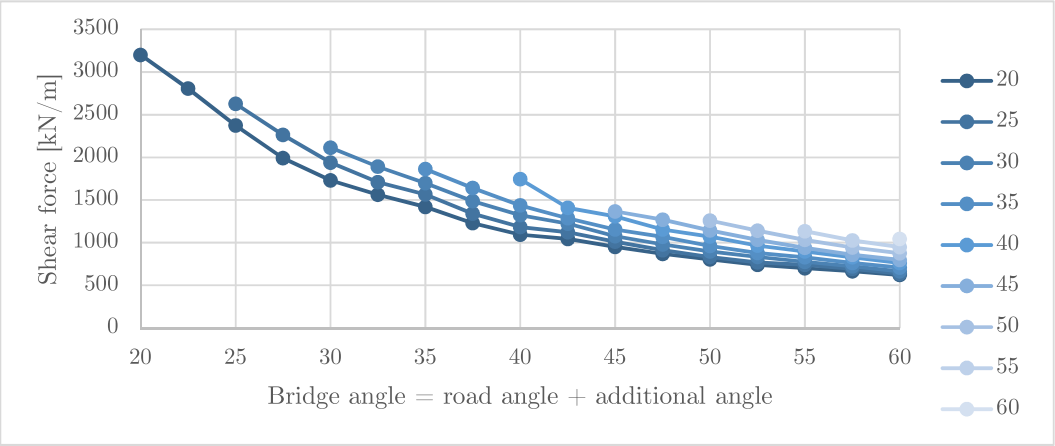

Figure D.2: Obtuse corner shear force versus the total bridge skew angle, for different road skew angles

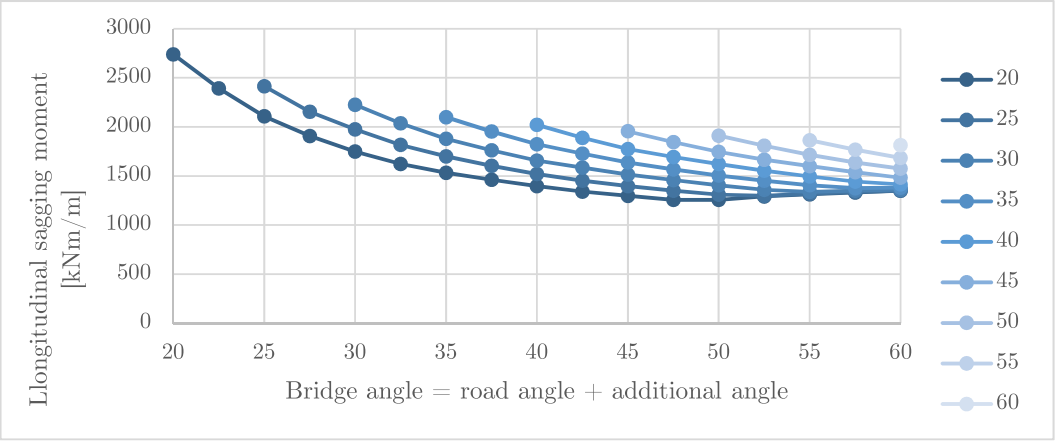

Figure D.3: Longitudinal sagging moment versus total the total bridge skew angle, for different road skew angles

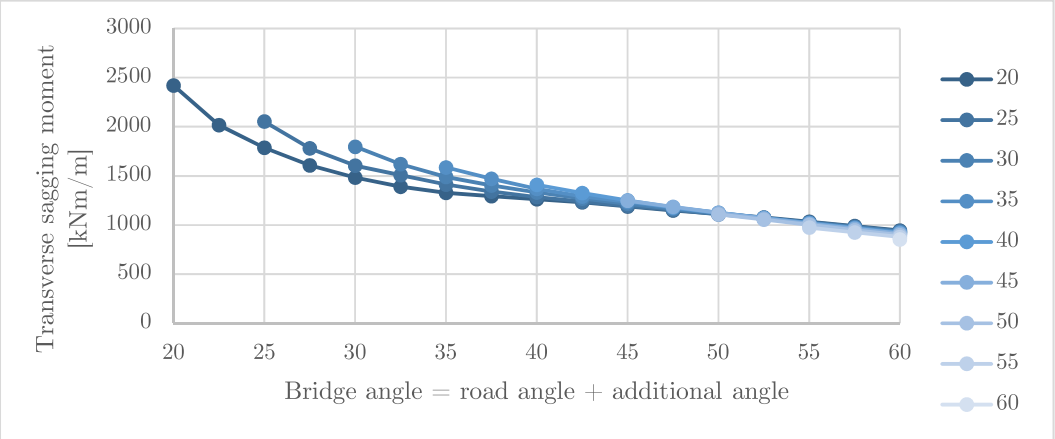

Figure D.4: Transverse sagging moment versus the total bridge skew angle, for different road skew angles

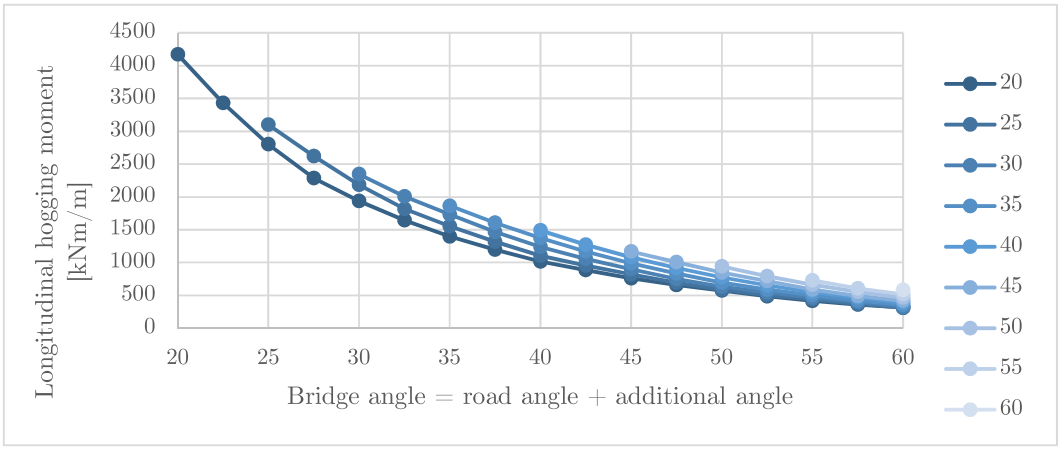

Figure D.5: Longitudinal hogging moment versus the total bridge skew angle, for different road skew angles

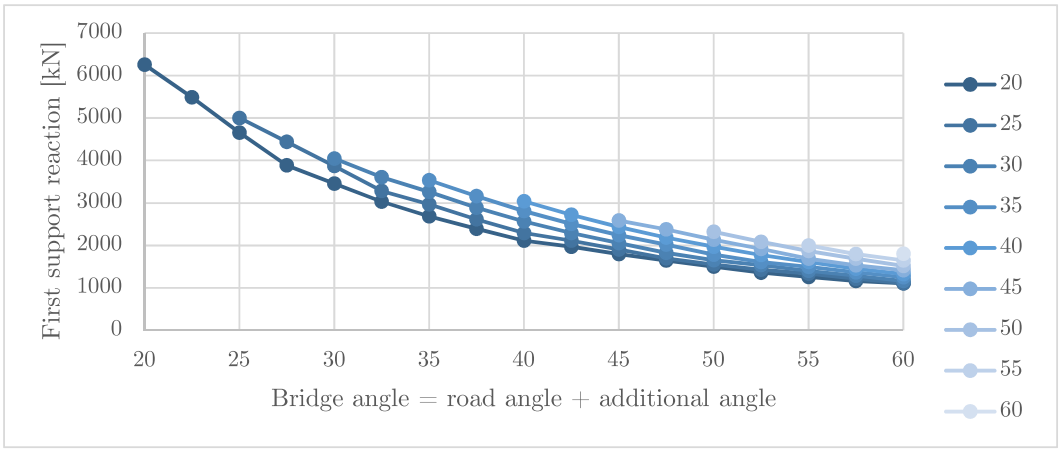

Figure D.6: Obtuse corner support reaction versus the total bridge skew angle, for different road skew angles

E | Flexural reinforcement determination based on crack width

In this appendix, the procedure for flexural reinforcement determination is explained. The procedure is based on Eurocode 2 [25] and a method as explained by R. Braam [43].

In the determination of flexural reinforcement below, pure bending is assumed. Results from the model in terms of principal stress showed only compression, so assuming pure bending is a conservative approach. The crack width is calculated by assuming a hidden tensile member in the are around the flexural reinforcement. This area is denoted as the width b times the height of this hidden tensile member $h_{c,eff}$.

The amount of reinforcement required to keep crack width to a certain limit, it first estimated, because height of the concrete compressive zone x is unknown by then. Once the amount of reinforcement is estimated, the Eurocode 2 validation is used to check whether the estimated amount of reinforcement indeed satisfies the set crack width limit.

E.1 Input parameters

Starting point is the bending moment in the Serviceability Limit State M_{sls}, which together with the upper limit crack width requirement w_k should be known. Furthermore, the following cross-sectional- and material parameters need to be chosen:

- height h (thickness of the bridge deck, known from the model)
- width $b \rightarrow$ taken as 1000 mm to consider a meter of plate
- cover c (determined by durability class)
- bar diameter ϕ_l
- concrete class, which determines following parameters:
  - characteristic compresssive cilinder strength: f_{ck}
  - mean axial tensile strength: f_{ctm}
  - secant modulus of elasticity: E_{cm}
- modulus of elasticity (design value) of reinforcing steel E_s

E.2 Initial reinforcement determination

First, the bending moment at the onset of crack is calculated, and a factor for the v for the relation between M_{sls} and M_{cr} is introduced.

$$M_{cr} = f_{ctm} * \frac{1}{6} * b * h^2$$
$$v = M_{sls}/M_{cr} \tag{E.1}$$

α_e is the relation between the E-moduli of concrete and the reinforcement steel:

$$\alpha_e = E_s/E_{cm} \tag{E.2}$$

Next, the factor λ of height from the assumed tensile area, divided by the total height is calculated. Because the height x of the concrete compressive zone is unknown, the limitation $h_{c,eff} \leq \frac{h-x}{3}$ is ignored for now (but will be checked later). Therefore $h_{c,eff}$ is estimated to be equal to 2.5 times the distance of the flexural reinforcement centre to the cross-section edge:

$$h - d = c + \frac{\phi_l}{2}$$
$$h_{c,eff} = 2.5 * (h - d) \tag{E.3}$$
$$\lambda = \frac{h_{c,eff}}{h}$$

Factor δ shows the relation between d and h:

$$\delta = \frac{d}{h} \tag{E.4}$$

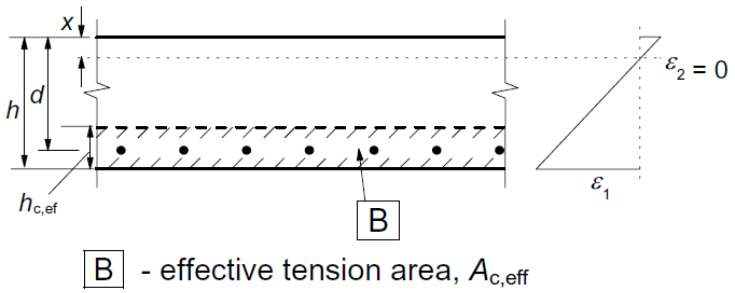

Figure E.1: The effective tensile area in a plate according to Eurocode 2 [25]

Next, v^* is introduced. It contains k_t, which is a factor for duration of the loading. Since traffic load is considered in this thesis, the value for short-term loading is taken, which is $k_t = 0.6$:

$$v^* = \frac{v}{1 - k_t * \frac{5.4 * \lambda * \delta}{v}} = \frac{v}{1 - 0.6\frac{5.4\lambda\delta}{v}} \tag{E.5}$$

Finally, the terms u_1 and u_2 are introduced:

$$u_1 = \frac{c}{\phi}$$
$$u_2 = \frac{w_k * E_s}{f_{ctm} * \phi_l} \tag{E.6}$$

What now remains is a quadratic equation that can be solved for p (assuming all parameters are known):

$$u_2 = \Big(\frac{v}{v^*}p - k_t\alpha_e\Big)\Big(3.4u_1 + 0.17(1 - \frac{v}{v^*})\frac{p}{k_t}\Big) \tag{E.7}$$

Now that p (a function of w_k) can be determined, all that is left is determining the reinforcement percentage ρ_s after which the required amount of reinforcement A_s can be determined:

$$\begin{gathered}\rho_s = \frac{v}{5.4p\delta} \\ A_s = \rho_s * b * h\end{gathered} \tag{E.8}$$

Tensile stress in the steel can also be calculated using p, since:

$$\sigma_s = p * f_{ctm} \tag{E.9}$$

E.3 Crack width validation with Eurocode 2

Now that the required amount of reinforcement is determined, a validation can be done through the method described in section 7.3.4 in Eurocode 2. In determination of p, the limitation for height of the tensile zone $h_{c,eff}$ that contains a term for the (average) compressive zone height x was not incorporated:

$$h_{c,eff} \leq \frac{h - x}{3} \tag{E.10}$$

With the formula below, the height of the compressive zone x can now be calculated, after which this limitation above can be taken into account as well:

$$\begin{gathered}x = \big(-\alpha_e\rho\sqrt{(\alpha\rho)^2 + 2\alpha_e\rho}\big)d \\ \text{with } \rho = \frac{A_s}{b * d}\end{gathered} \tag{E.11}$$

Now that the height of the compressive zone is known, the tensile stress σ_s in the flexural reinforcement due to the M_{sls} can be calculated by considering bending moment equilibrium around the centre of this concrete compressive zone:

$$\sigma_s = \frac{M_{sls}}{A_s * (d - \frac{1}{3}x)} \tag{E.12}$$

Since the height of the concrete compressive zone is known, only two more quantities need to be calculated before the crack width can be checked. $\rho_{s,eff}$ is the reinforcement ratio in the hidden tensile member, and σ_{sr} is the tensile stress in the reinforcement steel at the onset of cracking:

$$\begin{gathered}\rho_{s,eff} = \frac{A_s}{b * h_{c,eff}} \\ \sigma_{sr} = \frac{f_{ct,eff}}{\rho_{s,eff}}(1 + \alpha_e\rho_{s,eff})\end{gathered} \tag{E.13}$$

Finally, the formula for calculating the crack width from Eurocode 2 can be used for the validation:

$$w_k = \frac{\sigma_s}{E_s}\left(1 - k_t\frac{\sigma_{sr}}{\sigma_s}\right)\left(3.4c + 0.17\frac{\phi}{\rho_{s,eff}}\right) \tag{E.14}$$

It should now be checked whether the calculated crack width is below the limit set at the start of the calculation. If not, measures have to be taken and validation needs to be re-done.

If the calculated reinforcement proves to be sufficient, a layout can be designed. The bar diameter ϕ_l was already specified at the start, so only the centre-to-centre distance for the bar needs to be determined. The assumption has also been made that all bars fit into one layer. If this assumption proves to be wrong, the calculation should be redone, but with adjustments for a 2-layer reinforcement layout. In this calculation, the two reinforcement layers are treated as one equivalent layer.

Once the chosen layout is proven to have sufficient capacity, the bending moment capacity for the Ultimate Limit State (ULS) can also be calculated, see Appendix G.

E.4 Crack width calculation sheet

Below, the crack width calculation sheet can be found. The sheet is filled with values for example 2 of the case study, found in Section 7.3.

The orange-coloured cells indicate input cells. In part 1, the amount of required reinforcement to limit the cross-section to a certain crack width is estimated by approach. Next, in part 2, the reinforcement amount can be entered, after which the crack width is calculated according to Eurocode 2 (Concrete structures) [25].

Crack width calculation - 2 layers!

Input

h		900	mm	
b		1000	mm	
c_l	cover + shear bar diameter	66	mm	
ϕ_l		32	mm	
h - d_1	c + ϕ/2	82	mm	
d_1		818	mm	
h - d_2	c + 2.5ϕ	146	mm	assumption: vertical
d_2		754		ctc = 2ϕ
h - d_gem		114		
d_gem		786		
f_ck		35	N/mm2	
f_ctm		3.2	N/mm2	
E_cm		34000	N/mm2	
E_c		20000	N/mm2	
E_s		2.00E+05	N/mm2	
M_sls		1.80E+09	Nmm	
α_e	E_s / E_c	5.9	-	
α_e#	E_s / E_c	10.0	-	

Calculation of terms (from Cement article)

M_cr	1/6 * b * h^2 * f_ctm	4.32E+08	Nmm	
v	M_sls / M_cr	4.17	-	
h_c,eff	min{ 2.5(h-d) ; h/2 } , (h-x)/3 not used yet)	285	mm	CONSERVATIVE
λ	h_c,eff / h	0.32	-	
δ	d / h	0.87	-	
k_t	kortdurende belasting	0.6		
v*	v / (1 - k_t * ((5.4 δ λ) / v))	5.308		
u_1	c / ϕ	2.0625		
u_2	w_k * (E_s) / (f_ctm * ϕ)	1953.125	w_k	

$$u_2 = \left(\frac{v}{v^*}p - k_t\alpha_e\right)\left(3{,}4u_1 + 0{,}17(1 - \frac{v}{v^*})\frac{p}{k_t}\right)$$

term1	(v/v*) * p - k_t * α_e	0.785 p		-3.529
term2	3.4 * u_1 + 0.17 * (1 - (v / v*)) * (p / k_t)	7.0125	+	0.061 p

Part 1: reinforcement determination by approach

w_k	crack width (upper boundary)	0.1	mm

195.3125	=	0.048	p^2	+	5.289 p	+	-24.75	
		0.048	p^2	+	5.289 p	+	-220.06 =	0

ABC formula

a = 0.0478 b = 5.2894 c = -220.063

D 70.07815066 b^2 - 4*a*c

$$p = \frac{-b \pm SQRT(D)}{2*a}$$

p	32.21837105	of	p	-142.8117491

w_k	crack width (upper boundary)	0.2	mm

390.625 = 0.048 p^2 + 5.289 p + -24.75

0.048 p^2 + 5.289 p + -415.38 = 0

ABC formula

a = 0.0478 b = 5.2894 c = -415.375

D 107.4434577 b^2 - 4*a*c

$$p = \frac{-b \pm \mathrm{SQRT}(D)}{2*a}$$

p	53.06642259	of	p	-163.6598007

w_k	crack width (upper boundary)	0.3	mm

585.9375 = 0.048 p^2 + 5.289 p + -24.75

0.048 p^2 + 5.289 p + -610.69 = 0

ABC formula

a = 0.0478 b = 5.2894 c = -610.688

D 144.8087648 b^2 - 4*a*c

$$p = \frac{-b \pm \mathrm{SQRT}(D)}{2*a}$$

p	70.50570435	of	p	-181.0990824

by approach							
w_k	**p**	**σ_s** = p * f_ctm		**ρ_s** = v / (5.4 * p * δ)		**A_s** = ρ_s * b * h	
0.1	32.22	103.10	N/mm2	2.74%	-	**24680**	mm^2
0.2	53.07	169.81	N/mm2	1.66%	-	**14984**	mm^2
0.3	70.51	225.62	N/mm2	1.25%	-	**11278**	mm^2

Part 2: EC2 method crack width calculation

w_k	by approach	0.1	mm^2	
A_s		24680	mm^2	
ctc_l		65	mm	
ρ	A_s / (b*d)	3.14%	-	
x	(-α_e# * ρ + SQRT((α_e * ρ)^2 + 2α_e * ρ) * d	423.19	mm	0.78 d vs 0.9d
h_c,eff	min{ 2.5(h-d) ; h/2 ; (h-x)/3 }	158.94	mm	
ρ_s,eff	A_s / (b * h_c,eff)	15.53%	-	
σ_sr	(f_ctm / ρ_s,eff) * (1 + α_e * ρ_s,eff)	39.43	N/mm2	tension after cracking
z	d - x/3 (d_2?)	612.94	mm	0.78 d
σ_s	M_sls / (A_s * z)	119.0	N/mm2	
w_k	(σ_s / E_s) * (1 - k_t * (σ_sr / σ_s)) * (3.4*c + 0.17 * ϕ/ρ_s,eff)	0.124	mm	

w_k	by approach	0.2	mm^2	
A_s		16450	mm^2	**MANUAL INPUT**
ctc_l		98	mm	
ρ	A_s / (b*d)	2.09%	-	
x	(-α_e# * ρ + SQRT((α_e * ρ)^2 + 2α_e * ρ) * d	369.97	mm	0.8 d vs 0.9d
h_c,eff	min{ 2.5(h-d) ; h/2 ; (h-x)/3 }	176.68	mm	

ρ_s,eff	A_s / (b * h_c,eff)	9.31%	-	
σ_sr	(f_ctm / ρ_s,eff) * (1 + α_e * ρ_s,eff)	53.19	N/mm2	tension after cracking
z	d - x/3 (d_2?)	630.68	mm	0.80 d
σ_s	M_sls / (A_s * z)	173.5	N/mm2	
w_k	(σ_s / E_s) * (1 - k_t * (σ_sr / σ_s)) * (3.4*c + 0.17 * ϕ/ρ_s,eff)	0.200	mm	

w_k	by approach	0.3	mm^2	
A_s		11278	mm^2	
ctc_l		143	mm	
ρ	A_s / (b*d)	1.43%	-	
x	(-α_e# * ρ + SQRT((α_e * ρ)^2 + 2α_e * ρ) * d	323.12	mm	0.82 d vs 0.9d
h_c,eff	min{ 2.5(h-d) ; h/2 ; (h-x)/3 }	192.29	mm	
ρ_s,eff	A_s / (b * h_c,eff)	5.87%	-	
σ_sr	(f_ctm / ρ_s,eff) * (1 + α_e * ρ_s,eff)	73.38	N/mm2	tension after cracking
z	d - x/3 (d_2?)	646.29	mm	0.82 d
σ_s	M_sls / (A_s * z)	247.0	N/mm2	
w_k	(σ_s / E_s) * (1 - k_t * (σ_sr / σ_s)) * (3.4*c + 0.17 * ϕ/ρ_s,eff)	0.322	mm	

Crack width result comparison

w_k,approach	w_k,calc
0.1	**0.124**
0.2	**0.200**
0.3	**0.322**

remarks: Calculation method used a smaller effective tensile area (h_c,eff),
thus a larger reinforcement ratio (ρ_s,eff) (favorable in terms of crack_width)
This is expected to result in a smaller crack width (w_k)
However, for internal lever arm, in the approach z = 0.9d was used
In the calculated crack width however, a smaller lever arm was used (unfavorable)

Additionally, a higher reinforcement ratio leads to an increased maximum
crack distance s_r,max (ρ_s,eff increases, favorable)
On the other hand, average tensile strain is decreased (since σ_sr decreases)
which causes the effect of tension stiffening to decrease (unfavorable)

Minimum reinforcement $A_{s,min}\sigma_s = k_c\, k\, f_{ct,eff}\, A_{ct}$

k_c	0.65	-	
k	0.4	-	(assuming N=0)
f_ct,eff	3.2	N/mm2	(assuming concrete has hardened 28 days)
A_ct	450000	mm2	(assuming no reinforcement, since minimum is calculated here)
σ_s	500	N/mm2	(assuming σ_s = f_yk)
A_s,min	748.8	mm2	(EC2, 7.3.2)
A_s,min	1307.90	mm2	(EC2, 9.2.1.1: MAX[0.26 (f_ctm / f_yk) * b_t * d ; 0.0013 * b_t * d])

F | Shear reinforcement determination and validation

This chapter will treat the determination of shear reinforcement. The method is based on the formulas from Eurocode 2 (Concrete structures) [25]. Before determining the shear reinforcement, it is assumed that the flexural (longitudinal) reinforcement (based on SLS crack width and ULS capacity) has already been determined.

As stated before, the Eurocode mainly provides guidance in validation, which is also the case for shear reinforcement. For quick validation of a shear reinforcement layout, a sheet based on the Eurocode is set up, in which a cross section capacity will result from an input reinforcement layout.

F.1 Input parameters

For capacity calculation of a cross section and its reinforcement layout, the following geometrical and material properties need to be chosen:

- height h (thickness of the bridge deck, known from the model)
- width $b \rightarrow$ taken as 1000 mm to consider a meter of plate
- cover c (determined by durability class)
- longitudinal bar diameter ϕ_l
- centre-to-centre distance of longitudinal bars ctc_l
- concrete class, determines following parameters:
  - characteristic compresssive cilinder strength: f_{ck}
  - mean axial tensile strength: f_{ctm}
  - secant modulus of elasticity: E_{cm}
- modulus of elasticity (design value) of reinforcing steel E_s
- characteristic yield strength of reinforcing steel f_{yk}
- shear reinforcement bar diameter ϕ_{shear}
- amount of vertical bars in cross-section per meter width n_{bars} (1 stirrup = 2 bars)
- in plane centre-to-centre distance of shear bars s
- angle of compressive diagonals in truss-model θ

Once again, it is assumed that there is no normal force present: $N_{Ed} = 0$; $\sigma_{cp} = 0$.

F.2 Calculation of shear capacity

F.2.1 Concrete shear capacity

Calculation of shear capacity of a cross-section is done in a few steps. Firstly, the capacity of the concrete only $V_{Rd,c}$ is done, to check whether any reinforcement is required at all. This capacity is then validated: the prevailing shear force is checked against the pure concrete capacity. If this capacity is insufficient, shear reinforcement is needed. Additionally, according to Eurocode 2 [25] section 6.2.1, if the concrete shear capacity only is insufficient, it cannot be taken into account in calculating the total shear capacity including the reinforcement. In other words: if concrete shear capacity only is insufficient, the capacity is determined by the reinforcement capacity V_{Rd}.

Before calculating the concrete shear capacity, a few other parameters need to be determined:

$$A_{sl} = \frac{1}{4}\pi\phi_l^2 * \frac{b}{ctc_l}$$

$$k = 1 + \sqrt{\frac{200}{d}} \leq 2.0;\ d \text{ in } mm$$

$$\rho_l = \frac{A_{sl}}{b_w d} \leq 0.02 \tag{F.1}$$

$$C_{Rd,c} = \frac{0.18}{\gamma_c};\ \gamma_c = 1.5$$

$$v_{min} = 0.035 k^{1.5} f_{ck}^{0.5}$$

The concrete shear capacity is the highest value of formulas below (factor with σ_{cp} is zero):

$$\begin{gathered} V_{Rd,c} \text{ is the maximum of:} \\ \Big[C_{Rd,c} k (100\rho_l f_{ck})^{1/3} + k_1 \sigma_{cp}\Big] b_w d \\ \big(v_{min} + k_1 \sigma_{cp}\big) b_w d \end{gathered} \tag{F.2}$$

It can be seen that the concrete shear capacity (when disregarding shear reinforcement) actually is dependent on the longitudinal reinforcement. There is however another formula that determines the maximum capacity of the concrete, regardless of both shear and longitudinal reinforcement:

$$v = 0.6\left(1 - \frac{f_{ck}}{250}\right) \tag{F.3}$$

$$V_{Ed} \leq 0.5 * b_w d v f_{cd}$$

F.2.2 Cross-section shear capacity including reinforcement

The shear capacity calculation of a cross-section including the shear reinforcement is based on the truss model, as displayed in Figure F.1. Shear force is transferred to the top of the cross-section by the shear reinforcement. The angle with the horizontal of this shear reinforcement is denoted by α, which in a horizontal element is usually 90°. Assumed concrete compressive diagonals then transfer

the stress towards the longitudinal reinforcement in the bottom, over a certain horizontal length. This horizontal length depends on the angle θ which the compressive diagonal makes with the horizontal. The angle θ can be any value between 21.8° and 45°. Before calculation, an assumption for this angle θ should be made as it determines the equilibrium that is calculated and validated thereafter. As will be shown later, assumption of a relatively higher angle θ (closer to 45°) will lead to a higher maximum concrete capacity $V_{Rd,c,max}$ but a lower shear reinforcement capacity $V_{Rd,s}$.

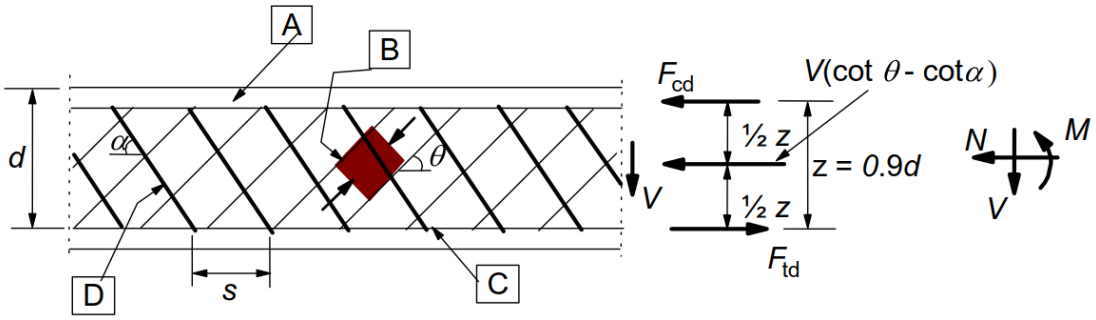

Figure F.1: The truss-model, from [25]. A=Compressive edge, B=compressive diagonal, C=Tensile edge, D=Shear reinforcement

Depending on the chosen angle θ, two capacities are calculated: $V_{Rd,s}$ denotes the capacity of the shear reinforcement, whereas $V_{Rd,c,max}$ denotes the maximum capacity of the concrete within the truss-model. When both values are calculated, the lowest value determines the governing failure mechanism and therefore the final capacity V_{Rd} of the cross-section due to shear.

For the calculation, the amount of shear reinforcement A_{sw} in the cross section is calculated first. It is the shear reinforcement per meter width. Next, the amount of shear reinforcement per (plate element) in-plane length (mm) is determined: A_{sw}/s

$$A_{sw} = \frac{1}{4}\pi\phi^2_{shear} * n_{bars}$$
$$A_{sw}/mm = \frac{A_{sw}}{s} \tag{F.4}$$

A quick check should be performed on whether the minimum shear reinforcement percentage is obtained:

$$\rho_{w,min} = \frac{0.08\sqrt{f_{ck}}}{f_{yk}}$$
$$\rho_w = \frac{A_{sw}}{s b_w \sin\alpha} \tag{F.5}$$
$$\text{Check: } \rho_w \geq \rho_{w,min}$$

The last parameters to be determined are z for the internal lever arm, α_{cw} as a factor for tension in the compressive side (=1 if there is no prestress present) and a reduction factor for concrete cracked due to shear v_1:

$$z = 0.9d$$

$$\alpha_{cw} = 1 \tag{F.6}$$

$$v_1 = v = 0.6\left(1 - \frac{f_{ck}}{250}\right)$$

What remains is calculation of the capacities in the assumed truss model of the concrete $V_{Rd,c,max}$ and the shear reinforcement $V_{Rd,s}$:

$$V_{Rd,s} = \frac{A_{sw}}{s} z f_{yd} \cot\theta$$

$$V_{Rd,c,max} = \frac{\alpha_{cw} b_w z v_1 f_{cd}}{\cot\theta + \tan\theta} \tag{F.7}$$

As stated before, final shear capacity of the cross-section becomes:

$$V_{Rd} = max\Big[V_{Rd,s}\ ;\ V_{Rd,c,max}\Big] \tag{F.8}$$

To obtain equilibrium in the truss-model with the assumed angle θ, a tensile capacity ΔF_{td} is required in the longitudinal (flexural) reinforcement. After the shear capacity calculation, it should be checked whether this (ULS) capacity in the tensile reinforcement is present. If not, measures have to be taken to either increase the tensile capacity or reduce this load.

F.3 Shear force validation sheet

Below, the shear force validation sheet can be found. The sheet is filled with values for example 2 of the case study, found in Section 7.3. Orange cells indicate input cells, grey cells indicate important output (capacity) values.

Shear reinforcement (ULS) determination

Input

h		900	mm	
b		1000	mm	
c		50	mm	
ϕ_l		32	mm	
ctc_l		98	mm	
LAYERS	number of layers	2		
h-d_gem	equivalent if two layers	98	mm	
d_gem	equivalent if two layers	802	mm	
f_ck		35	N/mm2	
ɣ_c		1.5	-	
f_cd		23.33	N/mm2	
E_cm		34000	N/mm2	
f_yk		500	N/mm2	
ɣ_s		1.15	-	
f_yd		435	N/mm2	
N_ed	normal force	0	N	
σ_cp	MIN [N_ed / A_c; 0.2 * f_cd]	0	N/mm2	
A_sl,calc	calculated	16413	mm2	
A_sl,man	Manual: MAKE EMPTY if no manual insertion		mm2	
A_sl	Takes manual if filled in	16413	mm2	
k	MIN [1 + SQRT(200 / d) ; 2.0]	1.50		
ρ_l	MIN[A_sl / (b * d) ; 2%]	2.00%		
C_Rd,c	0.18 / ɣ_c	0.12		NB
v_min	0.035 k ^ (3/2) f_ck ^ (1/2)	0.38		NB
k_1		0.15		NB

Concrete capacity

V_Rd,c	MAX[term1 ; term2]	**595**	kN
term1	(C_Rd,c * k * (100 * ρ_l * f_ck)^(1/3) + k_1 * σ_cp) * b_w * d	594701	N
term2	(v_min + k_1 * σ_cp) * b_w * d	304889	N
NIET HELEMAAL DUIDELIJK: eis voor dwarskracht nabij oplegging?			
Ved,max	0.5 * b_w * d * v * f_cd	4828	kN
v	0.6 * (1 - f_ck / 250)	0.516	

Shear reinforcement capacity

remarks:	based on truss-model				
	according to EC2, 9.2.2 (4), at least 50% of shear reinofrcement needs to be stirrups				
θ_max	based on 1 <= cot θ	= lowest capacity	45	deg	conservative

θ_min	based on cot θ <= 2.5	= highest capacity	21.8	deg	
note	Higher angle: higher concrete capacity, lower steel capacity				
θ	assumed angle of concrete compressive diagonal (truss model)		25	deg	
α	angle of shear reinforcement with horizontal (almost always 90)		90	deg	
ϕ_shear	diameter of shear reinforcement		16	mm	
A_sw / bar	0.25 * pi * ϕ_shear^2 (surface for 1 bar, 1 stirrup = 2 bars, etc)		201	mm2/bar	
n_bars	number of bars per meter width (1 stirrup = 2 bars)		4	bars/m	
A_sw	Surface of shear reinforcement in cross-section		804	mm2	(per m width)
s	centre to centre distance of stirrups length wise (in plane)		225	mm	
s_max	maximum allowed distance (EC2, 9.9): 0.75 d		601.5		
A_sw/mm	Shear reinforcement		3.57	mm^2/mm	(per m width)
z	internal lever arm (say z = 0.9d)		721.8	mm	
f_ywd	yield limit of shear reinforcement		435	N/mm2	
α_cw	factor for tension in compressive side, 1 for no pre-stress		1		
v_1	reduction factor for concrete cracked due to shear, =v		0.516		
V_Rd,s	(A_sw / s) * z * f_ywd * cot θ		**2406**	kN	
V_Rd,c,max	α_cw * b_w * z * v_1 * f_cd / (cot θ + tan θ)		**3329**	kN	
V_Rd	MIN [V_Rd,s ; V_Rd,max]		**2406**	kN	
note	**Shear reinforcement capacity is governing! (lowest capacity)**				
minimum required shear reinforcement					
ρ_w,min	0.08*SQRT(f_ck) / f_yk		0.09%		
ρ_w	A_sw / (s * b_w * sin(α))		0.36%		
(V_Ed)			2200	kN	
ΔF_td	0.5 * V_Ed * (cot θ - cot α)		**2359**	kN	
UC	V_Ed / V_Rd		0.91		

G | ULS bending moment capacity

Checking the ULS bending moment capacity is the last step in the reinforcement design phase. The longitudinal bending reinforcement has already been chosen and verified in terms of the SLS bending moment, based on the crack width criterion. In this last step, it is checked whether the ULS bending moment capacity is greater than the occurring ULS moment.

The ULS bending moment capacity can be seen as a value for the bending moment at which the cross-section is about to fail. Failure can happen in two ways:

- Crushing of the concrete: this means that the strain of the concrete has reached the compressive limit : $\varepsilon_c = \varepsilon_{cu3}$
- Tensile failure of the reinforcement: the steel has reached it ultimate strain limit and breaks: $\varepsilon_s = \varepsilon_{su}$

As stated before, longitudinal reinforcement in infrastructure is usually governed by the crack width criterion. With this in mind, the amount of reinforcement in the cross-section will be rather high. Additionally, the ultimate strain of the reinforcement steel ε_{su} is so high that is almost never reached in a normal reinforced concrete cross-section. Therefore, it is assumed that the failure mechanism with crushing of the concrete is governing.

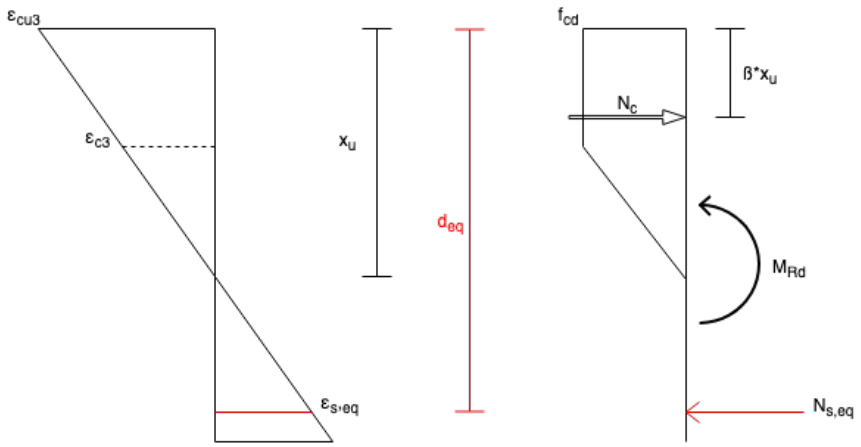

Figure G.1: Stress and strain diagram for the ULS moment capacity

G.1 Calculating the ULS bending moment capacity

Calculation of the ULS bending moment capacity is based on a few assumptions:

- The cross-section fails because the concrete ultimate strain is exceeded in the very top of the compressive zone: $\varepsilon_c \geq \varepsilon_{cu3}$
- Tensile reinforcement has a linear stress-strain relation ship, until it starts to yield. So before yielding, $\sigma_s = \varepsilon_s * E_s$. After yielding $\varepsilon_s \geq \varepsilon_{syd}$ and $\sigma_s = f_{yd}$

G.1.1 ULS moment capacity for 1 layer of reinforcement

Under the assumptions above, the ULS moment capacity is calculated. For 1 reinforcement layer, an extra assumption is added: the reinforcement steel has reached it yield strain ($\sigma_s = f_{yd}$).

First, the total force in the (equivalent) tensile reinforcement is calculated. Next, this force is set to be equal to the total equivalent load in the concrete compressive zone. From this equilibrium, height of the compressive zone is calculated:

$$\begin{aligned} N_s &= A_s * f_{yd} \\ N_c &= N_s \\ x_u &= \frac{N_c}{\alpha * b * f_{cd}};\ \alpha = 0.75 \end{aligned} \tag{G.1}$$

Now that the height of the concrete compressive zone x_u (at the moment of failure) is known, the ULS moment capacity can be calculated:

$$M_{Rd} = N_c * (d - \beta x_u);\ \beta = 0.389 \tag{G.2}$$

G.1.2 ULS moment capacity for 2 layers of reinforcement

Now that 2 layers of reinforcement are present, an analytic solution becomes harder to derive. The first (outer) layer of reinforcement should still have reached the yield strain to prevent brittle fracture of the cross-section. However, for the second (inner) reinforcement layer, this is most probably not the case. Procedure for determination of x_u is therefore changed into an iterative one: a height for x_u is first estimated. From this height, strain in the reinforcement of both layers is calculated, from which the stress follows. Next, the total force in the reinforcement is calculated, as well as the total force in the concrete compressive zone. Then both values are compared. If the difference is too great (more than 100 kN), a new value for x_u is entered and comparison is done again.

G.1.3 Ductility requirement

Considering the height of the concrete compressive zone in relation to the total cross-section height (specifically d_{eq}), a remark should be made. This remark concerns the calculated height x_u of the concrete compressive zone in the ULS moment capacity M_{Rd} equilibrium. The Dutch national annex on Eurocode 2 [26] contains a limitation of x_u, mainly for for statically indeterminate structures:

$$\frac{x_u}{d_{eq}} \leq \frac{500}{500 + f_{yd}} \approx 0.53 \tag{G.3}$$

This limit also prevents a cross-section from brittle failure: due to a relatively high amount of reinforcement, the concrete in the compressive zone can fail by compression before the reinforcement reaches the yield limit. In other words: no 'warning' in the form of visible extensive deformations of the structure can/will be observed before failure. The Eurocode 2 (Design of concrete structures) states that the effects of creep and shrinkage in ULS should be considered only when significant. They may be ignored in the ULS if ductility and eventual required rotation capacity are sufficient.

The limit contains the value of x_u, which is the height of the concrete compressive zone for the ULS bending moment capacity equilibrium. However, since longitudinal reinforcement for cross-sections in this thesis will be designed based on crack width criterion (SLS), rather than ULS bending moment, a question rises whether this limit should be followed. Reinforcement design based on SLS will mean that ULS moment capacity is not reached: the unity check $UC = \frac{M_{Ed}}{M_{Rd}}$ will

be well below 1. This means that the actual height of the compressive zone will be smaller than the calculated ultimate height x_u, and that brittle fracture will probably not occur. It is therefore decided that the cross-sections to be validated do not have to comply with this rule.